frontiers | Research Topics

Unraveling inflammaging: a pathway to prevent age-related disease in animals

Edited by
Toshiro Arai, Takahiro Teshima and Osamu Yamato

Coordinated by
Jose Ceron

Published in
Frontiers in Veterinary Science

ISSN 1664-8714
ISBN 978-2-8325-5894-2
DOI 10.3389/978-2-8325-5894-2

About Frontiers

Frontiers is more than just an open access publisher of scholarly articles: it is a pioneering approach to the world of academia, radically improving the way scholarly research is managed. The grand vision of Frontiers is a world where all people have an equal opportunity to seek, share and generate knowledge. Frontiers provides immediate and permanent online open access to all its publications, but this alone is not enough to realize our grand goals.

Frontiers journal series

The Frontiers journal series is a multi-tier and interdisciplinary set of open-access, online journals, promising a paradigm shift from the current review, selection and dissemination processes in academic publishing. All Frontiers journals are driven by researchers for researchers; therefore, they constitute a service to the scholarly community. At the same time, the *Frontiers journal series* operates on a revolutionary invention, the tiered publishing system, initially addressing specific communities of scholars, and gradually climbing up to broader public understanding, thus serving the interests of the lay society, too.

Dedication to quality

Each Frontiers article is a landmark of the highest quality, thanks to genuinely collaborative interactions between authors and review editors, who include some of the world's best academicians. Research must be certified by peers before entering a stream of knowledge that may eventually reach the public - and shape society; therefore, Frontiers only applies the most rigorous and unbiased reviews. Frontiers revolutionizes research publishing by freely delivering the most outstanding research, evaluated with no bias from both the academic and social point of view. By applying the most advanced information technologies, Frontiers is catapulting scholarly publishing into a new generation.

What are Frontiers Research Topics?

Frontiers Research Topics are very popular trademarks of the *Frontiers journals series*: they are collections of at least ten articles, all centered on a particular subject. With their unique mix of varied contributions from Original Research to Review Articles, Frontiers Research Topics unify the most influential researchers, the latest key findings and historical advances in a hot research area.

Find out more on how to host your own Frontiers Research Topic or contribute to one as an author by contacting the Frontiers editorial office: frontiersin.org/about/contact

Unraveling inflammaging: a pathway to prevent age-related disease in animals

Topic editors

Toshiro Arai — Nippon Veterinary and Life Science University, Japan

Takahiro Teshima — Nippon Veterinary and Life Science University, Japan

Osamu Yamato — Kagoshima University, Japan

Topic coordinator

Jose Ceron — University of Murcia, Spain

Citation

Arai, T., Teshima, T., Yamato, O., Ceron, J., eds. (2025). *Unraveling inflammaging: a pathway to prevent age-related disease in animals*. Lausanne: Frontiers Media SA. doi: 10.3389/978-2-8325-5894-2

Table of contents

frontiers | Frontiers in Veterinary Science

TYPE Original Research
PUBLISHED 29 September 2023
DOI 10.3389/fvets.2023.1275802

OPEN ACCESS

EDITED BY
Fazul Nabi,
Southwest University, China

REVIEWED BY
Sarah C. Pearce,
Agriculture Research Service, United States
Marcin Barszcz,
Polish Academy of Sciences, Poland

*CORRESPONDENCE
Ester Grilli
✉ ester.grilli@unibo.it

RECEIVED 10 August 2023
ACCEPTED 12 September 2023
PUBLISHED 29 September 2023

CITATION
Bonetti A, Toschi A, Tugnoli B, Piva A and Grilli E (2023) A blend of selected botanicals maintains intestinal epithelial integrity and reduces susceptibility to *Escherichia coli* F4 infection by modulating acute and chronic inflammation *in vitro*.
Front. Vet. Sci. 10:1275802.
doi: 10.3389/fvets.2023.1275802

A blend of selected botanicals maintains intestinal epithelial integrity and reduces susceptibility to *Escherichia coli* F4 infection by modulating acute and chronic inflammation *in vitro*

Andrea Bonetti[1], Andrea Toschi[2], Benedetta Tugnoli[2], Andrea Piva[1,2] and Ester Grilli[1,3]*

[1]Dipartimento di Scienze Mediche Veterinarie (DIMEVET), Università di Bologna, Ozzano dell'Emilia, Bologna, Italy, [2]Vetagro S.p.A., Reggio Emilia, Italy, [3]Vetagro Inc., Chicago, IL, United States

In the pig production cycle, the most delicate phase is weaning, a sudden and early change that requires a quick adaptation, at the cost of developing inflammation and oxidation, especially at the intestinal level. In this period, pathogens like enterotoxigenic *Escherichia coli* (ETEC) contribute to the establishment of diarrhea, with long-lasting detrimental effects. Botanicals and their single bioactive components represent sustainable well-recognized tools in animal nutrition thanks to their wide-ranging beneficial functions. The aim of this study was to investigate the *in vitro* mechanism of action of a blend of botanicals (BOT), composed of thymol, grapeseed extract, and capsicum oleoresin, in supporting intestinal cell health during inflammatory challenges and ETEC infections. To reach this, we performed inflammatory and ETEC challenges on Caco-2 cells treated with BOT, measuring epithelial integrity, cellular oxidative stress, bacterial translocation and adhesion, gene expression levels, and examining tight junction distribution. BOT protected enterocytes against acute inflammation: while the challenge reduced epithelial tightness by 40%, BOT significantly limited its drop to 30%, also allowing faster recovery rates. In the case of chronic inflammation, BOT systematically improved by an average of 25% the integrity of challenged cells ($p < 0.05$). Moreover, when cells were infected with ETEC, BOT maintained epithelial integrity at the same level as an effective antibiotic and significantly reduced bacterial translocation by 1 log average. The mode of action of BOT was strictly related to the modulation of the inflammatory response, protecting tight junctions' expression and structure. In addition, BOT influenced ETEC adhesion to intestinal cells (–4%, $p < 0.05$), also thanks to the reduction of enterocytes' susceptibility to pathogens. Finally, BOT effectively scavenged reactive oxygen species generated by inflammatory and H_2O_2 challenges, thus alleviating oxidative stress by 40% compared to challenge ($p < 0.05$). These results support the employment of BOT in piglets at weaning to help manage bacterial infections and relieve transient or prolonged stressful states thanks to the modulation of host-pathogen interaction and the fine-tuning activity on the inflammatory tone.

KEYWORDS

intestinal health, inflammation, oxidative stress, enterotoxigenic *Escherichia coli*, botanicals

1. Introduction

To cope with worldwide increasing meat demands (1), large-scale animal production systems have adopted intensive management procedures that expose animals to a wide variety of stressful stimuli that deeply impair their health and performance. When animals experience these pressures, they lose their homeostatic state to undergo an adaptation phase: if the new environmental conditions require considerable changes, stress is developed (2). This reaction is usually unfavorable to farmers, who need high animal resilience to ensure maximum production at the lowest cost.

For pigs, weaning represents the most delicate moment of their life, during which they experience sudden and dramatic changes in a short period of time. Common practice suggests that weaning should be carried out around 21–28 days of age, when piglets have not completed their gastrointestinal maturation (3), with consequences that can last for the entire production cycle (4, 5). The gastrointestinal tract of piglets is particularly affected by early weaning practices: the loss of intestinal integrity, the reduction of digestive enzyme production, the decrease in the absorptive surface, the arrival of new dietary antigens, and the lack of a full immune competence result in a state of considerable intestinal stress (6–8).

This detrimental condition triggers the onset of a prolonged inflammatory state, which impairs intestinal homeostasis and worsens the oxidative status of the gut mucosa (9, 10). Bacteria can take advantage of the host's susceptibility to overgrow in the intestinal lumen: the most frequent infection in weaning piglets is caused by enterotoxigenic *Escherichia coli* (ETEC), a group of pathogens that exacerbates the onset of diarrhea, further damaging the overall health and performance of piglets (11, 12).

Weaning stress and its symptoms, like diarrhea, were traditionally treated with antibiotics and pharmacological doses of zinc oxide (12, 13). The employment of antibiotics is now mainly restricted to full-blown cases, under veterinary prescription, and seriously limited due to the ever-expanding phenomenon of antimicrobial resistance, which is endangering the efficacy of antibiotics for both human and animal medicine (12, 14, 15). Similarly, high zinc oxide doses were banned in several areas of the world, such as the European Union, because of environmental pollution and bacterial resistance concerns (16).

Ground-breaking sustainable alternatives are urgently required to handle animal stress. A wide and varied source of novel and diverse compounds is represented by nature since plants innately produce numerous molecules to defend themselves against pathogens, predators, and stressors (17, 18). Botanicals such as essential oils, oleoresins, and powder extracts are broadly studied in animal nutrition thanks to their recognized antimicrobial, antioxidant, and anti-inflammatory properties (19, 20). Our previous studies showed that certain single terpene-rich botanicals and phenol-rich botanicals were able to modulate oxidative stress, ameliorate epithelial integrity of enterocytes, and support cells to manage ETEC infections *in vitro*, with specific mechanisms of action and peculiar individual properties (21, 22).

In this framework, the aim of this study was to investigate the ability of a blend of selected botanicals (BOT) in different stressful conditions on cultured Caco-2 enterocytes, a well-known model for intestinal studies. In particular, we assessed BOT ability to modulate acute and chronic inflammatory challenges, and explored its efficacy against an ETEC infection, while also elucidating its in-depth mechanism of action *in vitro*.

2. Materials and methods

2.1. Chemicals and reagents

Chemicals and cell culture reagents were provided by Merck KGaA (Darmstadt, Germany) unless otherwise specified. Capsicum oleoresin was purchased from Frey&Lau (Frey + Lau GmbH, Henstedt-Ulzburg, Germany) and grape seed extract was obtained from Layn Natural Ingredients (Guilin Layn Natural Ingredients Corp., Shanghai, China). The blend of botanicals (BOT) was composed of thymol, grape seed extract, and capsicum oleoresin, and tested at a concentration of 30 ppm (10 ppm of each component) in all the experiments. Stock solutions of the BOT components were prepared in ethanol 100% (v/v) and supplemented in a culture medium at a final working concentration of ethanol ≤1% (v/v).

2.2. Cell line and culture conditions

The human colon adenocarcinoma cell line (Caco-2) was obtained from DSMZ (DSMZ-German Collection of Microorganisms and Cell Cultures, Leibniz Institute, Germany). Caco-2 cells were maintained in a basal medium composed of Dulbecco's modified Eagle's medium (DMEM) supplemented with 10% fetal bovine serum (FBS), 1% L-glutamine, 1% non-essential amino acids, and 1% penicillin/streptomycin (P/S). Cells were incubated at 37°C in an atmosphere containing 5% CO_2 at 95% relative humidity.

2.3. Inflammatory challenge

To evaluate the monolayer integrity, Caco-2 cells were cultured into 24-well Transwell® inserts (0.4 µm diameter pores) (Corning, Massachusetts, United States), seeded at a density of 5×10^4 cells/transwell. Transepithelial Electrical Resistance (TER) was measured using an epithelial tissue voltohmmeter (Millicell ERS-2, Merk, Darmstadt, Germany). The experiment started 28 days after the seeding on filters when Caco-2 cells reached a TER value >600 Ω cm^2 which indicates adequate monolayer integrity and differentiation.

2.3.1. Acute inflammatory challenge

Once completely differentiated, Caco-2 cells were divided into five groups: a negative control group (CTR-) maintained in basal medium for the entire duration of the experiment, two positive control groups (CTR+) that were maintained in basal medium and challenged either at day 0 or day 6, and two treated groups (BOT+) that were supplemented with the blend of botanicals and challenged either at day 0 or day 6.

The acute inflammatory challenge was performed as described by Toschi et al., (23). Briefly, challenged cells were exposed for 24 h to a cocktail of pro-inflammatory cytokines (cytomix) including IL-1β (25 ng/mL), TNFα (50 ng/mL), and IFNγ (50 ng/mL), and LPS from *E. coli* O55:B5 (10 µg/mL). Depending on the experimental group, challenged cells received the cytomix + LPS either at day 0 (early acute inflammatory challenge) or at day 6 (late acute inflammatory challenge). Throughout the experiment, TER was measured on days 0, 1, 2, 5, 6, and 7.

2.3.2. Chronic inflammatory challenge

The chronic inflammatory challenge was adapted from Toschi et al., (23). To obtain continuous inflammatory stimulation on cells, the challenge was performed for 7 days with basal medium containing cytomix + LPS. The inflammatory cocktail was refreshed every 2 days adding incremental doses of LPS (10, 20, and 30 µg/mL on days 2, 4, and 6, respectively) to avoid eventual adaptation.

Cells were divided into 4 groups depending on the presence of the challenge and BOT (CTR-, CTR+, BOT-, BOT+), and treated for a total of 7 days during which TER was measured at days 0, 1, 2, 3, 6, and 7. At the end of the experiment, cells were washed with DPBS and harvested for gene expression analysis.

2.3.3. Measurement of reactive oxygen species (ROS) levels

ROS were measured using CellROX® Deep Red Reagent (Thermofisher Scientific, Milan, Italy) following the manufacturer's instructions. To perform the analysis, Caco-2 cells were seeded at a density of 1.5×10^4 cells/well onto 96-well plates and maintained in basal medium. Once reached the confluence, cells were treated with BOT for 24 h. Then, challenged groups were supplemented with cytomix + LPS for 24 h or 500 µM H_2O_2 for 1 h to induce ROS production before CellROX® assay. Fluorescence values were recorded with Varioskan™ LUX (Thermofisher Scientific, Waltham, MA, United States).

2.4. Bacterial challenge

The pathogen employed for the bacterial challenge was a field strain of ETEC with F4 adhesins, expressing heat-labile and heat-stable toxins (LT^+, STa^+, STb^+), and originally isolated from a weaning piglet affected by post-weaning diarrhea. Bacteria were cultured in brain-heart infusion broth (BHI, VWR International, Milan, Italy) at +37°C and daily passaged 1:100 to maintain an active culture (24). Caco-2 cells were obtained and routinary maintained as described in Section 2.2.

On challenge day, the bacterial inoculum was prepared by passing 1:80 the overnight culture in fresh BHI. After 4 h, when the late logarithmic growth phase was reached, bacterial turbidity at 630 nm was measured at the spectrophotometer. The resulting value was interpolated into an absorbance – CFU/mL curve previously prepared in order to standardize the bacterial inoculum at a precise concentration for the infection experiments, as previously described by Roselli et al. (25).

2.4.1. Infection of Caco-2 cells on porous filters

To recreate an ETEC infection on intestinal cells *in vitro*, Caco-2 cells were differentiated on porous Transwell® inserts (3.0 µm diameter pores) (Corning, Massachusetts, United States) in 12 well plates for 30 days.

The infection protocol was performed according to our previous study (22). Briefly, Caco-2 were differentiated and TER of all inserts measured as described in paragraph 2.3. Then, cells were washed twice with DPBS, and infected on the apical side with 5×10^7 CFU/mL ETEC (multiplicity of infection of 100) in basal medium without P/S and supplemented with the blend of botanicals (BOT+). Also the basolateral side of inserts contained the BOT treatment in basal medium without P/S. The experiment included three controls: a negative control (CTR-) without bacteria, a positive control (CTR+) with only the bacteria, and another group with the bacteria and 4 ppm colistin, a dose able to completely kill bacteria (COL+).

TER was measured at 2 and 4 h after the beginning of the infection to assess cellular integrity. At both time points, 100 µL of basolateral medium was collected from each filter and immediately diluted into sterile saline. Aliquots of the most appropriate dilutions were seeded on BHI agar plates, incubated for 24 h at +37°C, and then counted to enumerate viable bacteria translocated across the Caco-2 monolayer (bacterial translocation, BT).

To allow gene expression analysis, at the end of the experiment cells were washed twice with DPBS, then harvested and stored at −80°C until RNA extraction.

2.4.2. Adhesion assay

As previously described (22), to assess the ability of BOT to influence bacterial interaction with target cells, Caco-2 were differentiated on 24 well plates. On the infection day, cells were washed twice with DPBS, then infected with 5×10^7 CFU/mL ETEC in basal medium without P/S and supplemented with the blend of botanicals (BOT+). The experimental setup also included two controls: a positive control (CTR+) with only bacteria, and a group supplemented with bacteria and 4 ppm colistin (COL+), a dose able to completely kill bacteria.

After a 1 h infection, non-adhered bacteria were discarded, and then cells were washed four times with DPBS. Caco-2 was lysed with 0.5% Triton X-100 in DPBS for 10 min, then serially diluted in sterile saline to plate the most appropriate dilutions on BHI agar. Seeded plates were incubated for 24 h at +37°C, and viable bacteria adhered to cells were finally counted.

2.5. Gene expression assay

Gene expression was performed on cells harvested at the end of the chronic inflammatory challenge and the bacterial challenge. The assay's protocol was based on previous studies (21, 23). Briefly, RNA was extracted using NucleoSpin RNA Kit (Macherey-Nagel, Düren, Germany) with DNase digestion according to manufacturer's instructions. The RNA yield and purity were assessed by A230, A260, and A280 nm measurements at the spectrophotometer (µDrop Plate and Varioskan LUX, Thermo Fisher Scientific, Waltham, MA, United States).

RNA was reverse-transcribed using iScript cDNA Synthesis Kit (Bio-Rad Laboratories, Hercules, CA, United States) according to the manufacturer's instructions. Then, cDNA was diluted and used for qPCR in reaction mixes prepared with iTaq Universal SYBR Green Supermix (Bio-Rad Laboratories, Hercules, CA, United States). Table 1 shows forward and reverse primer sequences obtained from Merck (Darmstadt, Germany) and used for all the selected target genes.

qPCR analysis was performed by using a CFX96 Real-Time PCR Detection System (Bio-Rad Laboratories, Hercules, CA, United States) under the following conditions: 3 min at 95°C, followed by 40 cycles of 95°C for 10 s and 60°C for 30 s. The specificity of each reaction was evaluated by melting-curve analysis.

10.3389/fvets.2023.1275802

TABLE 1 Primers used for gene expression experiments in this study.

Function	Gene	Sequences (5′ → 3′)	Product length (bp)	Ref.
Tight-junction integrity	*ZO-1*	F: CGGGACTGTTGGTATTGGCTAGA R: GGCCAGGGCCATAGTAAAGTTTG	184	(26)
	ZO-2	F: CTAGCAGCGATCAACTTAGGGACAA R: CCCAGGAGTTTCATTACCAGCAA	158	(26)
	CLD-1	F: GCACATACCTTCATGTGGCTCAGF R: TGGAACAGAGCACAAACATGTCA	92	(26)
	OCCL	F: TCCTATAAATCCACGCCGGTTC R: CTCAAAGTTACCACCGCTGCTG	105	(26)
Innate immune response	*TNFα*	F: TCTCGAACCCCGAGTGACAA R: TATCTCTCAGCTCCACGCCA	124	(27)
	IL-1β	F: AATCTGTACCTGTCCTGCGTGTT R: TGGGTAATTTTTGGGATCTACACTCT	78	(28)
	IL-6	F: AGCCCTGAGAAAGGAGACATGT R: AGGCAAGTCTCCTCATTGAATCC	141	(28)
	IL-8	F: ATGACTTCCAAGCTGGC R: ACTTCTCCACAACCCT	174	(29)
Cellular response to ETEC	*MUC13*	F: CGCTTGTCAGAGAGGTGGTT R: AATGCTGGGGAGCTTTCCTC	131	This study
	BD1	F: CCTACCTTCTGCTGTTTACTC R: ACTTGGCCTTCCCTCTGTAAC	186	(30)
	GUCY2C	F: CGGGTGGCTGTCCTTTAGTT R: AGGCTGAGTTGCCCATCATC	89	This study
Housekeeping genes	*RPLP0*	F: GCAATGTTGCCAGTGTCTG R: GCCTTGACCTTTTCAGCAA	142	(31)
	GAPDH	F: TGCACCACCAACTGCTTAGC R: GGCATGGACTGTGGTCATGAG	87	(32)

Ref, reference; F, forward; R, reverse; ZO-1, zonula occludens 1; ZO-2, zonula occludens 2; CLD-1, claudin 1; OCCL, occludin; TNFα, tumor necrosis factor α; IL-1β, interleukin 1β; IL-6, interleukin 6; IL-8, interleukin 8; MUC13, mucin 13; BD1, beta defensin 1; GUCY2C, guanylyl cyclase 2C; RPLP0, ribosomal protein lateral stalk subunit P0; GAPDH, glyceraldehyde 3 phosphate dehydrogenase.

After collecting threshold cycles, gene expression levels were normalized using two reference genes, i.e., ribosomal protein lateral stalk subunit P0 (RPLP0) and glyceraldehyde-3-phosphate dehydrogenase (GAPDH). Relative changes in gene expression were calculated using the $2^{-\Delta\Delta Ct}$ method (33).

2.6. Immunofluorescence staining

To investigate the morphology of cells that experienced an inflammatory challenge or a bacterial infection, Caco-2 cells were stained by an immunofluorescence assay for zonula occludens 1 (ZO-1), a tight junction protein.

After having differentiated Caco-2 on glass coverslips (10 mm diameter) placed at the bottom of 6 well plates, with each well corresponding to a different group of treatment, cells were washed twice with DPBS, then challenged 24 h with cytomix + LPS or 2 h with 5×10^7 CFU/mL ETEC in basal medium without P/S and supplemented with the blend of botanicals (BOT+). The experimental design also included two controls: a negative control (CTR-) without any treatment or challenge, and a positive control (CTR+) with only the cytomix + LPS or bacteria.

After the challenge, cells were washed twice with DPBS, and then fixed in 4% paraformaldehyde in DPBS. Staining was performed according to our previous study (22). Briefly, Caco-2 were permeabilized with 0.5% Triton X-100, and subsequently blocked with 10% goat serum. Then, the rabbit anti-ZO-1 primary monoclonal antibody (ThermoFisher Scientific, Walthan, MA, United States) was diluted following manufacturer's instructions in DPBS with 2% bovine serum albumin (BSA) and 0.05% saponins and incubated on cells for 3 h at +4°C in humidified atmosphere. After three washes, a goat anti-rabbit secondary antibody conjugated to fluorescein isothiocyanate (FITC) (ThermoFisher Scientific, Walthan, MA, United States) was employed to bind the primary antibody for 1 h. After washing, nuclei were counterstained and slides mounted with Fluoroshield containing 4′,6-diamidino-2-phenylindole (DAPI). Pictures were visualized and acquired using a fluorescent microscope and images elaborated with NIS-Elements software (Nikon Corporation, Tokyo, Japan).

2.7. Statistical analysis

For each experiment, the experimental unit was the well, with $n = 6$ for each treatment group. Data are displayed on graphs as

means ± SEM. All data were processed using GraphPad Prism v.9.5.0 (GraphPad Software, Inc., San Diego, CA, United States). TER and BT were analyzed with Two-Way ANOVA analysis with Tukey post-hoc test comparing all experimental groups with each other. Adhesion assay, gene expression, and oxidative stress data were evaluated with One-Way ANOVA analysis with Tukey post-hoc test, comparing all experimental groups with each other. Differences were considered significant when $p \leq 0.05$, and trends were identified when $0.05 < p \leq 0.1$.

3. Results

3.1. Inflammatory challenge

3.1.1. Acute inflammatory challenge

Figure 1 reports the results of the acute inflammatory challenge, performed either at D0 or at D6 of BOT treatment.

When the inflammatory challenge was performed at the beginning of the experiment (Figure 1A), data showed that BOT was able to limit the drop (−27%) of cellular integrity caused by the challenge itself (−38%). The moderate drop in TER was also followed by a faster and higher recovery during the subsequent days: the BOT group showed always TER values higher than positive control and reached TER levels in line with or greater than the starting basal value (100%) one day in advance.

Similar results were obtained when Caco-2 was pre-treated with BOT and challenged for 24 h at D6 (Figure 1B). The application of BOT significantly improved the basal TER of intestinal epithelial cells, with an average of +20% in the first 6 days compared to the control. In addition, BOT allowed the maintenance of a higher integrity after the application of the cytomix + LPS: the challenge reduced by 30% the TER of the BOT+ group, while the drop was higher for CTR+ (40%).

3.1.2. Chronic inflammatory challenge

To investigate the effect of BOT on a prolonged inflammatory state on intestinal cells, Caco-2 was challenged for 7 days while simultaneously being treated with the blend of botanicals. Figure 2 displays the TER levels across the experiment. In normal conditions without the challenge, the treatment significantly increased the integrity of cells during the 7 days of treatment (BOT-) compared to control (CTR-), allowing enterocytes to reach a TER value up to 146% of the initial value on day 6.

The chronic inflammatory challenge (CTR+) systematically reduced cellular integrity during the experiment, keeping TER at values significantly lower than CTR-, between 75 to 55% of the initial ones. However, the BOT application consistently improved the integrity values of the BOT+ group, maintaining TER at levels significantly higher than the CTR+ group. On day 6, BOT+ integrity registered an enhancement that reached the unchallenged control (CTR-).

3.1.3. ROS levels

To examine the detailed mechanism of action of BOT, ROS levels were measured after both an inflammatory and an H_2O_2 challenge on Caco-2, and the results are reported in Figure 3. In both cases, when applied to normal intestinal cells, BOT did not significantly modify the ROS levels of the cellular system. However, in the presence of inflammatory and H_2O_2 challenges, both recognized to generate ROS, the application of BOT significantly reduced their production (−40% and −38%, respectively), restoring their concentration at the same level of the negative control (CTR-).

3.1.4. Gene expression

Caco-2 cells were harvested and mRNA levels were assessed to further elucidate the action of BOT in maintaining cellular integrity and modulating the inflammatory response during the chronic challenge.

Figure 4A shows the investigation of inflammation-related genes, like TNFα, IL-1β, IL-6, and IL-8. The challenge was able to increase the gene expression of IL-8 ($p < 0.05$) and IL-6 ($p < 0.1$), while for TNFα only numerical increases were measured, and no differences were registered for IL-1β. The BOT treatment alone, on healthy cells, did not significantly modify cytokines expression, even if some numerical reductions are displayed for TNFα, IL-1β, and IL-6. However, on challenged cells BOT was able to decrease the levels of IL-8 ($p < 0.05$)

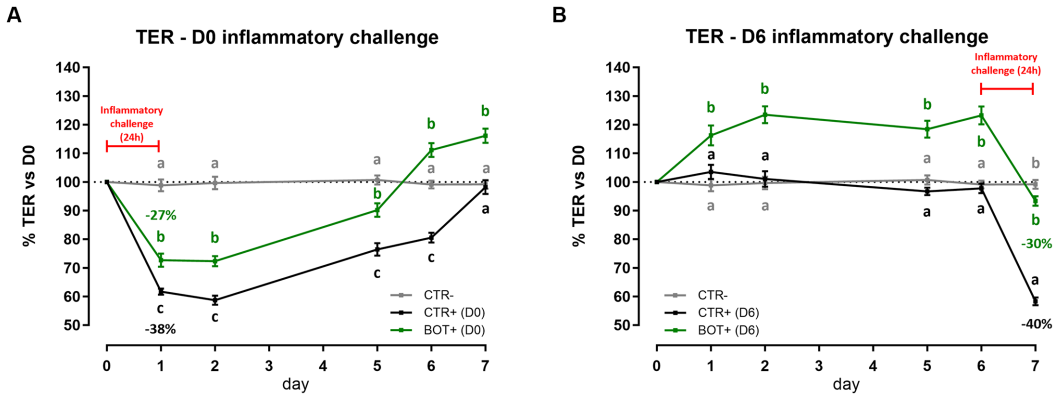

FIGURE 1
TER results during an acute LPS + cytomix challenge (24 h) on Caco-2 cells treated with a blend of botanicals (BOT). Panel **(A)** displays the TER of the challenge at D0, applied simultaneously to the treatment, while panel **(B)** shows the TER of the challenge at D6, applied on the last day of BOT treatment. Negative control (CTR-) was shared between the two challenges. Experimental groups with a "+" in the name were challenged. Data in graphs are represented as means ± SEM. Different letters indicate significant differences with $p < 0.05$ at each time point.

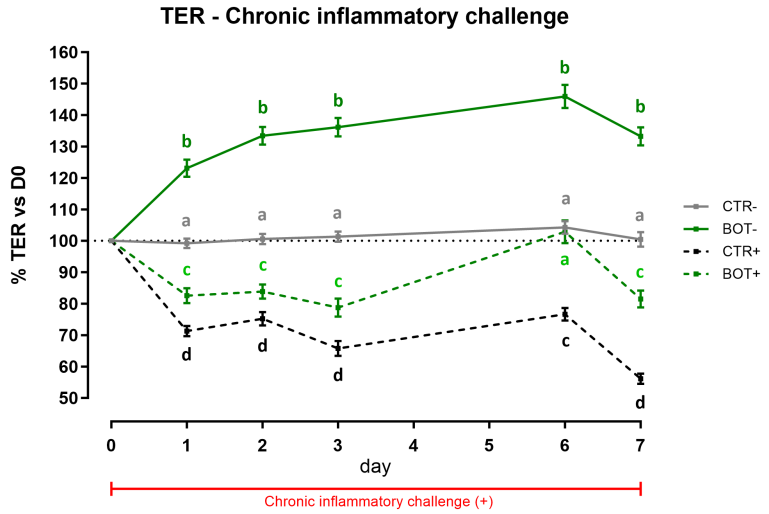

FIGURE 2
TER results during a chronic LPS + cytomix challenge (7 days) on Caco-2 cells treated with a blend of botanicals (BOT) for 7 days. Experimental groups with a "+" in the name were challenged. Data in graphs are represented as means ± SEM. Different letters indicate significant differences with $p < 0.05$ at each time point.

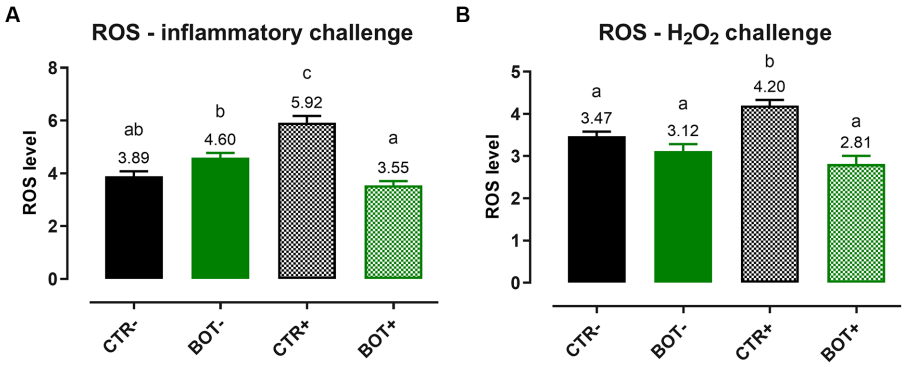

FIGURE 3
Reactive oxygen species levels in Caco-2 cells treated with a blend of botanicals (BOT) and challenged with LPS + cytomix for 24 h **(A)** or with hydrogen peroxide (H_2O_2) for 1 h **(B)**. Groups with the challenge are represented with a "+" in the name. Data in the graphs are reported as means ± SEM. Different letters denote significant differences with $p < 0.05$.

and IL-1β ($p < 0.1$) cytokines, with a numerical reduction for TNFα, and bringing back IL-6 expression in line with negative controls.

Figure 4B displays the expression levels of genes directly related to tight-junction integrity like zonula occludens 1 (ZO-1), zonula occludens 2 (ZO-2), claudin 1 (CLD-1), and occludin (OCCL). On healthy Caco-2 cells, BOT numerically increased the levels of ZO-1, CLD-1, and OCCL, with gene expression always significantly different from the positive control (CTR+). The inflammatory challenge (CTR+) worsened the expression of all the studied tight-junctions, with a significant effect on ZO-2, if compared to CTR-. The addition of BOT to the challenge enhanced the mRNA levels of all the studied tight-junction genes: although not significantly different from CTR+, gene expression was restored at the same level of the negative controls (CTR- and BOT-).

3.1.5. Immunofluorescence staining

The immunofluorescence staining for ZO-1 of cells experiencing an inflammatory challenge with or without BOT is shown in Figure 5. The application of the cytomix + LPS produced apparent alterations to the morphology of Caco-2, which tended to organize without a regular and ordered pattern. This resulted in areas of irregular ZO-1 disposition, partial loss of contact between adjacent cells, and the presence of localized acellular zones as a result of the detachment of cells. The supplementation of BOT significantly helped enterocytes to cope with the negative effects of the challenge by reducing the observed damages, with only some minor sites of ZO-1 misplacement or loss of tightness. No localized acellular areas were detected.

3.2. Bacterial challenge

3.2.1. Cellular integrity, bacterial translocation, and adhesion results

Figure 6A reports the results of Caco-2 cellular integrity during an ETEC challenge in the presence of BOT. Data show that ETEC significantly reduced TER of the epithelial monolayer at both 2 h and

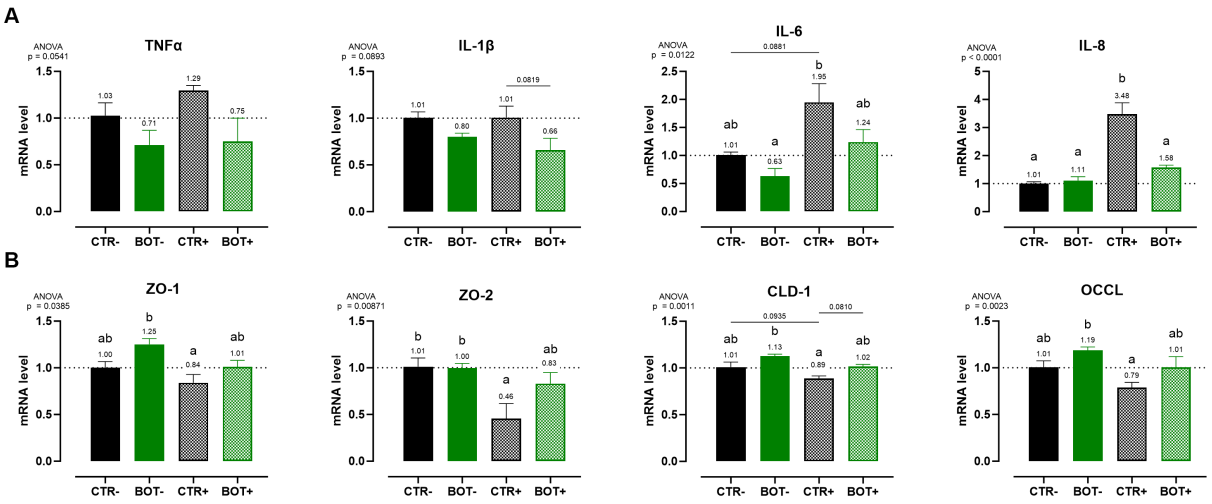

FIGURE 4
Gene expression analysis of Caco-2 cells treated with a blend of botanicals (BOT) and challenged with LPS + cytomix for 7 days. Panel **(A)** displays the inflammatory cytokines (TNFα, IL-1β, IL-6, IL-8), while panel **(B)** reports the data for tight-junction markers (ZO-1, ZO-2, CLD-1, OCCL). Groups with the inflammatory challenge are represented with a "+" in the name. Data in the graphs are reported as means ± SEM. Different letters denote significant differences with $p < 0.05$; tendencies ($p < 0.1$) are highlighted by reporting their respective p values and indicated by a line spanning the two evaluated groups.

4 h after the beginning of the infection. Damages were particularly pronounced at the end of the experiment, where the TER for the CTR+ group was only at 26% of the starting value. On the contrary, the addition of BOT to the system significantly protected cellular integrity throughout the entire experiment: TER values of the BOT+ group were in line with the negative control and colistin (COL+) at 2 h, with a slight reduction in TER only registered at 4 h, but still at values statistically equal to healthy unchallenged cells (CTR-).

To investigate the ability of BOT to influence the passage of bacteria across the Caco-2 monolayer, the bacterial translocation of ETEC was also assessed, and the results are presented in Figure 6B. Data demonstrate that, while colistin – at bactericidal dose – was able to completely avoid ETEC translocation across cells, the addition of BOT to the challenge allowed a significant reduction of the viable bacteria passage across Caco-2 at both time points. At 2 h, the reduction exerted by BOT was equal to 1 $\log_{10}$(CFU/mL), which was maintained at 4 h (0.9 $\log_{10}$(CFU/mL)).

Figure 6C displays the outcomes of the adhesion assay, performed to study BOT interference in the interaction between Caco-2 cells and ETEC. The blend of botanicals significantly reduced the adhesion of the bacteria to Caco-2 enterocytes (−4% compared to control), while colistin – at a bactericidal dose – completely inhibited its attachment.

3.2.2. Gene expression

At the end of the bacterial challenge, cells were harvested and mRNA extracted to investigate the expression of inflammatory (Figure 7A) and tight-junction (Figure 7B) related genes. Moreover, three genes related to the cellular response to bacteria were investigated, being mucin 13 (MUC13), bacterial beta defensin 1 (BD1), and guanylate cyclase 2C (GUCY2C) (Figure 7C).

The ETEC challenge significantly increased the expression of all the analyzed pro-inflammatory cytokines when compared to negative control. The application of BOT was not able to reduce the levels of IL-1β and IL-8 expression, while it tended to decrease TNFα ($p < 0.1$) and significantly lowered ($p < 0.05$) IL-6. The blend of botanicals also improved ZO-1, ZO-2, and CLD-1 expression, originally impaired by the presence of the ETEC challenge, bringing their levels between positive (CTR+) and negative (CTR-) controls.

During the challenge, BOT reduced the expression of MUC13, a putative receptor for ETEC on enterocytes. Moreover, the GUCY2C receptor for heat-stable ETEC toxins, while being already lowered by the challenge itself, was further decreased by BOT. Finally, the expression of BD1, impaired by the bacterial challenge, was partially restored by the addition of BOT to the system.

3.2.3. Immunofluorescence staining

The immunofluorescence staining results for ZO-1 of cells challenged with ETEC are shown in Figure 8. The ETEC challenge produced significant damage to the Caco-2 epithelial monolayer: compared to the healthy control, infected cells showed a swelling morphology with an irregular disposition of ZO-1 on cellular borders. Moreover, areas of cell-to-cell loss of contact left evident gaps between adjacent cell bodies. In certain areas, the degree of the damages reached a considerable extent, leading to cellular death, with acellular spaces open for bacterial translocation. The addition of BOT to the system significantly reduced the impairments exerted by ETEC, allowing the maintenance of a higher cellular tightness, with minor localized sites of ZO-1 irregular distribution or loss of contact between cellular margins. No areas of extensive cellular detachment were detected.

4. Discussion

Inflammation is a physiological response that occurs when the body needs to fight stressors (34, 35). In animal productions, common practices expose animals to a vast array of harmful stimuli, that can considerably impair their overall health and performance, with huge

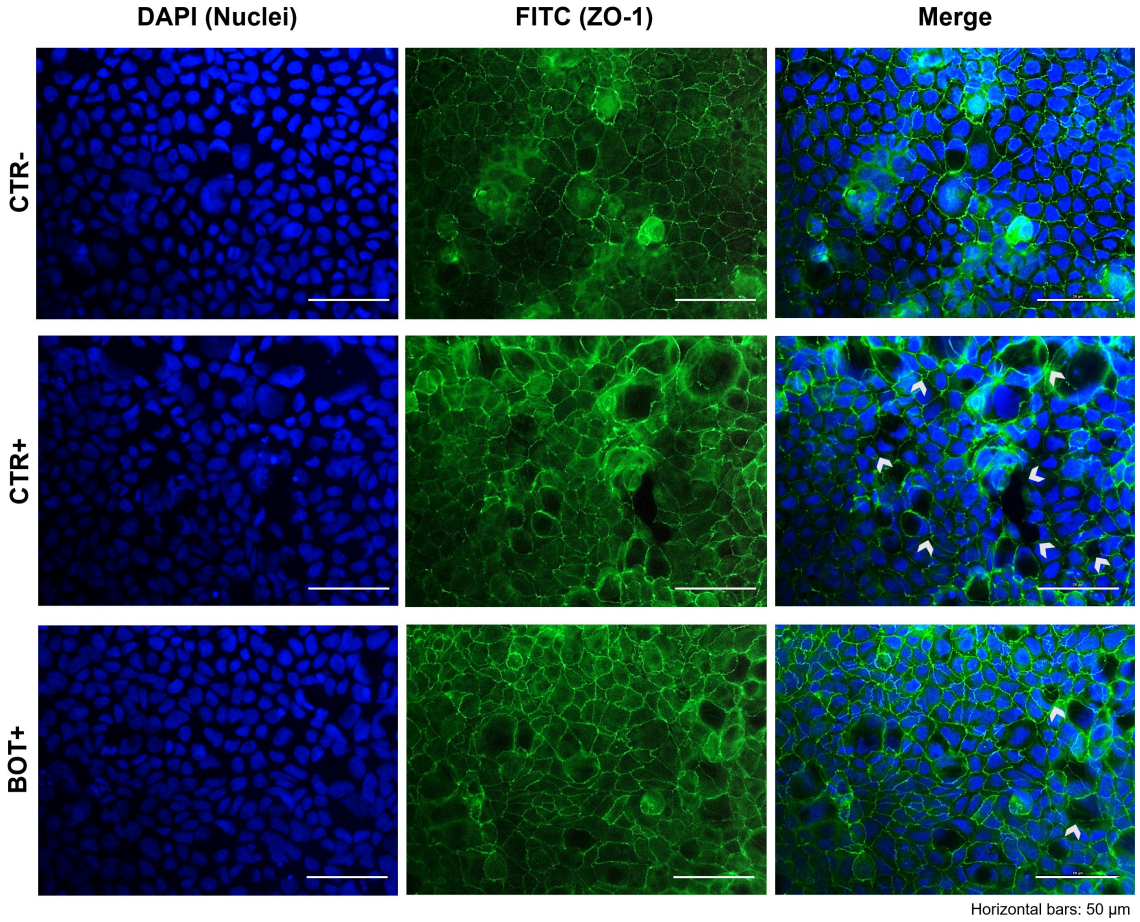

FIGURE 5
Immunofluorescence staining of Caco-2 cells treated with a blend of botanicals (BOT) and challenged with LPS + cytomix for 24 h. Groups with the inflammatory challenge are represented with a "+" in the name. The left pictures show the DAPI staining of cell nuclei, the central column depicts ZO-1 staining with FITC, while the right column displays the merge of the first two images. White arrows identify areas with anomalies of ZO-1 disposition, or loss of cells. Each row displays a different experimental group.

costs for producers (36, 37). In the pig productive cycle, the most delicate phase is weaning: its early occurrence elicits the onset of intestinal inflammation as a way to react to stress and adapt to the new dietary, environmental, and physiological conditions (10, 38). Caco-2 cells represent a recognized *in vitro* model to recreate a functional intestinal epithelium and to study its response against different detrimental stimuli (39, 40). The mix of cytokines and bacterial LPS employed in our investigations effectively recreated on intestinal cells the harmful state that piglets' gut undergoes at weaning: the health status of Caco-2 enterocytes was profoundly impaired–in the acute challenge model–as demonstrated by TER, a direct indicator of epithelial tightness. However, rather than acute, it is prolonged stress that is particularly common in actual pig husbandry, since stressors usually lasts for several days and need time to be completely resolved, especially during unfavorable periods like weaning (41). For this reason, we additionally developed a chronic challenge model, that equally proved efficient in reducing epithelial integrity of Caco-2 cells throughout time, while also activating the innate immune response of enterocytes.

The high interdependence and inverse relationship between tight junctions' state and inflammation are widely recognized in literature (42, 43). After the challenge, the drop in cellular integrity shown by our data is accompanied by the activation of a strong inflammatory status, proved by the increase of TNFα, IL-6, and IL-8 cytokine expression, and the subsequent deterioration of tight-junction mRNA levels. Consequently, the stimulation of the local inflammatory reaction triggers the release of reactive oxygen species (ROS), creating a self-amplifying cycle that further impairs homeostasis, leading to the loss of gut integrity and thus paving the way for pathogen's colonization of the intestinal mucosa (44). Our *in vitro* inflammatory challenge model significantly increased the ROS levels in Caco-2 cells, confirming the close connection between inflammation and oxidation, with the second being a physiological outcome of the first, but at the risk of excessively stimulating the overall stress response.

Historically, the employment of pharmacological doses of zinc oxide during the weaning phase was effective in reducing diarrheal symptoms and maintaining good zootechnical parameters despite the dramatic changes piglets must face (45, 46). The mechanism of action of zinc oxide is multi-factorial, and targets several sites of the gastrointestinal tract, avoiding excessive inflammation and ROS production (16). However, the excess of zinc oxide above nutritional requirements is excreted in feces, with severe environmental and bacterial resistance concerns (16, 47, 48). Thus, the European authorities banned zinc oxide medicinal doses in 2022, while other

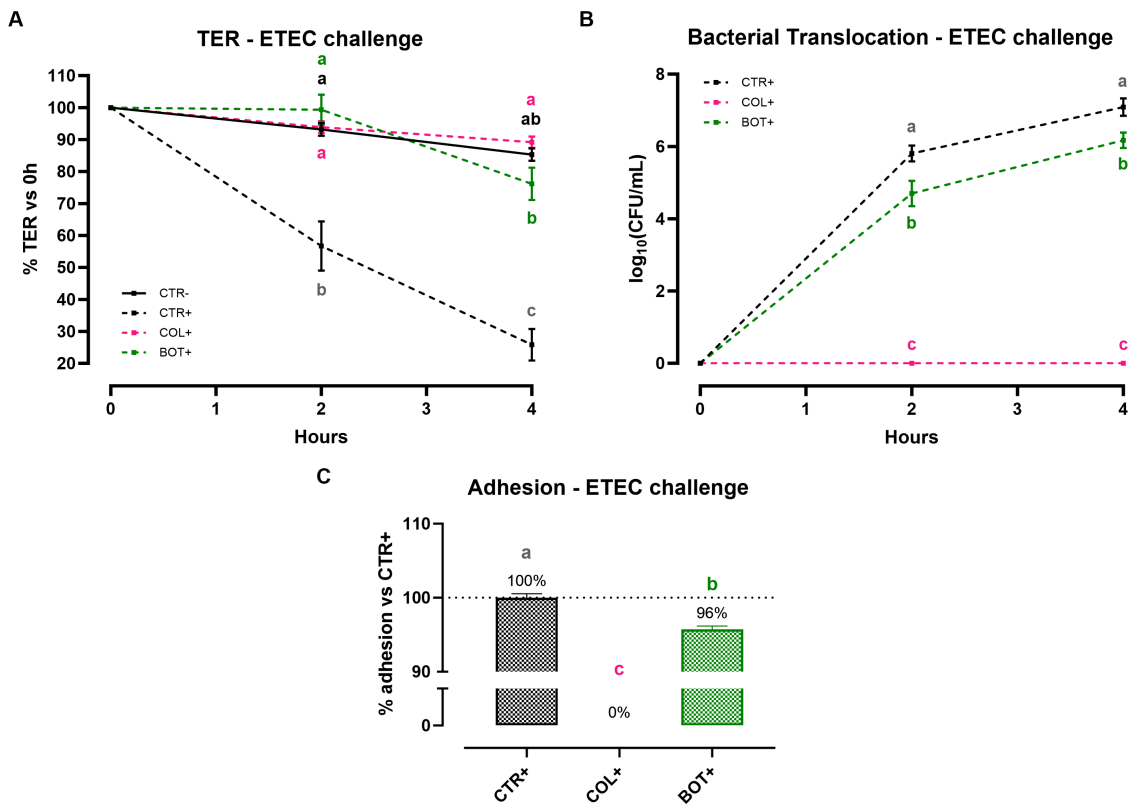

FIGURE 6
TER **(A)**, bacterial translocation **(B)**, and ETEC adhesion **(C)** assay results after an enterotoxigenic *E. coli* infection on Caco-2 cells treated with a blend of botanicals (BOT). Experimental groups with a "+" in the name were infected. Data in graphs are represented as means ± SEM. Different letters indicate significant differences with $p < 0.05$ at each timepoint.

countries are moving towards the same direction (49). Therefore, farmers are now requested to face weaning stress issues without pharmacological zinc oxide. Recognized powerful alternatives come from the bioactive compounds naturally available in fruits and plants, thanks to their diverse mechanisms of action that span both the pathogen and the host sides of the issue (19, 50, 51). When employed alone, single botanicals exert considerable supportive actions to maintain intestinal health and control bacterial overgrowth (52). Thymol, the main component of thyme essential oil, has a powerful antimicrobial and virulence-modulating action, and it is well known for its anti-inflammatory potential (53, 54). Capsaicin derived from capsicum oleoresin is a fine regulator of tight junction structure, owing also to its anti-inflammatory action and its ability to interact with the endocannabinoid system (55–57). Finally, the wide array of polyphenols inside grape seed extracts not only control bacterial toxin activity, but also exert a strong anti-inflammatory and antioxidant effect (58–60). In our study, we wanted to test the combination of the three botanicals (thymol, grape seed extract, and capsicum oleoresin; BOT) in different challenge models, complementing the individual efficacies of the single components.

The treatment with BOT was effective in protecting intestinal cells from the loss of integrity generated by an inflammatory challenge. In the case of enterocytes undergoing an acute challenge, the addition of BOT even allowed a faster recovery to normal integrity values. This beneficial effect was confirmed also when Caco-2 was pre-treated with the blend of botanicals: the pre-treatment with BOT improved the integrity of healthy cells before the challenge, and helped enterocytes to better deal with the inflammatory stimulus. In both acute challenges, even if still present, the drop in TER in BOT-treated groups was significantly limited.

When the inflammation was prolonged over time to recreate a chronic challenge model, BOT consistently supported enterocytes' health across the entire experiment, allowing cells to maintain a higher degree of tightness, and stimulating a complete recovery of TER if given sufficient time. Since weaning inflammation in pigs usually lasts for several days and requires time to be resolved (6, 61), the BOT-iterated supportive action is of central interest to maintain a healthier state, a higher animal performance, and to accelerate the recovery process to a homeostatic condition. The beneficial effects of BOT are related to its wide action against enterocytes' inflammatory response. Gene expression data at the end of the chronic challenge demonstrate that BOT significantly reduced the expression of pro-inflammatory cytokines like IL-6 and IL-8, while also numerically decreasing TNFα and IL-1β. These results are likely a consequence of thymol and capsaicin action, two BOT ingredients. The two terpenes possess phenolic hydroxyl groups that inhibit kinases responsible for NF-kB activation, one of the key transcription factors that elicit stress responses in cells (62, 63). Moreover, thymol and capsaicin directly interfere with NF-kB active sites, avoiding its translocation in the cell nucleus and the consequent inflammatory stimulation (64, 65). Finally, the two bioactives modulate the endocannabinoid system by binding TRPV1 and 3 receptors, triggering their anti-inflammatory

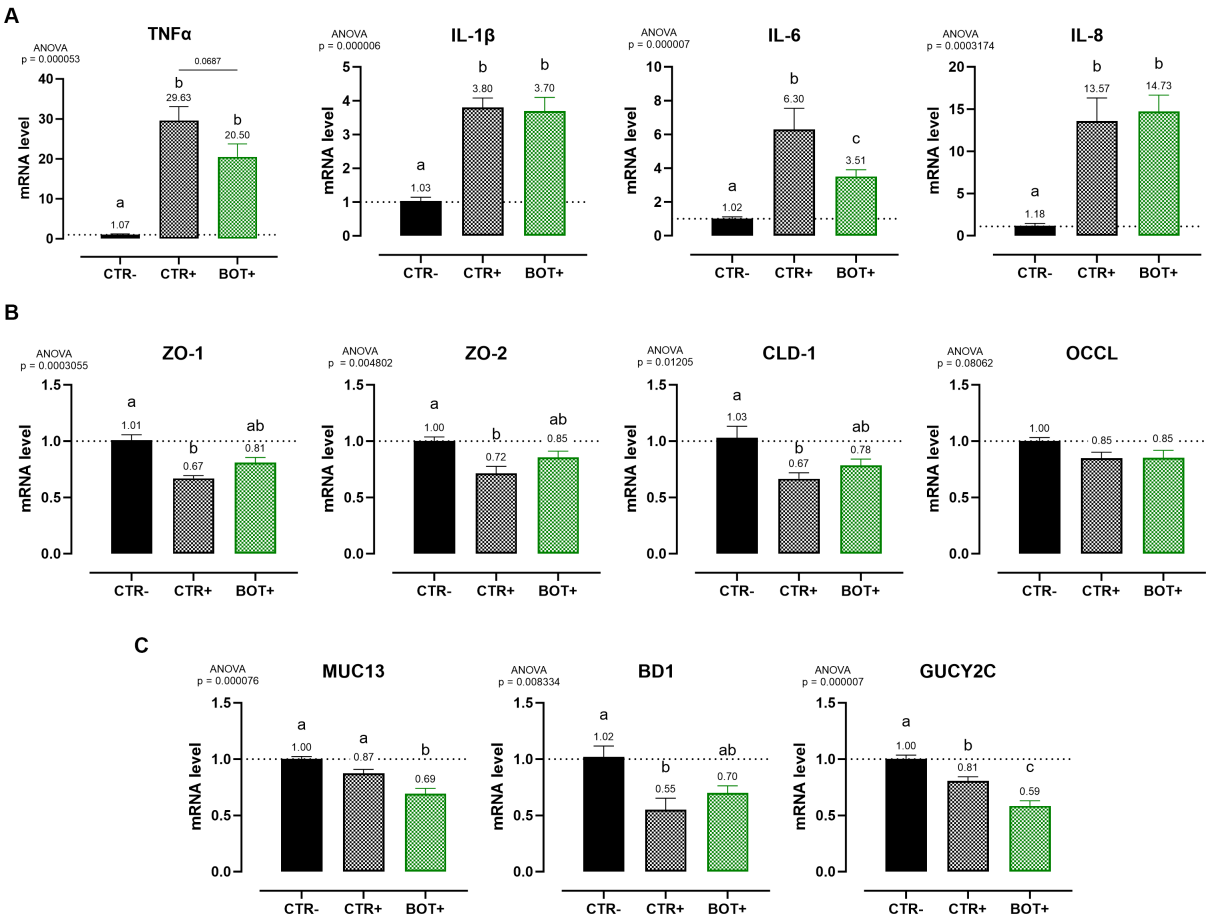

FIGURE 7
Gene expression analysis of Caco-2 cells treated with a blend of botanicals (BOT) and challenged with enterotoxigenic *E. coli* for 4 h. Panel **(A)** displays the inflammatory cytokines results (TNFα, IL-1β, IL-6, IL-8), panel **(B)** reports the data for tight-junction markers (ZO-1, ZO-2, CLD-1, OCCL), while panel C shows MUC13, BD1, and GUCY2C, three genes related to cellular response to bacterial infection. Groups with bacterial infection are represented with a "+" in the name. Data in the graphs are represented as means ± SEM. Different letters denote significant differences with $p < 0.05$; tendencies ($p < 0.1$) are highlighted by reporting their respective p values and indicated by a line spanning the two evaluated groups.

potential (66–68). The lowered inflammatory tone enabled the preservation of several tight junction components: during the challenge, BOT maintained higher expression levels of ZO-1 and-2, two scaffold-like proteins, and CLD-1 and OCCL, two sealing elements (69). These figures were also confirmed by the immunofluorescence staining for ZO-1: BOT-treated challenged cells showed a better tight junction distribution and only minor areas of loss of contact between adjacent cells. Since cytokines impair the distribution and function of tight junctions (70), the reduced inflammatory degree by BOT resulted in the preservation of a higher epithelial integrity and structure.

During the inflammatory cascade, the triggering of NF-kB stimulates the synthesis of oxidative enzymes to produce ROS as a physiological component of the inflammatory response (71, 72). However, the persistent accumulation of ROS promotes the activation of the inflammasome, with the onset of a loop that further exacerbates inflammation (73, 74). Polyphenols contained inside BOT may contribute to the disruption of this self-amplifying cycle (60, 75, 76). Our data showed that BOT reduced ROS generated by the LPS and cytokine challenge: enterocytes were safeguarded from an excessive inflammatory activation, thus avoiding the subsequent ROS synthesis. Moreover, BOT decreased the oxidative stress also during an H_2O_2 challenge, displaying its direct detoxifying action against ROS, the molecules that fuel the pro-oxidative loop.

During inflammation, the structure and function of the intestinal mucosa is deeply impaired. When the intestinal homeostasis is lost, pathogens can take over (77, 78). Weaning stress and inflammation in piglets represent the perfect condition for the overgrowth of enterotoxigenic *Escherichia coli* (ETEC) species, whose main representative is ETEC F4$^+$ (79). After adhering to the apical side of enterocytes, ETEC F4$^+$ produce heat-labile and heat-stable toxins, that elicit the release of ions in the intestinal lumen and, consequently, water (11). Piglets affected by this pathogen rapidly develop post-weaning diarrhea, that markedly reduces performance parameters and increases mortality (13). The botanical-based blend used in this study was effective in protecting Caco-2 enterocytes against an *in vitro* challenge with ETEC F4$^+$. As shown by TER levels, intestinal integrity of infected enterocytes treated with BOT was comparable to unchallenged cells and to cells treated with an effective antibiotic – colistin – used at a bactericidal dose. The protection of epithelial morphology was confirmed by the immunofluorescence staining of BOT treated cells, which displayed less damages and the preservation

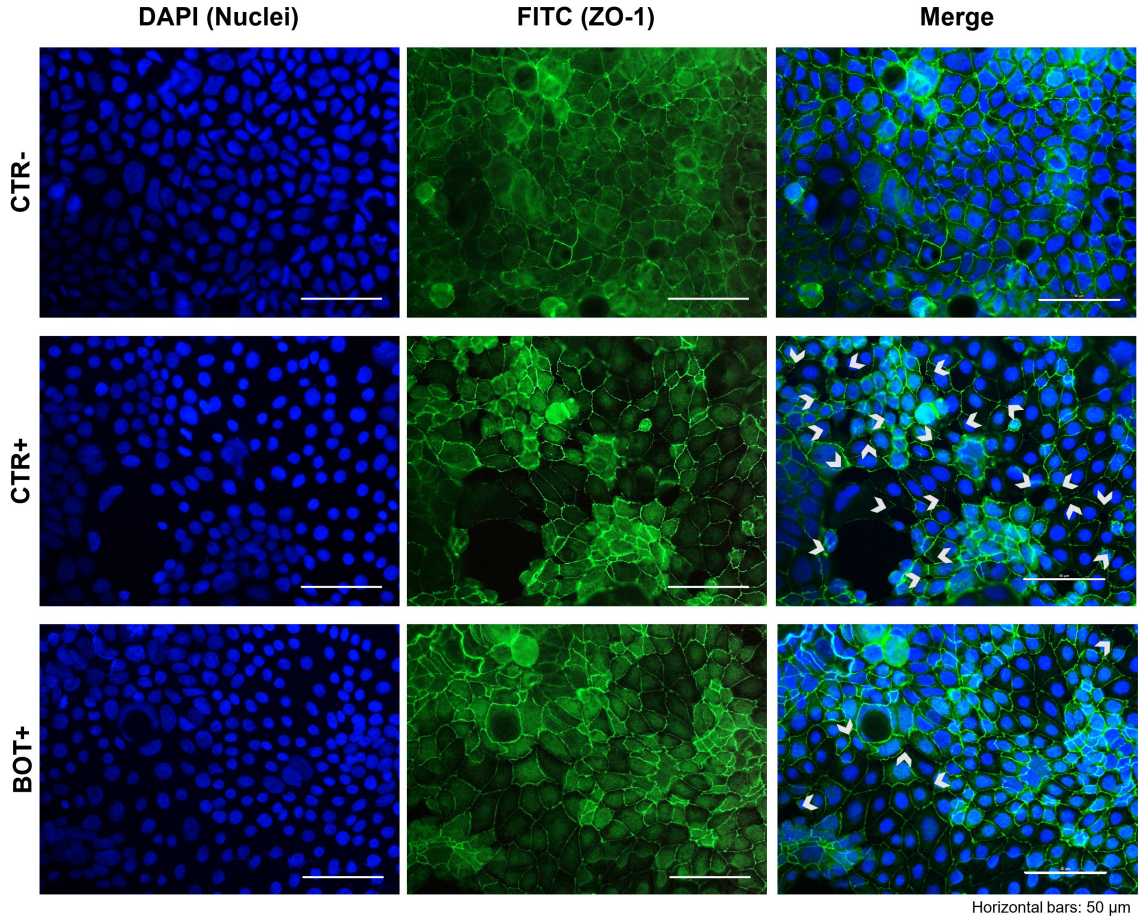

FIGURE 8
Immunofluorescence staining of Caco-2 cells treated with a blend of botanicals (BOT) and challenged with enterotoxigenic *E. coli* for 2 h. Groups with bacterial infection are represented with a "+" in the name. Left pictures show the DAPI staining of cell nuclei, the central column depicts ZO-1 staining with FITC, while the right column displays the merge of the first two images. White arrows identify areas with anomalies in ZO-1 disposition, or loss of cells. Each row displays a different experimental group.

of ZO-1 disposition if compared to the infected ones. As an indirect measurement of integrity, also bacterial translocation across Caco-2 was significantly reduced by BOT, highlighting the protective action of the blend and its ability to keep a tighter cellular monolayer. Even against the pathogen infection, the precise mechanism of action of BOT appears to be directed towards the modulation of the epithelial inflammatory response: the reduced expression of TNFα and IL-6 are indicators of a decreased inflammatory tone. On the opposite, the maintenance of higher levels of IL-8, a chemokine that attracts other immune cells in the site of inflammation (80), and the increased amount of BD1, a defensin involved in the protection against bacterial infections (81), might be a sign of an immune boosting effect, allowing the intestinal mucosa to be ready to efficiently respond in case of an excessive bacterial infection. The ability of BOT to lower inflammation is demonstrated also by the preservation of a higher tight-junction expression, similarly to the results of the inflammatory challenge. This BOT reinforcing action on intestinal mucosa integrity counteracts the disruptive effects that ETEC pathogens have on tight junctions (82, 83).

In addition, botanicals seemed to exert an effect on the susceptibility of intestinal cells to ETEC infection, as displayed by the BOT-driven reduction of MUC 13 expression, one of the candidate receptors that ETEC F4$^+$ exploits to target enterocytes (84, 85). This effect not only limits the adhesive capacity of the pathogen to Caco-2 cells, but opposes also NF-kB activity, mitigating the intestinal cell inflammatory response (86). This outcome further complements the available evidence about the virulence-modulating activity of the components inside BOT: thymol, polyphenols, and capsaicin interfere with the expression and activity of ETEC F4$^+$ toxins and adhesins (22, 24, 87, 88). Even if the bioactives inside BOT were used at sub-inhibitory doses, not directly able to prevent bacterial growth, it is likely possible that those low concentrations were still capable of decreasing ETEC ability to generate damages on the enterocytes, thus limiting the intestinal inflammatory response and the activation of ion channels responsible for the onset of diarrhea *in vivo*. Moreover, the BOT beneficial effect also extends to other markers, like GUCY2C, the receptor for the heat-stable STa bacterial toxin: data showed a significant decrease in its expression during the challenge, with a trend particularly marked in the BOT group. GUCY2C reduced signaling is physiologically linked to the stimulation of epithelial growth and regeneration: its downregulation might be correlated to an improved healing of damaged sites on intestinal surface, with the overall maintenance of an enhanced mucosal integrity (89, 90). Therefore, in the context of a bacterial infection, BOT displays interesting effects on

both the host and the pathogen side, deeply modulating their interaction at multiple levels.

5. Conclusion

In conclusion, the blend of botanicals (BOT) was effective in controlling acute and chronic stress originating from inflammatory and ETEC bacterial challenges, that strongly affect pigs at weaning. The mechanism of action of BOT combines the individual features of its single components to preserve epithelial integrity. In particular, BOT modulated enterocytes' inflammatory response, protected tight junction expression and function, controlled cellular oxidative stress, and reduced epithelial susceptibility against pathogens, while simultaneously acting on bacteria adhesive capacity. These outcomes enlighten the multifaceted activity of BOT at different stages of the host-pathogen interaction and support its employment in the feed to manage post-weaning diarrhea and weaning stress in piglets. Further studies should now explore BOT efficacy *in vivo*, both in field trials and challenge models. Moreover, other *in vitro* research could be addressed towards the investigation of BOT beneficial effects on additional complex models like intestinal organoids, and other cell lines like immune or liver cells, considering their role in the greater host response against stress.

Data availability statement

The raw data supporting the conclusions of this article will be made available by the authors, without undue reservation.

Ethics statement

Ethical approval was not required for the studies on humans in accordance with the local legislation and institutional requirements because only commercially available established cell lines were used.

Author contributions

AB: Conceptualization, Investigation, Writing – original draft, Methodology. AT: Conceptualization, Investigation, Writing – original draft. BT: Writing – review & editing. AP: Supervision, Writing – review & editing. EG: Conceptualization, Supervision, Writing – review & editing.

Funding

The author(s) declare financial support was received for the research, authorship, and/or publication of this article. This study received funding from Vetagro S.p.A. The funder had the following involvement with the study: participated in the study design, collection, analysis, and writing of the manuscript.

Conflict of interest

AP serves as a professor at the University of Bologna and is a member of the board of directors of Vetagro S.p.A. EG serves as an assistant professor at the University of Bologna and is a member of the board of directors of Vetagro Inc.

The remaining authors declare that the research was conducted in the absence of any commercial or financial relationships that could be construed as a potential conflict of interest.

Publisher's note

References

1. OECD-FAO Agricultural Outlook 2022-2031. OECD-FAO agricultural outlook. *OECD*. (2022). doi: 10.1787/f1b0b29c-en

2. Stott GH. What is animal stress and how is it measured? *J Anim Sci*. (1981) 52:150–3. doi: 10.2527/jas1981.521150x

3. Moeser AJ, Pohl CS, Rajput M. Weaning stress and gastrointestinal barrier development: implications for lifelong gut health in pigs. *Animal Nutr*. (2017) 3:313–21. doi: 10.1016/j.aninu.2017.06.003

4. Medland JE, Pohl CS, Edwards LL, Frandsen S, Bagley K, Li Y, et al. Early life adversity in piglets induces long-term upregulation of the enteric cholinergic nervous system and heightened, sex-specific secretomotor neuron responses. *Neurogastroenterol Motil*. (2016) 28:1317–29. doi: 10.1111/nmo.12828

5. Pohl CS, Medland JE, Mackey E, Edwards LL, Bagley KD, DeWilde MP, et al. Early weaning stress induces chronic functional diarrhea, intestinal barrier defects, and increased mast cell activity in a porcine model of early life adversity. *Neurogastroenterol Motil*. (2017) 29:e13118. doi: 10.1111/nmo.13118

6. Zheng L, Duarte ME, Sevarolli Loftus A, Kim SW. Intestinal health of pigs upon weaning: challenges and nutritional intervention. *Front Vet Sci*. (2021) 8:1–18. doi: 10.3389/fvets.2021.628258

7. Smith F, Clark JE, Overman BL, Tozel CC, Huang JH, Rivier JEF, et al. Early weaning stress impairs development of mucosal barrier function in the porcine intestine. *Am J Physiol Gastrointest Liver Physiol*. (2010) 298:G352–63. doi: 10.1152/ajpgi.00081.2009

8. Campbell JM, Crenshaw JD, Polo J. The biological stress of early weaned piglets. *J Anim Sci Biotechnol*. (2013) 4:2–5. doi: 10.1186/2049-1891-4-19

9. Lugrin J, Rosenblatt-Velin N, Parapanov R, Liaudet L. The role of oxidative stress during inflammatory processes. *Biol Chem*. (2014) 395:203–30. doi: 10.1515/hsz-2013-0241

10. Pié S, Lallès JP, Blazy F, Laffitte J, Sève B, Oswald IP. Weaning is associated with an upregulation of expression of inflammatory cytokines in the intestine of piglets. *J Nutr*. (2004) 134:641–7. doi: 10.1093/jn/134.3.641

11. Dubreuil JD, Isaacson RE, Schifferli DM. Animal enterotoxigenic Escherichia coli. *EcoSal Plus*. (2016) 7:1–47. doi: 10.1128/ecosalplus.ESP-0006-2016

12. Luppi A. Swine enteric colibacillosis: diagnosis, therapy and antimicrobial resistance. *Porcine Health Manag*. (2017) 3:16–8. doi: 10.1186/s40813-017-0063-4

13. Rhouma M, Fairbrother JM, Beaudry F, Letellier A. Post weaning diarrhea in pigs: risk factors and non-colistin-based control strategies. *Acta Vet Scand*. (2017) 59:31–19. doi: 10.1186/s13028-017-0299-7

14. Castro J, Barros MM, Araújo D, Campos AM, Oliveira R, Silva S, et al. Swine enteric colibacillosis: current treatment avenues and future directions. *Front Vet Sci*. (2022) 9:981207. doi: 10.3389/fvets.2022.981207

15. Bonetti A, Tugnoli B, Piva A, Grilli E. Thymol as an adjuvant to restore antibiotic efficacy and reduce antimicrobial resistance and virulence gene expression in enterotoxigenic Escherichia coli strains. *Antibiotics*. (2022) 11:1073. doi: 10.3390/antibiotics11081073

16. Bonetti A, Tugnoli B, Piva A, Grilli E. Towards zero zinc oxide: feeding strategies to manage post-weaning diarrhea in piglets. *Animals*. (2021) 11:1–24. doi: 10.3390/ani11030642

17. Tiku AR. Antimicrobial compounds and their role in plant defense. *Mol Aspects Plant-Pathogen Inter*. (2018) 71:283–307. doi: 10.1007/978-981-10-7371-7_13/COVER/

18. Kumar S, Abedin MM, Singh AK, Das S. Role of phenolic compounds in plant-defensive mechanisms. Plant phenolics in sustainable. *Agriculture*. (2020) 22:517–32. doi: 10.1007/978-981-15-4890-1_22/COVER

19. Zhai H, Liu H, Wang S, Wu J, Kluenter A-M. Potential of essential oils for poultry and pigs. *Animal Nutr*. (2018) 4:179–86. doi: 10.1016/j.aninu.2018.01.005

20. Zeng Z, Zhang S, Wang H, Piao X. Essential oil and aromatic plants as feed additives in non-ruminant nutrition: a review. *J Anim Sci Biotechnol*. (2015) 6:7. doi: 10.1186/s40104-015-0004-5

21. Toschi A, Piva A, Grilli E. Phenol-rich botanicals modulate oxidative stress and epithelial integrity in intestinal epithelial cells. *Animals*. (2022) 12:172188. doi: 10.3390/ani12172188

22. Bonetti A, Piva A, Grilli E. Botanicals as a zinc oxide alternative to protect intestinal cells from an Escherichia coli F4 infection in vitro by modulation of enterocyte inflammatory response and bacterial virulence. *Front Vet Sci*. (2023) 10:642. doi: 10.3389/fvets.2023.1141561

23. Toschi A, Rossi B, Tugnoli B, Piva A, Grilli E. Nature-identical compounds and organic acids ameliorate and prevent the damages induced by an inflammatory challenge in caco-2 cell culture. *Molecules*. (2020) 25:184296. doi: 10.3390/molecules25184296

24. Bonetti A, Tugnoli B, Rossi B, Giovagnoni G, Piva A, Grilli E. Nature-identical compounds and organic acids reduce E. coli K88 growth and virulence gene expression in vitro. *Toxins*. (2020) 12:468. doi: 10.3390/toxins12080468

25. Roselli M, Finamore A, Garaguso I, Britti MS, Mengheri E. Zinc oxide protects cultured enterocytes from the damage induced by Escherichia coli. *J Nutr*. (2003) 133:4077–82. doi: 10.1093/jn/133.12.4077

26. Park H-Y, Kunitake Y, Hirasaki N, Tanaka M, Matsui T. Theaflavins enhance intestinal barrier of Caco-2 cell monolayers through the expression of AMP-activated protein kinase-mediated Occludin, Claudin-1, and ZO-1. *Biosci Biotechnol Biochem*. (2015) 79:130–7. doi: 10.1080/09168451.2014.951027

27. Furrie E, Macfarlane S, Kennedy A, Cummings JH, Walsh SV, O'Neil DA, et al. Synbiotic therapy (Bifidobacterium longum/synergy 1) initiates resolution of inflammation in patients with active ulcerative colitis: a randomised controlled pilot trial. *Gut*. (2005) 54:242–9. doi: 10.1136/gut.2004.044834

28. Chang KW, Kuo CY. 6-Gingerol modulates proinflammatory responses in dextran sodium sulfate (DSS)-treated Caco-2 cells and experimental colitis in mice through adenosine monophosphate-activated protein kinase (AMPK) activation. *Food Funct*. (2015) 6:3334–41. doi: 10.1039/c5fo00513b

29. Parlesak A, Haller D, Brinz S, Baeuerlein A, Bode C. Modulation of cytokine release by differentiated CACO-2 cells in a compartmentalized coculture model with mononuclear leucocytes and nonpathogenic Bacteria. *Scand J Immunol*. (2004) 60:477–85. doi: 10.1111/j.0300-9475.2004.01495.x

30. Wehkamp J, Fellermann K, Herrlinger KR, Baxmann S, Schmidt K, Schwind B, et al. Human β-defensin 2 but not β-defensin 1 is expressed preferentially in colonic mucosa of inflammatory bowel disease. *Eur J Gastroenterol Hepatol*. (2002) 14:745–52. doi: 10.1097/00042737-200207000-00006

31. Bondo Dydensborg A, Herring E, Auclair J, Tremblay E, Beaulieu J-F, Bondo A. Innovative methodology normalizing genes for quantitative RT-PCR in differentiating human intestinal epithelial cells and adenocarcinomas of the colon. *Am J Physiol Gastrointest Liver Physiol*. (2006) 290:1067–74. doi: 10.1152/ajpgi.00234.2005.-As

32. Vandesompele J, De Preter K, Pattyn F, Poppe B, Van Roy N, De Paepe A, et al. Accurate normalization of real-time quantitative RT-PCR data by geometric averaging of multiple internal control genes. *Genome Biol*. (2002) 3:RESEARCH0034. doi: 10.1186/gb-2002-3-7-research0034

33. Livak KJ, Schmittgen TD. Analysis of relative gene expression data using real-time quantitative PCR and the 2-ΔΔCT method. *Methods*. (2001) 25:402–8. doi: 10.1006/meth.2001.1262

34. Jiminez JA, Uwiera TC, Inglis GD, Uwiera RRE. Animal models to study acute and chronic intestinal inflammation in mammals. *Gut Pathog*. (2015) 7:29. doi: 10.1186/s13099-015-0076-y

35. Broom LJ, Kogut MH. Inflammation: friend or foe for animal production? *Poult Sci*. (2018) 97:510–4. doi: 10.3382/ps/pex314

36. Guevara RD, Pastor JJ, Manteca X, Tedo G, Llonch P. Systematic review of animal-based indicators to measure thermal, social, and immune-related stress in pigs. *PLoS One*. (2022) 17:e0266524. doi: 10.1371/journal.pone.0266524

37. Scheffer M, Bolhuis JE, Borsboom D, Buchman TG, Gijzel SMW, Goulson D, et al. Quantifying resilience of humans and other animals. *Proc Natl Acad Sci*. (2018) 115:11883–90. doi: 10.1073/pnas.1810630115

38. Kim SW, Duarte ME. Understanding intestinal health in nursery pigs and the relevant nutritional strategies. *Anim Biosci*. (2021) 34:338–44. doi: 10.5713/ab.21.0010

39. Lea T., Caco-2 cell line., the impact of food bioactives on health, *Vitro and ex vivo models*. Cham: Springer International Publishing (2015). p. 103–111

40. Sambuy Y, De Angelis I, Ranaldi G, Scarino ML, Stammati A, Zucco F. The Caco-2 cell line as a model of the intestinal barrier: Influence of cell and culture-related factors on Caco-2 cell functional characteristics. *Cell Biol Toxicol*. (2005). 21:1–26. doi: 10.1007/s10565-005-0085-6

41. Martínez-Miró S, Tecles F, Ramón M, Escribano D, Hernández F, Madrid J, et al. Causes, consequences and biomarkers of stress in swine: an update. *BMC Vet Res*. (2016) 12:171. doi: 10.1186/s12917-016-0791-8

42. Al-Sadi R, Boivin M, Ma T. Mechanism of cytokine modulation of epithelial tight junction barrier. *Front Biosci*. (2009) 34:2765–78. doi: 10.2741/3413

43. Förster C. Tight junctions and the modulation of barrier function in disease. *Histochem Cell Biol*. (2008) 130:55–70. doi: 10.1007/s00418-008-0424-9

44. Chatterjee S. Oxidative stress, inflammation, and disease. *Oxidative Stress Biomater Elsevier*. (2016) 69:35–58. doi: 10.1016/B978-0-12-803269-5.00002-4

45. Poulsen HD. Zinc oxide for weanling piglets. *Acta Agricult Scand A*. (1995) 45:159–67. doi: 10.1080/09064709509415847

46. Grilli E, Tugnoli B, Vitari F, Domeneghini C, Morlacchini M, Piva A, et al. Low doses of microencapsulated zinc oxide improve performance and modulate the ileum architecture, inflammatory cytokines and tight junctions expression of weaned pigs. *Animal*. (2015) 9:1760–8. doi: 10.1017/S1751731115001329

47. Gräber I, Hansen JF, Olesen SE, Petersen J, Østergaard HS, Krogh L. Accumulation of copper and zinc in Danish agricultural soils in intensive pig production areas. *Geografisk Tidsskrift*. (2005) 105:15–22. doi: 10.1080/00167223.2005.10649536

48. Slifierz MJ, Friendship R, Weese JS. Zinc oxide therapy increases prevalence and persistence of methicillin-resistant staphylococcus aureus in pigs: a randomized controlled trial. *Zoonoses Publ Health*. (2015) 62:301–8. doi: 10.1111/zph.12150

49. EMA, CVMP. EMA – zinc oxide – annex II – scientific conclusions and grounds for the refusal of the marketing authorisation and for withdrawal of the existing marketing authorisations. Amsterdam, (2017). Available at: https://www.ema.europa.eu/en/medicines/veterinary/referrals/zinc-oxide (Accessed October 12, 2019).

50. Franz C, Baser K, Windisch W. Essential oils and aromatic plants in animal feeding – a European perspective. A review. *Flavour Fragr J*. (2010) 25:327–40. doi: 10.1002/ffj.1967

51. Omonijo FA, Ni L, Gong J, Wang Q, Lahaye L, Yang C. Essential oils as alternatives to antibiotics in swine production. *Animal Nutrition*. (2018) 4:126–36. doi: 10.1016/j.aninu.2017.09.001

52. Rossi B, Toschi A, Piva A, Grilli E. Single components of botanicals and nature-identical compounds as a non-antibiotic strategy to ameliorate health status and improve performance in poultry and pigs. *Nutr Res Rev*. (2020) 33:218–34. doi: 10.1017/S0954422420000013

53. Marchese A, Orhan IE, Daglia M, Barbieri R, Di Lorenzo A, Nabavi SF, et al. Antibacterial and antifungal activities of thymol: a brief review of the literature. *Food Chem*. (2016) 210:402–14. doi: 10.1016/j.foodchem.2016.04.111

54. Ezzat Abd El-Hack M, Alagawany M, Ragab Farag M, Tiwari R, Karthik K, Dhama K, et al. Beneficial impacts of thymol essential oil on health and production of animals, fish and poultry: a review. *J Essent Oil Res*. (2016) 28:365–82. doi: 10.1080/10412905.2016.1153002

55. Han J, Isoda H, Maekawa T. Analysis of the mechanism of the tight-junctional permeability increase by capsaicin treatment on the intestinal Caco-2 cells. *Cytotechnology* (2002). 40:93–98. doi: 10.1023/A:1023922306968

56. Wang Y, Cui L, Xu H, Liu S, Zhu F, Yan F, et al. TRPV1 agonism inhibits endothelial cell inflammation via activation of eNOS/NO pathway. *Atherosclerosis*. (2017) 260:13–9. doi: 10.1016/j.atherosclerosis.2017.03.016

57. Alhamoruni A, Wright K, Larvin M, O'Sullivan S. Cannabinoids mediate opposing effects on inflammation-induced intestinal permeability. *Br J Pharmacol*. (2012) 165:2598–610. doi: 10.1111/j.1476-5381.2011.01589.x

58. Dubreuil JD. Antibacterial and antidiarrheal activities of plant products against enterotoxinogenic Escherichia coli. *Toxins*. (2013) 5:2009–41. doi: 10.3390/toxins5112009

59. Brenes A, Viveros A, Chamorro S, Arija I. Use of polyphenol-rich grape by-products in monogastric nutrition. A review. *Anim Feed Sci Technol*. (2016) 211:1–17. doi: 10.1016/j.anifeedsci.2015.09.016

60. Hussain T, Tan B, Yin Y, Blachier F, Tossou MCB, Rahu N. Oxidative stress and inflammation: what polyphenols can do for us? *Oxidative Med Cell Longev*. (2016) 2016:1–9. doi: 10.1155/2016/7432797

61. Tang X, Xiong K, Fang R, Li M. Weaning stress and intestinal health of piglets: a review. *Front Immunol*. (2022) 13:42778. doi: 10.3389/fimmu.2022.1042778

62. Liang D, Li F, Fu Y, Cao Y, Song X, Wang T, et al. Thymol inhibits LPS-stimulated inflammatory response via down-regulation of NF-κB and MAPK signaling pathways in mouse mammary epithelial cells. *Inflammation*. (2014) 37:214–22. doi: 10.1007/s10753-013-9732-x

63. Kim C-S, Kawada T, Kim B-S, Han I-S, Choe S-Y, Kurata T, et al. Capsaicin exhibits anti-inflammatory property by inhibiting IkB-a degradation in LPS-stimulated peritoneal macrophages. *Cell Signal*. (2003) 15:299–306. doi: 10.1016/S0898-6568(02)00086-4

64. Surh YJ, Han Seoung Su, Keum YS, Seo HJ, Lee Sang Sup. *Inhibitory effects of curcumin and capsaicin on phorbol ester-induced activation of eukaryotic transcription factors, NF-κB and AP-1*. BioFactors. IOS Press (2000). 107–112

65. Nagoor Meeran MF, Javed H, Al TH, Azimullah S, Ojha SK. Pharmacological properties and molecular mechanisms of thymol: prospects for its therapeutic potential and pharmaceutical development. *Front Pharmacol*. (2017) 8:380. doi: 10.3389/fphar.2017.00380

66. Toschi A, Tugnoli B, Rossi B, Piva A, Grilli E. Thymol modulates the endocannabinoid system and gut chemosensing of weaning pigs. *BMC Vet Res*. (2020) 16:289. doi: 10.1186/s12917-020-02516-y

67. Xu H, Delling M, Jun JC, Clapham DE. Oregano, thyme and clove-derived flavors and skin sensitizers activate specific TRP channels. *Nat Neurosci*. (2006) 9:628–35. doi: 10.1038/nn1692

68. Kobayashi M, Watanabe K, Yokoyama S, Matsumoto C, Hirata M, Tominari T, et al. Capsaicin, a TRPV1 ligand, suppresses bone resorption by inhibiting the prostaglandin E production of osteoblasts, and attenuates the inflammatory bone loss induced by lipopolysaccharide. *ISRN Pharmacol*. (2012) 2012:1–6. doi: 10.5402/2012/439860

69. Schneeberger EE, Lynch RD. The tight junction: a multifunctional complex. *Am J Physiol Cell Physiol*. (2004) 286:1213–28. doi: 10.1152/ajpcell.00558.2003.-Multicellular

70. Capaldo CT, Nusrat A. Cytokine regulation of tight junctions. *Biochim Biophys Acta Biomembranes*. (2009) 1788:864–71. doi: 10.1016/j.bbamem.2008.08.027

71. Morgan MJ, Liu ZG. Crosstalk of reactive oxygen species and NF-κB signaling. *Cell Res*. (2011) 21:103–15. doi: 10.1038/cr.2010.178

72. Lingappan K. NF-κB in oxidative stress. *Curr Opin Toxicol*. (2018) 7:81–6. doi: 10.1016/j.cotox.2017.11.002

73. Kelley N, Jeltema D, Duan Y, He Y. The NLRP3 inflammasome: an overview of mechanisms of activation and regulation. *Int J Mol Sci*. (2019) 20:133328. doi: 10.3390/ijms20133328

74. Harijith A, Ebenezer DL, Natarajan V. Reactive oxygen species at the crossroads of inflammasome and inflammation. *Front Physiol*. (2014) 5:352. doi: 10.3389/fphys.2014.00352

75. Gessner DK, Fiesel A, Most E, Dinges J, Wen G, Ringseis R, et al. Supplementation of a grape seed and grape marc meal extract decreases activities of the oxidative stress-responsive transcription factors NF-κB and Nrf2 in the duodenal mucosa of pigs. *Acta Vet Scand*. (2013) 55:18. doi: 10.1186/1751-0147-55-18

76. Erlejman AG, Jaggers G, Fraga CG, Oteiza PI. TNFα-induced NF-κB activation and cell oxidant production are modulated by hexameric procyanidins in Caco-2 cells. *Arch Biochem Biophys*. (2008) 476:186–95. doi: 10.1016/j.abb.2008.01.024

77. Okumura R, Takeda K. Maintenance of intestinal homeostasis by mucosal barriers. *Inflamm Regen*. (2018) 38:5. doi: 10.1186/s41232-018-0063-z

78. Groschwitz KR, Hogan SP. Intestinal barrier function: molecular regulation and disease pathogenesis. *J Allergy Clin Immunol*. (2009) 124:3–20. doi: 10.1016/j.jaci.2009.05.038

79. Fairbrother JM, Nadeau É, Gyles CL. Escherichia coli in postweaning diarrhea in pigs: an update on bacterial types, pathogenesis, and prevention strategies. *Anim Health Res Rev*. (2005) 6:17–39. doi: 10.1079/AHR2005105

80. Andrews C, McLean MH, Durum SK. Cytokine tuning of intestinal epithelial function. *Front Immunol*. (2018) 9:1270. doi: 10.3389/fimmu.2018.01270

81. Blyth GAD, Connors L, Fodor C, Cobo ER. The network of colonic host defense peptides as an innate immune defense against enteropathogenic bacteria. *Front Immunol*. (2020) 11:965. doi: 10.3389/fimmu.2020.00965

82. Dubreuil JD. Enterotoxigenic Escherichia coli targeting intestinal epithelial tight junctions: an effective way to alter the barrier integrity. *Microb Pathog*. (2017) 113:129–34. doi: 10.1016/j.micpath.2017.10.037

83. Johnson AM, Kaushik RS, Hardwidge PR. Disruption of transepithelial resistance by enterotoxigenic Escherichia coli. *Vet Microbiol*. (2010) 141:115–9. doi: 10.1016/j.vetmic.2009.08.020

84. Ren J, Yan X, Ai H, Zhang Z, Huang X, Ouyang J, et al. Susceptibility towards enterotoxigenic Escherichia coli F4ac diarrhea is governed by the MUC13 gene in pigs. *PLoS One*. (2012) 7:e44573–11. doi: 10.1371/journal.pone.0044573

85. Zhang B, Ren J, Yan X, Huang X, Ji H, Peng Q, et al. Investigation of the porcine MUC13 gene: isolation, expression, polymorphisms and strong association with susceptibility to enterotoxigenic Escherichia coll F4ab/ac. *Anim Genet*. (2008) 39:258–66. doi: 10.1111/j.1365-2052.2008.01721.x

86. Sheng YH, Triyana S, Wang R, Das I, Gerloff K, Florin TH, et al. MUC1 and MUC13 differentially regulate epithelial inflammation in response to inflammatory and infectious stimuli. *Mucosal Immunol*. (2013) 6:557–68. doi: 10.1038/mi.2012.98

87. Dubreuil JD. Fruit extracts to control pathogenic *Escherichia coli*: a sweet solution. *Heliyon*. (2020) 6:e03410. doi: 10.1016/j.heliyon.2020.e03410

88. Füchtbauer S, Mousavi S, Bereswill S, Heimesaat MM. Antibacterial properties of capsaicin and its derivatives and their potential to fight antibiotic resistance – a literature survey. *Eur J Microbiol Immunol*. (2021) 11:10–7. doi: 10.1556/1886.2021.00003

89. Rappaport JA, Waldman SA. The guanylate cyclase C-cGMP signaling axis opposes intestinal epithelial injury and neoplasia. Front. *Oncologia*. (2018) 8:299. doi: 10.3389/fonc.2018.00299

90. Amarachintha S, Harmel-Laws E, Steinbrecher KA. Guanylate cyclase C reduces invasion of intestinal epithelial cells by bacterial pathogens. *Sci Rep*. (2018) 8:1521. doi: 10.1038/s41598-018-19868-z

frontiers | Frontiers in Veterinary Science

TYPE Original Research
PUBLISHED 03 November 2023
DOI 10.3389/fvets.2023.1140417

OPEN ACCESS

EDITED BY
Galileu Barbosa Costa,
United States Food and Drug Administration, United States

REVIEWED BY
Susan Hazel,
University of Adelaide, Australia
Benjamin Hart,
University of California, Davis, United States

*CORRESPONDENCE
Kiersten K. Forsyth
✉ kkforsyt@purdue.edu

RECEIVED 09 January 2023
ACCEPTED 16 October 2023
PUBLISHED 03 November 2023

CITATION
Forsyth KK, McCoy BM, Schmid SM, Promislow DEL, Snyder-Mackler N, the DAP Consortium and Creevy KE (2023) Lifetime prevalence of owner-reported medical conditions in the 25 most common dog breeds in the Dog Aging Project pack.
Front. Vet. Sci. 10:1140417.
doi: 10.3389/fvets.2023.1140417

Lifetime prevalence of owner-reported medical conditions in the 25 most common dog breeds in the Dog Aging Project pack

Kiersten K. Forsyth[1]*, Brianah M. McCoy[2], Sarah M. Schmid[3], Daniel E. L. Promislow[4,5], Noah Snyder-Mackler[2,6,7], the DAP Consortium and Kate E. Creevy[8]

[1]Department of Veterinary Clinical Sciences, College of Veterinary Medicine, Purdue University, West Lafayette, IN, United States, [2]School of Life Sciences, Arizona State University, Tempe, AZ, United States, [3]Department of Small Animal Clinical Sciences, College of Veterinary Medicine, University of Tennessee, Knoxville, TN, United States, [4]Department of Laboratory Medicine and Pathology, University of Washington School of Medicine, Seattle, WA, United States, [5]Department of Biology, University of Washington, Seattle, WA, United States, [6]Center for Evolution and Medicine, Arizona State University, Tempe, AZ, United States, [7]School for Human Evolution and Social Change, Arizona State University, Tempe, AZ, United States, [8]Department of Small Animal Clinical Sciences, College of Veterinary Medicine & Biomedical Sciences, Texas A&M University, College Station, TX, United States

Introduction: Large scale data on the prevalence of diverse medical conditions among dog breeds in the United States are sparse. This cross-sectional study sought to estimate the lifetime prevalence of medical conditions among US dogs and to determine whether purebred dogs have higher lifetime prevalence of specific medical conditions compared to mixed-breed dogs.

Methods: Using owner-reported survey data collected through the Dog Aging Project (DAP) Health and Life Experience Survey for 27,541 companion dogs, we identified the 10 most commonly reported medical conditions in each of the 25 most common dog breeds within the DAP cohort. Lifetime prevalence estimates of these medical conditions were compared between mixed-breed and purebred populations. The frequency of dogs for whom no medical conditions were reported was also assessed within each breed and the overall mixed-breed and purebred populations.

Results: A total of 53 medical conditions comprised the top 10 conditions for the 25 most popular breeds. The number of dogs for whom no medical conditions were reported was significantly different ($p = 0.002$) between purebred (22.3%) and mixed-breed dogs (20.7%). The medical conditions most frequently reported within the top 10 conditions across breeds were dental calculus (in 24 out of 25 breeds), dog bite (23/25), extracted teeth (21/25), osteoarthritis (15/25), and Giardia (15/25).

Discussion: Purebred dogs in the DAP did not show higher lifetime prevalence of medical conditions compared to mixed-breed dogs, and a higher proportion of purebred dogs than mixed-breed dogs had no owner-reported medical conditions. Individual breeds may still show higher lifetime prevalence for specific conditions.

KEYWORDS

lifetime prevalence, purebred, mixed-breed, epidemiology, cross-sectional

1. Introduction

The domestic dog (*Canis familiaris*) is a highly morphologically diverse species including various breeds developed over the past few hundred years resulting in dramatic phenotypic variations (20, 64). Humans have selected for specific phenotypic traits leading to the development of many pedigree dog breeds. There are currently 197 registered breeds with the American Kennel Club (AKC) and approximately 400 breeds recognized internationally (1). Inbreeding or line-breeding has been deployed in the development of most dog breeds, raising the concern that purebred dogs will have a greater chance of carrying genetic disorders (1, 12, 20). Inbreeding can lead to an increased prevalence of recessive genetic disorders, making what would normally be a rare disease more common within that breed or familial line (12, 20, 58); however, it can also lead to purging of the genetic load and associated elimination of inbreeding depression (10, 65). It is a common belief that purebred dogs are at a greater risk for disease compared to mixed-breed dogs, often due to concerns for genetic or inherited disorders; however, research has shown that this is not always the case. Some studies suggest specific breeds or groups of breeds are at greater risk for certain disorders, but simply being purebred may not necessarily be associated with increased disorder prevalence overall (43, 55).

The majority of studies evaluating breed predilections focus on either the breeds affected by a certain medical condition or the medical conditions most prevalent in a specific breed (32, 33, 37–39, 41, 42, 48, 60). For example, dilated cardiomyopathy has been determined to be far more common in Doberman Pinschers, Boxers, and Great Danes (32) than other dog breeds, whereas studies on the Cavalier King Charles Spaniel have found a high prevalence of cardiac, dermatological, and ocular disease (60). Comparatively, there are few studies that investigate the overall prevalence of disorders within and across breeds (21, 22, 66). Such studies are accomplished through either retrospective review of medical records or insurance data, or through health surveys completed by owners or veterinarians. Each of these methods of data acquisition have their own benefits and limitations.

Historically, prevalence data have been obtained via survey questionnaires distributed through breed clubs and associations; however, these surveys are often small-scale including only a few hundred to a few thousand dogs (12). With advancements in data sharing programs like VetCompass in the UK and Australia and the increased implementation of electronic medical record systems, large quantities of data can be collected and used to evaluate the demographic risk factors for various medical conditions (27, 33, 37–42, 44, 45, 50, 60). Pet insurance data has also been utilized to assess disease prevalence and mortality in the insured pet population (15). There are not currently any publicly accessible data sources like VetCompass in the US, making it difficult to perform a large-scale review of medical records to estimate prevalence of veterinary medical conditions in the US. Large-scale health surveys offer the chance to collect information from a more representative population, including those dogs who may not have seen a veterinarian within the timeframe of the study (66). The Dog Aging Project (DAP) is a nationwide community science research initiative; at its core is a long-term longitudinal study following companion dogs through annual surveys collecting biological, environmental, and lifestyle data.

This cross-sectional study aimed to estimate the lifetime prevalence of the most common owner-reported medical conditions (ORMC) for the top 25 breeds in the DAP, to identify differences in lifetime medical condition prevalence between the mixed-breed and purebred populations, and to identify differences in lifetime medical condition prevalence for the top 25 breeds when compared to other purebreds and to mixed-breed dogs. A secondary aim of this study was to determine whether or not there is a difference in prevalence of dogs with no ORMC between the purebred and mixed-breed populations.

2. Materials and methods

The DAP is a community science project in which owners enroll their companion dogs through a series of online surveys (8). The data collection instrument offered to all owners at the time of enrollment is a detailed Health and Life Experience Survey (HLES). All dogs whose owners complete HLES in its entirety become members of the DAP Pack for the duration of the study (or until the dog's death or the owner drops out of the study). The DAP is an open data initiative with HLES data becoming available for analysis in yearly releases. The methodology of the DAP, including survey distribution and data collection, has been detailed previously (8). The University of Washington IRB deemed that recruitment of dog owners for the Dog Aging Project, and the administration and content of the DAP Health and Life Experience Survey (HLES), are human subjects research that qualifies for Category 2 exempt status (IRB ID no. 5988, effective 10/30/2018). No interactions between researchers and privately owned dogs occurred; therefore, IACUC oversight was not required. This cross-sectional study was performed using data collected from 27,541 dogs enrolled in the DAP Pack between December 26, 2019 and December 31, 2020.

HLES consists of 10 topical sections including owner and dog demographics, health status, diet, behavior, physical activity, and environmental factors. The full HLES questionnaire is publicly available for review online (13). Data from the Dog Demographics section of HLES were used to identify the 25 most common AKC-recognized breeds within the DAP Pack and to calculate descriptive statistics for the various breed groups. Data from the Health Status section of HLES were used to identify the top 10 ORMC for each of those 25 most common breeds. Because these data are collected directly from owners and because all medical problems may not have been fully investigated, term lists in the Health Status section include specific diagnoses, syndromes, and clinical signs; here we use the term "medical conditions" to embrace all of these findings. Within the Health Status section, owners are asked to report all medical conditions their dogs have experienced. Respondents select medical conditions within pathophysiologic (e.g., "Cancer or tumors" or "Infectious or parasitic disease") and organ system [e.g., "Cardiac disorders" or "Kidney or urinary disorders" categories, and each category includes the option of "other (please describe)]." Free text responses recorded in these "other (please describe)" items were not included in the analysis of the medical conditions because this response choice does not represent a single medical condition and was therefore beyond the scope of this study. Free text categories for which the choice of "other (please describe)" would have ranked in the top 10 medical conditions for one or more of the 25 breeds include: other

trauma, other oral condition, other eye condition, other orthopedic condition, and other skin condition. These "other (please describe)" free text responses will be coded and analyzed in a future study, and coded results will be made available in future data releases. For purposes of the study reported here, we do not attempt to refine, combine or otherwise modify participant responses, and present the data as reported by the participant. For instance, while it is plausible that a dog with "intervertebral disc disease" or "fibrocartilagenous embolism" also had "limb paralysis," and vice versa, we report precisely what the participant indicated, without assuming that other related conditions were present.

2.1. Statistical analysis

Statistical analysis was performed using R software (version 4.1.1, R Foundation for Statistical Computing, Vienna, Austria). Dogs were separated into groups of mixed-breed dogs or purebred dogs based on owner-reported breed classification, which has been shown to be reliable (35). Here, we focused on the 25 most common AKC-recognized breeds within the DAP Pack. Descriptive statistics for dogs in each of the breeds were calculated including median age and median weight at the time survey data were collected. On average, small dogs live longer than large dogs, and often by a substantial margin. For this reason, simple chronological age is insufficient to describe the life stage (e.g., juvenile to adult to senior) in dogs of various sizes (18). Using the AAHA Canine Life Stage Guidelines (9), and the authors' prior work on companion dog lifespan (62), average lifespan estimates were generated for groups of dog sizes in 10-kg increments, and life stages were assigned within size categories, as shown in Table 1. All dogs were assigned to a specific life stage based on age and body size. The mean and median life stage was determined for each of the 25 breeds and the mixed-breed category.

Within each of the 25 breeds, we calculated the lifetime prevalence of the 10 most commonly reported ORMC and generated 95% confidence intervals using the Wilson method. Lifetime prevalence estimates for these medical conditions were also calculated for all purebred, and all mixed-breed dogs, respectively, within the DAP Pack. We used a binomial model with logit link and adjusting for age with a linear effect to test: (1) whether mixed-breed and purebred dogs differed in lifetime medical condition prevalence and then (2) whether specific breeds exhibited statistically higher (or lower) lifetime prevalence of a given medical condition compared to all other purebred dogs in the dataset. The result of these models were age-adjusted log-odds ratios of medical conditions prevalence for a given breed compared to all other purebred dogs (or a comparison of mixed vs. purebred dogs). In the case where multiple statistical comparisons were carried out, we adjusted the threshold for significance using the Bonferroni correction. With 53 unique medical conditions (see below), this led to an adjusted significance threshold of $p \leq 0.05/53 = 0.00095$ (e.g., Tables 2–5). When comparing the lifetime prevalence of dogs with no owner-reported medical conditions between the 25 breeds and mixed-breed dogs, this led to an adjusted significance threshold of $p \leq 0.05/25 = 0.002$ (e.g., Table 6).

TABLE 1 Life stages by dog size.

Size	Puppy	Young adult	Mature adult	Senior
<10 kg	0–0.75 yr	> 0.75–3 yr	> 3–12 yr	> 12 yr
10–19.9 kg	0–0.75 yr	> 0.75–3 yr	> 3–12 yr	> 12 yr
20–29.9 kg	0–0.75 yr	> 0.75–3 yr	> 3–11 yr	> 11 yr
30–39.9 kg	0–1 yr	> 1.0–3 yr	> 3–10.5 yr	> 10.5 yr
≥ 40 kg	0–1.5 yr	> 1.5–3 yr	> 3–9.5 yr	> 9.5 yr

3. Results

Data from 27,541 companion dogs were included in the study. Of those dogs, 50.6% were mixed-breed dogs ($n = 13{,}923$) and 49.4% were purebred dogs ($n = 13{,}618$). Of the purebred dogs, the 25 most commonly represented breeds are included in Table 7. These 25 breeds ($n = 8{,}438$) make up 62.0% of the purebred dog population and 30.6% of the overall DAP Pack. The remaining 38.0% of purebred dogs included members of 258 breeds. Demographic data describing these breed groups is summarized in Table 7. Both the mean and median life stage for all 25 breeds and the mixed-breed category fell into the mature adult life stage. The distribution of life stages within individual breeds was similar across the 25 breeds.

A total of 53 unique medical conditions were identified making up the top 10 ORMC for these 25 breeds. The top 10 ORMC in mixed-breed dogs were a subset of these 53 medical conditions. The ORMC reported most frequently across breeds were dental calculus, dog bites, extracted teeth, osteoarthritis, and *Giardia* (Figure 1). Data on all 53 medical conditions and their lifetime prevalence in individual breeds are available in Supplementary Table 1. Data on the top 10 ORMC and their lifetime prevalence in individual breeds are available as Supplementary Table 2. A Heatmap (Figure 2) demonstrates the scaled prevalence of these 53 medical conditions across the 25 most popular dog breeds in the DAP Pack.

3.1. Dogs with no reported medical conditions

Purebred dogs (22.3%) were significantly more likely ($p = 0.002$) to have no ORMC than mixed-breed dogs (20.7%). Considering each breed compared to the population of mixed-breed dogs, significantly more Golden Retrievers (25.1%; $p = 1.16 \times 10^{-4}$), Poodles (26.9%; $p = 0.001$), Australian Shepherds (29.2%; $p = 2.3 \times 10^{-5}$), Border Collies (31.5%; $p = 5.84 \times 10^{-6}$), and Siberian Huskies (34.8%; $p = 1.53 \times 10^{-5}$) had no ORMC compared to mixed-breed dogs (Table 6). Conversely, the frequency of Greyhounds with no ORMC was significantly lower (8.8%; $p = 2.15 \times 10^{-4}$) than mixed-breed dogs.

3.2. Overall purebred vs. mixed-breed results

A total of 14 ORMC were significantly more prevalent in the overall purebred dog population compared to the overall mixed-breed dog population, and similarly, 13 ORMC were significantly more prevalent in mixed-breed dogs compared to purebred dogs (Table 2). The remaining 26 ORMC were not significantly different between the mixed-breed and purebred dog populations. The most common

TABLE 2 Lifetime prevalence of 53 medical conditions in the purebred and mixed-breed dog populations.

	N (mixed-breed/ purebred)	Mixed-breed Prevalence (%; *n* = 13,923)	Purebred Prevalence (%; *n* = 13,618)	*p*-value
No ORMC	2888/3031	20.74	22.26	**0.002**
Dental calculus	2089/2011	15.00	14.77	0.058
Extracted teeth	1877/810	13.48	5.95	$\mathbf{1.66 \times 10^{-98}}$
Dog bite	1663/1305	11.94	9.58	$\mathbf{2.64 \times 10^{-10}}$
Fractured teeth	997/810	7.16	5.95	$\mathbf{4.82 \times 10^{-5}}$
Seasonal allergies	994/884	7.14	6.49	**0.033**
Giardia	952/1006	6.84	7.39	0.076
Osteoarthritis	908/869	6.52	6.38	0.636
Ear infection	860/1138	6.18	8.36	$\mathbf{3.11 \times 10^{-12}}$
Torn or broken toenail	788/658	5.66	4.83	**0.002**
Chocolate ingestion	746/546	5.36	4.01	$\mathbf{1.21 \times 10^{-7}}$
Bordatella and/or *parainfluenza*	719/558	5.16	4.10	$\mathbf{2.57 \times 10^{-5}}$
Heart murmur	647/709	4.65	5.21	**0.032**
Pruritis	641/523	4.60	3.84	**0.002**
Laceration	540/433	3.88	3.18	**0.002**
Cruciate ligament rupture	535/447	3.84	3.28	**0.012**
Cataracts	527/626	3.79	4.60	$\mathbf{7.71 \times 10^{-4}}$
Fleas	485/325	3.48	2.39	$\mathbf{7.17 \times 10^{-8}}$
Sebaceous cysts	460/482	3.30	3.54	0.282
Food or medicine allergies that affect the skin	415/427	2.98	3.14	0.455
Gingivitis	414/475	2.97	3.49	**0.016**
Roundworms	412/366	2.96	2.69	0.174
Conjunctivitis	390/369	2.80	2.71	0.643
Hookworms	388/319	2.79	2.34	**0.020**
Chronic/recurrent hot spots	386/442	2.77	3.25	**0.022**
Lyme disease	377/333	2.71	2.45	0.169
Chronic/recurrent diarrhea	375/411	2.69	3.02	0.106
Patellar luxation	372/321	2.67	2.36	0.096
Anal sac impaction	353/367	2.54	2.69	0.407
Urinary tract infection (chronic/ recurrent)	346/466	2.49	3.42	$\mathbf{4.32 \times 10^{-6}}$
GI foreign body	329/357	2.36	2.62	0.169
Food or medicine allergies	309/337	2.22	2.47	0.162
Hip dysplasia	307/333	2.20	2.45	0.186
Hearing loss (incompletely deaf)	306/347	2.20	2.55	0.056
Urinary incontinence	303/332	2.18	2.44	0.148
Seizures	283/323	2.03	2.37	0.055
Pancreatitis	263/324	1.89	2.38	**0.005**
Underbite	252/115	1.81	0.84	$\mathbf{2.82 \times 10^{-12}}$
Hypothyroidism	245/275	1.76	2.02	0.113
Lameness (chronic/recurrent)	240/240	1.72	1.76	0.807
Deafness	223/249	1.60	1.83	0.147

(Continued)

TABLE 2 (Continued)

	N (mixed-breed/ purebred)	Mixed-breed Prevalence (%; *n* = 13,923)	Purebred Prevalence (%; *n* = 13,618)	*p*-value
Urinary crystals or stones in bladder or urethra	194/228	1.39	1.67	0.058
Coccidia	184/254	1.32	1.87	$\mathbf{3.12\times10^{-4}}$
Anaplasmosis	151/150	1.08	1.10	0.892
Fractured bone (limb)	146/170	1.05	1.25	0.120
Lick granuloma	144/142	1.03	1.04	0.945
Corneal ulcer	113/208	0.81	1.53	$\mathbf{3.14\times10^{-8}}$
Intervertebral disc disease (IVDD)	112/206	0.80	1.51	$\mathbf{3.78\times10^{-8}}$
Chronic kidney disease	109/105	0.78	0.77	0.911
Retained deciduous teeth	96/148	0.69	1.09	$\mathbf{4.35\times10^{-4}}$
Keratoconjunctivitis sicca (KCS)	85/206	0.61	1.51	$\mathbf{2.46\times10^{-13}}$
Tracheal collapse	76/93	0.55	0.68	0.145
Entropion	41/132	0.29	0.97	$\mathbf{1.37\times10^{-12}}$
Stenotic/narrow nares	5/50	0.04	0.37	$\mathbf{7.44\times10^{-10}}$

The bold values included in the tables are the *p*-values that are statistically significant.

ORMC in mixed-breed dogs were dental calculus, extracted teeth, dog bite, seasonal allergies, fractured teeth, giardia, osteoarthritis, ear infection, torn or broken toenail, and chocolate toxicity (Table 2).

3.3. Breed specific results

Data on the eight of the most popular breeds are described in detail here; data for the remaining 17 breeds in the top 25 are available in Supplementary Table 2. Additional information including the lifetime prevalence of the other ORMC within the union set of 53 medical conditions that did not rank in the top 10 ORMC within each breed are available in Supplementary Table 1. The top ORMC in Labrador Retrievers were ear infections, dog bites, osteoarthritis, *Giardia*, dental calculus, seasonal allergies, fractured teeth, cruciate ligament rupture, extracted teeth, and *Bordetella* and/or parainfluenza (Table 3). Labrador Retrievers were significantly more likely to be reported to have had ear infections (logOR = 0.66, $p = 1.33\times10^{-16}$), osteoarthritis (logOR = 0.55, $p = 7.42\times10^{-8}$), and cruciate ligament rupture (logOR = 1.03, $p = 8.54\times10^{-20}$) compared to other purebred dogs. Labrador Retrievers were significantly less likely to be reported to have dental calculus (logOR = −0.85, $p = 2.99\times10^{-17}$) and extracted teeth (logOR = −0.99, $p = 9.64\times10^{-20}$) compared to other purebred dogs.

TABLE 3 Lifetime prevalence of the top 10 medical conditions in Labrador Retrievers compared to the total purebred population.

Medical condition	Number affected	Lifetime Prevalence (%)	95% CI (%)	*p*-value
Ear Infection	226	13.51	11.95–15.23	$\mathbf{1.33\times10^{-16}}$
Dog bite	159	9.50	8.19–11.00	0.836
Osteoarthritis	138	8.25	7.02–9.66	$\mathbf{7.42\times10^{-8}}$
Giardia	126	7.53	6.36–8.90	0.912
Dental calculus	120	7.17	6.03–8.51	$\mathbf{2.99\times10^{-17}}$
Seasonal allergies	120	7.17	6.03–8.51	0.170
Fractured teeth	119	7.11	5.98–8.45	0.006
Cruciate ligament rupture	115	6.87	5.76–8.19	$\mathbf{8.54\times10^{-20}}$
Extracted teeth	102	6.10	5.05–7.35	$\mathbf{9.64\times10^{-20}}$
Bordetella and/or parainfluenza ("kennel cough")	91	5.44	4.45–6.63	0.004

The bold values included in the tables are the *p*-values that are statistically significant.

The top ORMC in Golden Retrievers were ear infections, *Giardia*, chronic/recurrent hot spots, dental calculus, seasonal allergies, dog bites, osteoarthritis, *Bordetella* and/or parainfluenza, fractured teeth, and pruritis (Table 4). Golden Retrievers were significantly more likely to be reported to have ear infections (logOR = 0.56, $p = 1.19\times10^{-10}$) and chronic/ recurrent hot spots (logOR = 1.28, $p = 3.67\times10^{-29}$) compared to the overall purebred population. Golden Retrievers were significantly less likely to be reported to have dental calculus (logOR = −0.68,$p = 2.68\times10^{-10}$) compared to other purebred dogs.

The top ORMC in German Shepherd Dogs were seasonal allergies, ear infections, *Giardia*, dog bites, hip dysplasia, osteoarthritis, fractured teeth, pruritis, sebaceous cysts, and torn or broken toenails (Table 5). German Shepherd Dogs were significantly more likely to be reported to have hip dysplasia (logOR = 1.48, $p = 9.76\times10^{-19}$) and seasonal allergies (logOR = 0.61, $p = 9.95\times10^{-6}$) than other purebred dogs. The lifetime prevalence of the remaining eight ORMC in German Shepherd Dogs were not significantly different compared to other purebred dogs.

Compared to the overall purebred population, the lifetime prevalence of the top 10 ORMC in Australian Shepherds, Australian Cattle Dogs, Boxers, and Siberian Huskies were not significantly different from other purebred dogs (Supplementary Table 1). Both

TABLE 4 Lifetime prevalence of the top 10 medical conditions in Golden Retrievers compared to the total purebred population.

Medical condition	Number affected	Lifetime Prevalence (%)	95% CI (%)	*p*-value
Ear Infection	179	12.23	10.65–14.00	$\mathbf{1.19 \times 10^{-10}}$
Giardia	120	8.20	6.90–9.71	0.578
Chronic or recurrent hot spots	115	7.86	6.58–9.35	$\mathbf{3.67 \times 10^{-29}}$
Dental calculus	103	7.04	5.83–8.46	$\mathbf{2.68 \times 10^{-10}}$
Seasonal allergies	91	6.22	5.09–7.57	0.942
Dog bite	91	6.22	5.09–7.57	1.80×10^{4}
Osteoarthritis	78	5.33	4.29–6.60	0.147
Bordetella and/or parainfluenza ("kennel cough")	72	4.92	5.76–8.19	0.126
Fractured teeth	57	3.89	3.02–5.01	0.022
Pruritis (itchy skin)	57	3.89	3.02–5.01	0.640

The bold values included in the tables are the *p*-values that are statistically significant.

Australian Shepherds and Siberian Huskies were also found to have a significantly higher percentage of dogs with no ORMC than the mixed-breed population (Table 6).

Four of the 10 most commonly reported ORMC in Chihuahuas involved dental conditions: extracted teeth, dental calculus, gingivitis, and retained deciduous teeth (Supplementary Table 2). Specifically, 47.60% (41.22–54.05%) of Chihuahuas were reported to have had teeth extracted and 33.62% (27.82–39.97%) had dental calculus reported. This is significantly more frequently than either of those ORMC were reported in the purebred population ($p = 6.12 \times 10^{-22}$ and $p = 4.52 \times 10^{-6}$, respectively).

TABLE 5 Lifetime prevalence of the top 10 medical conditions in German Shepherd Dogs compared to the total purebred population.

Medical condition	Number affected	Lifetime Prevalence (%)	95% CI (%)	*p*-value
Seasonal allergies	63	10.36	8.18–13.04	$\mathbf{9.95 \times 10^{-6}}$
Ear Infection	55	9.05	7.02–11.59	0.246
Giardia	53	8.72	6.73–11.23	0.421
Dog bite	51	8.39	6.44–10.86	0.783
Hip dysplasia	46	7.57	5.72–9.94	$\mathbf{9.76 \times 10^{-19}}$
Osteoarthritis	43	7.07	5.29–9.39	5.95×10^{-5}
Fractured teeth	39	6.41	4.73–8.65	0.085
Pruritis (itchy skin)	34	5.59	4.03–7.71	0.009
Sebaceous cysts	33	5.43	3.89–7.52	3.96×10^{-5}
Torn or broken toenail	32	5.26	3.75–7.34	0.330

The bold values included in the tables are the *p*-values that are statistically significant.

4. Discussion

The primary objective of this study was to describe the medical conditions most commonly reported by owners of the most popular breeds in the DAP Pack. Although there was the potential for 250 unique ORMC when looking at the 10 most common conditions for each of the 25 breeds, only 53 ORMC were identified. While the majority of these ORMC only placed in the top 10 for one or two of the 25 breeds, 10 of the ORMC were identified as highly common among at least 10 of the 25 breeds.

Dental calculus was among the top 10 ORMC in 24 of the 25 breeds, and extracted teeth were among the top 10 ORMC in 21 of the 25 breeds. This shows that dental conditions and dental care are relatively common across breeds in the US. Although dental conditions are seen across breeds, certain breeds are impacted more greatly, like Chihuahuas, for whom owners reported dental calculus in approximately one-third of breed members in the DAP Pack and extracted teeth in nearly half the breed members. O'Neill and others reported a 19% prevalence of dental disease among the Chihuahua population in the UK (41); it is possible that the difference is attributable to the fact that their study was a period prevalence estimate for the year 2016, whereas our study considers lifetime prevalence. A 1999 study demonstrated a prevalence of dental calculus at 20.5% as reported by veterinarians for dogs attending private small animal practices in the US (30). This is a higher rate of dental calculus for dogs overall than was noted in our study. This difference may be due to changes in prevalence and improved dental care and prophylaxis over the past 20 years, or may be due to a difference between veterinarian-reported and owner-reported information. Additional studies have shown that dental disorders are one of the most common medical conditions amongst various breeds in the UK (40, 45) and US (17), and dental conditions are a priority area of interest for future health-related welfare improvement in the UK dog population (59), particularly considering that regular veterinary dental scaling is associated with longer lifespan in dogs (63).

Interestingly, dog bite injuries were the second most common ORMC reported across breeds, identified in 23 of the top 25 breeds in the DAP Pack. Most prevalence data for dog bite injuries report on humans being bitten, with scarce data on dogs being bitten by other dogs (5, 23, 29, 49, 61). As a result, there are no recent prevalence data for dog-on-dog bite injuries in the US. The 23 affected breeds included dogs of all body sizes, from toy and small breeds to large and giant breed dogs. While owners and veterinarians may have concern that small dogs may be bitten by larger dogs, this study shows that bite injuries are quite common regardless of size. This highlights the

TABLE 6 Lifetime prevalence of dogs with no owner-reported medical conditions (ORMC) in the total purebred dog population and the 25 most popular individual breeds compared to the mixed-breed dog population.

	No ORMC (*N*)	No ORMC (%)	95% CI	*p*-value
Purebred Dogs (all)	3,031	22.26%	21.57–22.96%	**0.002**
Mixed-Breed Dogs	2,888	20.74%	20.08–21.42%	
Labrador Retriever	378	22.59%	20.65–24.66%	0.079
Golden Retriever	367	25.07%	22.92–27.35%	$\mathbf{1.16\times10^{-4}}$
German Shepherd Dog	150	24.67%	21.41–28.25%	0.020
Poodle	125	26.88%	23.05–31.09%	**0.001**
Australian Shepherd	126	29.17%	25.08–33.62%	$\mathbf{2.30\times10^{-5}}$
Dachshund	72	21.11%	17.12–25.76%	0.867
Border Collie	94	31.54%	26.53–37.03%	$\mathbf{5.84\times10^{-6}}$
Chihuahua	39	17.03%	12.72–22.43%	0.169
Beagle	41	19.90%	15.02–25.88%	0.768
Pembroke Welsh Corgi	53	26.50%	20.87–33.02%	0.047
Boxer	42	21.21%	16.09–27.43%	0.871
Shih Tzu	29	15.03%	10.67–20.75%	0.051
Miniature Schnauzer	39	20.31%	15.23–26.56%	0.884
Pug	30	15.96%	11.41–21.87%	0.108
Havanese	32	17.78%	12.88–24.02%	0.329
Cavalier King Charles Spaniel	41	24.12%	18.30–31.07%	0.281
Yorkshire Terrier	30	17.75%	12.73–24.21%	0.340
Great Dane	42	25.77%	19.67–32.98%	0.116
Greyhound	14	8.81%	5.32–14.24%	$\mathbf{2.15\times10^{-4}}$
Boston Terrier	37	23.27%	17.38–30.42%	0.435
Siberian Husky	55	34.81%	27.82–42.52%	$\mathbf{1.53\times10^{-5}}$
Shetland Sheepdog	33	21.43%	15.68–28.56%	0.835
English Springer Spaniel	35	23.33%	17.28–30.72%	0.437
Australian Cattle Dog	28	19.31%	13.71–26.49%	0.672
Doberman Pinscher	40	27.78%	21.11–35.60%	0.039

The bold values included in the tables are the *p*-values that are statistically significant.

importance of client education along with training and early socialization of dogs, to try to reduce the incidence of bite wounds in the future. Owner-reported dog bite injuries were more common in our study than previously reported in other studies (30); in fact, most prior studies did not even include dog bite injuries or animal bite injuries specifically in their analyses (17, 27, 33, 37–42, 45, 60, 66). It may be that dog bite injuries are being included in more broad categories such as trauma in other studies. Alternatively, it is possible that dog bite injuries are being overlooked in breed-related disease prevalence studies, as trauma of any kind may not be considered a form of disease. The study reported here described individual medical conditions, rather than overarching categories such as "trauma." Within the category of trauma, conditions that occurred within the top 10 most frequent ORMC for any of the top 25 breeds were dog bite wound, torn or broken toenail, laceration and fractured bone. Other factors, such as lifestyle and environment, likely contribute to risk of medical conditions among dogs, and perhaps more significantly for traumatic conditions. However, it is likely that breed remains a significant risk factor for some traumatic conditions. For instance, certain breeds may be inherently more active, or may be disproportionately chosen by owners for active lifestyles; in either case, breed and environment could interact to increase the risk of traumatic injury. Future studies can further investigate these interrelationships.

The secondary objective of this study was to investigate whether or not there is a difference between purebred or mixed-breed dogs in lifetime prevalence of ORMC, or dogs with no ORMC. This study showed that the lifetime prevalence of dogs with no ORMC was higher in the purebred population (22.3%) compared to the mixed-breed population (20.7%) in the DAP Pack. This is contrary to the common belief that purebred dogs have a greater risk for developing medical conditions due to breed predispositions. This is also a higher proportion of dogs with no medical conditions than the 6.8% reported in the previously mentioned study which used veterinarian-reported data from small animal practices (30). It is possible that the difference between the two studies' findings reflects the fact that, despite the survey instructions to report all known medical conditions, owners may not recall or choose to report all of their dogs' medical conditions in the survey-based data used here. Alternatively, it is possible that the DAP Pack captures data from dogs from a general population of healthy dogs who do not require or receive veterinary care and therefore are not represented in manuscripts reporting only data derived from veterinary practice records. This intriguing possibility merits further investigation by determining the frequency of veterinary visits among DAP Pack members, and by comparing owner-reported data to data captured in medical records; such analyses are currently underway by the DAP. Although the difference between dogs with no ORMC in the purebred and mixed-breed populations was statistically significant, the difference was only 1.5%. The mixed-breed population had a significantly higher lifetime prevalence than the purebred population for 13 of the 53 ORMC described here; similarly, the purebred population had a significantly higher lifetime prevalence than the mixed-breed population for 14 of the 53 ORMC as well. Additionally, our study revealed that certain breeds were shown to have a higher lifetime prevalence of specific medical conditions. Overall, 23 of the 25 breeds evaluated showed a significantly increased lifetime prevalence of at least one ORMC when compared to other purebred dogs. Of the breeds evaluated, only the Australian Shepherd, Australian Cattle Dog, Boxer, and Siberian Husky showed no significant difference in lifetime prevalence for their 10 most commonly reported medical conditions when compared to other purebred dogs. Even when evaluating for lifetime prevalence in all 53 of the included ORMC, there was no significant difference in

10.3389/fvets.2023.1140417

TABLE 7 Descriptive data for the DAP Pack including mixed-breed dogs, purebred dogs, and the 25 most popular individual breeds.

	Number of dogs	Age [years, mean (range)]	Life stage (mean)	Weight [kg, mean (range)]	Neutered Male [*n* (%)]	Intact Male [*n* (%)]	Spayed Female [*n* (%)]	Intact Female [*n* (%)]
Mixed-Breed Dogs	13,923	7.2 (0.1–24.8)	Mature adult	21.6 (<0.1–90.9)	6,593 (47.4)	222 (1.59)	6,982 (50.1)	162 (1.16)
Purebred Dogs (total)	13,618	7.4 (0.1–25.5)	Mature adult	24.0 (0.3–104.5)	5,852 (43.0)	1,147 (8.42)	5,991 (44.0)	628 (4.61)
Labrador Retriever	1,673	8.1 (0.2–24.8)	Mature adult	33.7 (4.2–59.1)	687 (41.1)	127 (7.59)	794 (47.5)	65 (3.89)
Golden Retriever	1,464	6.1 (0.3–19.4)	Mature adult	32.3 (7.0–57.7)	604 (41.3)	167 (11.41)	607 (41.5)	86 (5.87)
German Shepherd Dog	608	6.0 (0.3–19.4)	Mature adult	36.9 (14.7–67.3)	214 (35.2)	67 (11.02)	296 (48.7)	31 (5.1)
Poodle	465	7.2 (0.3–19.0)	Mature adult	20.1 (2.4–44.1)	230 (49.5)	38 (8.17)	183 (39.4)	14 (3.01)
Australian Shepherd	432	6.6 (0.2–17.7)	Mature adult	21.3 (3.2–44.1)	199 (46.1)	33 (7.64)	177 (41.0)	23 (5.32)
Dachshund	341	9.1 (0.2–20.8)	Mature adult	6.8 (1.8–18.2)	157 (46.0)	22 (6.45)	158 (46.3)	4 (1.17)
Border Collie	298	7.3 (0.3–17.0)	Mature adult	19.6 (10.6–42.7)	114 (38.3)	21 (7.05)	145 (48.7)	18 (6.04)
Chihuahua	229	9.7 (0.3–22.3)	Mature adult	3.7 (0.9–10.9)	109 (47.6)	5 (2.18)	104 (45.4)	11 (4.80)
Beagle	206	8.9 (0.6–21.0)	Mature adult	13.2 (6.4–25.0)	92 (44.7)	6 (2.91)	102 (49.5)	6 (2.91)
Pembroke Welsh Corgi	200	6.1 (0.3–20.3)	Mature adult	13.1 (4.5–21.4)	91 (45.5)	9 (4.50)	91 (45.5)	9 (4.5)
Boxer	198	6.3 (0.5–20.8)	Mature adult	29.2 (16.8–44.5)	89 (44.9)	11 (5.56)	90 (45.5)	8 (4.04)
Shih Tzu	193	9.4 (0.3–18.0)	Mature adult	6.5 (2.3–14.5)	106 (54.9)	11 (5.70)	73 (37.8)	3 (1.55)
Miniature Schnauzer	192	7.9 (0.3–17.8)	Mature adult	8.0 (3.0–15.5)	85 (44.3)	9 (4.69)	95 (49.5)	3 (1.56)
Pug	188	8.8 (0.3–17.3)	Mature adult	9.5 (4.7–17.3)	93 (49.5)	1 (0.53)	90 (47.9)	4 (2.13)
Havanese	180	7.7 (0.4–19.2)	Mature adult	6.6 (2.7–13.6)	92 (52.4)	5 (2.78)	78 (43.3)	5 (2.78)
Cavalier King Charles Spaniel	170	7.1 (0.3–14.9)	Mature adult	9.1 (2.7–17.7)	89 (52.4)	7 (4.12)	70 (41.2)	4 (2.35)
Yorkshire Terrier	169	9.4 (0.9–22.0)	Mature adult	3.9 (1.4–9.8)	80 (47.3)	4 (2.37)	82 (48.5)	3 (1.78)
Great Dane	163	5.1 (0.3–12.2)	Mature adult	59.6 (22.7–88.6)	55 (33.7)	21 (12.88)	79 (48.5)	8 (4.91)
Greyhound	159	7.5 (1.8–14.2)	Mature adult	31.8 (21.4–45.5)	78 (49.1)	2 (1.26)	77 (48.4)	2 (1.26)
Boston Terrier	159	7.2 (0.1–16.0)	Mature adult	9.9 (2.3–20.0)	70 (44.0)	7 (4.40)	75 (47.2)	7 (4.4)
Siberian Husky	158	7.2 (0.7–19.3)	Mature adult	25.4 (13.2–45.9)	65 (41.1)	7 (4.43)	80 (50.6)	6 (3.8)
Shetland Sheepdog	154	8.0 (0.5–19.0)	Mature adult	12.0 (5.5–22.7)	81 (52.6)	11 (7.14)	58 (37.7)	4 (2.6)
English Springer Spaniel	150	7.6 (0.4–16.7)	Mature adult	21.1 (10.5–35.5)	52 (34.7)	4 (2.67)	85 (56.7)	9 (6.0)
Australian Cattle Dog	145	7.4 (0.3–18.5)	Mature adult	21.2 (11.8–33.6)	64 (44.1)	5 (3.45)	71 (49.0)	5 (3.45)
Doberman Pinscher	144	6.1 (0.4–13.6)	Mature adult	34.5 (5.0–54.5)	55 (38.2)	15 (10.42)	67 (46.5)	7 (4.86)

lifetime prevalence for the Australian Cattle Dog and Siberian Husky compared to other purebred dogs (Supplementary Table 1). Similarly, the Australian Shepherd and Siberian Husky were the breeds with the highest frequency of dogs with no ORMC in our study and significantly more dogs from these breeds had no ORMC compared to the mixed-breed population. Because the data utilized in this study are owner-reported and individual medical records associated with each dog were not evaluated as part of this study, we are unable to determine the severity of the ORMC or how that severity might vary between breeds. Future studies of severity of disease among breeds,

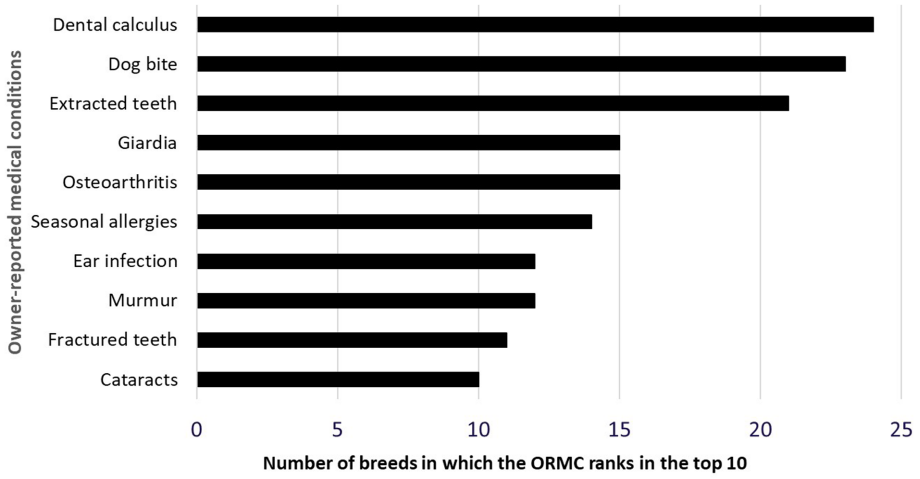

FIGURE 1
Medical conditions which rank in the top 10 medical conditions in at least 10 of the 25 most popular individual dog breeds in the DAP Pack.

and response to therapies deployed, are important targets of this research.

The most common breeds and ORMC seen in the DAP Pack are likely to be representative of the United States canine population. Most previous studies evaluating dogs within the US have been performed at veterinary referral centers (6, 16, 54) or within a single large private-practice chain (44, 50, 55). This creates a bias as these studies do not include dogs whose owners are unable to or elect not to pursue veterinary specialty referral (3), or target only a particular consumer group who may not be representative of the overall population. Because the dogs within the DAP Pack are recruited directly from owners, not through veterinarians or veterinary clinics, there is the possibility to include dogs who are evaluated by veterinarians less frequently, who are never seen at veterinary referral centers, and potentially those who have never seen a veterinarian at all. Any owner within the US can sign up at any time. While there is currently a trend towards older dogs and older owners within the DAP Pack, the DAP is actively recruiting for dogs of all ages and owners from more varying backgrounds. There is also a trend towards dogs which have been neutered within the DAP Pack. Because the majority of dogs within the DAP Pack are neutered, sex, neuter status, and age of neutering have not been assessed within this study. This is a limitation of this study, as these factors can influence medical conditions (21, 22).

The top 25 breeds making up the DAP Pack vary somewhat when compared to the top 25 breeds according to AKC registration numbers for 2020. Border Collie, Chihuahua, Pug, Greyhound, Shetland Sheepdog, and English Springer Spaniel all ranked higher in the DAP Pack than they did in AKC registration, as they were not even included in the AKC top 25 breeds (2). These differences between the reported AKC numbers and DAP Pack numbers are likely due to the fact that there are many purebred dogs in the US that are never registered with the AKC. Greyhounds are an excellent example of this as many of the Greyhounds in the DAP Pack are retired racing dogs, which are often registered with the National Greyhound Association instead of the AKC (36). It is also possible that this is the reason our study found significantly fewer greyhounds with no ORMC, as many racing greyhounds are retired due to injuries. However, despite these differences there are also similarities between popular DAP Pack and AKC breeds, such as the top 3 breeds in the DAP Pack ranking within the top 4 breeds in the AKC (2). This study classified all mixed-breed dogs as part of the mixed-breed population, including new "designer breeds" such as goldendoodles or cockapoos. While designer breeds are actually F1 hybrids and not purebred dog breeds, many are becoming popular within the United States. As a result, performing a similar study evaluating F1 hybrids as a third breed-background group could provide useful information for practicing veterinarians in the United States.

One of the main limitations of this study is that the data were collected through owner-reported survey results, meaning there is an inherent risk of recall bias and reporting bias affecting results. This may be because of lack of understanding of one or more conditions, lack of recollection of one or more condition and/or lack of comprehensive diagnostic investigation of one or more conditions. With these limitations in mind, our survey was intentionally designed to include clinical signs, as well as discrete diagnoses, among the options presented to participants. Additionally, data were intentionally analyzed as reported, and no attempt was made to interpret responses as components of a larger disease syndrome, or to assume the presence of common comorbidities. No previous large studies have been performed analyzing the accuracy of owner-reported medical data in veterinary medicine. Further research comparing owner-reported survey data to veterinary medical records is needed. Studies in human pediatrics show reasonable accuracy in parental recall of children's health information, with greater accuracy for acute and significant health events (4, 11, 14, 19, 24, 34, 51–53, 57). Assuming that dog owners will have similar recall accuracy and biases as parents completing surveys about their children's health, it is reasonable to assume that owner-reported surveys will be relatively accurate to their dog's medical conditions with a potential bias towards recalling medical conditions which owners regard as more significant. As a result, this study may highlight those medical conditions that owners most recall or are most concerned about for their dogs. This means that there may be an underrepresentation of medical conditions that owners do not find concerning, or a lack of recognition of all

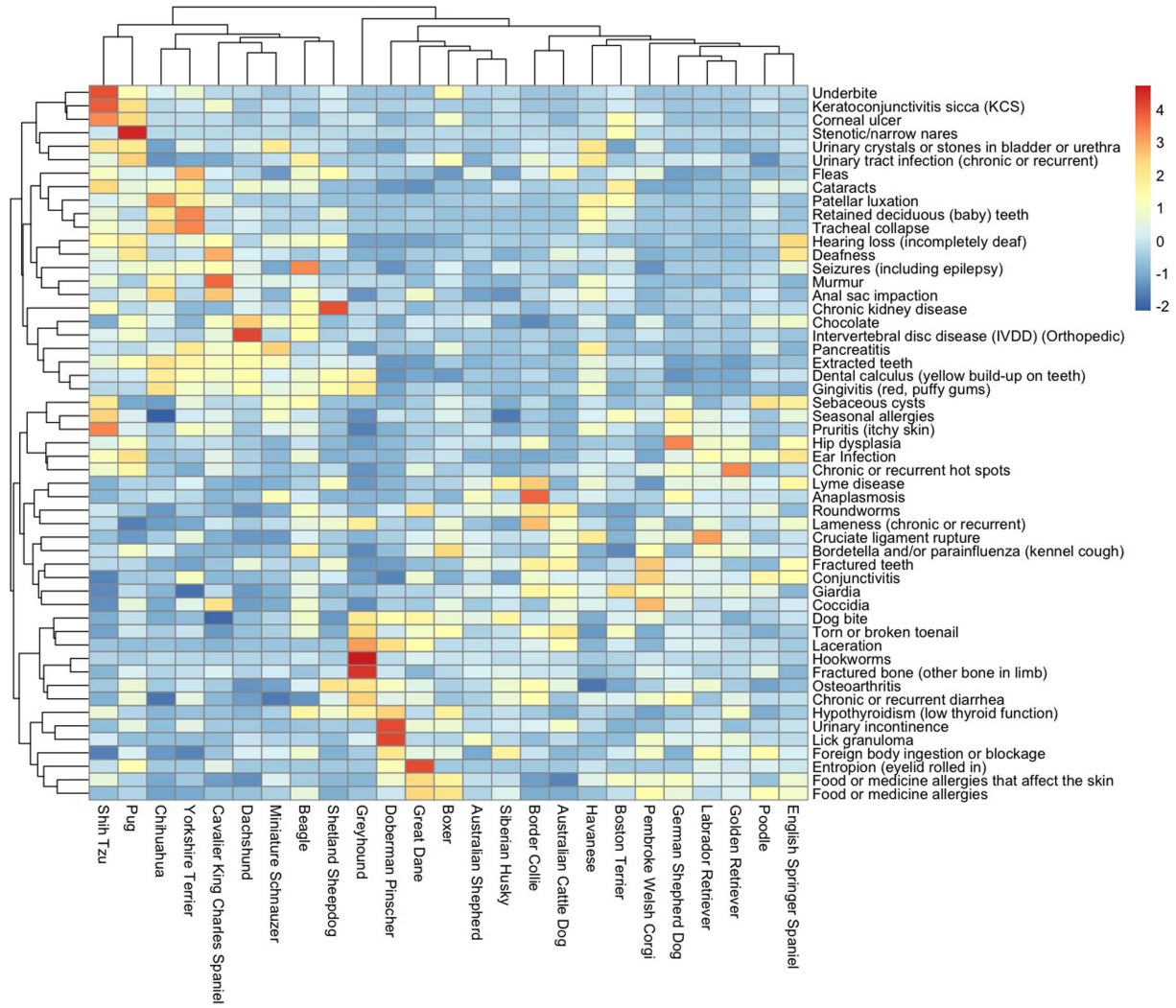

FIGURE 2
Heatmap showing the scaled lifetime prevalence of the 53 medical conditions (vertical axis) within the 25 most popular individual breeds (horizontal axis) in the DAP pack, with medical condition and breed clustered by similarity. The red color denotes higher lifetime prevalence, while the blue color denotes lower lifetime prevalence.

components of a given medical syndrome by some respondents. An example of this is the low lifetime prevalence of stenotic nares, underbite, and tracheal collapse in this study. These three conditions were each reported in less than 1% of the purebred population and less than 2% of the mixed-breed population, much less frequent than reported in previous studies (25, 28, 31). Stenotic nares and underbite are often associated with brachycephalic breeds and may potentially be considered a breed standard in some, and as a result may not be recognized as a medical condition by owners or veterinarians (28, 46, 47). Furthermore, dogs with externally apparent brachycephalic features often have hypoplastic trachea as well (7, 26, 56), which less likely to be apparent to an owner, and may be under-reported in our data. We did not attempt to re-classify reports of external brachycephalic features into an overarching diagnosis of "brachycephalic syndrome" that assumed hypoplastic trachea was also present. Additional studies comparing ORMC to what is reported in the medical records are indicated to determine the accuracy of survey data in veterinary medicine.

Another limitation is the risk that owners will only recall the most recent medical conditions, resulting in underreporting of congenital disorders or medical conditions more commonly associated with young age. While dogs of all ages were included in this study, the DAP Pack is predominantly older dogs with the median ages of the different breeds ranging from 5.1 years (Great Dane) to 9.7 years (Chihuahua). All the breeds included in this study and the mixed-breed category had a majority of the participating dogs in the mature adult life stage. If owners do fail to recall medical conditions that were further in the past, the median age of the DAP Pack population may lead to a reporting towards medical conditions more common in older dogs. However, since the median life stages are similar among breeds in the DAP Pack, there should be minimal age-related biases in direct breed-to-breed comparisons. Furthermore, as the DAP is a longitudinal study, ORMC will be collected each year which will make it possible to construct a more accurate description of the timing of ORMC acquisition across the lifespan.

Another limitation of this study is that sex, neuter status, and age of neutering were not assessed in relation to the ORMC.

Overall, our study found that purebred dogs did not have an increased lifetime prevalence of ORMC compared to mixed-breed dogs; in fact the frequency of dogs with no ORMC was higher within the purebred population. However, specific breeds often show an increased lifetime prevalence of certain medical conditions. As a result, it is important for veterinarians to consider potential breed predispositions when monitoring and treating their patients. This study also revealed that dental conditions and dog bites are common across breeds, and as a result prevention for these conditions should be addressed by primary care veterinarians.

Data availability statement

The datasets presented in this study can be found in online repositories. The names of the repository/repositories and accession number(s) can be found at: https://dogagingproject.org/open_data_access/.

Ethics statement

The University of Washington IRB deemed that recruitment of dog owners for the Dog Aging Project, and the administration and content of the DAP Health and Life Experience Survey (HLES), are human subjects research that qualifies for Category 2 exempt status (IRB ID no. 5988, effective 10/30/2018). No interactions between researchers and privately owned dogs occurred; therefore, IACUC oversight was not required. The studies were conducted in accordance with the local legislation and institutional requirements. The participants provided their written informed consent to participate in this study.

Author contributions

The DAP Consortium designed the DAP study, implemented data collection, and developed and curated the DAP databases. KKF, KEC, and SS designed the specific study. KKF, BMM, NS-M, and DELP completed the analyses and made the figures. KKF wrote the first draft of the manuscript. All authors contributed to the article and approved the submitted version.

DAP Consortium

Joshua M. Akey[1], Brooke Benton[2], Elhanan Borenstein[3,4,5], Marta G. Castelhano[6,7], Amanda E. Coleman[8], Kate E. Creevy[9], Kyle Crowder[10,11], Matthew D. Dunbar[11], Virginia R. Fajt[12], Annette L. Fitzpatrick[13,14,15], Unity Jeffery[16], Erica C Jonlin[2,17], Matt Kaeberlein[2], Elinor K. Karlsson[18,19], Kathleen F. Kerr[20], Jonathan M. Levine[9], Jing Ma[21], Robyn L McClelland[20], Daniel E. L. Promislow[2,22], Audrey Ruple[23], Stephen M. Schwartz[24,14], Sandi Shrager[25], Noah Snyder-Mackler[26,27,28], M. Katherine Tolbert[9], Silvan R. Urfer[2], Benjamin S. Wilfond[29,30]

[1]Lewis-Sigler Institute for Integrative Genomics, Princeton University, Princeton, NJ, United States

[2]Department of Laboratory Medicine and Pathology, University of Washington School of Medicine, Seattle, WA, United States

[3]Department of Clinical Microbiology and Immunology, Sackler Faculty of Medicine, Tel Aviv University, Tel Aviv, Israel

[4]Blavatnik School of Computer Science, Tel Aviv University, Tel Aviv, Israel

[5]Santa Fe Institute, Santa Fe, NM, United States

[6]Cornell Veterinary Biobank, College of Veterinary Medicine, Cornell University, Ithaca, NY, United States

[7]Department of Clinical Sciences, College of Veterinary Medicine, Cornell University, Ithaca, NY, United States

[8]Department of Small Animal Medicine and Surgery, College of Veterinary Medicine, University of Georgia, Athens, GA, United States

[9]Department of Small Animal Clinical Sciences, Texas A&M University College of Veterinary Medicine & Biomedical Sciences, College Station, TX, United States

[10]Department of Sociology, University of Washington, Seattle, WA, United States

[11]Center for Studies in Demography and Ecology, University of Washington, Seattle, WA, United States

[12]Department of Veterinary Physiology and Pharmacology, Texas A&M University College of Veterinary Medicine and Biomedical Sciences, College Station, TX, United States

[13]Department of Family Medicine, University of Washington, Seattle, WA, United States

[14]Department of Epidemiology, University of Washington, Seattle, WA, United States

[15]Department of Global Health, University of Washington, Seattle, WA, United States

[16]Department of Veterinary Pathobiology, Texas A&M University College of Veterinary Medicine & Biomedical Sciences, College Station, TX, United States

[17]Institute for Stem Cell and Regenerative Medicine, University of Washington, Seattle, WA, United States

[18]Bioinformatics and Integrative Biology, University of Massachusetts Chan Medical School, Worcester, MA, United States

[19]Broad Institute of MIT and Harvard, Cambridge, MA, United States

[20]Department of Biostatistics, University of Washington, Seattle, WA, United States

[21]Division of Public Health Sciences, Fred Hutchinson Cancer Research Center, Seattle, WA, United States

[22]Department of Biology, University of Washington, Seattle, WA, United States

[23]Department of Population Health Sciences, Virginia-Maryland College of Veterinary Medicine, Virginia Tech, Blacksburg, VA, United States

[24]Epidemiology Program, Fred Hutchinson Cancer Research Center, Seattle, WA, United States

[25]Collaborative Health Studies Coordinating Center, Department of Biostatistics, University of Washington, Seattle, WA, United States

[26]School of Life Sciences, Arizona State University, Tempe, AZ, United States

[27]Center for Evolution and Medicine, Arizona State University, Tempe, AZ, United States

[28]School for Human Evolution and Social Change, Arizona State University, Tempe, AZ, United States

[29]Treuman Katz Center for Pediatric Bioethics, Seattle Children's Research Institute, Seattle, WA, United States

[30]Department of Pediatrics, Division of Bioethics and Palliative Care, University of Washington School of Medicine, Seattle, WA, United States

Funding

The Dog Aging Project is supported by National Institute on Aging grant U19AG057377 (PI: Promislow) and private donations. This content is solely the responsibility of the authors and does not necessarily reflect the official views of the National Institutes of Health.

Acknowledgments

We would like to thank the Dog Aging Project participants, their dogs, and community veterinarians for their important contributions to the Dog Aging Project.

Conflict of interest

The authors declare that the research was conducted in the absence of any commercial or financial relationships that could be construed as a potential conflict of interest.

Publisher's note

Supplementary material

The Supplementary material for this article can be found online at: https://www.frontiersin.org/articles/10.3389/fvets.2023.1140417/full#supplementary-material

References

1. American-Kennel-Club (2021). Becoming Recognized by the AKC: The American Kennel Club Inc. Available at: https://www.akc.org/press-center/articles-resources/facts-and-stats/becoming-recognized/ (Accessed February 1, 2023).

2. American-Kennel-Club (2021). The Most popular dog breeds of 2020: The American Kennel Club Inc. Available at: https://www.akc.org/expert-advice/dog-breeds/the-most-popular-dog-breeds-of-2020/ (Accessed February 1, 2023).

3. Bartlett PC, Van Buren JW, Neterer M, Zhou C. Disease surveillance and referral bias in the veterinary medical database. *Prev Vet Med*. (2010) 94:264–71. doi: 10.1016/j.prevetmed.2010.01.007

4. Binyaruka P, Borghi J. Validity of parental recalls to estimate vaccination coverage: evidence from Tanzania. *BMC Health Serv Res*. (2018) 18:440. doi: 10.1186/s12913-018-3270-z

5. Brooks A, Moxon R, England GCW. Incidence and impact of dog attacks on guide dogs in the UK. *Vet Rec*. (2010) 166:778–81. doi: 10.1136/vr.b4855

6. Bryan JN, Keeler MR, Henry CJ, Bryan ME, Hahn AW, Caldwell CW. A population study of neutering status as a risk factor for canine prostate cancer. *Prostate*. (2007) 67:1174–81. doi: 10.1002/pros.20590

7. Coyne BE, Fingland RB. Hypoplasia of the trachea in dogs: 103 cases (1974-1990). *J Am Vet Med Assoc*. (1992) 201:768–72.

8. Creevy KE, Akey JM, Kaeberlein M, Promislow DEL, Barnett BG, Benton B, et al. An open science study of ageing in companion dogs. *Nature*. (2022) 602:51–7. doi: 10.1038/s41586-021-04282-9

9. Creevy KE, Grady J, Little SE, Moore GE, Strickler BG, Thompson S, et al. 2019 AAHA Canine Life Stage Guidelines. *J Am Anim Hosp Assoc*. (2019) 55:267–90. doi: 10.5326/JAAHA-MS-6999

10. Crnokrak P, Barrett SC. Perspective: purging the genetic load: a review of the experimental evidence. *Evolution*. (2002) 56:2347–58. doi: 10.1111/j.0014-3820.2002.tb00160.x

11. Cummings P, Rivara FP, Thompson RS, Reid RJ. Ability of parents to recall the injuries of their young children. *Inj Prev*. (2005) 11:43–7. doi: 10.1136/ip.2004.006833

12. Dodds WJ. Estimating disease prevalence with health surveys and genetic screening. *Adv Vet Sci Comp Med*. (1995) 39:29–96. doi: 10.1016/S0065-3519(06)80017-0

13. Dog-Aging-Project (2021). Dog Aging Project Survey Instruments: GitHub Inc. Available at: https://github.com/dogagingproject/survey_instruments/tree/main/HLES/annotated_with_terra_names

14. D'Souza-Vazirani D, Minkovitz CS, Strobino DM. Validity of maternal report of acute health care use for children younger than 3 years. *Arch Pediatr Adolesc Med*. (2005) 159:167–72. doi: 10.1001/archpedi.159.2.167

15. Egenvall A, Nødtvedt A, Häggström J, Ström Holst B, Möller L, Bonnett BN. Mortality of life-insured Swedish cats during 1999-2006: age, breed, sex, and diagnosis. *J Vet Intern Med*. (2009) 23:1175–83. doi: 10.1111/j.1939-1676.2009.0396.x

16. Fleming JM, Creevy KE, Promislow DE. Mortality in north American dogs from 1984 to 2004: an investigation into age-, size-, and breed-related causes of death. *J Vet Intern Med*. (2011) 25:187–98. doi: 10.1111/j.1939-1676.2011.0695.x

17. Freeman LM, Abood SK, Fascetti AJ, Fleeman LM, Michel KE, Laflamme DP, et al. Disease prevalence among dogs and cats in the United States and Australia and proportions of dogs and cats that receive therapeutic diets or dietary supplements. *J Am Vet Med Assoc*. (2006) 229:531–4. doi: 10.2460/javma.229.4.531

18. Galis F, Van der Sluijs I, Van Dooren TJ, Metz JA, Nussbaumer M. Do large dogs die young? *J Exp Zool B Mol Dev Evol*. (2007) 308:119–26. doi: 10.1002/jez.b.21116

19. Gareaballah ET, Loevinsohn BP. The accuracy of mother's reports about their children's vaccination status. *Bull World Health Organ*. (1989) 67:669–74.

20. Gough A, Thomas A. *Breed predispositions to disease in dogs and cats*, vol. *xvii. 2nd* ed. Chichester, West Sussex; Ames, Iowa: Wiley-Blackwell (2010). 330 p.

21. Hart BL, Hart LA, Thigpen AP, Willits NH. Assisting decision-making on age of neutering for mixed breed dogs of five weight categories: associated joint disorders and cancers. *Front Vet Sci*. (2020) 7:472. doi: 10.3389/fvets.2020.00472

22. Hart BL, Hart LA, Thigpen AP, Willits NH. Assisting decision-making on age of neutering for 35 breeds of dogs: associated joint disorders, cancers, and urinary incontinence. *Front Vet Sci*. (2020) 7:388. doi: 10.3389/fvets.2020.00388

23. Heyward CL, Hazel S, Peacock R, Nielsen T. Characteristics and outcomes of dog attacks to dogs and cats in Melbourne, Australia: a retrospective study of 459 cases (2018). *Prev Vet Med*. (2022) 201:105609. doi: 10.1016/j.prevetmed.2022.105609

24. Infante-Rivard C, Jacques L. Empirical study of parental recall bias. *Am J Epidemiol*. (2000) 152:480–6. doi: 10.1093/aje/152.5.480

25. Johnson LR, Pollard RE. Tracheal collapse and bronchomalacia in dogs: 58 cases (7/2001–1/2008). *J Vet Intern Med*. (2010) 24:298–305. doi: 10.1111/j.1939-1676.2009.0451.x

26. Kaye BM, Boroffka SA, Haagsman AN, Ter Haar G. Computed tomographic, radiographic, and endoscopic tracheal dimensions in English bulldogs with grade 1 clinical signs of brachycephalic airway syndrome. *Vet Radiol Ultrasound*. (2015) 56:609–16. doi: 10.1111/vru.12277

27. Kim E, Choe C, Yoo JG, Oh SI, Jung Y, Cho A, et al. Major medical causes by breed and life stage for dogs presented at veterinary clinics in the Republic of Korea: a survey of electronic medical records. *PeerJ*. (2018) 6:e5161. doi: 10.7717/peerj.5161

28. Liu NC, Troconis EL, Kalmar L, Price DJ, Wright HE, Adams VJ, et al. Conformational risk factors of brachycephalic obstructive airway syndrome (BOAS) in pugs, French bulldogs, and bulldogs. *PLoS One*. (2017) 12:e0181928. doi: 10.1371/journal.pone.0181928

29. Loder RT. The demographics of dog bites in the United States. *Heliyon*. (2019) 5:e01360. doi: 10.1016/j.heliyon.2019.e01360

30. Lund EM, Armstrong PJ, Kirk CA, Kolar LM, Klausner JS. Health status and population characteristics of dogs and cats examined at private veterinary practices in the United States. *J Am Vet Med Assoc*. (1999) 214:1336–41.

31. Marolf A, Blaik M, Specht A. A retrospective study of the relationship between tracheal collapse and bronchiectasis in dogs. *Vet Radiol Ultrasound*. (2007) 48:199–203. doi: 10.1111/j.1740-8261.2007.00229.x

32. Martin MW, Stafford Johnson MJ, Celona B. Canine dilated cardiomyopathy: a retrospective study of signalment, presentation and clinical findings in 369 cases. *J Small Anim Pract*. (2009) 50:23–9. doi: 10.1111/j.1748-5827.2008.00659.x

33. McGreevy PD, Wilson BJ, Mansfield CS, Brodbelt DC, Church DB, Dhand N, et al. Labrador retrievers under primary veterinary care in the UK: demography, mortality and disorders. *Canine Genet Epidemiol*. (2018) 5:8. doi: 10.1186/s40575-018-0064-x

34. Modi RN, King C, Bar-Zeev N, Colbourn T. Caregiver recall in childhood vaccination surveys: systematic review of recall quality and use in low- and middle-income settings. *Vaccine*. (2018) 36:4161–70. doi: 10.1016/j.vaccine.2018.05.089

35. Morrill K, Hekman J, Li X, McClure J, Logan B, Goodman L, et al. Ancestry-inclusive dog genomics challenges popular breed stereotypes. *Science*. (2022) 376:eabk0639. doi: 10.1126/science.abk0639

36. National-Greyhound-Association (2021). National Greyhound Association. Available at: https://www.ngagreyhounds.com/ (Accessed February 1, 2023).

37. O'Neill DG, Butcher C, Church DB, Brodbelt DC, Gough AG. Miniature schnauzers under primary veterinary care in the UK in 2013: demography, mortality and disorders. *Canine Genet Epidemiol*. (2019) 6:1. doi: 10.1186/s40575-019-0069-0

38. O'Neill DG, Coulson NR, Church DB, Brodbelt DC. Demography and disorders of German shepherd dogs under primary veterinary care in the UK. *Canine Genet Epidemiol*. (2017) 4:7. doi: 10.1186/s40575-017-0046-4

39. O'Neill DG, Darwent EC, Church DB, Brodbelt DC. Demography and health of pugs under primary veterinary care in England. *Canine Genet Epidemiol*. (2016) 3:5. doi: 10.1186/s40575-016-0035-z

40. O'Neill DG, James H, Brodbelt DC, Church DB, Pegram C. Prevalence of commonly diagnosed disorders in UK dogs under primary veterinary care: results and applications. *BMC Vet Res*. (2021) 17:69. doi: 10.1186/s12917-021-02775-3

41. O'Neill DG, Packer RMA, Lobb M, Church DB, Brodbelt DC, Pegram C. Demography and commonly recorded clinical conditions of Chihuahuas under primary veterinary care in the UK in 2016. *BMC Vet Res*. (2020) 16:42. doi: 10.1186/s12917-020-2258-1

42. O'Neill DG, Rooney NJ, Brock C, Church DB, Brodbelt DC, Pegram C. Greyhounds under general veterinary care in the UK during 2016: demography and common disorders. *Canine Genet Epidemiol*. (2019) 6:4. doi: 10.1186/s40575-019-0072-5

43. Oberbauer AM, Belanger JM, Bellumori T, Bannasch DL, Famula TR. Ten inherited disorders in purebred dogs by functional breed groupings. *Canine Genet Epidemiol*. (2015) 2:9. doi: 10.1186/s40575-015-0021-x

44. Okafor CC, Lefebvre SL, Pearl DL, Yang M, Wang M, Blois SL, et al. Risk factors associated with calcium oxalate urolithiasis in dogs evaluated at general care veterinary hospitals in the United States. *Prev Vet Med*. (2014) 115:217–28. doi: 10.1016/j.prevetmed.2014.04.006

45. O'Neill DG, Church DB, McGreevy PD, Thomson PC, Brodbelt DC. Prevalence of disorders recorded in dogs attending primary-care veterinary practices in England. *PLoS One*. (2014) 9:e90501. doi: 10.1371/journal.pone.0091532

46. Packer RMA, Hendricks A, Burn CC. Do dog owners perceive the clinical signs related to conformational inherited disorders as 'normal' for the breed? A potential constraint to improving canine welfare. *Anim Welf*. (2012) 21:81–93. doi: 10.7120/096272812X13345905673809

47. Packer RM, Tivers MS. Strategies for the management and prevention of conformation-related respiratory disorders in brachycephalic dogs. *Vet Med*. (2015) 6:219–32. doi: 10.2147/VMRR.S60475

48. Parker HG, Meurs KM, Ostrander EA. Finding cardiovascular disease genes in the dog. *J Vet Cardiol*. (2006) 8:115–27. doi: 10.1016/j.jvc.2006.04.002

49. Patronek GJ, Slavinski SA. Animal bites. *J Am Vet Med Assoc*. (2009) 234:336–45. doi: 10.2460/javma.234.3.336

50. Plant JD, Lund EM, Yang M. A case-control study of the risk factors for canine juvenile-onset generalized demodicosis in the USA. *Vet Dermatol*. (2011) 22:95–9. doi: 10.1111/j.1365-3164.2010.00922.x

51. Pless CE, Pless IB. How well they remember. The accuracy of parent reports. *Arch Pediatr Adolesc Med*. (1995) 149:553–8. doi: 10.1001/archpedi.1995.02170180083016

52. Porth JM, Wagner AL, Tefera YA, Boulton ML. Childhood immunization in Ethiopia: accuracy of maternal recall compared to vaccination cards. *Vaccines*. (2019) 7:313–18. doi: 10.3390/vaccines7020048

53. Rafferty E, Hetherington E, Tough S, Aujla S, McNeil D, Saini V, et al. The impact of time since vaccination and study design on validity in parental recall of childhood vaccination status in the all our families cohort. *Vaccine*. (2018) 36:2953–9. doi: 10.1016/j.vaccine.2018.04.045

54. Raghavan M, Glickman N, Moore G, Caldanaro R, Lewis H, Glickman L. Prevalence of and risk factors for canine tick infestation in the United States, 2002-2004. *Vector Borne Zoonotic Dis*. (2007) 7:65–75. doi: 10.1089/vbz.2006.0570

55. Rettenmaier JL, Keller GG, Lattimer JC, Corley EA, Ellersieck MR. Prevalence of canine hip dysplasia in a veterinary teaching hospital population. *Vet Radiol Ultrasound*. (2002) 43:313–8. doi: 10.1111/j.1740-8261.2002.tb01010.x

56. Riecks TW, Birchard SJ, Stephens JA. Surgical correction of brachycephalic syndrome in dogs: 62 cases (1991-2004). *J Am Vet Med Assoc*. (2007) 230:1324–8. doi: 10.2460/javma.230.9.1324

57. Spencer NJ, Coe C. Validation of the Warwick child health and morbidity profile in routine child health surveillance. *Child Care Health Dev*. (2000) 26:323–36. doi: 10.1046/j.1365-2214.2000.00148.x

58. Summers JF, Diesel G, Asher L, McGreevy PD, Collins LM. Inherited defects in pedigree dogs. Part 2: disorders that are not related to breed standards. *Vet J*. (2010) 183:39–45. doi: 10.1016/j.tvjl.2009.11.002

59. Summers JF, O'Neill DG, Church D, Collins L, Sargan D, Brodbelt DC. Health-related welfare prioritisation of canine disorders using electronic health records in primary care practice in the UK. *BMC Vet Res*. (2019) 15:163. doi: 10.1186/s12917-019-1902-0

60. Summers JF, O'Neill DG, Church DB, Thomson PC, McGreevy PD, Brodbelt DC. Prevalence of disorders recorded in Cavalier King Charles Spaniels attending primary-care veterinary practices in England. *Canine Genet Epidemiol*. (2015) 2:4. doi: 10.1186/s40575-015-0016-7

61. Tuckel PS, Milczarski W. The changing epidemiology of dog bite injuries in the United States, 2005–2018. *Inj Epidemiol*. (2020) 7:57. doi: 10.1186/s40621-020-00281-y

62. Urfer SR, Kaeberlein M, Promislow DEL, Creevy KE. Lifespan of companion dogs seen in three independent primary care veterinary clinics in the United States. *Canine Med Genet*. (2020) 7:7. doi: 10.1186/s40575-020-00086-8

63. Urfer SR, Wang M, Yang M, Lund EM, Lefebvre SL. Risk factors associated with lifespan in pet dogs evaluated in primary care veterinary hospitals. *J Am Anim Hosp Assoc*. (2019) 55:130–7. doi: 10.5326/JAAHA-MS-6763

64. Wayne RK, Ostrander EA. Lessons learned from the dog genome. *Trends Genet*. (2007) 23:557–67. doi: 10.1016/j.tig.2007.08.013

65. Wellmann R, Pfeiffer I. Pedigree analysis for conservation of genetic diversity and purging. *Genet Res*. (2009) 91:209–19. doi: 10.1017/S0016672309000202

66. Wiles BM, Llewellyn-Zaidi AM, Evans KM, O'Neill DG, Lewis TW. Large-scale survey to estimate the prevalence of disorders for 192 Kennel Club registered breeds. *Canine Genet Epidemiol*. (2017) 4:8. doi: 10.1186/s40575-017-0047-3

frontiers | Frontiers in Veterinary Science

TYPE Original Research
PUBLISHED 06 March 2024
DOI 10.3389/fvets.2024.1332337

OPEN ACCESS

EDITED BY
Valentina Meucci,
University of Pisa, Italy

REVIEWED BY
Victor Alejandro Castillo,
University of Buenos Aires, Argentina
Dianne McFarlane,
University of Florida, United States
Teresa Burns,
The Ohio State University, United States
Harold Schott,
Michigan State University, United States

*CORRESPONDENCE
David Rendle
✉ daverendle@me.com

RECEIVED 02 November 2023
ACCEPTED 23 February 2024
PUBLISHED 06 March 2024

CITATION
Sundra T, Kelty E, Rossi G and Rendle D (2024) Retrospective assessment of the use of extended-release cabergoline in the management of equine pituitary pars intermedia dysfunction.
Front. Vet. Sci. 11:1332337.
doi: 10.3389/fvets.2024.1332337

Retrospective assessment of the use of extended-release cabergoline in the management of equine pituitary pars intermedia dysfunction

Tania Sundra[1,2], Erin Kelty[3], Gabriele Rossi[2] and David Rendle[4]*

[1]Avon Ridge Equine Veterinary Services, Brigadoon, WA, Australia, [2]School of Veterinary Medicine, Murdoch University, Murdoch, WA, Australia, [3]School of Population and Global Health, University of Western Australia, Crawley, WA, Australia, [4]EMT Consulting, Tiverton, United Kingdom

Introduction: Dopaminergic agonists are accepted as the most effective treatment for pituitary pars intermedia dysfunction. However, some horses are refractory to daily oral pergolide, the recommended registered treatment. Extended-release cabergoline (ERC) injection may offer an alternative. The objective of this retrospective case series was to describe clinical and endocrinological responses to ERC.

Methods: Medical records of horses treated with weekly intramuscular injections of ERC (5 mg/mL, BOVA Aus) at either 0.01 mg/kg (high dose, HD) ($n = 10$) or 0.005 mg/kg (low dose, LD) ($n = 30$) were reviewed. Short-term ACTH responses were assessed at 5–8 days using a Wilcoxon signed ranked test. Longer-term ACTH responses (30 to 365 days) were assessed using generalised estimating equations.

Results: Five to eight days after the first dose of LDERC, median adrenocorticotropic hormone (ACTH) concentration was lower ($p = 0.001$), changing from 153 pg/mL (IQR: 78, 331) to 57 pg/mL (IQR: 30, 102). With HDERC, median ACTH concentration was also 153 pg/mL (IQR: 96, 185) before and then 56 pg/mL (IQR: 29, 86) after 5–8 days of treatment ($p = 0.047$). Over 12 months of treatment, ACTH concentration ranged from 14 to >1,250 pg/mL (median: 51 pg/mL) in horses treated with LDERC and 20 to 472 pg/mL (median: 50 pg/mL) in horses treated with HDERC. Measurements remained above the seasonal reference range in 39.3 and 52.3% of horses treated with LDERC and HDERC, respectively. Clinical improvement was reported by owners in 78.3 and 100% of horses treated with LDERC and HDERC, respectively. Partial, self-limiting inappetence was reported in 30.0% of LDERC and 60% HDERC cases. Seven horses exhibited lethargy (5 LDERC, 2 HDERC). Insulin concentrations measured 30 days post-ERC treatment were no different from baseline.

Discussion: Clinical and endocrinological responses were consistent with results of previous reports of oral pergolide treatment. Weekly injection of ERC may be an effective alternative to pergolide; the 0.005 mg/kg dose appeared to be as effective, with less risk of inappetence, than the 0.01 mg/kg dose that has been reported previously.

KEYWORDS

horse, endocrine, laminitis, geriatric, dopamine, ACTH

Introduction

Pituitary pars intermedia dysfunction (PPID) is a neurodegenerative condition that results in loss of dopaminergic inhibition of the pars intermedia and leads to an overproduction of peptides, including adrenocorticotrophic hormone (ACTH) (1). PPID is the most common endocrine condition in geriatric horses and is encountered frequently in clinical practice (2). Epidemiological studies have demonstrated a disease prevalence of approximately 15–30% in horses over the age of 15 yrs (3). Clinical signs associated with PPID include hypertrichosis, laminitis, polyuria, polydipsia, lethargy, muscle wastage, and delayed wound healing (1, 4). In addition to good husbandry, the treatment of PPID involves the use of dopaminergic agonists, which reduce peptide secretion from the pars intermedia (1, 2, 5).

Pergolide, a dopaminergic agonist, has been used widely for the treatment of PPID for over two decades (5, 6). Pergolide is currently registered as tablet and (in some countries) liquid preparation; however, some horses are refractory to daily oral administration, and previous studies have reported that owners might be less committed to lifelong therapy in older animals (7–9). A recent study demonstrated poor compliance with the administration of pergolide tablets, and this may have implications for the control of clinical signs even though it did not appear to affect ACTH responses (9).

Cabergoline is a dopaminergic agonist that has the same mechanism of action as pergolide but is available as an extended-release intramuscular injection, alleviating the need for daily oral administration of medication (10, 11). For several decades, cabergoline was used to treat functional pituitary adenomas in humans, including cases refractory to pergolide therapy, as it has a high affinity for dopaminergic receptors in the hypothalamus and pituitary gland (12–16). Previous studies in horses have investigated the effects of cabergoline on prolactin, MSH and insulin concentrations (10, 11, 17) and shown that these hormones have reduced consistent with the drug having an inhibitory effect on both melanotrophs and lactotrophs in the equine pituitary gland.

Anecdotally, extended-release cabergoline (ERC) administered as a low-volume intramuscular injection is an effective alternative to pergolide. The objectives of the current study were to: (1) review and describe the initial (5–8 days) and longer-term (12 months) clinical and endocrinological responses to two dose rates of an intramuscular extended release cabergoline (ERC) injection that is being used widely in clinical practice for the treatment of PPID.

Materials and methods

Horses

Clinical records of privately-owned horses treated by Avon Ridge Equine Clinic (anonymised for peer review) between June 2021 and October 2022 were reviewed to identify horses that had been treated with ERC for the management of PPID. Horse weight was estimated using a validated weigh tape.[1]

Treatment

In accordance with previous reports (10, 11, 17), horses initially received treatment with ERC as an intramuscular injection (5 mg/mL)[2] at a "high" dose of 0.01 mg/kg (HDERC). Some horses were reported by owners to experience in appetence at this higher dose, and prompting a change in the practice protocol to use a "low" dose of 0.005 mg/kg (LDERC) for subsequent cases in an attempt to mitigate issues with appetite reduction.

Site selection and correct intramuscular injection technique were demonstrated by the treating veterinarian when administering the first dose. The injection site was cleaned with isopropyl alcohol[3] prior to injection, and the total dose of cabergoline (maximum 1 mL) was administered at a single injection site in either the neck or gluteal musculature. Owners administered subsequent doses and were advised to record clinical changes and to contact their veterinarian immediately if any adverse effects were observed. Cabergoline is not currently registered for use in horses; thus, informed client consent for the use of an unregistered medicine was obtained prior to commencing treatment. Clinical signs were assessed and recorded at repeat veterinary examinations in consultation with the owners responsible for day-to-day care of the horses.

Laboratory investigations

ACTH data was collated and grouped relative to cabergoline administration. For all cases ACTH results were available from up to 3 days prior to treatment, 5 to 8 days after the first injection of ERC, and thereafter at less consistent but regular intervals as dictated by the clinical progress of each case. Post-prandial insulin concentrations were also available from up to 3 days prior to, and after 30 (+/−3), days of treatment. Insulin was measured approximately 90 min after the provision of the horse's normal feed and forage in the morning. Insulin and ACTH concentrations were measured using an Immulite 2000.[4]

Data analysis

Signalment and clinical data were transposed from case records to Microsoft Excel[5] for subsequent analysis. Age, sex, and baseline ACTH were compared between high and low doses of ERC using Wilcoxon sign-rank or Chi-squared tests. Median ACTH concentration and interquartile range (IQR) were calculated for baseline (up to 30 days prior to treatment), 5–8 days, 30–90 days, 91–180 days, and 181–365 days post treatment. Where horses had had ACTH concentration measured more than once during a period, the mean of the results was used. Each ACTH concentration measurement was also classified as being within or above the geographical and seasonal reference range (18) for the month of collection. The percentage of horses with one or more ACTH concentrations above the normal range was reported for each period.

1 Virbac, 361 Horsley Road, Milperra, NSW 2214, Australia.

2 BOVA Aus, Suite 1, 304-318 Kingsway Caringbah, NSW 2229.

3 Isopropyl Alcohol; PharmAust Manufacturing, Malaga, WA, Australia.

4 Siemens, 885 Mountain Highway, Bayswater, Victoria 3,153, Australia.

5 Microsoft corporation, Redmond, USA.

TABLE 1 Short-term adrenocorticotropic hormone responses following a single dose of extended release cabergoline, stratified by low (LDERC) and high dose (HDERC).

	LDERC				HDERC			
	n	Pre-treatment[a]	Day 5–8	*p*-value	*n*	Pre-treatment[a]	Day 5–8	*p*-value
ACTH, median (IQR)	22	153 (78, 331)	57 (30, 102)	0.001	10	153 (96, 185)	56 (29. 86)	0.047
Above reference range[b], *n* (%)	22	22 (100%)	13 (59.1%)	–	10	10 (100%)	6 (60.0%)	–

[a]0 to 31 days prior to the commencement of treatment.
[b]Percentage of horses with one or more ACTH concentrations above the seasonally adjusted reference range.

Efficacy of HDERC and LDERC were examined by comparing the ACTH responses at different time points with baseline ACTH concentration. Comparisons between measures taken at baseline and 5–8 days were made using a Wilcoxon signed ranked test, overall and stratified by high and low dose. Comparison between ACTH concentration at each longer-term follow-up period and baseline was performed using generalised estimating equations, using a negative binomial distribution for ACTH values and a binomial distribution for normal/high ACTH values. Analysis was carried out in StataMP version 17.[6]

Animal ethics approval

An ethics committee was consulted, and it was determined that ethics committee oversight was not required for the retrospective review of clinical data.

Results

Horses

Data from 40 horses were included. Mean (±standard deviation) age was 22.4 (±5.1 years), with 25 geldings (62.5%) and 15 mares (37.5%). The average weight of horses at baseline was 344 ± 146 kg. A variety of breeds were represented, including Welsh and Welsh crosses ($n = 18$, 45.0%), Thoroughbreds ($n = 4$, 10.0%), Standardbreds ($n = 3$, 7.5%), Quarter horses ($n = 3$, 7.5%), Shetlands ($n = 2$, 5.0%), Miniatures and Miniature crosses ($n = 2$, 5.0%), Warmblood and Warmblood crosses ($n = 2$, 5.0%), and a range of other mixed breeds ($n = 6$, 15.0%). There were insufficient data to compare groups but there were no obvious differences in breed distributions between the HDERC and LDERC groups. Horses started treatment at all times of year: January 9, February 2, March 0, April 1, May 3, June 0, July 7, August 7, September 1, October 2, November 2, and December 6, with no apparent difference between groups.

Clinical signs of PPID at initial evaluation included hypertrichosis ($n = 28$, 70.0%), weight loss ($n = 10$, 25.0%), laminitis (or a history of laminitis) ($n = 10$, 25.0%), muscle atrophy ($n = 9$, 22.5%), lethargy ($n = 4$, 10.0%), recurrent infections ($n = 2$, 5.3%), polyuria and polydipsia ($n = 1$, 2.6%) and poor wound healing ($n = 2$, 5.3%). Fifteen horses had previously received treatment with pergolide with a mean of 15.2 days (range 1–60 days) between receiving their last dose of pergolide and commencing treatment with ERC. Seven had received pergolide within a week of starting pergolide treatment (3 HDERC, 4 LDERC).

Treatment

The most common reason for commencing ERC was actual or anticipated difficulty administering daily oral medication ($n = 38$, 97.4%). Three horses also displayed signs of partial anorexia whilst on treatment with pergolide at 2 mcg/kg. One horse demonstrated high ACTH concentration, complete anorexia and somnolence when treated with pergolide at 2 mcg/kg. Ten horses (25.0%) were treated with 0.01 mg/kg HDERC, 30 (75.0%) with 0.005 mg/kg LDERC. There was no significant difference between the two groups in terms of age ($p = 0.253$), sex ($p = 0.187$), or baseline ACTH ($p = 0.179$). Owners did not report missing any treatment doses.

At the end of the study period, 25 horses continued on treatment (5 HDERC, 20 LDERC) and seven horses were lost to follow up (3 HDERC, 4 LDERC). Of the horses that discontinued treatment, 2 (LDERC) stopped due to marked anorexia or colic, 2 due to owner finances (LDERC), 2 became refractory to injections (LDERC), 3 were euthanased for unrelated accidents or illness (2 LDERC, 1 HDERC), and 1 was switched to pergolide (HDERC).

Short-term ACTH responses

Measurements of ACTH concentration were available for 32 horses on day 0 and after a single dose of cabergoline at days 5–8. The median ACTH concentration reduced from 153 pg/mL (IQR: 79, 245) to 57 pg/mL (30, 96) ($p < 0.001$). All horses had an ACTH concentration above the seasonal reference range prior to treatment; 19 horses (59.4%) remained above the seasonal reference after a single dose of cabergoline. Short-term ACTH responses stratified by dose are shown in Table 1; the reduction in ACTH concentration was significant in both groups.

Longer-term ACTH responses

In horses with longer-term follow-up data available, ACTH concentration ranged from 59 to >1,250 pg/mL (median: 162 pg/mL) prior to treatment with all horses having an ACTH concentration above the seasonal reference range (Table 2). In the year following the commencement of treatment, ACTH concentrations ranged from 13 to 1,250 pg/mL (median: 50 pg/mL), with 46.4% of measurements remaining above the seasonal reference range. Longer-term ACTH responses are shown in Table 2 and are stratified by dose in Table 3.

6 StataCorp, Texas, USA.

TABLE 2 Adrenocorticotropic hormone concentration (pg/mL) in 40 horses treated with extended release cabergoline.

	n	Median (IQR)	*p*-value	Above reference[b] (%)
Baseline[a]	40	162 (90, 286)	–	40 (100%)
Day 31–90	30	61 (41, 83)	<0.001	17 (56.7%)
Day 91–180	24	47 (38, 106)	<0.001	11 (45.8%)
Day 181–365	16	68 (50, 100)	<0.001	11 (68.8%)

[a]0 to 31 days prior to the commencement of treatment.
[b]Horses with one or more ACTH concentrations above the seasonally adjusted ACTH range.

TABLE 3 Longer-term adrenocorticotropic concentration (pg/mL) following treatment with extended release cabergoline, stratified by low (LDERC) and high dose (HDERC).

	LDERC				HDERC			
	N	Median (IQR)	*p*-value	Above reference (%)	*N*	Median (IQR)	*p*-value	Above reference (%)
Baseline	26	170 (88, 331)	–	26 (100%)	9	150 (96, 178)	–	9 (100%)
Day 31–90	21	46 (32, 83)	<0.001	8 (38.1%)	9	67 (47, 80)	<0.001	9 (100%)
Day 91–180	16	48 (33, 119)	<0.001	8 (50.0%)	8	47 (42, 71)	<0.001	3 (37.5%)
Day 181–365	9	63 (34, 65)	<0.001	4 (55.6%)	7	102 (71, 280)	0.684	6 (85.7%)

Reduction in ACTH concentration was significant with both doses at all time points, with the exception of the day 181–365 HDERC group.

Insulin responses

Measurement of insulin concentration was performed at day 0 and day 30 in seven horses in the HDERC group. All horses were already being managed for equine metabolic syndrome with a diet consisting of <10% NSC for at least one week prior to measurement of insulin concentration. The diet of the horses remained consistent at both testing timepoints. Median insulin concentration prior to treatment was 185 µu/mL (IQR: 113, 279) and after treatment was 241 µu/mL (IQR: 113, 284) ($p = 0.563$).

Longer-term clinical response to treatment

The owners' perceived response to treatment was recorded in 31 of the 40 horses (23 LDERC and 8 HDERC). In the horses treated with LDERC, 78.3% reported an improvement ($n = 17$), while no change was reported by 13.0% of owners ($n = 3$) and 8.7% reported worsening of clinical signs ($n = 2$). Of the horses which improved, 77.8% demonstrated improved coat shedding ($n = 14$), 66.7% increased energy levels ($n = 12$), and 22.2% showed signs of improved body condition ($n = 4$). All owners reported good compliance with the weekly injection of ERC. Improvement was reported in 100% of the horses treated with HDERC ($n = 8$). Of these, 87.5% demonstrated improved coat shedding ($n = 7$), 25% increased energy levels ($n = 2$), and 25% showed signs of improved body condition ($n = 2$).

Adverse reactions

Adverse events including self-limiting lethargy (HDERC: $n = 2$, 20%; LDERC: $n = 5$, 16.7%), partial anorexia (HDERC: $n = 6$, 60%; LDERC: $n = 9$, 30.0%), and mild colic (LDERC: $n = 2$, 6.7%) occurred within 12–36 h following the injection of ERC. Where partial anorexia was observed, horses displayed a preference for hay and grass over concentrate feed for approximately 12–24 h following injection with ERC. No reactions were reported at the injection sites in any of the horses that were treated.

The owners of one horse receiving HDERC opted to switch to pergolide after two injections, as anorexia and lethargy were observed for 12 h following each dose. The horse displayed no adverse effects when treated with pergolide. One horse receiving LDERC displayed lethargy and inappetence for 72 h. Treatment with LDERC was discontinued after the third dose, and the horse commenced treatment with pergolide at 2 mcg/kg. No adverse events were observed on pergolide. Of the three horses which demonstrated anorexia on pergolide, only one showed signs of partial anorexia (for 12 h) following treatment with LDERC. The horse which demonstrated marked anorexia and became an obtunded following each daily dose of pergolide displayed signs of partial anorexia for 18 h following each weekly injection with LDERC but remained clinically normal between doses after this time. Three horses that displayed partial anorexia on ERC (HDERC: $n = 2$; LDERC: $n = 1$) did not previously demonstrate any adverse effects on pergolide. One horse treated with LDERC was partially anorexic and displayed signs of low-grade colic for 6 days following the first dose. No further doses were administered, and no further episodes of colic or anorexia were reported.

Discussion

In the horses studied, once weekly injection of cabergoline was associated with a reduction in ACTH concentration and an improvement in clinical signs of PPID at the previously reported 0.01 mg/kg dose and also at a lower 0.005 mg/kg dose.

Although median ACTH concentration decreased using both doses of ERC, ACTH concentration remained above the seasonal reference range in around half the treated horses. Whilst this appears

disappointing, similar responses are identified in response to treatment of PPID with pergolide, with only 30% of horses having seasonally normal ACTH concentrations following treatment with this oral dopaminergic agonist (19, 20). Season has a profound effect on ACTH concentrations (21–23); however, it remains unclear whether the return of ACTH concentrations to within seasonal reference ranges should be an objective of treatment to optimise equine welfare in PPID (24). Inconsistent responses to treatment, as observed among horses treated with ERC in the present study, has also been reported following pergolide treatment (20). Inconsistency of response has been attributed both to inter-horse variability in pharmacokinetics and pharmacodynamics of dopaminergic agonists and to the heterogeneous and progressive nature of PPID (20, 25).

Whilst it can be challenging to assess objectively, clinical response to PPID treatment is ultimately more important than endocrine response (2, 24), and the owners of 83.9% of horses in this study reported improvement in clinical signs. However, owners were not blinded and were therefore subject to bias. Hypertrichosis, weight loss, history of laminitis, and muscle atrophy were the most common presenting signs in this study, consistent with previous reports (24, 26, 27). Decreases in hypertrichosis, laminitis occurrence and the reversal of weight loss and muscle atrophy have been used to assess clinical response to pergolide (24, 26, 27), with time to the improvement of clinical signs ranging from 2 months to 3–4 years (20, 26, 27). Clinical responses observed in this study are therefore consistent with those reported with pergolide. Treatment with ERC was not associated with post-prandial insulin responses in the small subset of horses where insulin measurements were performed. This is consistent with a previous study in horses which demonstrated that cabergoline does not affect the insulin response to a glucose challenge (17), and similar findings have also been reported with pergolide (28).

All but one owner in the current study cited difficulty in administering a daily oral medication as a reason to commence ERC treatment. All owners reported good compliance with ERC treatment. A study in Australia estimated that almost 70% of horses over 15 years of age lived exclusively at pasture, suggesting ageing horses are managed less intensively, which may make it more challenging and less appealing to medicate them daily in feed or by mouth (3). The extended-release nature of cabergoline offers an advantage in cases where daily administration of pergolide presents challenges with practicality and, therefore, compliance (29). Compliance in human and veterinary medicine is an emerging area of research in which equine medicine lags behind, with few studies having been performed. One report found that horse owners were less compliant compared to small animal owners, and veterinarians significantly overestimated client compliance (30). This is further supported by a recent survey from the UK, which compared the amount of pergolide used with the amount that should have been dispensed and showed that compliance was very poor, with only 48% of owners purchasing ≥90% of the amount required to supply the prescribed dose (9). This study also found that age and breed had a significant effect, with compliance being extremely low in owners of Shetland ponies and horses ≥26 yrs old (9). Previous studies have also demonstrated that routine health care was less frequently performed in aged animals (7, 8), suggesting that owners may be less committed to, and compliant with, healthcare recommendations in older horses (9). In addition to reducing the time and effort involved in treating PPID, the ERC injection allows for precise dosing, which may also offer advantages over pergolide tablets in smaller ponies where splitting of tablets may pose challenges for owners and potentially reduce compliance (9).

The HDERC initially used in this study was based on previous studies in horses (10, 11, 17). One report compared the effects of this 0.01 mg/kg dose of cabergoline (a different formulation to the one used in the current study) and pergolide on prolactin concentration and demonstrated that the suppressive effects of cabergoline lasted at least 10 days compared to an intra-muscular injection of pergolide, which only produced 24 h of suppression (11). Following injection every 10 days, cabergoline has also been shown to suppress plasma MSH concentrations (17). The authors' anecdotal experience of using the ERC preparation used in the current study suggests a rapid onset of action and variable duration of effect, with ACTH concentration dropping within a few days and remaining suppressed for up to 2 weeks. In most horses, ACTH concentration appears to start to increase after 7 to 10 days hence the recommended 7 days treatment interval. Pharmacokinetic and pharmacodynamic studies of ERC in horses are required to determine the optimal dosing regimen. Preliminary observations from this study suggest the LDERC might be more appropriate for further study than the HDERC, as clinical responses were similar and there were less unwanted effects. Adverse events were noted in both groups; however, fewer cases of anorexia were reported in the LDERC compared with HDERC (30.0% vs. 60%), albeit case numbers were small. Anorexia is also reported following pergolide administration (1, 31); however, in this study, some horses demonstrated anorexia following pergolide administration but not ERC and vice versa. It is unclear why this is the case. Despite the variability which exists, ERC may offer an alternative treatment for horses which are unable to tolerate pergolide due to adverse effects.

Previous studies investigating the use of ERC in normal horses have not reported any adverse effects (10, 11, 17). In all cases where partial anorexia was reported in the current study, the owners observed that horses had a preference for long-stem forage (hay or grass) over cereal-based feeds. In humans, the use of dopaminergic agonists has been associated with feelings of nausea (32, 33), which may explain the reduction in feed intake in horses. A significant reduction in feed intake has also been observed in dairy cows following a single injection of ERC (34). The reduction in prolactin concentration that occurs with cabergoline administration (10) may suppress appetite, as prolactin has been shown to stimulate food intake in other species (34, 35). The two horses that suffered from anorexia for longer than 24 h had significant dental disease, both having lost several molars and having had incisors extracted for the treatment of equine odontoclastic tooth resorption and hypercementosis, a common disorder affecting older horses (36, 37). As a result, neither were able to chew long-stem forage. Whilst anorexia from pergolide administration might be resolved by abruptly reducing the dose (1), the long-acting nature of ERC does not allow for such rapid drug withdrawal. Until further investigations are performed, veterinary surgeons should be cognisant of the possibility that ERC may have a more profound effect on feed intake in horses with significant dental pathology.

This study provides preliminary data and is limited by retrospective data collection, lack of an untreated control or placebo group, small sample size, and short follow-up period. However, the results suggest that once weekly injection of extended release cabergoline may be an effective treatment for horses with PPID and provides a basis for designing more robust investigations. A dose of

0.005 mg/kg may be more appropriate for the treatment of PPID than the 0.01 mg/kg dose that has been reported in horses previously. Larger, blinded, randomised clinical trials and studies on the pharmacokinetics and pharmacodynamics of ERC are warranted.

Data availability statement

The original contributions presented in the study are included in the article/supplementary material, further inquiries can be directed to the corresponding author.

Ethics statement

The requirement of ethical approval was waived by University of Murdoch Animal Ethics Committee, Perth for the studies involving animals because collation of clinical data was retrospective. The studies were conducted in accordance with the local legislation and institutional requirements. Written informed consent was obtained from the owners for the participation of their animals in this study.

Author contributions

TS: Conceptualization, Investigation, Methodology, Supervision, Writing – original draft, Writing – review & editing. EK: Conceptualization, Data curation, Formal analysis, Investigation, Methodology, Writing – original draft, Writing – review & editing. GR: Conceptualization, Formal analysis, Writing – review & editing. DR: Investigation, Supervision, Writing – review & editing.

Funding

The author(s) declare that financial support was received for the research, authorship, and/or publication of this article. BOVA Aus subsidised the costs of the extended release cabergoline and some laboratory testing.

Acknowledgments

The authors are grateful to the owners of the horses for sharing their clinical data.

Conflict of interest

DR provides consultancy services to BOVA Aus, BOVA UK and Luoda Pharma, who have developed and produced the extended release cabergoline preparation that was investigated. TS has received subsidised travel expenses from BOVA Aus for attending CPD events.

The remaining authors declare that the research was conducted in the absence of any commercial or financial relationships that could be construed as a potential conflict of interest.

Publisher's note

References

1. McFarlane D. Equine pituitary pars intermedia dysfunction. *Vet Clin North Am Equine Pract*. (2011) 27:93–113. doi: 10.1016/j.cveq.2010.12.007

2. Durham AE. Endocrine disease in aged horses. *Vet Clin North Am Equine Pract*. (2016) 32:301. doi: 10.1016/j.cveq.2016.04.007

3. McGowan T, Pinchbeck G, Phillips C, Perkins N, Hodgson D, McGowan C. A survey of aged horses in Queensland, Australia. Part 1: management and preventive health care. *Aust Vet J*. (2010) 88:420–7. doi: 10.1111/j.1751-0813.2010.00637.x

4. Secombe C, Bailey S, Laat M d, Hughes K, Stewart A, Sonis J, et al. Equine pituitary pars intermedia dysfunction: current understanding and recommendations from the Australian and New Zealand equine endocrine group. *Aust Vet J*. (2018) 96:233–42. doi: 10.1111/avj.12716

5. Durham A, McGowan C, Fey K, Tamzali Y, Van Der KJ. Pituitary pars intermedia dysfunction: diagnosis and treatment. *Equine vet Educ*. (2014) 26:216–23. doi: 10.1111/eve.12160

6. Tatum R, McGowan C, Ireland J. Efficacy of pergolide for the management of equine pituitary pars intermedia dysfunction: a systematic review. *Vet J*. (2020) 266:105562–2. doi: 10.1016/j.tvjl.2020.105562

7. Ireland JL, Clegg PD, McGowan CM, McKane SA, Pinchbeck GL. A cross-sectional study of geriatric horses in the United Kingdom. Part 2: health care and disease. *Equine Vet J*. (2011) 43:37–44. doi: 10.1111/j.2042-3306.2010.00142.x

8. Ireland JL, McGowan CM, Clegg PD, Chandler KJ, Pinchbeck GL. A survey of health care and disease in geriatric horses aged 30 years or older. *Vet J*. (2010) 192:57–64. doi: 10.1016/j.tvjl.2011.03.021

9. Hague N, Durham AE, Menzies-Gow NJ. Pergolide dosing compliance and factors affecting the laboratory control of equine pituitary pars intermedia dysfunction. *Vet Rec*. (2021) 189:e142. doi: 10.1002/vetr.142

10. Hebert R, Thompson D, Mitcham P, Lestelle J, Gilley R, Burns P. Inhibitory effects of Pergolide and Cabergoline formulations on daily plasma prolactin concentrations in geldings and on the daily prolactin responses to a small dose of Sulpiride in mares. *J Equine Vet*. (2013) 33:773–8. doi: 10.1016/j.jevs.2012.12.006

11. Valencia NA, Thompson DL, Oberhaus EL. Long-term and short-term dopaminergic (Cabergoline) and Antidopaminergic (Sulpiride) effects on insulin response to glucose, glucose response to insulin, or both in horses. *J Equine Vet*. (2017) 59:95–103. doi: 10.1016/j.jevs.2017.10.008

12. Curran MP, Perry CM. Cabergoline. *Drugs*. (2004) 64:2125–41. doi: 10.2165/00003495-200464180-00015

13. Ferriere A, Cortet C, Chanson P, Delemer B, Caron P, Chabre O, et al. Cabergoline for Cushing's disease: a large retrospective multicenter study. *Eur J Endocrinol*. (2017) 176:305–14. doi: 10.1530/eje-16-0662

14. Alexandraki KI, Grossman AB. Pituitary-targeted medical therapy of Cushing's disease. *EOIDER*. (2008) 17:669. doi: 10.1517/13543784.17.5.669

15. Contin M, Riva R, Albani F, Baruzzi A. Pharmacokinetic optimisation of dopamine receptor agonist therapy for Parkinson's disease. *CNS Drugs*. (2000) 14:439–55. doi: 10.2165/00023210-200014060-00003

16. Shaojian L, Anke Z, Xun Z, Zhe BW. Treatment of pituitary and other tumours with Cabergoline: new mechanisms and potential broader applications. *Neuroendocrinology*. (2020) 110:477–88. doi: 10.1159/000504000

17. Valencia NA, Thompson DL, Oberhaus EL, Gilley RM. Long-term treatment of insulin-insensitive mares with Cabergoline: effects on prolactin and melanocyte stimulating hormone responses to sulpiride and on indices of insulin sensitivity. *J Equine Vet*. (2014) 34:680–6. doi: 10.1016/j.jevs.2013.12.015

18. Secombe CJ, Tan RHH, Perara DI, Byrne DP, Watts SP, Wearn JG. The effect of geographic location on circannual adrenocorticotropic hormone plasma concentrations in horses in Australia. *J Vet Intern Med*. (2017) 31:1533–40. doi: 10.1111/jvim.14782

19. Schott H, Coursen C, Sw E, Nachreiner R, Refsal K, Ewart S, et al. *The Michigan Cushing's project. Proceedings of the annual convention of the Association of American Equine Practitioners*. (2001) 22–24.

20. Durham AE. Therapeutics for equine endocrine disorders. *Vet Clin North Am: Equine Pr*. (2017) 33:127–39. doi: 10.1016/j.cveq.2016.11.003

21. McFarlane D, Banse H, Knych HK, Maxwell LK. Pharmacokinetic and pharmacodynamic properties of pergolide mesylate following long-term administration to horses with pituitary pars intermedia dysfunction. *J Vet Pharmacol Ther*. (2017) 40:158–64. doi: 10.1111/jvp.12339

22. McFarlane D, Donaldson MT, McDonnell SM, Cribb AE. Effects of season and sample handling on measurement of plasma α-melanocyte-stimulating hormone concentrations in horses and ponies. *Am J Vet Res*. (2004) 65:1463–8. doi: 10.2460/ajvr.2004.65.1463

23. Schreiber CM, Stewart AJ, Kwessi E, Behrend EN, Wright JC, Kemppainen RJ, et al. Seasonal variation in results of diagnostic tests for pituitary pars intermedia dysfunction in older, clinically normal geldings. *J Am Vet Med Assoc*. (2012) 241:241–8. doi: 10.2460/javma.241.2.241

24. Perkins GA, Lamb S, Erb HN, Schanbacher B, Nydam DV, Divers TJ. Plasma adrenocorticotropin (ACTH) concentrations and clinical response in horses treated for equine Cushing's disease with cyproheptadine or pergolide. *Equine Vet J*. (2002) 34:679–85. doi: 10.2746/042516402776250333

25. Meyer JC, Hunyadi LM, Ordóñez-Mena JM. The accuracy of ACTH as a biomarker for pituitary pars intermedia dysfunction in horses: a systematic review and meta-analysis. *Equine Vet J*. (2022) 54:457–66. doi: 10.1111/evj.13500

26. Rohrbach BW, Stafford JR, Clermont RSW, Reed SM, Schott HC, Andrews FM. Diagnostic frequency, response to therapy, and long-term prognosis among horses and ponies with pituitary par intermedia dysfunction, 1993–2004. *J Vet Intern Med*. (2012) 26:1027–34. doi: 10.1111/j.1939-1676.2012.00932.x

27. Spelta C, Axon J. Case series of equine pituitary pars intermedia dysfunction in a tropical climate. *Aust Vet J*. (2012) 90:451–6. doi: 10.1111/j.1751-0813.2012.00997.x

28. Gehlen H, May A, Bradaric Z. Comparison of insulin and glucose metabolism in horses with pituitary pars intermedia dysfunction treated versus not treated with Pergolide. *J Equine Vet*. (2014) 34:508–13. doi: 10.1016/j.jevs.2013.11.001

29. Furtado T, Rendle D. To improve welfare in the equine species should we place greater emphasis on understanding our own? *Equine Vet J*. (2022) 54:1001–4. doi: 10.1111/evj.13869

30. Verker M, van Stokrom M, Endenburg N. How can veterinarians optimise owner compliance with medication regimes. *Eur J Companion Anim Pract*. (2008) 18:73–7.

31. Schott HC. Pituitary pars intermedia dysfunction: equine Cushing's disease. *Vet Clin North Am Equine Pract*. (2002) 18:237–70. doi: 10.1016/s0749-0739(02)00018-4

32. Pivonello R, Martino MCD, Cappabianca P, Leo MD, Faggiano A, Lombardi G, et al. The medical treatment of Cushing's disease: effectiveness of chronic treatment with the dopamine agonist Cabergoline in patients unsuccessfully treated by surgery. *J Clin Endocrinol Metab*. (2009) 94:223–30. doi: 10.1210/jc.2008-1533

33. Martins D, Mehta MA, Prata D. The "highs and lows" of the human brain on dopaminergics: evidence from neuropharmacology. *Neurosci Biobehav Rev*. (2017) 80:351–71. doi: 10.1016/j.neubiorev.2017.06.003

34. Larsen M, Franchi G, Herskin M, Foldager L, Larsen M, Hernández-Castellano L, et al. Effects of feeding level, milking frequency, and single injection of cabergoline on feed intake, milk yield, milk leakage, and clinical udder characteristics during dry-off in dairy cows. *J Dairy Sci*. (2021) 104:11108–25. doi: 10.3168/jds.2021-20289

35. Woodside B. Prolactin and the hyperphagia of lactation. *Physiol Behav*. (2007) 91:375–82. doi: 10.1016/j.physbeh.2007.04.015

36. Henry TJ, Puchalski SM, Arzi B, Kass PH, Verstraete FJM. Radiographic evaluation in clinical practice of the types and stage of incisor tooth resorption and hypercementosis in horses. *Equine Vet J*. (2017) 49:486–92. doi: 10.1111/evj.12650

37. Staszyk C, Bienert A, Kreutzer R, Wohlsein P, Simhofer H. Equine odontoclastic tooth resorption and hypercementosis. *Vet J*. (2008) 178:372–9. doi: 10.1016/j.tvjl.2008.09.017

frontiers | Frontiers in Veterinary Science

TYPE Case Report
PUBLISHED 09 April 2024
DOI 10.3389/fvets.2024.1334813

OPEN ACCESS

EDITED BY
Mindaugas Tamosiunas,
University of Latvia, Latvia

REVIEWED BY
Masahiro Murakami,
Purdue University, United States
Pete Mantis,
Dick White Referrals, United Kingdom

*CORRESPONDENCE
Elli Elizabeth Michaelidou
✉ elli.el.micha@gmail.com

†These authors have contributed equally to this work and share senior authorship

RECEIVED 07 November 2023
ACCEPTED 26 March 2024
PUBLISHED 09 April 2024

CITATION
Michaelidou EE, Kaczmarska A, Gutierrez-Quintana R, Morris J, Hammond G and Cloquell A (2024) Case report: MRI and CT imaging features of a melanocytic tumour affecting a cervical vertebra in an adult dog, and review of differential diagnosis for T1W-hyperintense lesions.
Front. Vet. Sci. 11:1334813.
doi: 10.3389/fvets.2024.1334813

Case report: MRI and CT imaging features of a melanocytic tumour affecting a cervical vertebra in an adult dog, and review of differential diagnosis for T1W-hyperintense lesions

Elli Elizabeth Michaelidou*, Adriana Kaczmarska, Rodrigo Gutierrez-Quintana, Joanna Morris, Gawain Hammond† and Ana Cloquell†

Institute of Biodiversity, Animal Health and Comparative Medicine, University of Glasgow, Glasgow, United Kingdom

A 7-year-old Lhasa Apso presented with a history of left thoracic limb lameness and neck pain. Magnetic resonance imaging revealed a well-defined, extradural lesion that was hyperintense on T1-weighted (T1W) images and isointense on T2-weighted (T2W) images and T2* images located at the left lamina of the C4 vertebra. Computed tomography showed an isoattenuating and contrast-enhancing mass centered on the left C4 vertebral lamina with associated osteolysis. The mass was surgically debulked, and histopathology revealed a malignant melanocytic tumour. The patient recovered completely and received radiotherapy and three doses of the melanoma vaccine as adjunctive treatment. Eighteen months following treatment, the patient presented with neck pain again, but further investigations were declined at this stage, and the patient was euthanised. To the author's knowledge, this is the first case report describing the imaging characteristics of a cervical extradural melanocytic tumour in a dog. This case illustrates the MRI and CT imaging features and treatment of a canine melanocytic tumour of the cervical vertebrae.

KEYWORDS

melanocytic neoplasia, Melan-A, T1W hyperintensity, cervical vertebra, melanoma of unknown primary, melanotic schwannoma, case report

1 Introduction

Primary melanocytic tumours of the central nervous system (CNS) are rare pathologies, with metastatic melanocytic tumours being more frequent (1). In humans, the majority of melanocytic tumours display characteristic signal patterns on MRI showing T1 and T2 shortening, resulting in T1W hyperintensity and T2W hypointensity (2). In general, apart from lipids, methaemoglobin and proteinaceous material, this T1W hyperintense appearance of the lesion is rarely observed on MRI (3) and only a few substances amongst which melanin, can create this T1W hyperintensity of the lesion (4). This case report describes the imaging

findings and treatment of a melanocytic tumour affecting the cervical vertebra in an adult dog and a systematic approach to T1W hyperintense lesions on MRI.

2 Case description

A 7-year-old, 6.6 kg, male-neutered Lhasa Apso presented with a 3-month history of progressive left thoracic limb lameness and episodes of yelping. On presentation, the physical examination was unremarkable. Neurological examination revealed mild lameness and reduced postural reactions of the left thoracic limb, with severe pain on ventroflexion of the neck. The remainder of the neurological examination was normal. Neuroanatomical localisation was consistent with a left-sided lesion of the C6-T2 spinal cord segments. Haematology and serum biochemistry were normal. The patient was anaesthetised for cervical magnetic resonance imaging (MRI) using a 1.5-Tesla system (Magnetom Essenza, Siemens, Camberley, United Kingdom; MRI acquisition protocol is summarized in Supplementary Table S1) with a head–neck coil. A solitary, rounded, 10 mm diameter extradural, well-defined mass lesion was observed at the level of the left lamina and pedicle of the C4 vertebra, causing osteolysis (Figure 1). The mass was isointense on T2-weighted (T2W) images (with a central hyperintense cleft) (Figure 1A), markedly hyperintense on T1-weighted (T1W) images (Figure 1C), and with no signal voids on T2* (Figure 1D). Although the mass was suppressed on the short tau inversion recovery (STIR) sequence, there was no suppression on the specific fat-saturation (FAT-SAT) sequences, excluding a lipid-containing lesion (Figures 1B,E). Due to marked T1W hyperintensity, subtraction images were used for further evaluation of the contrast enhancement, which was homogenous and marked, associated with a linear and irregular enhancement of the adjacent periosteum and meninges. The lesion was causing spinal cord compression at the level of C4. The C4 left nerve root appeared enlarged and T1W hyperintense, with contrast enhancement of the adjacent cervical epaxial muscle.

Given the suspicion of a melanin-containing lesion following the MRI, a careful examination of the skin, oral cavity, and eyes was performed, which did not reveal any lesions. Computed tomography (CT) of the entire vertebral column, thorax, and abdomen was performed using an 80-slice helical scanner with 120 kVp, 112 mAs, and 1.0 mm slice thickness (Aquilion Lightning, Canon, Duluth, United States). Images were reconstructed using medium- and high-frequency spatial algorithms after intravenous ioversol (Optiray 300 mg/mL, Guerbet, Roissy CdG, France) was administered (2 mL/kg) via a power injector (Injectron 82CT, MedTron AG, Germany) at a rate of 5 mL/s through the cephalic vein. CT demonstrated an osteodestructive, isoattenuating, well-demarcated, homogenously enhancing mass within the left lamina, also affecting the left pedicle and the cranial and caudal articular processes of C4 extending into the vertebral canal and into the left transverse foramen (Figure 2). Bone proliferation was not observed, nor was there evidence of metastatic disease or other primary neoplasms.

The patient underwent a left C4 hemilaminectomy, which revealed a black pigmented mass bulging through the C4 lamina. The left lamina of C4 and the articular process were removed, which allowed an en-block debulking of the mass. Although no infiltration or attachment to the meninges or nerve roots were

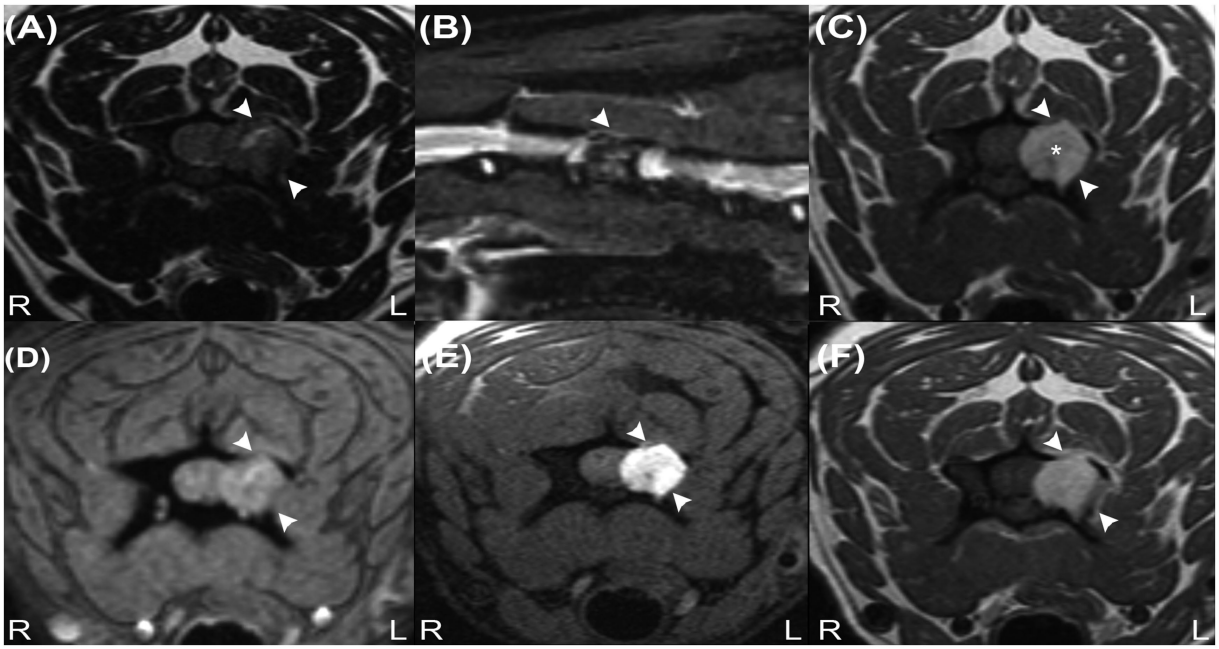

FIGURE 1
Transverse T2W image **(A)**, sagittal STIR image **(B)**, transverse precontrast T1W images **(C)**, transverse T2* image **(D)**, transverse T1W fat-suppressed precontrast image **(E)** and transverse contrast-enhanced T1W image **(F)** revealing an extradural mass at the level of the C4 vertebra (arrowheads). Note the characteristic hyperintense signal on image **(C)** (asterisk) and signal suppression on image **(B)** but absence of signal suppression on image **(E)**, indicating that the lesion does not contain fat tissue. The absence of signal voids on image **(D)** reveals that haemorrhage and calcifications are unlikely to be present in the mass.

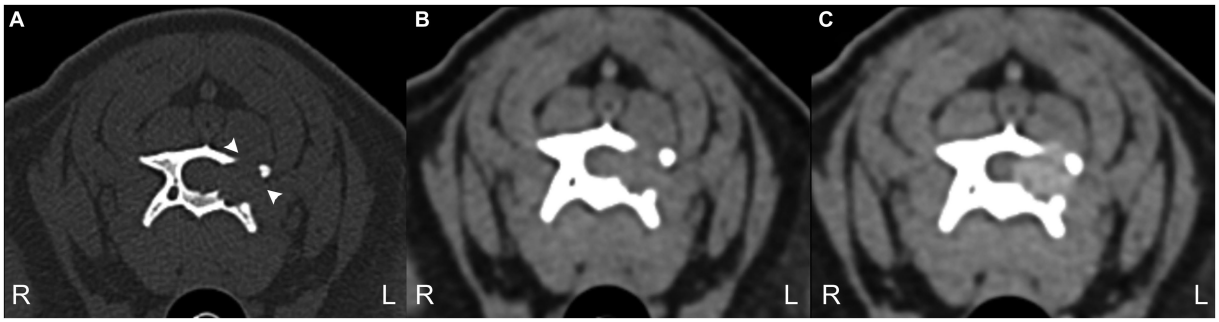

FIGURE 2
3 CT transverse images bone window **(A)** and soft tissue window precontrast **(B)** and post-contrast **(C)** at the level of C4 vertebra. Note the geographical bone resorption of the left lamina of C4 (arrowheads) and the moderate contrast enhancement of the mass. The mass demonstrated a mean of 58 Hounsfield units.

observed, the ventrolateral aspect of the exposed vertebra following mass dissection retained a black discolouration, suggesting neoplastic infiltration. The cavitron ultrasonic surgical aspirator (CUSA: Integra LifeSciences Corporation, NJ, United States) was used at that level. As clear margins were not achievable, adjunctive radiotherapy was implemented 4 weeks after surgery (48Gy in 16 daily fractions). Histopathological and immunohistochemical examination of the mass revealed a well-differentiated infiltrating tumour with a high mitotic count (12 per 10HPF), positive for Melan-A, confirming a malignant melanocytic neoplasm. To delay metastatic spread, the patient also received three doses of the melanoma vaccine (Oncept, Merial Inc., Athens, GA, United States). The patient recovered after initial treatment, but 15 months following treatment, the patient exhibited an episode of neck pain. Further investigations at this stage were declined, and the patient was euthanised 18 months following the diagnosis. A post-mortem examination was declined.

3 Discussion

This case report presents a T1W hyperintense lesion of the cervical vertebra. On MRI, most substances and pathologies are hypointense on T1W images (3), as only a few naturally occurring substances are known to reduce T1 relaxation times (4), including; lipids, methaemoglobin, minerals (calcium, iron, copper, and manganese), proteins (including vasopressin-neurophysin II-copeptin complex), melanin, and gadolinium contrast agents (3, 4). Melanocytic tumours have been described as having the following imaging characteristics on MRI; T1W hyperintensity and T2W isointensity to hypointensity (5). In human literature, the paramagnetic properties of melanin are thought to be the reason behind these signal intensities (4). The melanocytic tumour in our case shares these typical MRI characteristics. Moreover, these have also been reported in a cat with an extradural melanoma within the lumbar region (6). However, there are reports indicating that this is not always the case. An example of this includes a recent case of an extradural melanoma affecting a thoracic vertebra in a dog, where the lesion was hyperintense on both T1W and T2W images (7). Similarly, a case of meningeal melanomatosis characterised by T1W hyperintensity and T2W hyperintensity with a few small areas demostrating T2W hypointensity has also been described in the literature (8). The cause of these atypical MRI findings is not completely understood. One of the current hypotheses includes alteration of the typical MRI signals by blood products from intratumoral haemorrhage (6).

The differential diagnoses for a T1W hyperintense lesion can be narrowed using can be narrowed using localization and morphology of pathologies that cause the characteristic T1W hyperintensity, along with the evaluation of other MRI sequences or imaging techniques (3, 4). We propose a systematic approach detailed in Figure 3. The first step evaluates adipose tissue content using fat suppression sequences such as STIR and FAT-SAT (9). In this case, the mass' signal was suppressed on STIR. However, as other tissues with short T1 relaxation may also be suppressed (10), fat-saturation was applied, showing a hyperintense mass, which excluded a lipid-containing lesion. To evaluate the content of haemoglobin and calcium, the T2* sequence was used. Signal voids on T2* were not observed, ruling out a calcified and likely haemorrhagic lesion. It is important to note that not all stages of haemorrhage will demonstrate a signal void on T2*. Oxyhaemoglobin, a diamagnetic substance (seen in the initial stages of haemorrhage), does not create signal voids, which in contrast to deoxyhaemoglobin and methaemoglobin, which have paramagnetic properties and induce faster T2* relaxation times, which result in signal voids (11–14). The CT characteristics supported these findings, as the Hounsfield units of the mass were not compatible with lipid, haemorrhage, or mineralization. Other minerals, such as iron, copper, and manganese, were considered unlikely, as their accumulation in the body is related to metabolic disturbances, usually creating bilateral and symmetrical parenchymal lesions (4). Similarly, based on the mass' localisation, the presence of vasopressin was excluded (4, 15). Thus, a melanin-containing or proteinaceous lesion was the most likely cause of the T1W hyperintensity. Protein-containing lesions are usually hyperintense on T2W sequences. However, T2 relaxation times may vary depending on the amount of free water, protein content, and viscosity (3, 4). The T2W intensity in our case, suggested a melanin-containing lesion, which was considered more likely as it usually appears hypointense on these sequences (16). Despite the accuracy that may be achieved via evaluating all imaging sequences and diagnostic methods, histopathology remains the gold standard technique (17, 18). In this case report, the histopathological analysis and the positive result for Melan-A immunohistochemistry confirmed the presence of a melanocytic neoplasm.

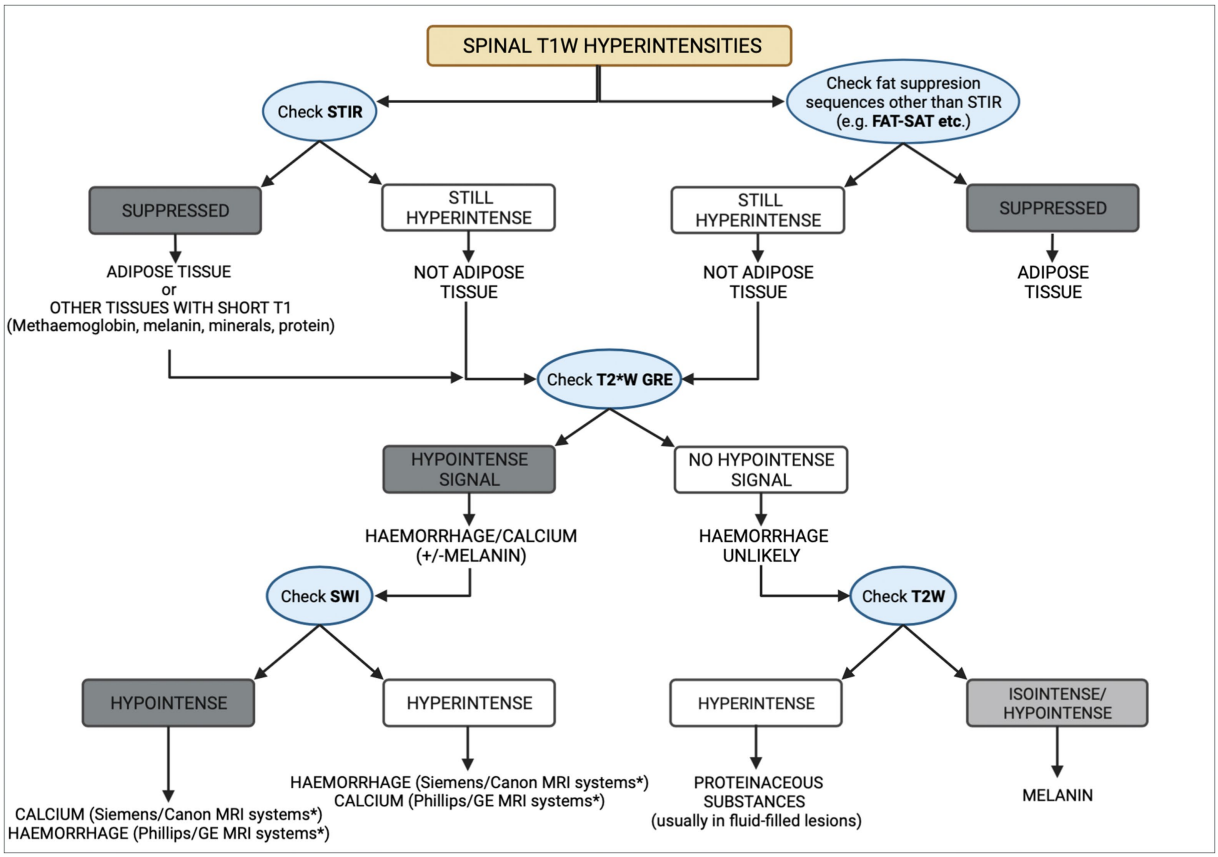

FIGURE 3
Diagram representing a methodical approach to the differential diagnoses of T1W spinal hyperintensities. CT can aid in the process, by taking into consideration the Hounsfield units of different substances. Asterisk (*) indicates the appearance of haemorrhage and calcium on susceptibility weighted imaging (SWI) studies which depends on the system manufacturer, with Siemens and Canon using a left-handed reference scheme and GE and Phillips using a right-handed reference scheme.

Melanocytic neoplasms arise from melanocytes, which originate from the neural crest during embryogenesis and migrate to the skin, mucous membranes, and the CNS. Melanoma is common in dogs, usually involving the oral cavity, nailbed, eye, skin, and genitals (19, 20), with metastases reported in lymph nodes, the lung, brain, heart, spleen, and bone (20). Primary melanocytic tumours (melanocytoma, melanoma, melanocytosis, and melanomatosis) of the CNS are rare (1) but metastatic melanomas are more common (1, 21), with intracranial (22), intramedullary (23), and vertebral (24) involvement being documented in veterinary medicine. Additionally, primary CNS tumours such as schwannomas (25) and gliomas (26) may undergo melanisation. In human medicine, melanoma of unknown primary (MUP) refers to metastatic melanoma occurring in lymph nodes, subcutaneous tissue, or visceral sites in the absence of a detectable primary tumour (27). MUP may affect the vertebral column in humans (28–30), but it has not been documented in veterinary medicine.

Despite the imaging and histopathological findings in this case, it was not possible to differentiate between a MUP affecting the C4 vertebra (no primary lesion was found) or a melanotic schwannoma. Although MUP has not been previously described in dogs, there was no obvious involvement of the nerve roots or meninges observed during surgery, making melanocytic schwannoma less likely. Achieving a final diagnosis between melanotic schwannomas and melanocytic lesions can be challenging because both are histologically similar. Immunohistochemical stains are not always useful because all lesions generally express S-100 and one or more melanocytic markers. Stains for components of the basement membrane can be used to discriminate schwannomas, but overlapping staining patterns have been observed with other melanocytic lesions. Therefore, in human medicine, mutational analyses are being developed (31).

To the author's knowledge, MRI and CT findings of a solitary melanocytic mass affecting the cervical vertebral column, without an identified primary site, have not been previously reported in dogs. These findings may provide the imaging characteristics for future recognition of melanin-containing masses, as well as a systematic approach to T1W hyperintense lesions. Although MRI can assist with the differential diagnosis, histopathological examination remains essential for a definitive diagnosis (32).

4 Conclusion

To the author's knowledge, this case describes the first documented melanocytic neoplasia affecting the cervical vertebra in an adult canine and its surgical and medical management. This report provides

the basis for recognizing such neoplasms in the future, as well as a diagram that can aid the clinician in narrowing down their differential diagnoses of a T1W hyperintense lesion in the spine.

Data availability statement

The original contributions presented in the study are included in the article/Supplementary material, further inquiries can be directed to the corresponding author.

Ethics statement

Ethical approval was not required for the studies involving animals in accordance with the local legislation and institutional requirements because this was a retrospective case report of a canine patient seen at the Neurology Department of Glasgow's University Small Animal Hospital. The patient was referred for further veterinary care due to cervical pain and thoracic lameness. Written informed consent was obtained from the owners for the participation of their animals in this study.

Author contributions

EM: Conceptualization, Software, Writing – original draft, Writing – review & editing. AK: Conceptualization, Supervision, Validation, Visualization, Writing – review & editing, Writing – original draft. RG-Q: Supervision, Validation, Visualization, Writing – review & editing, Writing – original draft. JM: Supervision, Validation, Visualization, Writing – review & editing, Writing – original draft. GH: Software, Supervision, Validation, Visualization, Writing – review & editing, Writing – original draft. AC: Conceptualization, Supervision, Validation, Visualization, Writing – review & editing, Writing – original draft.

Funding

The author(s) declare that no financial support was received for the research, authorship, and/or publication of this article.

Acknowledgments

The authors gratefully acknowledge Dr. Angie Rupp's and Dr. Francesco Marchesi's contribution to the histopathological examination and radiographers Nicola Brennan and Gill Cameron.

Conflict of interest

The authors declare that the research was conducted in the absence of any commercial or financial relationships that could be construed as a potential conflict of interest.

Publisher's note

All claims expressed in this article are solely those of the authors and do not necessarily represent those of their affiliated organizations, or those of the publisher, the editors and the reviewers. Any product that may be evaluated in this article, or claim that may be made by its manufacturer, is not guaranteed or endorsed by the publisher.

Supplementary material

The Supplementary material for this article can be found online at: https://www.frontiersin.org/articles/10.3389/fvets.2024.1334813/full#supplementary-material

References

1. Van der Weyden L, Brenn T, Patton EE, Wood GA, Adams DJ. Spontaneously occurring melanoma in animals and their relevance to human melanoma. *J Pathology*. (2020) 252:4–1. doi: 10.1002/path.5505

2. Marx HF, Colletti PM, Raval JK, Boswell WD Jr, Zee CS. Magnetic resonance imaging features in melanoma. *Magn Reson Imaging*. (1990) 8:223–9. doi: 10.1016/0730-725X(90)90093-H

3. Zimny A, Zińska L, Bladowska J, Neska-Matuszewska M, Sąsiadek M. Intracranial lesions with high signal intensity on T1-weighted MR images - review of pathologies. *Pol J Radiol*. (2013) 78:36–46. doi: 10.12659/PJR.889663

4. Ginat DT, Meyers SP. Intracranial lesions with high signal intensity on T1-weighted MR images: differential diagnosis. *Radiographics*. (2012) 32:499–516. doi: 10.1148/rg.322105761

5. Albastaki A, Ahmed S, Khan A, Farhan A, Almayman T. Malignant Melanoma Presenting as Spinal Cord and Pleural Lesions. *Case Rep Oncol Med*. (2023) 2023:1–6. doi: 10.1155/2023/9647892

6. Fert S, River P, Bondonny L, Cauzinille L. Metastatic extradural melanoma of the lumbar spine in a cat. *Vet Med Sci*. (2023) 9:2393–8. doi: 10.1002/vms3.1248

7. Prodger A, Rodriguez TE, Mallol C, Costa T, Benito M. Atypical magnetic resonance imaging findings of a vertebral melanotic melanoma in a dog. *Vet Rec Case Rep*. (2024):e800. doi: 10.1002/vrc2.800

8. Wu CC, Huang WH, Liao PW, Chang YP. Diagnosis of meningeal melanomatosis in a dog using magnetic resonance imaging and cerebrospinal fluid findings. *J Vet Med Sci*. (2021) 83:94–9. doi: 10.1292/jvms.20-0556

9. D'anjou MA, Carmel EN, Tidwell AS. Value of fat suppression in gadolinium-enhanced magnetic resonance neuroimaging. *Vet Radiol Ultrasound*. (2011) 52:S85–90. doi: 10.1111/j.1740-8261.2010.01789.x

10. Krinsky G, Rofsky NM, Weinreb JC. Nonspecificity of short inversion time inversion recovery (STIR) as a technique of fat supression: pitfalls in image interpretation. *AJR Am J Roentgenol*. (1996) 166:523–6. doi: 10.2214/ajr.166.3.8623620

11. Bradley WG Jr. MR appearance of hemorrhage in the brain. *Radiology*. (1993) 189:15–26. doi: 10.1148/radiology.189.1.8372185

12. Bren KL, Eisenberg R, Gray HB. Discovery of the magnetic behavior of hemoglobin: A beginning of bioinorganic chemistry. *Proc Natl Acad Sci USA*. (2015) 112:13123–7. doi: 10.1073/pnas.1515704112

13. Mallol C, Gutierrez-Quintana R, Hammond G, Schweizer-Gorgas D, De Decker S, Novellas R, et al. MRI features of canine hemangiosarcoma affecting the central nervous system. *Vet Radiol Ultrasound*. (2022) 63:185–96. doi: 10.1111/vru.13041

14. Weston P, Morales C, Dunning M, Parry A, Carrera I. Susceptibility weighted imaging at 1.5 Tesla magnetic resonance imaging in dogs: Comparison with T2*-weighted gradient echo sequence and its clinical indications. *Vet Radiol Ultrasound*. (2020) 61:566–76. doi: 10.1111/vru.12894

15. Bonneville F, Cattin F, Marsot-Dupuch K, Dormont D, Bonneville JF, Chiras J. T1 signal hyperintensity in the sellar region: spectrum of findings. *Radiographics*. (2006) 26:93–113. doi: 10.1148/rg.261055045

16. Lee NK, Lee BH, Hwang YJ, Sohn MJ, Chang S, Kim YH, et al. Findings from CT, MRI, and PET/CT of a primary malignant melanoma arising in a spinal nerve root. *Eur Spine J*. (2010) 19:174–S178. doi: 10.1007/s00586-010-1285-1

17. Laborda-Vidal P, Martin M, Orts-Porcar M, Vilalta L, Melendez-Lazo A, de Carellán AG, et al. Computed tomography guided needle biospies of vertebral and paravertebral lesions in small animals. *Animals (Basel)*. (2022) 12:1688. doi: 10.3390/ani12131688

18. Prömmel P, Pilgram-Pastor S, Sitter H, Buhk JH, Strik H. Neoplastic meningitis: how MRI and CSF cytology are influenced by CSF cell count and tumor type. *Sci World J*. (2013) 2013:248072:1–5. doi: 10.1155/2013/248072

19. Cotchin E. Melanotic tumors of dogs. *J Comp Path Therapeutics*. (1955) 65:115–IN14. doi: 10.1016/S0368-1742(55)80011-2

20. Kim DY, Royal AB, Villamil JA. Disseminated melanoma in a dog with involvement of leptomeninges and bone marrow. *Vet Pathol*. (2009) 46:80–3. doi: 10.1354/vp.46-1-80

21. Razmara AM, Wittenburg LA, Al-Nadaf S, Toedebusch RG, Meyers FJ, Toedebusch CM. Prevalence and Clinicopathologic Features of Canine Metastatic Melanoma Involving the Central Nervous System: A Retrospective Analysis and Comparative Review. *Front Oncol*. (2022) 12:868004. doi: 10.3389/fonc.2022.868004

22. Kesdangsakonwut S, Chankow K, Rungsipipat A. Disseminated oral melanoma with brain and gastrointestinal tract involvements in a cocker spaniel: a case report. *Thai J Vet Med*. (2015) 45:141–5. doi: 10.56808/2985-1130.2618

23. Waters DJ, Hayden DW. Intramedullary spinal cord metastasis in the dog. *J Vet Intern Med*. (1990) 4:207–15. doi: 10.1111/j.1939-1676.1990.tb00899.x

24. Rovesti GL, Guandalini A, Peiffer R. Suspected latent vertebral metastasis of uveal melanoma in a dog: a case report. *Vet Ophthalmol*. (2001) 4:75–7. doi: 10.1046/j.1463-5224.2001.00130.x

25. Warren AL, Miller AD, De Lahunta A, Kortz G, Summers BA. Four cases of the melanotic variant of malignant nerve sheath tumour: a rare, aggressive neoplasms in young dogs with a predilection for the spinal cord. *J Comp Pathol*. (2020) 178:1–8. doi: 10.1016/j.jcpa.2020.03.010

26. Schkeeper AE, Moon R, Shrader S, Koehler JW, Linden D, Taylor AR. Imaging diagnosis-magnetic resonance imaging features of a multifocal oligodendrioglioma in the spinal cord and brain of a dog. *Vet Radiol Ultrasound*. (2017) 58:E49–54. doi: 10.1111/vru.12401

27. Scott JF, Gerstenblith MR. *Noncutaneous Melanoma*. Brisbane: Codon Publications (2018).

28. Kakutani K, Doita M, Nishida K, Miyamoto H, Kurosaka M. Radiculopathy due to malignant melanoma in the sacrum with unknown primary site. *Eur Spine J*. (2008) 17:271–4. doi: 10.1007/s00586-007-0561-1

29. Ku A, Henry A, Tunkel R, Lachmann E, Nagler W. Lumbosacral radiculopathy secondary to L5 metastatic melanoma of unknown primary. *Arch Phys Med Rehabil*. (1996) 77:307–9. doi: 10.1016/S0003-9993(96)90118-5

30. Tang S, Zuo J, Zhang H, Wu Z, Liang B. Spinal metastatic melanoma with unknown primary lesions presenting as radiculopathy: case report and literature review. *World Neurosurg*. (2020) 140:320–4. doi: 10.1016/j.wneu.2020.05.067

31. Küsters-Vandevelde HVN, Van Engen-van Grunsven ACH, Küsters B, van Dijk MRCF, Groenen PJTA, Wesseling P, et al. Improved discrimination of melanotic schwannoma from melanocytic lesions by combined morphological and GNAQ mutational analysis. *Acta Neuropathol*. (2010) 120:755–64. doi: 10.1007/s00401-010-0749-z

32. Sun L, Song Y, Gong Q. Easily misdiagnosed delayed metastatic intraspinal extradural melanoma of the lumbar spine: a case report and review of the literature. *Oncology Lett*. (2013) 5:1799–802. doi: 10.3892/ol.2013.1299

frontiers | Frontiers in Veterinary Science

TYPE Brief Research Report
PUBLISHED 31 May 2024
DOI 10.3389/fvets.2024.1345548

OPEN ACCESS

EDITED BY
Ozgur Kaynar,
Kastamonu University, Türkiye

REVIEWED BY
Francesca Arfuso,
University of Messina, Italy
W. Jean Dodds,
Independent Researcher, Santa Monica, California, United States

*CORRESPONDENCE
Toshiro Arai
toshiarai74@gmail.com

RECEIVED 28 November 2023
ACCEPTED 15 May 2024
PUBLISHED 31 May 2024

CITATION
Asahi Y, Arai T and Tanaka Y (2024) Changes in plasma metabolite concentrations and enzyme activities in aging riding horses. *Front. Vet. Sci.* 11:1345548. doi: 10.3389/fvets.2024.1345548

Changes in plasma metabolite concentrations and enzyme activities in aging riding horses

Yukari Asahi, Toshiro Arai* and Yoshikazu Tanaka

School of Veterinary Medicine, Nippon Veterinary and Life Science University, Musashino, Japan

In older horses, basal metabolic rate decreases, and plasma metabolite and hormone concentrations related to energy metabolism change. The occurrence of age-related diseases, which increases in old animals, may enhance inflammatory reactivity (inflammaging). Finding the appropriate treatment for inflammaging at an early stage may prevent various age-related diseases. Changes in metabolite and hormone concentrations and enzyme activities involved in energy metabolism in the plasma of clinically healthy riding horses of various ages were measured to identify biomarkers of inflammaging (persistent low-grade inflammation that occurs with aging). All horses were clinically healthy, and their body condition scores (BCSs) were 4 or 5 (9-point scale). Plasma triglyceride (TG), total cholesterol (T-Cho), blood urea nitrogen (BUN), insulin concentrations, malondialdehyde (MDA), and serum amyloid A (SAA) concentrations generally increased with age. Adiponectin concentrations, plasma superoxide dismutase (SOD), and leukocyte AMP-activated protein kinase (AMPK) activities decreased, while plasma aspartate aminotransferase (AST), alanine aminotransferase (ALT), and glutathione peroxidase (GPx) remained unchanged as horses aged. Although riding horses that partake in continuous exercise seems to be less likely to develop inflammaging, horses over 17 years of age tend to show proinflammatory signs with disordered lipid metabolism. In riding horses, SAA, in combination with other markers, may be a useful biomarker for inflammaging and dysregulated lipid metabolism in aging horses.

KEYWORDS

adiponectin, age-related disease, chronic inflammation, inflammaging, serum amyloid A

1 Introduction

The percentage of horses considered "aged" has been increasing, with estimates of all horses older than 15 years of age ranging from 22 to 34% (1, 2). In older horses, basal metabolic rate decreases (3), and plasma metabolite and hormone concentrations related to energy metabolism change with age (4). The occurrence of age-related diseases increases in old animals (5, 6), and enhanced inflammatory reactivity known as inflammaging may arise with their onset (7, 8). Franceschi et al. termed the persistence of low-grade chronic inflammatory status as inflammaging (9), which involves the accumulation of damaged macromolecules and cellular debris because of increased production and chronically inhibited damage surveillance and repair functions in multiple tissues (10). The secretion of proinflammatory cytokines from senescent cells accumulates in tissues with age, termed "senescence-associated secretory phenotype (SASP)," and contributes to the onset of inflammaging (11). As plasma

concentrations of macromolecules, metabolites, hormones, and enzymes involved in energy metabolism change in animals with age, monitoring these concentrations can aid in detecting inflammaging. Appropriate treatment for inflammaging at an early stage may prevent various age-related diseases. Arfuso et al. reported that serum C-reactive protein (CRP) and α2 macroglobulin concentrations increased in horses with aging, and acute phase proteins (APPs) such as CRP could be good parameters to assess inflammaging in horses (12). In this study, changes in metabolite and hormone concentrations and enzyme activities involved in energy metabolism in the plasma of clinically healthy riding horses of various ages were measured. Macromolecules that vary with age are considered to be useful biomarkers for diagnosing inflammaging in riding horses.

2 Materials and methods

2.1 Animals

In this study, 18 riding horses (Thoroughbred, gelding, 2–23 years of age) maintained at Niiza Riding Club (Saitama, Japan) and Saitama Horse Riding Club (Saitama, Japan) were examined. Their body condition score (BCS) was classified using a 9-point system. Six horses were selected for each of three groups based on age: Group A (adolescent, <10 years old), Group B (middle age, 10–16 years old), and Group C (old age, >17 years old). The horses were fed 5.2–6.4 kg of hay cube, 3.0–4.0 kg of good quality hay, 0–1.3 kg of wheat bran, and 0–1.8 kg of barley at 6:00 and 16:00 daily. Each horse was subjected to exercise, which included walking (2–3 m/s for 5–10 min) and trotting (4–6 m/s for 15–20 min) every day of the week, resting on Sunday, over a 10-week period.

2.2 Collection and preparation of blood samples

Blood samples were taken from the jugular veins of horses and placed in heparinized tubes. Plasma was then recovered by centrifugation at 800 × g for 10 min at 4°C and stored at −25°C until needed for further analysis. Leukocytes were isolated by centrifugation using hypotonic and hypertonic solutions. Cytosolic fractions of leukocytes were prepared and isolated according to the method previously described (13).

2.3 Plasma metabolite and hormone assay

Plasma glucose, triglyceride (TG), total cholesterol (T-Cho), total protein (TP), creatinine, and blood urea nitrogen (BUN) concentrations were measured using an automatic clinical chemistry analyzer (BioMajesty™ JCA-BM2250, JEOL Ltd., Tokyo, Japan) with the manufacturer reagents at FUJIFILM VET Systems Co., Ltd. (Tokyo, Japan). Non-esterified fatty acids (NEFAs) and malondialdehyde (MDA) concentrations were measured using NEFA C-test Wako (FUJIFILM Wako Pure Chemical Corporation, Osaka, Japan) and NWLSS™ Malondialdehyde Assay (Northwest Life Science Specialties, LLC, WA, USA) commercial kits, respectively. Serum amyloid A (SAA) concentrations were measured using a biochemistry automatic analyzer (Hitachi 7,180, Hitachi High-Tech Corporation, Tokyo, Japan) with a commercial kit, VET-SAA (EIKEN CHEMICAL CO., LTD., Tokyo, Japan). Insulin and adiponectin concentrations were measured using LBIS Rat Insulin ELISA kit (FUJIFILM Wako Pure Chemical Corporation, Osaka, Japan) and Mouse/rat adiponectin ELISA kit (Otsuka Pharmaceutical Co., Ltd., Tokyo, Japan), respectively. Insulin and adiponectin concentrations were measured by the ELISA analysis (14), and 100 times diluted plasma was used for the adiponectin assay. All calibrators and samples were run in duplicate, and the samples exhibited parallel displacement to the standard curve for the ELISA analysis. The intra- and inter-assay coefficients of variation were at <10% in both insulin and adiponectin assay.

2.4 Plasma enzyme activity assay

Aspartate aminotransferase (AST) and alanine aminotransferase (ALT) activities were measured using an automatic clinical chemistry analyzer (BioMajesty™ JCA-BM2250, JEOL Ltd., Tokyo, Japan) with the manufacturer's reagents at FUJIFILM VET Systems Co., Ltd. (Tokyo, Japan). Glutathione peroxidase (GPx) and superoxide dismutase (SOD) activities were measured using commercial kits, GPx activity assay (Northwest Life Science Specialties, LLC, WA, USA) and SOD assay kit-WST (DOJINDO LABORATORIES, Kumamoto, Japan), respectively. Malate dehydrogenase (MDH) and lactate dehydrogenase (LDH) activities were measured using the methods previously described (15, 16). The M/L ratio was calculated as MDH activities divided by LDH activities. A higher M/L ratio reflects elevated energy metabolism, leading to higher ATP production in some tissues, such as muscle and the liver (17). AMP-activated protein kinase (AMPK) activities in the cytosolic fraction of peripheral leukocytes were measured using a commercial kit (CycLex AMPK Assay Kit, MEDICAL & BIOLOGICAL LABORATORIES CO., LTD., Tokyo, Japan). The protein concentration in the cytosolic fraction was determined by the Bradford method (18).

2.5 Statistical analysis

The measured values are expressed as a means±standard error (SE). Statistical significance was determined by Student's *t*-test. The significance level was set at a *p*-value of <0.05. Measured values outside the reference range were excluded.

3 Results

All horses were clinically healthy, and their BCS values were 4 or 5 on the 9-point scale. Plasma glucose, TP, creatinine, and NEFA concentrations in horses remained unchanged through adolescence, middle age, and old age. TG, T-Cho, BUN, and insulin concentrations increased with age, while adiponectin concentrations decreased. MDA and SAA concentrations did not change between adolescence and middle age but increased with aging beyond middle age. The MDA concentrations in the old age group were significantly higher than those in the adolescent group (Table 1). Plasma AST, ALT, and GPx activities did not change in the horses with age, while plasma SOD and

leukocyte AMPK activities decreased. The plasma M/L ratio did not change with aging (Table 2).

4 Discussion

According to their plasma ALT and AST activities and creatinine and BUN concentrations, it could be presumed that no riding horses in this study had any specific lesions in their livers, kidneys, or skeletal muscles. Although the BCS of riding horses did not increase with aging, they showed symptoms of insulin resistance, including increases in both plasma insulin and TG. In healthy, middle-aged humans, insulin resistance and dyslipidemia associated with the accumulation of excess visceral adipose tissue are frequently observed (19, 20). A horse at 17 years of age is equivalent to a human at 50 years of age (21). Dysregulation of lipid metabolism became clear in riding horses aged over 17 years. The increases in plasma MDA and SAA concentrations and decreases in SOD activities were notable. White adipose tissue dysfunction and the accumulation of visceral fat occur in elderly humans (22, 23). Although older riding horses did not show marked obesity, they accumulated more dysregulated adipocytes (enlarged adipocytes) as visceral fat compared to younger horses (4). In older riding horses, plasma adiponectin concentrations decreased, as is the case for aging humans. The molecular mechanisms responsible for adiponectin concentrations may be the direct result of inflammatory cells suppressing reactive oxygen species (ROS) and cytokines, inhibiting the NF-κB inflammatory signaling pathway, and downregulating inflammatory responses (24, 25). Decreasing adiponectin concentrations lead to dyslipidemia and insulin resistance (26). Obesity is known to affect immunity and inflammation in horses, and failure to control for BCS can obscure the interpretation of these results (27, 28). Increased plasma SAA concentrations in obese animals could be the result of normal fat mass and/or increased expression and secretion of SAA from dysfunctional adipose tissue or other tissues (26). Concentrations of MDA as a product of lipid peroxidation (29) increase with chronic inflammation as a result of ROS. Increased MDA in older riding horses is considered to be induced by lower adiponectin concentrations and decreased SOD activities.

SAA from dysfunctional adipose tissue may act locally to alter cytokine production and fat metabolism. Additionally, it may act systemically on the liver, muscle, cells of the immune system, and the

TABLE 1 Changes in plasma metabolite and hormone concentrations in aging riding horses.

		Group A ($n = 6$) adolescent, <10 years old	Group B ($n = 6$) middle age, 10–16 years old	Group C ($n = 6$) old age, >17 years old
Glucose	(mg/dL)	90 ± 3	92 ± 2	90 ± 2
TG	(mg/dL)	14 ± 2	18 ± 3	20 ± 3
T-Cho	(mg/dL)	77 ± 7	79 ± 6	95 ± 5
NEFA	(μEq/L)	89 ± 12	98 ± 20	82 ± 7
TP	(g/dL)	5.9 ± 0.2	6.1 ± 0.2	5.9 ± 0.1
Creatinine	(mg/dL)	1.2 ± 0.1	1.2 ± 0.1	1.2 ± 0.0
BUN	(mg/dL)	16 ± 1	19 ± 1	20 ± 1
MDA	(μmol/L)	7.6 ± 2.5	7.6 ± 2.5	13.8 ± 0.9 *
SAA	(mg/L)	1.4 ± 0.4	0.6 ± 0.1	2.3 ± 1.3
Insulin	(ng/mL)	0.9 ± 0.4	1.0 ± 0.5	1.4 ± 0.8
Adiponectin	(μg/mL)	9.1 ± 2.0	8.1 ± 1.5	7.1 ± 1.1

*Significant differences ($p < 0.05$) from the value in Group A (Student's t-test).

TABLE 2 Changes in plasma enzyme activities in riding horses with aging.

		Group A ($n = 6$)	Group B ($n = 6$)	Group C ($n = 6$)
AST	(U/L)	221 ± 18	226 ± 18	253 ± 25
ALT	(U/L)	7.0 ± 0.9	6.8 ± 0.6	7.5 ± 1.2
GPx	(U/L)	5.5 ± 1.9	5.9 ± 0.8	5.4 ± 0.3
SOD	(unit/mL)	114 ± 29	97 ± 11	94 ± 13
MDH	(U/L)	152 ± 12	155 ± 18	167 ± 15 *
LDH	(U/L)	215 ± 28	214 ± 20	246 ± 37
M/L	Ratio	0.72 ± 0.05	0.73 ± 0.04	0.70 ± 0.04
AMPK**	(μg/min/mg)	1.4 ± 0.3	1.3 ± 0.3	1.0 ± 0.1

A: <10 years B: 10–16 years C: >17 years.
*Significant differences ($p < 0.05$) from the value in Group A (Student's t-test).
**AMPK activities were measured in the cytosol of peripheral leukocytes.

vasculature to impact insulin resistance and atherosclerosis (26). Although SAA is commonly used as a marker for APP in cats and horses (30, 31), it may be used as a marker of inflammaging in riding horses when combined other lipid metabolism markers.

Although riding horses with sufficient exercise continually seem to be less likely to develop inflammaging, horses older than 17 years tend to show a proinflammatory status with dysregulated lipid metabolism. Current SAA reagents do not have enough sensitivity to confirm a significant difference; however, it is expected that improved reagent performance will allow SAA to become a biomarker that can differentiate the presence or absence of inflammaging with dysregulated lipid metabolism in riding horses.

This study has some limitations. First, the number of horses in each group was small. Second, the insulin, adiponectin, and SAA antibodies for measurements were not specific to the equine species. An age- and sex-matched control group, fed on a similar diet, would be required to help eliminate the possible influence of the aforementioned factors. Further studies should be performed to evaluate the usefulness of SAA and other macromolecules such as TG, NEFA, MDA, and SOD as biomarkers for diagnosing inflammaging in riding horses.

5 Conclusion

Changes in metabolite and hormone concentrations and enzyme actiMalate dehydrogenase UV assayities relating to energy metabolism in the plasma of clinically healthy riding horses of various ages were measured. All horses had BCS values of 4 or 5, without obesity. Plasma TG, T-Cho, BUN, and insulin concentrations increased gradually with aging, whereas plasma adiponectin concentrations decreased. MDA and SAA concentrations increased with aging, while plasma AST, ALT, and GPx activities did not change. Furthermore, plasma SOD and leukocyte AMPK activities decreased. Although riding horses with sufficient and continuous exercise seem to be less likely to develop inflammaging, horses over the age of 17 years tend to show a proinflammatory status with the disorder of lipid metabolism. SAA, in combination with other lipid metabolism markers, may be a useful biomarker for inflammaging with dysregulated lipid metabolism in riding horses.

Data availability statement

The original contributions presented in the study are included in the article/supplementary material, further inquiries can be directed to the corresponding author.

Ethics statement

The animal study was approved by the Nippon Veterinary and Life Science University Animal Research Committee. The study was conducted in accordance with the local legislation and institutional requirements.

Author contributions

YA: Writing – original draft, Validation, Resources, Methodology, Investigation, Formal analysis, Data curation, Conceptualization. TA: Writing – review & editing, Validation, Supervision, Project administration, Formal analysis, Data curation, Conceptualization. YT: Writing – review & editing, Validation, Resources, Methodology, Data curation.

Funding

The author(s) declare that no financial support was received for the research, authorship, and/or publication of this article.

Acknowledgments

The authors would like to thank the staff at the Niiza Riding Club and Saitama Horse Riding Club for their contribution to the sample collection from riding horses.

Conflict of interest

The authors declare that the research was conducted in the absence of any commercial or financial relationships that could be construed as a potential conflict of interest.

Publisher's note

References

1. DeNotta S, McFarlane D. Immunosenescence and inflammaging in the aged horse. *Immun Ageing*. (2023) 20:2. doi: 10.1186/s12979-022-00325-5

2. McGowan TW, Pinchbeck G, Phillips CJC, Perkins N, Hodgson DR, McGowan CM. A survey of aged horses in Queensland, Australia. Part 1: management and preventive health care. *Aust Vet J*. (2010) 88:420–7. doi: 10.1111/j.1751-0813.2010.00637.x

3. Argo CM. Nutritional management of the older horse. *Vet Clin North Am Equine Pract*. (2016) 32:343–54. doi: 10.1016/j.cveq.2016.04.010

4. Kawasumi K, Yamamoto M, Koide M, Okada Y, Mori N, Yamamoto I, et al. Aging effect on plasma metabolites and hormones concentrations in riding horses. *Open Vet J*. (2015) 5:154–7. doi: 10.5455/OVJ.2015.v5.i2.p154

5. Ireland JL, McGowan CM, Clegg PD, Chandler KJ, Pinchbeck GL. A survey of health care and disease in geriatric horses aged 30 years or older. *Vet J*. (2012) 192:57–64. doi: 10.1016/j.tvjl.2011.03.021

6. Jahns H, Callanan JJ, McElroy MC, Sammin DJ, Bassett HF. Age-related and non-age-related changes in 100 surveyed horse brains. *Vet Pathol*. (2006) 43:740–50. doi: 10.1354/vp.43-5-740

7. Estrada McDermott JE, Pezzanite L, Goodrich L, Santangelo K, Chow L, Dow S, et al. Role of innate immunity in initiation and progression of osteoarthritis, with emphasis on horses. *Animals*. (2021) 11:3247. doi: 10.3390/ani11113247

8. Hansen S, Otten ND, Fjeldborg J, Baptiste KE, Horohov DW. Age-related dynamics of pro-inflammatory cytokines in equine bronchoalveolar lavage (BAL) fluid and

peripheral blood from horses managed on pasture. *Exp Gerontol*. (2019) 124:110634. doi: 10.1016/j.exger.2019.110634

9. Franceschi C, Bonafè M, Valensin S, Olivieri F, De Luca M, Ottaviani E, et al. Inflamm-aging. An evolutionary perspective on immunosenescence. *Ann N Y Acad Sci*. (2000) 908:244–54. doi: 10.1111/j.1749-6632.2000.tb06651.x

10. Franceschi C, Campisi J. Chronic inflammation (inflammaging) and its potential contribution to age-associated diseases. *J Gerontol A Biol Sci Med Sci*. (2014) 69:S4–9. doi: 10.1093/gerona/glu057

11. Robbins PD. Extracellular vesicles and aging. *Stem Cell Investig*. (2017) 4:98. doi: 10.21037/sci.2017.12.03

12. Arfuso F, Piccione G, Guttadauro A, Monteverde V, Giudice E, Giannetto C. Serum C-reactive protein and protein electrophoretic pattern correlated with age in horses. *J Equine Vet*. (2023) 126:104561. doi: 10.1016/j.jevs.2023.104561

13. Washizu T, Takahashi M, Azakami D, Ikeda M, Arai T. Activities of enzymes in the malate-aspartate shuttle in the peripheral leukocytes of dogs and cats. *Vet Res Commun*. (2001) 25:623–9. doi: 10.1023/a:1012787012433

14. Okada Y, Kawasumi K, Koide M, Hirakawa Y, Mori M, Yamamoto I, et al. Changes in energy metabolic indicators with aging in thoroughbred riding horses. *Asian J Anim Vet Adv*. (2016) 11:253–7. doi: 10.3923/ajava.2016.253.257

15. Bergmeyer HU, Bernt E. Malate dehydrogenase UV assay In: HU Berg-meyer, editor. *Methods of enzymatic analysis*. New York: Academic Press (1974). 613–7.

16. Kaloustian HD, Stolzenbach FE, Everse J, Kaplan NO. Lactate dehydrogenase of lobster (*Homarus americanus*) tail muscle. I. Physical and chemical properties. *J Biol Chem*. (1969) 244:2891–901. doi: 10.1016/S0021-9258(18)91709-6

17. Li G, Lee P, Mori N, Yamamoto I, Arai T. Long term intensive exercise training leads to a higher plasma malate/lactate dehydrogenase (M/L) ratio and increased level of lipid mobilization in horses. *Vet Res Commun*. (2012) 36:149–55. doi: 10.1007/s11259-012-9515-0

18. Bradford MM. A rapid and sensitive method for the quantitation of microgram quantities of protein utilizing the principle of protein-dye binding. *Anal Biochem*. (1976) 72:248–54. doi: 10.1016/0003-2697(76)90527-3

19. Correa-Rodríguez M, González-Ruíz K, Rincón-Pabón D, Izquierdo M, García-Hermoso A, Agostinis-Sobrinho C, et al. Normal-weight obesity is associated with increased cardiometabolic risk in young adults. *Nutrients*. (2020) 12:1106. doi: 10.3390/nu12041106

20. Wittert G, Grossmann M. Obesity, type 2 diabetes, and testosterone in ageing men. *Rev Endocr Metab Disord*. (2022) 23:1233–42. doi: 10.1007/s11154-022-09746-5

21. Rogers CW, Gee EK, Dittmer KE. Growth and bone development in the horse: when is a horse skeletally mature? *Animals*. (2021) 11:3402. doi: 10.3390/ani11123402

22. Reyes-Farias M, Fos-Domenech J, Serra D, Herrero L, Sánchez-Infantes D. White adipose tissue dysfunction in obesity and aging. *Biochem Pharmacol*. (2021) 192:114723. doi: 10.1016/j.bcp.2021.114723

23. Ko SH, Jung Y. Energy metabolism changes and dysregulated lipid metabolism in postmenopausal women. *Nutrients*. (2021) 13:4556. doi: 10.3390/nu13124556

24. Ouchi N, Walsh K. Adiponectin as an anti-inflammatory factor. *Clin Chim Acta*. (2007) 380:24–30. doi: 10.1016/j.cca.2007.01.026

25. Nigro E, Scudiero O, Sarnataro D, Mazzarella G, Sofia M, Bianco A, et al. Adiponectin affects lung epithelial A549 cell viability counteracting TNFα and IL-1β toxicity through adipoR1. *Int J Biochem Cell Biol*. (2013) 45:1145–53. doi: 10.1016/j.biocel.2013.03.003

26. Yang RZ, Lee MJ, Hu H, Pollin TI, Ryan AS, Nicklas BJ, et al. Acute-phase serum amyloid a: an inflammatory adipokine and potential link between obesity and its metabolic complications. *PLoS Med*. (2006) 3:e287. doi: 10.1371/journal.pmed.0030287

27. Herbst AC, Reedy SE, Page AE, Horohov DW, Adams AA. Effect of aging on monocyte phagocytic and inflammatory functions, and on the ex vivo inflammatory responses to lipopolysaccharide, in horses. *Vet Immunol Immunopathol*. (2022) 250:110459. doi: 10.1016/j.vetimm.2022.110459

28. Adams AA, Katepalli MP, Kohler K, Reedy SE, Stilz JP, Vick MM, et al. Effect of body condition, body weight and adiposity on inflammatory cytokine responses in old horses. *Vet Immunol Immunopathol*. (2009) 127:286–94. doi: 10.1016/j.vetimm.2008.10.323

29. Ayala A, Muñoz MF, Argüelles S. Lipid peroxidation: production, metabolism, and signaling mechanisms of malondialdehyde and 4-hydroxy-2-nonenal. *Oxidative Med Cell Longev*. (2014) 2014:360438. doi: 10.1155/2014/360438

30. Hultén C, Sandgren B, Skiöldebrand E, Klingeborn B, Marhaug G, Forsberg M. The acute phase protein Serum Amyloid A (SAA) as an inflammatory marker in equine influenza virus infection. *Acta Vet Scand*. (1999) 40:323–33. doi: 10.1186/BF03547012

31. Tuna GE, Ulutas B. Investigation of acute-phase protein concentrations in healthy and various diseased cats. *Pol J Vet Sci*. (2022) 25:589–97. doi: 10.24425/pjvs.2022.143545

frontiers | Frontiers in Veterinary Science

TYPE Original Research
PUBLISHED 17 June 2024
DOI 10.3389/fvets.2024.1389070

OPEN ACCESS

EDITED BY
Yatta Linhares Boakari,
Texas A&M University System, United States

REVIEWED BY
Charles Bradley Shuster,
New Mexico State University, United States
Jason T. Magnuson,
United States Geological Survey, United States

*CORRESPONDENCE
Essaikiammal Sodalai Muthu Konar
ekonar@frov.jcu.cz

RECEIVED 20 February 2024
ACCEPTED 30 May 2024
PUBLISHED 17 June 2024

CITATION
Konar ESM, Mai K, Brachs S, Waghmare SG, Samarin AM, Policar T and Samarin AM (2024) Evaluation of viability, developmental competence, and apoptosis-related transcripts during *in vivo* post-ovulatory oocyte aging in zebrafish *Danio rerio* (Hamilton, 1822).
Front. Vet. Sci. 11:1389070.
doi: 10.3389/fvets.2024.1389070

Evaluation of viability, developmental competence, and apoptosis-related transcripts during *in vivo* post-ovulatory oocyte aging in zebrafish *Danio rerio* (Hamilton, 1822)

Essaikiammal Sodalai Muthu Konar[1]*, Knut Mai[2,3], Sebastian Brachs[2,3], Swapnil Gorakh Waghmare[1], Azadeh Mohagheghi Samarin[1], Tomas Policar[1] and Azin Mohagheghi Samarin[1]

[1]Research Institute of Fish Culture and Hydrobiology, South Bohemian Research Center of Aquaculture and Biodiversity of Hydrocenoses, Faculty of Fisheries and Protection of Waters, University of South Bohemia in Ceske Budejovice, Vodnany, Czechia, [2]Department of Endocrinology and Metabolism, Charité – Universitätsmedizin Berlin, Corporate Member of Freie Universität Berlin and Humboldt-Universität zu Berlin, Berlin, Germany, [3]DZHK (German Centre for Cardiovascular Research), Partner Site Berlin, Berlin, Germany

Introduction: Post-ovulatory aging is a time-dependent deterioration of ovulated oocytes and a major limiting factor reducing the fitness of offspring. This process may lead to the activation of cell death pathways like apoptosis in oocytes.

Methodology: We evaluated oocyte membrane integrity, egg developmental competency, and mRNA abundance of apoptosis-related genes by RT-qPCR. Oocytes from zebrafish *Danio rerio* were retained *in vivo* at 28.5°C for 24 h post-ovulation (HPO). Viability was assessed using trypan blue (TB) staining. The consequences of in vivo oocyte aging on the developmental competence of progeny were determined by the embryo survival at 24 h post fertilization, hatching, and larval malformation rates.

Results: The fertilization, oocyte viability, and hatching rates were 91, 97, and 65% at 0 HPO and dropped to 62, 90, and 22% at 4 HPO, respectively. The fertilizing ability was reduced to 2% at 8 HPO, while 72% of oocytes had still intact plasma membranes. Among the apoptotic genes *bcl-2* (b-cell lymphoma 2), *bada* (bcl2-associated agonist of cell death a), *cathepsin D, cathepsin Z, caspase 6a, caspase 7, caspase 8, caspase 9, apaf1, tp53* (tumor protein p53), *cdk1* (cyclin-dependent kinase 1) studied, mRNA abundance of anti-apoptotic *bcl-2* decreased and pro-apoptotic *cathepsin D* increased at 24 HPO. Furthermore, *tp53* and *cdk1* mRNA transcripts decreased at 24 HPO compared to 0 HPO.

Discussion: Thus, TB staining did not detect the loss of oocyte competency if caused by aging. TB staining, however, could be used as a simple and rapid method to evaluate the quality of zebrafish oocytes before fertilization. Taken together, our results indicate the activation of cell death pathways in the advanced stages of oocyte aging in zebrafish.

KEYWORDS

apoptosis, cell death, fertilization, membrane integrity, trypan blue, zebrafish

1 Introduction

The fertilization rate and subsequent normal embryo and larval developmental stages can be used to define the quality of gametes (1). A delay in fertilization of ovulated oocytes leads to post-ovulatory aging or over-ripeness. Post-ovulatory aging is a factor that adversely affects the quality of oocytes and is complicated to manage. This aging process causes a loss of developmental competence of the egg, as well as deterioration, and may lead to oocyte death. Based on previous studies using murine, porcine and bovine models, oxidative stress (2, 3), mitochondrial dysfunction (4–6), degradation of maternal RNAs (7, 8), loss of survival factors (9, 10), epigenetic modifications (11, 12), and apoptosis (13–15) are probably involved in this process of oocyte aging. Mitochondrial microRNAs for cell death and signal transduction, stress response and DNA damage, RNA degradation, as well as energy and transcription regulation, were downregulated in rainbow trout (*Oncorhynchus mykiss*) due to post-ovulatory aging (16). However, oxidative stress does presumably not initiate oocyte aging in common carp (*Cyprinus carpio*) and goldfish (*Carassius auratus*) (17, 18). Histone acetylation pattern at histone H4 altered during the oocyte aging in common carp (19) indicating the involvement of epigenetic regulation. The first report of upregulation of apoptotic genes in aged oocytes from common carp speculated about the involvement of apoptosis in the degenerative process of fish oocytes (17).

The optimal time window for fertilization after ovulation highly varies among species and environmental conditions like temperature and storage (20). Several studies have been carried out to understand the *in vitro* and *in vivo* oocyte aging process using different model species. For example, the fertilization rate of *in vivo* aged curimata (*Prochilodus marggravii*) oocytes declined more prominently compared to *in vitro* aged at 26°C (21). The successful *in vitro* storage of Caspian brown trout (*Salmo trutta caspius*) oocytes was for 2 days at 2–3°C (22), whereas *in vivo* storage was for 30 days even at a higher temperature of 7°C (23). The most suitable duration for *in vitro* storage of rainbow trout oocytes was 9 days (24), and for *in vivo* storage was 30 days even at the same temperature, i.e., 2°C (25). The *in vivo* storage of northern pike (*Esox lucius*) oocytes retained the maximum fertilizing ability till 4 days post ovulation, whereas *in vitro* aging of 24 h resulted in a low fertilization rate at 10°C (26). In this study, we established a 24-h *in vivo* oocyte aging of zebrafish (*Danio rerio*) for the first time, as *in vivo* studies are important to understand the fate of oocytes retained inside the fish body after ovulation.

The underlying mechanisms of the degeneration process of post-ovulatory aged oocytes in fish remain elusive. Therefore, in this study, we used zebrafish as the experimental animal to investigate the decrease of trypan blue (TB) -based viability during *in vivo* aging of zebrafish oocytes and their quality before fertilization. Furthermore, the developmental competence was analyzed by estimating fertilization capability, embryo survival, hatching, and larval malformation rates after fertilization. Moreover, we analyzed the mRNA abundance of the pro-survival factor *bcl-2* (b-cell lymphoma 2), cell cycle regulator *cdk1* (cyclin-dependent kinase 1), and the main pro-apoptotic protein *bada* (*bcl2*-associated agonist of cell death a) during oocyte aging. The pro-apoptotic regulators like *cathepsin D* and *cathepsin Z*, *tp53* (tumor protein p53), and *apaf1* (apoptosis peptidase activating factor 1) mRNA abundance were also investigated. In addition, *caspase 6a*, *caspase 7*, *caspase 8,* and *caspase 9* were also studied. The successful *in vivo* storage of the zebrafish AB strain oocytes was identified.

2 Materials and methods

2.1 Animal maintenance

The zebrafish (AB strain) used in this study were initially obtained from the European Zebrafish Resource Centre (Karlsruhe, Germany) and later donated to the Faculty of Fisheries and Protection of Waters, the University of South Bohemia, Vodnany, Czech Republic. The fish were maintained in the ZebTec Active Blue rearing system (Techniplast, UK) under optimal photoperiod (14:10 h for light:dark cycle) and temperature (28.5°C). The broodstock was fed an adequate amount of Skretting M-300 Gemma Micro (Skretting, UK), according to the manufacturers' recommendation. The females were bred at two-week intervals to maintain a fresh reproductive cycle. For this experiment, approximately 12-month-old fish were used. The males and females were prepared for gamete Research Topic based on the protocol by Westerfield (27). Briefly, males and females were separated overnight in 1 L spawning tanks by a glass partition in the 2:1 ratio. The spawning was induced by the light on the subsequent morning.

2.2 Oocyte sampling

Ovulation was detected by observing the release of a few eggs by the female fish. After that, the females were anaesthetized with 0.05% tricaine methanesulfonate (methyl-aminobenzoate, MS222). The hand-stripping method was followed for the Research Topic of oocytes. A smidgen of oocytes (approx. 150 oocytes) was stripped from each of the six experimental females and considered as the fresh group or 0 h post-ovulation (HPO). The remaining oocytes were retained in the fish body for *in vivo* aging at 28.5°C. The cycle of collecting oocytes was continued at 2, 4, 8, and 24 HPO. Six individual females were used to strip at 0, 2 and 24 HPO, and another set of six females were used to strip at 0, 4 and 8 HPO since stripping the same females five times is unfeasible. The oocytes collected at each time point were divided into two different 35 mm petri dishes to assess viability loss using TB and for *in vitro* fertilization. The oocyte samples from 0, 8, and 24 HPOs were immediately frozen in liquid nitrogen and stored at −80°C till further use for total RNA extraction.

2.3 Oocyte membrane integrity assessment

Trypan blue dye exclusion test was used to analyze the oocytes' membrane integrity. The stock solution of 0.2% trypan blue (Sigma-Aldrich, Missouri, United States) was prepared in 1X Phosphate Buffered Saline (PBS, Sigma-Aldrich). 30–60 oocytes were stained with TB staining solution (0.1% in PBS) for 2 min at room temperature in a 35 mm petri dish immediately after stripping. Following staining, the oocytes were rinsed with PBS before visualization. TB stain, a large negatively charged molecule, is impermeable to cells with an intact plasma membrane and permeable to a cell with a disrupted membrane and enters the cytoplasm, making non-viable cells dark blue (28). The total and the viable number of oocytes were counted under a stereo

microscope (Olympus SZX16, Olympus Life Science, Japan). The number of viable oocytes to the total number of oocytes used for staining was used to calculate the viability rates.

2.4 Artificial insemination

The males were anaesthetized in MS222 (0.05%), and milt was collected from them in the immobilizing solution (Kurokura 180) (29). While stripping the male fish, a 2.5 µL pipette was used to collect the milt simultaneously. The milt collected from 5 males were pooled together in 50 µL of Kurokura 180 solution. The milt was pooled to eliminate the effect of individual male sperm quality and to have an equal volume of sperm for fertilization of all females. The motility of pooled sperm was analyzed using an Olympus CX31 light microscope (Olympus Life Science, Japan) before fertilization, according to Fauvel et al. (30). The pooled milt showed >75% of active spermatozoa movement. The oocytes stripped at 0, 2, and 24 HPO from six individual females, and 0, 4, and 8 HPO from another set of six females were fertilized immediately. Fertilization was carried out by adding 200 µL of water and 10 µL of sperm to 50–90 oocytes, as the number varied at different time points of aging in a 35 mm glass petri plate. The eggs were thereafter transferred into a Pyrex® Petri plate (9 cm in diameter, Germany) (31). After 90 min of incubation at 28.5°C, the fertilization rate was assessed by examining the cleavage pattern of embryos. The eggs showing cleavage were counted under a Nikon SMZ745T stereo microscope (Nikon, Japan). The fertilization rate was defined by the number of eggs showing cleavage to the total number of oocytes inseminated.

2.5 Assessment of egg developmental indices

Embryo survival, mortality, hatching, and malformation rates were calculated to determine the developmental competence of differently aged oocytes, according to Waghmare et al. (31). Briefly, the fertilized eggs were re-examined after 24 h of fertilization. The number of viable embryos after 24 h of fertilization to the total number of inseminated oocytes was used to determine the embryo survival rate. The successful development of fertilized eggs was examined by calculating embryo mortality (between 24 h and the hatching period) and hatching (48-72 h after fertilization) rates. The embryo mortality rate was determined by counting the viable embryos between 24 h and the hatching period to the total number of 24 h survived embryos. The number of hatched larvae to the total number of inseminated eggs was used to determine the hatching rate. After hatching, the larvae were observed under the Nikon SMZ745T stereomicroscope (Nikon, Japan) for the body shape. The larvae with body shape curved, bent, or curled were counted (72 h after fertilization) to the total number of hatched larvae for malformation rate.

2.6 RNA isolation and cDNA synthesis

Total RNA was isolated from 10 mg of oocytes sampled at 0, 8, and 24 HPOs from four individual females by the Trizol (Invitrogen, United States) method. The RNA concentration and quality were assessed using Nanodrop 2000 (Thermo Scientific, United States). The isolated RNA was treated with DNAse I, Amplification Grade (Invitrogen, United States) to digest residual DNA. Maxima First Strand cDNA Synthesis Kit (Thermo Scientific™, United States) was used for reverse transcription of 1,000 ng of RNA to first strand cDNA according to the manufacturer's instructions. Reverse transcription was carried out by incubating samples for 10 min at 25°C followed by 15 min at 50°C and final termination at 85°C for 5 min.

2.7 Quantitative expression analysis

Real-time quantitative expression analysis was performed to determine the apoptosis-related gene (*bcl-2*, *bada*, *cathepsin D*, *cathepsin Z*, *caspase 6a*, *caspase 7*, *caspase 8*, *caspase 9*, *apaf1*, *p53*, *cdk1*) expression using LightCycler 480 (Roche Applied Science, Germany). The primers of targeted genes were designed by Primer3web (https://primer3.ut.ee/) and were provided by Eurofins Genomics, Germany (Table 1). The reaction mixture contained 2 µL of diluted cDNA (1:10), 1 µL forward and reverse primers (500 nM), 2 µL of nuclease-free water, and 5 µL PowerUp™ SYBR™ Green Master Mix (Thermo scientific™, United States). 18S ribosomal RNA (*18 s*), beta-actin (*βactin*), and elongation factor 1 alpha (*ef1α*) were tested as reference genes. Among those, 18S was found to be the most stable reference gene to normalize the expression of selected genes. All data were presented as mean ± SD from three samples with three parallel repetitions, and all the primers were validated by melt curve analysis. The relative expression levels were analyzed by the $2^{-\Delta\Delta Ct}$ method (32).

2.8 Data analysis

The statistical evaluation and graph generation were performed using GraphPad Prism 9.4.1 (GraphPad Software, San Diego, CA, United States). The viability, fertilization, egg development indices, and relative gene expression were analyzed for variance by one-way ANOVA followed by Tukey's multiple comparisons tests for *post hoc* comparisons. Viability and fertilization rates between the high- and low-quality oocytes were analyzed by Mann Whitney test as data were not normally distributed. Statistical significance was considered with $^{*}p \leq 0.05$, $^{**}p \leq 0.01$, $^{***}p \leq 0.001$, and, $^{****}p \leq 0.0001$.

2.9 Compliance with ethical standards

All methodological protocols, experimental manipulations, and sampling procedures used in the present study were approved by the expert committee of the Institutional Animal Care and Use Committee of the University of South Bohemia, Czech Republic. The co-authors of this study deal with the manipulation and artificial reproduction of fish and hold certificates authorizing them to work with laboratory animals according to section 15d paragraph 3 of Act no. 246/1992 Coll. For the purposes of stripping gametes, fish were anesthetized with 0.05% tricaine methanesulfonate (MS-222; Sigma-Aldrich, United States) to ensure their welfare and minimize any associated stress.

TABLE 1 primer sequence of selected genes for quantitative expression analysis.

Gene	Forward primer (5′-3′)	Reverse primer (5′-3′)	Genbank accession no
bcl2	GTCGAGTGTGTGGAGAAGGA	CCGCTGCATCTTTTCCAAAG	NM_131807.1
bada	ACCTCGCATGACCATCAAGA	AGATTCCGAATAGAGCCGCA	XM_005161364.4
cathepsin D (ctsd)	CCTGAAATACAACCTGGGCT	TGAAGGTCTGGACAGGAGTG	NM_131710.2
cathepsin Z (ctsz)	GCACTACACGCAACCAACAT	CCACAGTCAATCACGTTCTGG	NM_001006043.1
caspase 6a	ATGTCGTAGTCTTGTGGGCA	CCATCGGAGTCACAGGATCA	NM_001020497.1
caspase 7	ACCATGACCTCGCTCTTCAA	TATTGTGTCATTGGGCGGTC	NM_001020607.1
caspase 8	ATCTTCCAAGGGCAAAGCTG	GCCCAAGCCTCTGTTGTTTT	NM_131510.2
caspase 9	TCATCGCCCTCCTGTCATTT	AGGCTTTCAGGTCTCAGTGG	NM_001007404.2
p53	CTCTCCCACCAACATCCACT	TGCCAGCTGACAGAAGAGTT	U60804.1
apaf-1	CACAAACTCCCAGAACAGGC	AATGCGCTTGAACTGCTTCT	NM_131608.1
cdk1	CATCTTTGCTGAACTCGCCA	AGAGACTCAACATCTGGCCA	NM_212564.2
βactin	TAGTCATTCCAGAAGCGTTTACC	TACAGAGACACCCTGGCTTACAT	AF057040.1
18S rRNA	GAATTCCCAGTAAGCGCAGG	GATCCGAGGACCTCACTGAG	BX296557.35
ef1α	ACAGCTGATCGTTGGAGTCA	GTATGCGCTGACTTCCTTGG	L23807.1

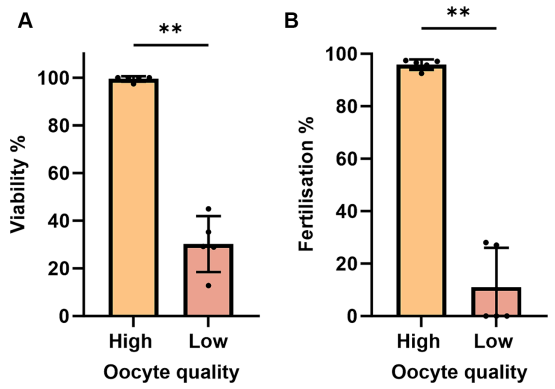

FIGURE 1
Evaluation of TB-based viability **(A)** and fertilization rates **(B)** during post-ovulatory aging in zebrafish. Data represents mean ± SD. Statistical significance calculated by one-way ANOVA followed by Tukeys multiple comparison test are shown by ns, non-significant; *$p \leq 0.05$; **$p < 0.01$; ***$p < 0.001$; ****$p < 0.0001$.

3 Results

3.1 Viability loss and fertilization during *in vivo* oocyte aging

To account for quality eggs, we estimated oocyte viability by measuring the TB-based staining rate. An oocyte batch from a female with less than 50% viability rate at 0 HPO was considered poor and excluded from the study at further time points (Figure 1A). Those oocytes also exhibited very low fertilization rates of 27% at 0 HPO and were categorized as low-quality oocytes (Figure 1B). We observed hardly any impact during the first 4 h of *in vivo* oocyte aging with approximately 97% viability at 0 and 2 HPO, and 90% at 4 HPO without differences compared to 0 HPO (Figure 2A). The viability rate significantly decreased to 72% at 8 HPO and drastically to 16% at 24 HPO. The fertilization rate for oocytes fertilized immediately after ovulation was 91% and slightly decreased at 2 HPO to 78%, not reaching statistical significance (Figure 2B). However, this decrease significantly intensified at 4 HPO and 8 HPO to 62 and 2%, respectively. As expected, the fertilization rate at 24 HPO was nil.

3.2 Egg developmental indices

To further analyze the impact of post-ovulatory aging on oocytes, we measured the survival and hatching of the fertilized eggs. We found that within 2 h of oocyte aging, embryo survival, and hatching rates had significantly declined from 67 and 65% at 0 HPO to 28 and 26% at 2 HPO, respectively. We did not reveal a further drop toward 4 HPO, which showed values of 27 and 22% (Figures 3A,B). Beyond that, the developmental indices are only shown up to 4 HPO, as no embryos developed from 8 HPO. Embryo mortality and larval malformation rates were assessed to further specify oocyte quality. Therefore, larva morphology was examined and classified as malformed if a curled, curved, or bent body shape was observed. The embryo mortality and larval malformation rates barely occurred at 0 HPO with 1 and 9%, respectively (Figures 3C,D). Although the mortality and malformation rates slightly rose to 5 and 33%, respectively, we did not detect significant differences for 2 HPO in either parameter (Figures 3C,D). However, at 4 HPO, a significant increase in the mortality and malformation rates to 12 and 41% was found (Figures 3C,D).

3.3 mRNA abundance of apoptosis-related genes in post-ovulatory aged oocytes

To investigate possible mechanisms of post-ovulatory oocyte degradation, we studied the mRNA abundance of apoptosis-related genes during oocyte aging. Based on previous findings (17, 18, 33), mRNA abundance of pro- and anti-apoptotic genes were quantified at

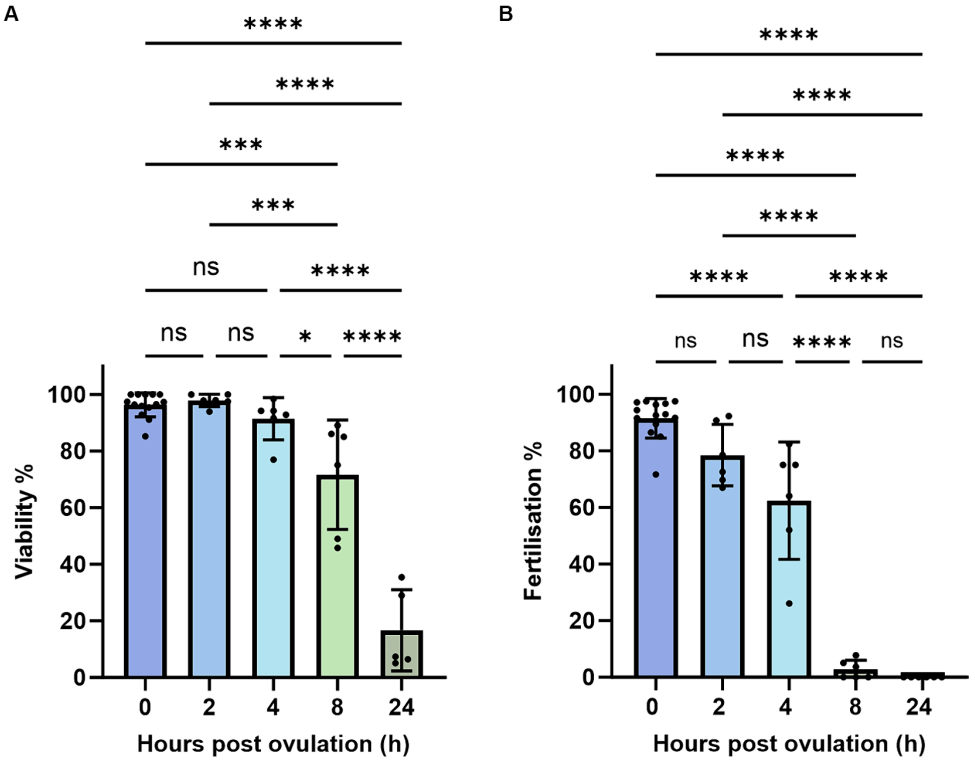

FIGURE 2
Oocyte quality of zebrafish assessed by TB-based viability **(A)** and fertilization rates **(B)**. Data represents mean ± SD. Statistical significance calculated by Mann Whitney test are shown by *$p \leq 0.05$; **$p < 0.01$.

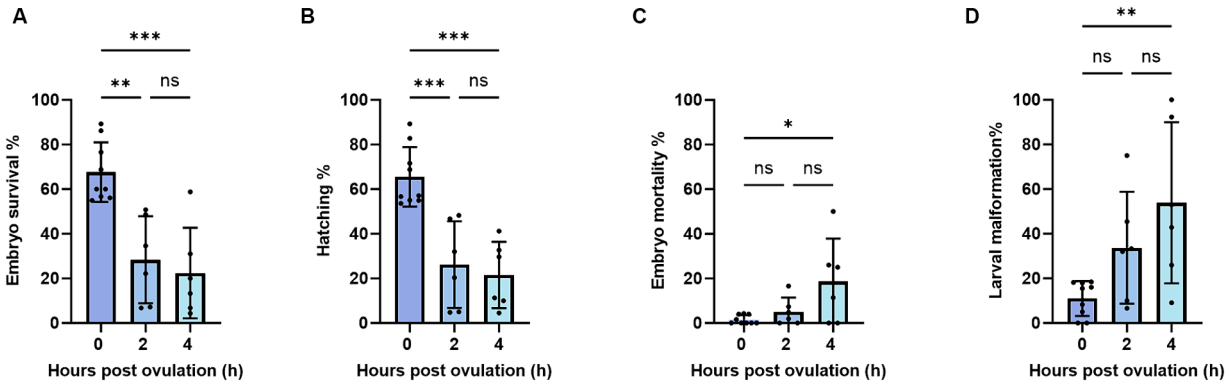

FIGURE 3
Embryo survival **(A)**, embryo mortality **(B)**, hatching **(C)**, and larval malformation **(D)** rates during post-ovulatory aging in zebrafish. Data represents mean ± SD. Statistical significance calculated by one-way ANOVA followed by Tukeys multiple comparison tests is shown by ns, non-significant; *$p \leq 0.05$; **$p < 0.01$; ***$p < 0.001$; ****$p < 0.0001$.

0, 8, and 24 HPO. We observed a strong increase in the pro-apoptotic gene *cathepsin D* at 24 HPO compared to 0 and 8 HPO (Figure 4A). In line with the induction of apoptosis during oocyte aging, we also revealed a significant downregulation of the anti-apoptotic gene *bcl-2* at 24 HPO (Figure 4C). The pro-apoptotic gene *bada* showed constant transcript levels during all time points (Figure 4D). In contrast, the transcript level of *tp53* was significantly decreased at 8 and 24 HPO compared to 0 HPO (Figure 4E). The transcript level of the cell cycle-related gene *cdk1* significantly decreased at 24 HPO (Figure 4K). Furthermore, *cathepsin Z, caspase 6a, caspase 7, caspase 8, caspase 9*, and *apaf-1* enhibited no significant change at the examined time points (Figures 4B,F–J).

4 Discussion

The observed decrease in the fertilization rates during *in vivo* aging of zebrafish oocytes is consistent with findings in other species,

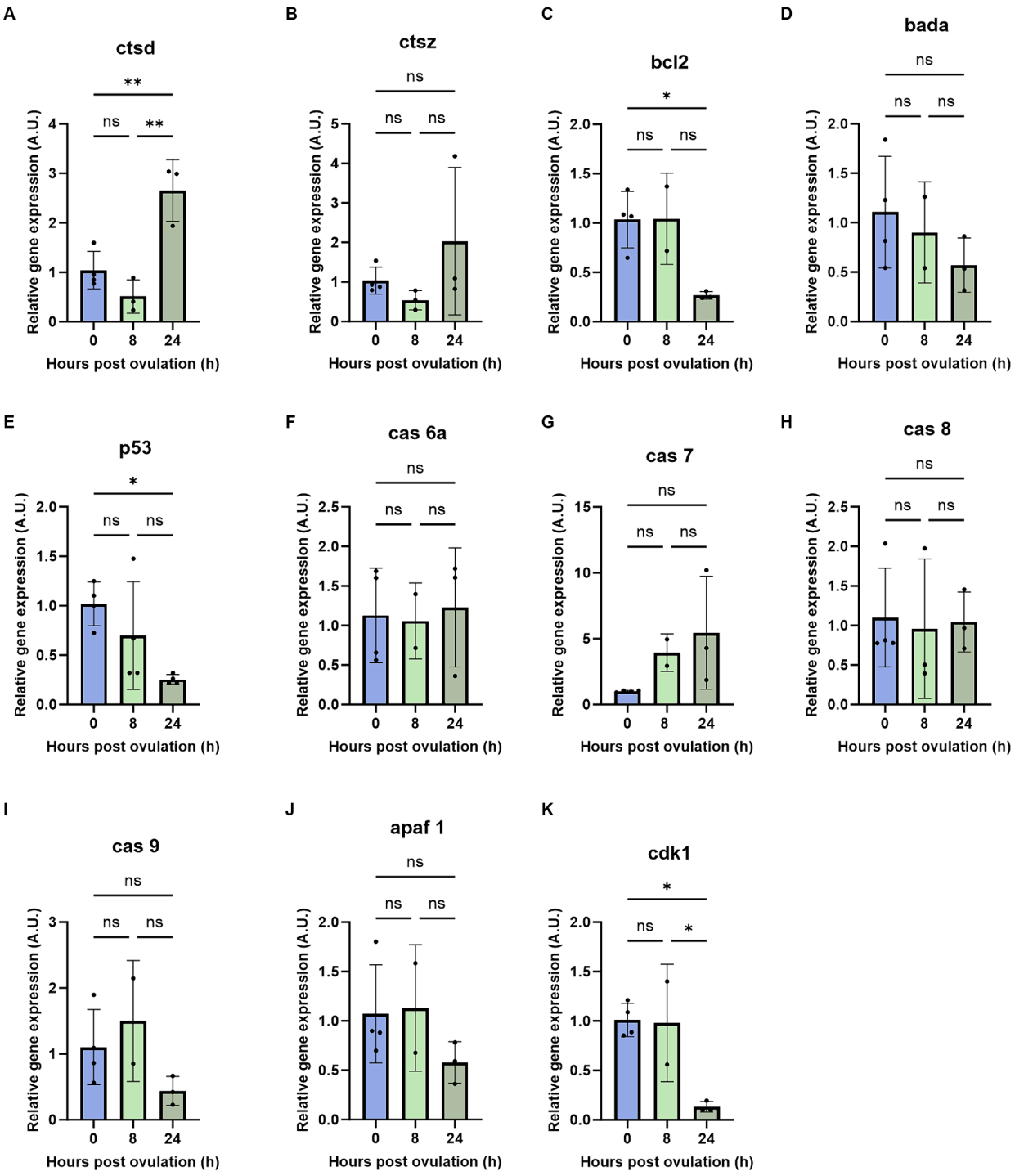

FIGURE 4
Regulation of pro- and anti-apoptotic genes during post-ovulatory oocyte aging. Depicted are the pro- and anti-apoptotic genes *cathepsin D* **(A)**, *cathepsin Z* **(B)**, *bcl2* **(C)**, bada **(D)**, *tp53* **(E)**, *caspase 6a* **(F)**, *caspase7* **(G)**, *caspase 8* **(H)**, *caspase 9* **(I)**, *apaf 1* **(J)** and *cdk1* **(K)**. A.U. represents arbitrary units. Data represents mean ± SD. Statistical significance calculated by one-way ANOVA followed by Tukeys multiple comparison test is shown by ns, non-significant; *$p \leq 0.05$; **$p < 0.01$; ***$p < 0.001$; ****$p < 0.0001$.

such as rainbow trout, Japanese eel (*Anguilla japonica*), common carp, northern pike, and yellowtail tetra (*Alestopetersius caudalis*) (26, 34–37). However, the duration of oocyte storage assuring the fertilization success is relatively short in zebrafish compared to those other species. Zebrafish oocytes from certain females exhibited low TB-based viability rates at the time of ovulation, and hence, this decrease in viability was not solely attributed to aging. Various factors, such as nutrition, temperature, photoperiod, salinity, captivity management, stress, chemical elements, and diseases, can affect the oocyte quality (1) thus contributing to low viability rates at the time

of ovulation. The *in vitro* aging of zebrafish AB strain oocytes at 26°C had no significant difference in fertilization rates until 2 h post-stripping, which aligns with our findings (31). However, it's worth noting that the fertilization capacity of oocytes at 4 h of *in vivo* aging was higher, even at a higher storage temperature, compared to *in vitro* aging (31). Zebrafish Tubingen strain oocytes stored in Chinook Salmon ovarian fluid retained fertilizing ability for a longer duration (38) compared to our study. Conversely, gold-strain zebrafish oocytes stored at 8°C in a modified Hanks medium lost their fertilizing ability (39) earlier than *in vivo* storage of AB strain oocytes in our study. These variations in fertilization rates may be attributed to specific storage conditions (e.g., temperature and medium) as well as genetic strain differences. Although we observed high TB-based viability rates after 4 h *in vivo* aging, their fertilization rates significantly decreased. Hence, aging may cause the developmental capacity loss of oocytes at the early stage and viability loss in the later stage of aging.

The current results showed that the embryo mortality and larval malformation rates increased significantly with *in vivo* oocyte aging. However, it's noteworthy that only 50% of the larvae were found to be malformed at 4 HPO, which contrasts with the findings from *in vitro* aging experiment where all larvae developed from 4-h-aged oocytes exhibited morphological malformations (31). Studies involving other fish species, such as northern pike, common carp, and rainbow trout, have consistently reported a higher occurrence of malformations in larvae originating from *in vitro* aged oocytes compared to those aged *in vivo* (17, 25, 26). This suggests that *in vitro* oocyte aging is more likely to result in malformation in the resulting larvae compared to *in vivo* aging. While it's known that ovarian fluid components may contribute to maintaining the fertilizing ability and embryo development during oocyte aging (40), the precise role of ovarian fluid in the oocyte aging process remains elusive and requires further investigation.

The lysosomal proteases, including cathepsin D, cathepsin Z, and cathepsin B, can indirectly act as pro-apoptotic modulators (41). These cathepsins disrupt mitochondrial membrane potential, thereby triggering the mitochondrial pathway of apoptosis (42). In our study, we observed a significant increase in *cathepsin D* in 24-h-aged oocytes, while *cathepsin Z* showed a non-significant upward trend. Studies with other fish species have shown variability in cathepsin activity during oocyte aging. For example, sea bream (*Sparus aurata*) eggs with high cathepsin D activity exhibited activation of apoptosis (43), while mRNA abundance of *cathepsin D* showed no significant change during *in vivo* aging of rainbow trout oocytes (44). Similarly, studies with African catfish (*Clarias gariepinus*) and common carp showed varying trends in *cathepsin D* and *cathepsin Z* mRNA level (17, 33). Considering that matured oocytes are transcriptionally silent until the initiation of zygotic transcription and early embryo development relies on stored mRNAs (45), the increase in *cathepsin D* transcripts at 24 h post-ovulation in our study could be linked to the spontaneous activation of oocytes, which ceases transcriptional silence and presumably triggering cell death. Cathepsins are also known to potentially activate caspases, which are key regulators of apoptosis (46). In our study, we did not find a significant difference in the mRNA level of *caspase 6a*, *caspase 7*, *caspase 8*, and *caspase 9* in zebrafish aged oocytes. This contrasts with findings from studies involving common carp, where the mRNA abundance of *caspase 9* increased during oocyte aging (17). However, future research focusing on cathepsin and caspase enzyme activity may provide a clearer understanding of their roles and interactions during oocyte aging.

Another critical factor in cell fate determination is the ratio of pro-apoptotic to anti-apoptotic Bcl-2 family proteins. An excess of bcl-2 typically results in cell survival, while an excess of bax leads to cell death (47). In our study, we observed a significant decrease in *bcl-2* abundance in 24-h *in vivo* aged oocytes, which is consistent with findings in aged oocytes of pigs and mice (9, 10). However, the *bcl-2* transcript level remained unchanged in common carp aged oocytes during 14 h of *in vivo* aging (17). The *bax* gene is upregulated during oocyte aging in common carp (17), whereas it remains unchanged in mouse oocytes during *in vitro* aging (14). Additionally, in the current study, the expression of *bada*, which has a similar function to *bax*, showed no statistical difference during oocyte aging in zebrafish. This could be due to low levels of maturation promoting factor (MPF) and mitogen-activated protein kinase (MAPK) in aged oocytes (48) potentially influencing the downregulation of *bcl-2* without affecting *bada* expression (14). The decrease in the pro-survival gene *bcl-2* and the increase in pro-apoptotic *cathepsin D* might make aged oocytes prone to apoptosis.

p53can directly bind to PUMA/NOXA (49) and increase mitochondrial membrane permeability, resulting in leakage of pro-apoptotic proteins and cytochrome c, or indirectly activate pro-apoptotic genes, such as *bax*, *puma*, *bbc3*, *igfbp3*, *noxa*, and *apaf1* (50–52). The mRNA level of *tp53* decreased significantly at 24 HPO, which is consistent with the results observed in post-ovulatory aged rainbow trout oocytes (53). The transcript levels of tp53 orthologous decreased in maternally aged oocytes (54). The tp53 protein level decreased significantly in mouse oocytes (55), whereas the mRNA level remained constant in pig oocytes during post-ovulatory aging (56). Maternally derived *tp53* mRNA is essential for embryonic development in mice and frog (57, 58). Thus, a decrease in *tp53* transcripts along with *bcl-2* might contribute to abnormal cleavage, increased mortality, and increased malformations in embryos developed from the aged oocytes. However, the detailed role of *tp53* in oocyte developmental competence and aging is yet unexplored.

Cdk1 kinase is a major component of the maturation-promoting factor, MPF that maintains the ovulated oocytes at the metaphase arrest (59). Deficiency of *cdk1* in mouse ovulated oocytes prevents the cells from resuming the meiotic cycle and resulting in infertility (60). Post-ovulatory aged frog oocytes exhibited low cdk1 activity followed by spontaneous meiotic exit (61), which is a prerequisite for the activation of apoptosis (62). The drastic decrease in *cdk1* transcript at 24 HPO in our study might be due to the spontaneous activation to exit metaphase arrest and execute the cell death. In the current study, the 8-h-aged oocytes lost their fertilizing capacity and exhibited membrane blebbing phenotype after activation with water (unpublished data), which is a morphological indicator of apoptosis. Additional analyzes are required to elaborate on the mechanism behind spontaneous activation followed by cell death in post-ovulatory aged oocytes.

5 Conclusion

Zebrafish AB strain oocytes can be stored *in vivo* for 2 h with minimal loss of competency, and complete loss of egg fertilizing ability

occurs at 8 h of ovulation. TB staining does not accurately detect oocyte post-ovulatory aging. However, it can be used as a simple and rapid method to estimate the quality of oocytes before fertilization in zebrafish. The upregulation of *cathepsin D* and downregulation of *bcl-2* and *cdk1* after 24 h of *in vivo* oocyte aging was observed. Based on the results obtained in the current study, the apoptotic pathway is activated in the advanced stage of aging, attributing to viability loss. Complementary analyses like DNA fragmentation, detection of proteins involved in the activation of cell death pathway, and examining mitochondrial changes would contribute to thoroughly understanding the involvement of apoptosis in the oocyte aging process.

Data availability statement

The raw data supporting the conclusions of this article will be made available by the authors, without undue reservation.

Ethics statement

The experiment was carried out under controlled conditions of RAS in the Laboratory of Intensive Aquaculture (LIA), which is part of the University of South Bohemia, Faculty of Fisheries and Protection of Waters (USB FFPW) (Vodňany, Czech Republic). All fish manipulations during the experiment were governed by valid legislative regulations of the Czech Republic (Act No. 166/1996 and No. 246/1992); the permit was issued No. 58672/2020-MZE-18134 and No. 33446/2020-MZE-18134 in the NAZV QK22020144 project.

Author contributions

EK: Conceptualization, Formal analysis, Investigation, Methodology, Writing – original draft. KM: Writing – review & editing. SB: Writing – review & editing. SW: Formal analysis, Investigation, Methodology, Writing – review & editing. AAS: Formal analysis, Investigation, Methodology, Writing – review & editing. TP: Funding acquisition, Writing – review & editing. AIS: Conceptualization, Formal analysis, Funding acquisition, Investigation, Methodology, Supervision, Writing – review & editing.

Funding

The author(s) declare that financial support was received for the research, authorship, and/or publication of this article. This study was financially supported by the Ministry of Agriculture of the Czech Republic (NAZV QK22020144) and by the Czech Science Foundation (GACR No. 20-01251S).

Acknowledgments

We thank Diana Woellner, Department of Endocrinology and Metabolism, Charité – Universitätsmedizin Berlin, for excellent technical assistance.

Conflict of interest

The authors declare that the research was conducted in the absence of any commercial or financial relationships that could be construed as a potential conflict of interest.

Publisher's note

Supplementary material

The Supplementary material for this article can be found online at: https://www.frontiersin.org/articles/10.3389/fvets.2024.1389070/full#supplementary-material

References

1. Bobe J, Labbé C. Egg and sperm quality in fish. *Gen Comp Endocrinol*. (2010) 165:535–48. doi: 10.1016/j.ygcen.2009.02.011

2. Tarin JJ, Perez-Albala S, Cano A. Consequences on offspring of abnormal function in ageing gametes. *Hum Reprod Update*. (2000) 6:532–49. doi: 10.1093/humupd/6.6.532

3. Takahashi T, Takahashi E, Igarashi H, Tezuka N, Kurachi H. Impact of oxidative stress in aged mouse oocytes on calcium oscillations at fertilization. *Mol Reprod Dev*. (2003) 66:143–52. doi: 10.1002/mrd.10341

4. Perez GI, Trbovich AM, Gosden RG, Tilly JL. Mitochondria and the death of oocytes. *Nature*. (2000) 403:500–1. doi: 10.1038/35000651

5. Hamatani T, Falco G, Carter MG, Akutsu H, Stagg CA, Sharov AA, et al. Age-associated alteration of gene expression patterns in mouse oocytes. *Hum Mol Genet*. (2004) 13:2263–78. doi: 10.1093/hmg/ddh241

6. Takahashi T, Igarashi H, Amita M, Hara S, Kurachi H. Cellular and molecular mechanisms of various types of oocyte aging. *Reprod Med Biol*. (2011) 10:239–49. doi: 10.1007/s12522-011-0099-0

7. Kosubek A, Klein-Hitpass L, Rademacher K, Horsthemke B, Ryffel GU. Aging of *Xenopus tropicalis* eggs leads to deadenylation of a specific set of maternal mRNAs and loss of developmental potential. *PLoS One*. (2010) 5:e13532. doi: 10.1371/journal.pone.0013532

8. Dankert D, Demond H, Trapphoff T, Heiligentag M, Rademacher K, Eichenlaub-Ritter U, et al. Pre-and postovulatory aging of murine oocytes affect the transcript level and poly (a) tail length of maternal effect genes. *PLoS One*. (2014) 9:e108907. doi: 10.1371/journal.pone.0108907

9. Ma W, Zhang D, Hou Y, Li Y-H, Sun Q-Y, Sun X-F, et al. Reduced expression of MAD2, BCL2, and MAP kinase activity in pig oocytes after in vitro aging are associated with defects in sister chromatid segregation during meiosis II and embryo fragmentation after activation. *Biol Reprod*. (2005) 72:373–83. doi: 10.1095/biolreprod.104.030999

10. Tatone C, Carbone MC, Gallo R, Delle Monache S, Di Cola M, Alesse E, et al. Age-associated changes in mouse oocytes during postovulatory in vitro culture: possible role for meiotic kinases and survival factor BCL21. *Biol Reprod*. (2006) 74:395–402. doi: 10.1095/biolreprod.105.046169

11. Huang J-C, Yan L-Y, Lei Z-L, Miao Y-L, Shi L-H, Yang J-W, et al. Changes in histone acetylation during postovulatory aging of mouse oocyte. *Biol Reprod*. (2007) 77:666–70. doi: 10.1095/biolreprod.107.062703

12. Ge Z-J, Schatten H, Zhang C-L, Sun Q-Y. Oocyte ageing and epigenetics. *Reproduction*. (2015) 149:R103–14. doi: 10.1530/REP-14-0242

13. Perez GI, Tao X-J, Tilly JL. Fragmentation and death (aka apoptosis) of ovulated oocytes. *Mol Hum Reprod*. (1999) 5:414–20. doi: 10.1093/molehr/5.5.414

14. Gordo AC, Rodrigues P, Kurokawa M, Jellerette T, Exley GE, Warner C, et al. Intracellular calcium oscillations signal apoptosis rather than activation in in vitro aged mouse eggs. *Biol Reprod*. (2002) 66:1828–37. doi: 10.1095/biolreprod66.6.1828

15. Tokmakov AA, Sato K-I, Stefanov VE. Postovulatory cell death: why eggs die via apoptosis in biological species with external fertilization. *J Reprod Dev*. (2017) 64:1–6. doi: 10.1262/jrd.2017-100

16. Ma H, Weber GM, Hostuttler MA, Wei H, Wang L, Yao J. MicroRNA expression profiles from eggs of different qualities associated with post-ovulatory ageing in rainbow trout (*Oncorhynchus mykiss*). *BMC Genomics*. (2015) 16:201. doi: 10.1186/s12864-015-1400-0

17. Samarin A, Samarin A, Østbye T-KK, Ruyter B, Sampels S, Burkina V, et al. Alteration of mRNA abundance, oxidation products and antioxidant enzyme activities during oocyte ageing in common carp *Cyprinus carpio*. *PLoS One*. (2019) 14:e0212694. doi: 10.1371/journal.pone.0212694

18. Samarin AM, Samarin AM, Østbye T-KK, Ruyter B, Sampels S, Burkina V, et al. The possible involvement of oxidative stress in the oocyte ageing process in goldfish *Carassius auratus* (Linnaeus, 1758). *Sci Rep*. (2019) 9:10469. doi: 10.1038/s41598-019-46895-1

19. Waghmare SG, Samarin AM, Samarin AM, Danielsen M, Møller HS, Policar T, et al. Histone acetylation dynamics during in vivo and in vitro oocyte aging in common carp *Cyprinus carpio*. *Int J Mol Sci*. (2021) 22:6036. doi: 10.3390/ijms22116036

20. Samarin AM, Policar T, Lahnsteiner F. Fish oocyte ageing and its effect on egg quality. *Rev Fish Sci Aquacul*. (2015) 23:302–14. doi: 10.1080/23308249.2015.1053560

21. Rizzo E, Godinho HP, Sato Y. Short-term storage of oocytes from the neotropical teleost fish Prochilodus marggravii. *Theriogenology*. (2003) 60:1059–70. doi: 10.1016/S0093-691X(03)00108-0

22. Niksirat H, Sarvi K, Amiri BM, Karami M, Hatef A. In vitro storage of unfertilized ova of endangered Caspian brown trout (*Salmo trutta* caspius) in artificial media. *Anim Reprod Sci*. (2007) 100:356–63. doi: 10.1016/j.anireprosci.2006.08.019

23. Bahre Kazemi M, Soltani M, Matinfar A, Abtahi B, Pusti I, SamarinA M, et al. Biochemical and histological studies of over-ripened oocyte in the Caspian brown trout (*Salmo trutta* caspius) to determine biomarkers for egg quality. *Iran J Fish Sci*. (2010) 9:33–48. doi: 10.22092/IJFS.2018.114081

24. Niksirat H, Sarvi K, Amiri BM, Hatef A. Effects of storage duration and storage media on initial and post-eyeing mortality of stored ova of rainbow trout *Oncorhynchus mykiss*. *Aquaculture*. (2007) 262:528–31. doi: 10.1016/j.aquaculture.2006.10.031

25. Samarin AM, Ahmadi MR, Azuma T, Rafiee GR, Amiri BM, Naghavi MR. Influence of the time to egg stripping on eyeing and hatching rates in rainbow trout *Oncorhynchus mykiss* under cold temperatures. *Aquaculture*. (2008) 278:195–8. doi: 10.1016/j.aquaculture.2008.03.034

26. Samarin AM, Blecha M, Uzhytchak M, Bytyutskyy D, Zarski D, Flajshans M, et al. Post-ovulatory and post-stripping oocyte ageing in northern pike, *Esox lucius* (Linnaeus, 1758), and its effect on egg viability rates and the occurrence of larval malformations and ploidy anomalies. *Aquaculture*. (2016) 450:431–8. doi: 10.1016/j.aquaculture.2015.08.017

27. Westerfield M. *The zebrafish book. A guide for the laboratory use of Zebrafish (Danio rerio), 4th Edition*. Eugene: University of Oregon Press (2000).

28. Strober W. Trypan blue exclusion test of cell viability. *Curr Protoc Immunol*. (2015) 111:A–3B. doi: 10.1002/0471142735.ima03bs111

29. Rodina M, Cosson J, Gela D, Linhart O. Kurokura solution as immobilizing medium for spermatozoa of Tench (*Tinca tinca* L.). *Aquac Int*. (2004) 12:119–31. doi: 10.1023/B:AQUI.0000017192.75993.e3

30. Fauvel C, Suquet M, Cosson J. Evaluation of fish sperm quality. *J Appl Ichthyol*. (2010) 26:636–43. doi: 10.1111/j.1439-0426.2010.01529.x

31. Waghmare SG, Samarin AM, Franěk R, Pšenička M, Policar T, Linhart O, et al. Oocyte ageing in zebrafish *Danio rerio* (Hamilton, 1822) and its consequence on the viability and ploidy anomalies in the progeny. *Animals*. (2021) 11:912. doi: 10.3390/ani11030912

32. Livak KJ, Schmittgen TD. Analysis of relative gene expression data using real-time quantitative PCR and the 2(-Delta Delta C(T)) method. *Methods*. (2001) 25:402–8. doi: 10.1006/meth.2001.1262

33. Samarin AM, Sampels S, Policar T, Rodina M, Hematyar N, Samarin AM. mRNA abundance changes during in vitro oocyte ageing in African catfish *Clarias gariepinus* (Burchell, 1822). *Aquac Res*. (2018) 49:1037–45. doi: 10.1111/are.13552

34. Azuma T, Ohta H, Oda S, Muto K, Yada T, Unuma T. Changes in fertility of rainbow trout eggs retained in coelom. *Fish Sci*. (2003) 69:131–6. doi: 10.1046/j.1444-2906.2003.00597.x

35. Nomura K, Takeda Y, Unuma T, Morishima K, Tanaka H, Arai K, et al. Post-ovulatory oocyte aging induces spontaneous occurrence of polyploids and mosaics in artificial fertilization of Japanese eel, Anguilla japonica. *Aquaculture*. (2013) 404-405:15–21. doi: 10.1016/j.aquaculture.2013.04.016

36. Samarin AM, Blecha M, Bytyutskyy D, Policar T. Post-ovulatory oocyte ageing in pikeperch (*Sander lucioperca* L.) and its effect on egg viability rates and the occurrence of larval malformations and ploidy anomalies. *Turk J Fish Aquat Sci*. (2015) 15:429–35. doi: 10.4194/1303-2712-v15_2_29

37. do Nascimento NF, Lázaro TM, de Alcântara NR, Senhorini JA, dos Santos SCA, Nakaghi LSO, et al. In vivo storage of oocytes leads to lower survival, increased abnormalities and may affect the ploidy status in the yellowtail tetra *Astyanax altiparanae*. *Zygote*. (2018) 26:471–5. doi: 10.1017/S0967199418000527

38. Siripattarapravat K, Busta A, Steibel JP, Cibelli J. Characterization and in vitro control of MPF activity in zebrafish eggs. *Zebrafish*. (2009) 6:97–105. doi: 10.1089/zeb.2008.0527

39. Cardona-Costa J, Perez-Camps M, Garcia-Ximenez F, Espinos FJ. Effect of gametes aging on their activation and fertilizability in zebrafish (*Danio rerio*). *Zebrafish*. (2009) 6:93–5. doi: 10.1089/zeb.2008.0578

40. Rime H, Guitton N, Pineau C, Bonnet E, Bobe J, Jalabert B. Post-ovulatory ageing and egg quality: a proteomic analysis of rainbow trout coelomic fluid. *Reprod Biol Endocrinol*. (2004) 2:26. doi: 10.1186/1477-7827-2-26

41. Kågedal K, Johansson U, Öllinger K. The lysosomal protease cathepsin D mediates apoptosis induced by oxidative stress. *FASEB J*. (2001) 15:1592–4. doi: 10.1096/fj.00-0708fje

42. Paquet C, Sane A, Beauchemin M, Bertrand R. Caspase-and mitochondrial dysfunction-dependent mechanisms of lysosomal leakage and cathepsin B activation in DNA damage-induced apoptosis. *Leukemia*. (2005) 19:784–91. doi: 10.1038/sj.leu.2403717

43. Carnevali O, Polzonetti V, Cardinali M, Pugnaloni A, Natalini P, Zmora N, et al. Apoptosis in sea bream *Sparus aurata* eggs. *Mol Reprod Dev*. (2003) 66:291–6. doi: 10.1002/mrd.10356

44. Aegerter S, Jalabert B, Bobe J. Large scale real-time PCR analysis of mRNA abundance in rainbow trout eggs in relationship with egg quality and post-ovulatory ageing. *Mol Reprod Dev*. (2005) 72:377–85. doi: 10.1002/mrd.20361

45. Lubzens E, Bobe J, Young G, Sullivan CV. Maternal investment in fish oocytes and eggs: the molecular cargo and its contributions to fertility and early development. *Aquaculture*. (2017) 472:107–43. doi: 10.1016/j.aquaculture.2016.10.029

46. Conus S, Perozzo R, Reinheckel T, Peters C, Scapozza L, Yousefi S, et al. Caspase-8 is activated by cathepsin D initiating neutrophil apoptosis during the resolution of inflammation. *J Exp Med*. (2008) 205:685–98. doi: 10.1084/jem.20072152

47. Adams JM, Cory S. The Bcl-2 protein family: arbiters of cell survival. *Science*. (1998) 281:1322–6. doi: 10.1126/science.281.5381.1322

48. Xu Z, Abbott A, Kopf GS, Schultz RM, Ducibella T. Spontaneous activation of ovulated mouse eggs: time-dependent effects on M-phase exit, cortical granule exocytosis, maternal messenger ribonucleic acid recruitment, and inositol 1, 4, 5-trisphosphate sensitivity. *Biol Reprod*. (1997) 57:743–50. doi: 10.1095/biolreprod57.4.743

49. Nakano K, Vousden KH. PUMA, a novel proapoptotic gene, is induced by p53. *Mol Cell*. (2001) 7:683–94. doi: 10.1016/S1097-2765(01)00214-3

50. Miyashita T, Reed JC. Tumor suppressor p53 is a direct transcriptional activator of the human bax gene. *Cell*. (1995) 80:293–9. doi: 10.1016/0092-8674(95)90412-3

51. Robles AI, Bemmels NA, Foraker AB, Harris CC. APAF-1 is a transcriptional target of p53 in DNA damage-induced apoptosis. *Cancer Res*. (2001) 61:6660–4.

52. Yu J, Zhang L. The transcriptional targets of p53 in apoptosis control. *Biochem Biophys Res Commun*. (2005) 331:851–8. doi: 10.1016/j.bbrc.2005.03.189

53. Aegerter S, Jalabert B, Bobe J. Messenger RNA stockpile of cyclin B, insulin-like growth factor I, insulin-like growth factor II, insulin-like growth factor receptor Ib, and p53 in the rainbow trout oocyte in relation with developmental competence. *Mol Reprod Dev*. (2004) 67:127–35. doi: 10.1002/mrd.10384

54. Guglielmino MR, Santonocito M, Vento M, Ragusa M, Barbagallo D, Borzì P, et al. TAp73 is downregulated in oocytes from women of advanced reproductive age. *Cell Cycle*. (2011) 10:3253–6. doi: 10.4161/cc.10.19.17585

55. Jeon H-J, Cui X-S, Guo J, Lee JM, Kim J-S, Oh JS. TCTP regulates spindle assembly during postovulatory aging and prevents deterioration in mouse oocyte quality. Biochimica et Biophysica Acta (BBA) - molecular. *Cell Res*. (2017) 1864:1328–34. doi: 10.1016/j.bbamcr.2017.05.002

56. Wang T, Gao YY, Chen L, Nie ZW, Cheng W, Liu X, et al. Melatonin prevents postovulatory oocyte aging and promotes subsequent embryonic development in the pig. *Aging*. (2017) 9:1552–64. doi: 10.18632/aging.101252

57. Armstrong JF, Kaufman MH, Harrison DJ, Clarke AR. High-frequency developmental abnormalities in p53-deficient mice. *Curr Biol*. (1995) 5:931–6. doi: 10.1016/S0960-9822(95)00183-7

58. Wallingford JB, Seufert DW, Virta VC, Vize PD. p53 activity is essential for normal development in Xenopus. *Curr Biol*. (1997) 7:747–57. doi: 10.1016/S0960-9822(06)00333-2

59. Masui Y, Markert CL. Cytoplasmic control of nuclear behavior during meiotic maturation of frog oocytes. *J Exp Zool*. (1971) 177:129–45. doi: 10.1002/jez.1401770202

60. Adhikari D, Zheng W, Shen Y, Gorre N, Ning Y, Halet G, et al. Cdk1, but not Cdk2, is the sole Cdk that is essential and sufficient to drive resumption of meiosis in mouse oocytes. *Hum Mol Genet*. (2012) 21:2476–84. doi: 10.1093/hmg/dds061

61. Iguchi S, Iwasaki T, Fukami Y, Tokmakov AA. Unlaid Xenopus eggs degrade by apoptosis in the genital tract. *BMC Cell Biol*. (2013) 14:11. doi: 10.1186/1471-2121-14-11

62. Tokmakov AA, Iguchi S, Iwasaki T, Fukami Y. Unfertilized frog eggs die by apoptosis following meiotic exit. *BMC Cell Biol*. (2011) 12:56. doi: 10.1186/1471-2121-12-56

frontiers | Frontiers in Veterinary Science

TYPE Original Research
PUBLISHED 03 July 2024
DOI 10.3389/fvets.2024.1407928

OPEN ACCESS

EDITED BY
Toshiro Arai,
Nippon Veterinary and Life Science University, Japan

REVIEWED BY
Antonio González Cantalapiedra,
University of Santiago de Compostela, Spain
Claudia Interlandi,
University of Messina, Italy

*CORRESPONDENCE
Zhenlei Zhou
✉ zhouzl@njau.edu.cn

RECEIVED 15 April 2024
ACCEPTED 17 May 2024
PUBLISHED 03 July 2024

CITATION
Guo Y, Mao S and Zhou Z (2024) Effects of intramuscular alfaxalone and dexmedetomidine alone and combined on ocular, electroretinographic, and cardiorespiratory parameters in normal cats. *Front. Vet. Sci.* 11:1407928. doi: 10.3389/fvets.2024.1407928

Effects of intramuscular alfaxalone and dexmedetomidine alone and combined on ocular, electroretinographic, and cardiorespiratory parameters in normal cats

Yizhe Guo, Sichao Mao and Zhenlei Zhou*

College of Veterinary Medicine, Nanjing Agricultural University, Nanjing, China

Background: This study aimed to determine the effects of intramuscular (IM) administration of alfaxalone with or without dexmedetomidine on short electroretinography (ERG), ocular parameters and cardiorespiratory in healthy cats.

Methods: Eight healthy female spayed cats were treated with three sedation protocols: IM administration of 5 μg/kg dexmedetomidine (DEX), 5 mg/kg alfaxalone (ALF), and 5 μg/kg dexmedetomidine plus 5 mg/kg alfaxalone (DEX + ALF). The washout period after each treatment was 2 weeks. Physiological parameters, time metrics, intraocular pressure (IOP), Schirmer tear test 1 (STT-1) and a short ERG protocol were recorded. For age data, weight data, time metrics and ERG data, one-way ANOVA with Bonferroni posterior comparisons were performed. For physiological parameters, IOP and STT-1 data, two-way repeated measures ANOVA with Bonferroni posterior comparisons were performed. Statistical significance was set at a p-value <0.05.

Results: IOPs were increased in all three groups compared to baseline and showed no significant differences among three groups at any time point. STT-1 values were decreased significantly during the process. Significant differences were noticed between a-wave amplitude in the dark-adapted response between DEX and ALF, and a-wave amplitude in light-adapted response between ALF and DEX + ALF.

Conclusion: This study demonstrates the feasibility of three sedation protocols for short ERG recording in cats. All these treatments resulted in increased IOP values and reduced STT-1 values. But baseline data of ERG was not obtained as a blank control in cats.

KEYWORDS

alfaxalone, dexmedetomidine, electroretinography, intraocular pressure, cats

1 Introduction

The electroretinogram (ERG) has been an important tool in clinical ophthalmology for evaluating retinal function since 1865 (1). It provides an invaluable mean of assessing retinal function with opaque media or during the early phases of diseases without significant funduscopic changes (2). Glaucoma is an ocular disorder characterized by increased intraocular pressure (IOP), and the rebound tonometry is a widely used method of IOP measurement (3). Aqueous tear deficiency (dry eye) can lead to serious ocular complications, and Schirmer tear test-1 (STT-1) examination is commonly used in clinical practice (4).

In addition to a quick retinal check performed in partially conscious animal, anesthesia is preferred during the ERG examination to prevent artifacts caused by involuntary eyelid twitch, body or globe movements as well as minimize stress induced by physical restraint (2, 5–7). The results of IOP and STT-1 will be affected by anesthesia, the majority of measurements are taken without anesthesia. Intraocular pressure (IOP) is primarily determined by aqueous humor dynamics and other factors including intraocular blood volume, central venous pressure, and extraocular muscle tone (8). Anesthetic drugs influence IOP mainly though extraocular muscles, affecting the success of ophthalmic procedures (9, 10). Previous studies reported an increase in IOP in cats administered with propofol (11). Moreover, reduced tear production is observed in cats with administration of medetomidine-ketamine (12). Corneal exposure and tear film evaporation during sedation may lead to ocular complications such as ulcerative keratitis (13). But sedation of less compliant animals provides ideal conditions for optimal ophthalmic examination and enhances safety for both the patient and examiner (14). Furthermore, general anesthesia carries inherent risks like cardiopulmonary depression (15). Thus, there is an urgent need for a simple, safe, and effective chemical restraint for short ERG recordings in cats.

Alfaxalone is a progesterone analog that have rapid onset and brief duration of action through γ-aminobutyric acid type A (GABAA) receptors (16–18). Compared to other anesthetic agents, alfaxalone offers advantages such as minimal cardiovascular depression in cats (19–21), dogs (22), and human (23). But alfaxalone is associated with certain side effects. Intravenous (IV) administration of alfaxalone at doses ranging from 0 to 50 mg/kg has been shown to induce dose-dependent suppressive effect on cardiorespiratory function and hyperkinesia during recovery in unpremedicated cats (21, 24). The most common adverse effects of alfaxalone administration in cats include apnea and hypoventilation (21). Dexmedetomidine is a sedative drug that commonly used in veterinary medicine. It is an alpha-2 adrenoceptor agonist witch exerts sedative effects through activation of central presynaptic and postsynaptic alpha-2 receptors in the locus coeruleus (25). Cats administered with alfaxalone (5 mg/kg) intramuscularly (IM) were deeply sedated, while cats administered with alfaxalone IM (5 mg/kg) combined with 20 and 40 μg/kg dexmedetomidine were anaesthetized (26). Induction with alfaxalone alone or in combination with dexmedetomidine intramuscularly (IM) is reported in cats, however, there is a lack of data specifically about their effects on the ERG, IOP, and STT-1 in cats (22).

We hypothesized that similar to anesthetic drugs such as propofol, IM administration of alfaxalone would increase IOP, decrease tear production, and have no effect on the ERG recordings in cats, while the use of dexmedetomidine could influence the ERG recordings and physiological variables. This study was designed to compare the effects of IM administration of alfaxalone alone or in combination with dexmedetomidine on the short ERG protocol, IOP, STT-1, sedative effect, reversal times, and physiological variables in cats.

2 Materials and methods

2.1 Animals

All procedures were performed following the guidelines of the Association for Research in Vision and Ophthalmology Statement for the Use of Animals in Ophthalmic and Vision Research. Eight spayed female cats were recruited for this study. They were housed individually in a room under controlled temperature (21°C) and light (7:00–19:00): dark (19:00–7:00 next day) cycle. Cats were socialized and adapted to human handling for 2 months prior to the study. Two weeks before study, the cats were specifically assimilated to tonometry. The animal study was approved by the Institutional Animal Care and Use Committee of Nanjing Agricultural University. The approval number was NJAU2022025.

The American Society of Anesthesiologists (ASA) classification was utilized in this study (27). Before the study, physical examination and ophthalmic examinations, including X-ray examination (InnoVet Versa DR Veterinary System; Radiology Imaging Solutions), echocardiography examination (W70 Vet; Esaote), complete blood count test (BC-5000 Vet; Mindray Animal Care), blood biochemistry test (Catalyst One Chemistry Analyzer; Idexx), blood gas analysis (i-STAT 1 analyzer; Abbott), electrocardiogram (ECG, BeneHeart R3A; Mindray), Schirmer tear test I (I-DEW Tear strips Schirmer Test; Ophtalmo), fluorescein staining (I-DEW FLO Fluorescein 1MG Strips; Ophtalmo), intraocular pressure with rebound tonometry setting as "do" (Tonovet; Icare Finland), slit lamp biomicroscopy (SL-17; Kowa), and fundus imaging system examination (Clear View 2; Menicon) were conducted on the cats. The inclusion criteria for cats included in this trial were that there are no abnormalities in the above examinations and the ASA classification was class I. All cats received an ASA class I assessment without ocular abnormalities.

2.2 Study design

The process of this study was shown in Figure 1. The right eye was treated with 5 mg/mL tropicamide (Tropicamide Eye Drops, Bausch + Lomb) to dilate the pupil 30 min before the injection of drugs. The cats were treated using three different protocols with a washout period of 2 weeks after each treatment. IM injection of 5 μg/kg dexmedetomidine (Dexdomitor, Orion Pharma) and 5 mg/kg alfaxalone (Alfaxan, Jurox Animal Health) was the DEX + ALF group; IM injection of 5 μg/kg dexmedetomidine was the DEX group; IM injection of 5 mg/kg alfaxalone was the ALF group. The drugs were mixed in one syringe. Sodium chloride 0.9% solution was administrated for DEX (0.5 mL/kg) and ALF (0.01 mL/kg) groups, respectively, to ensure a same amount of IM fluid. The time of drug administration was considered T0, with various interventions performed at 5 min intervals for 30 min (represented as T5, T10, T15, T20, T25, and T30) except ECG, STT-1 and ERG.

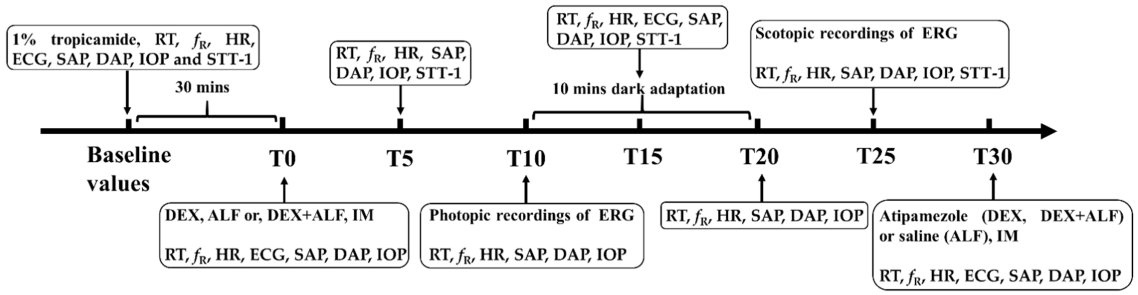

FIGURE 1
Flow chart of this study. Baseline values were measured 30 min before the administrated of drugs. T0 was the timepoint after administrated of drugs. DEX + ALF, the group received a combination of dexmedetomidine (5 μg/kg) and alfaxalone (5 mg/kg) intramuscularly (IM); DEX, the group received dexmedetomidine (5 μg/kg) intramuscularly; ALF, the group received alfaxalone (5 mg/kg) intramuscularly; IM, intramuscular injection, $n = 8$ cats; ERG, electroretinography; RT, rectal temperature; f_R, respiratory rate; HR, heart rate; ECG, electrocardiogram; SAP, systolic arterial pressure; DAP, diastolic arterial pressure; IOP, the intraocular pressure; STT-1, Schirmer tear test 1.

This study was performed between 15:00 and 17:00. The cats were fasted for 6 h before the experiment, but water was available until 1 h before the start of the experiment. A 22 G intravenous catheter was placed in the cephalic vein before sedation. The cats were positioned in sternal recumbency and received oxygen via a face mask (2 L/min). Body temperatures were preserved using an air blanket. The Lift-head time (LH), sternal recumbency time (SRr), and standing time (ST) were recorded to evaluate sedative effects of drugs during recovery from anesthesia (26). The LH was determined from drug injection to the first instance of the cat autonomously raising its head. The SRr was determined from drug injection to the first occurrence of the cat returning to the sternal recumbency. The ST was determined from drug injection to the first instance of the cat autonomously standing.

2.3 Physiological variables evaluations

Systolic arterial pressure (SAP), diastolic arterial pressure (DAP), rectal temperature (RT), heart rate (HR) and respiratory rate (f_R) were measured at baseline and every 5 min from 0 to 30 min after treatment. The ECG was evaluated at baseline and every 15 min from 0 to 30 min after treatment. The SAP and the DAP was determined by a veterinary blood pressure monitor (SunTech Vet20; SunTech Medical) with a cuff width approximately 40% of the limb circumference positioned on the right forelimb (28). Three measurements were taken and the average was considered as the blood pressure for that time point. The RT was determined by a compact anesthesia monitor (S/5; GE Healthcare) using an intrarectal sensor. The HR and the ECG were determined by a lead II electrocardiogram (BeneHeart R3A; Mindray). The f_R was counted by observing chest movement during the respiratory cycle for a period of 30 s. All physiological variables evaluations, LH, SRr and ST were recorded by the same experienced veterinarian who was blinded to group allocation.

2.4 Ophthalmic examination

IOP and STT-1 were measured from the left eye of each cat in different groups. IOP and STT-1 examinations were performed by the same experienced veterinarian who was blinded to group allocation. IOP was registered at baseline and every 5 min from 0 to 30 min after treatment. STT-1 was registered at baseline and 5, 15, 25 min after treatment. IOP was recorded on the central cornea without topical anesthesia. Three measurements were taken. If the differences between three measurements were not greater than 3 mmHg, the second measurement value was considered as the IOP value for that time point. Measurements were performed with cats in sternal recumbency. The head was kept above the level of the heart for each measurement using a soft pillow and the jugular vein was not compressed. STT-1 was measured by placing the commercial strip in the inferior conjunctival fornix for exactly 60 s and reading immediately.

2.5 The ERG procedure

A short ERG protocol was recorded from the right eye of each cat using a full-field ERG device (RETevetTM device; LKC Technologies) for veterinary ophthalmology. The ERG protocol was performed by another experienced veterinarian who was blinded to group allocation. The cats were prepared in normal ambient room light. The corneas of right eye were intermittently irrigated with saline to prevent keratopathy, and the eyelids were fixed by a eyelid speculum. Pupil size was assessed frequently to ensure that the pupils were fully dilated during the examination. The flash was placed 15 cm away from the cats. The ERG device included three electrodes: 1. The active electrode, a contact lens with a platinum wire, was placed on the cornea; 2. The reference electrode, a subcutaneous needle electrode (12 mm * 29 gauge), was fully inserted at the bottom of the right ear; 3. Ground electrode, a subcutaneous needle electrode (12 mm * 29 gauge), was fully inserted at the occipital crest. The ERG protocol used in this study was modified from ECVO (European College of Veterinary Ophthalmologists) 5-step single flash Protocol. The specific process was shown in Table A1. The conditions of the photic stimulator without a filter were set at maximum brightness (350 candela s/m^2). The photopic recordings were conducted 10 min after the cats were administrated with drugs. Then the light was turned off and retinal function was tested after 10 min of dark adaptation.

The implicit times and amplitudes were measured in all ERG responses. Three ERG responses were recorded and the mean values were used for subsequent analysis. The amplitude of a-wave was

TABLE 1 Basic information about the cats in this study.

	Values
Age (months)	3.4 ± 0.6 kg
Weight (kg)	13–25 (18)

Weight data are reported as mean ± SD. Age data are reported as minimum – maximum (median), $n = 8$ cats.

TABLE 2 Times to head-lift (LH), sternal recumbency (SRr), and standing position (ST) after received drugs.

Group	LH (mins)	SRr (mins)	ST (mins)
DEX	30.7 ± 9.6 * ($p = 0.019$)	36.1 ± 4.1	38.2 ± 3.3
ALF	21.8 ± 3.8 *#	35.0 ± 5.3	47.1 ± 11.5
DEX + ALF	37.6 ± 11.4 # ($p = 0.001$)	42.0 ± 10.7	46.8 ± 11.6

DEX + ALF, the group received a combination of dexmedetomidine (5 μg/kg) and alfaxalone (5 mg/kg) intramuscularly; DEX, the group received dexmedetomidine (5 μg/kg) intramuscularly; ALF, the group received alfaxalone (5 mg/kg) intramuscularly, $n = 8$ cats; data are reported as mean ± SD. *Significantly different between the value of DEX and ALF ($p < 0.05$). #Significantly different between the value of DEX + ALF and ALF ($p < 0.05$).

defined as the difference between baseline and the negative deflection trough. The b-wave amplitude was defined as the difference in amplitude between the a-wave trough and the peak of the b-wave.

2.6 Recovery

The effects of dexmedetomidine were reversed with IM atipamezole (12.5 μg/kg; Antisedan, Orion Pharma) for the DEX and DEX + ALF groups 30 min after the treatment. The ALF group was injected with same volume of saline. Subsequent to the experiment, cats received oxygen supplementation for 5 min before being transferred to a temperature-controlled kennel to facilitate recovery.

2.7 Data analyses

Data analyses were conducted using SPSS software, version 25 (SPSS Inc., IL, United States), operating on a Windows platform. Normality was assessed by the evaluation of descriptive statistics, plotting histograms and the Shapiro–Wilk test. All age data, weight data, physiological parameters (RT, HR, SAP, DAP and f_R), time metrics (LH, SRr and ST), IOP and STT-1 data were normally distributed. For weight data, time metrics (LH, SRr and ST), and ERG data, means ± standard deviations (SD) were computed and one-way ANOVA with Bonferroni posterior comparisons were performed. For age data, minimum – maximum (median) were computed and one-way ANOVA with Bonferroni posterior comparisons were performed. For physiological parameters (RT, HR, SAP, DAP and fR), IOP and STT-1 data, means ± SD were computed and a two-way repeated measures ANOVA was performed. The statistical significance of the main effects was compared using Bonferroni corrections *post hoc* tests. Statistical significance was set at a p-value <0.05.

The sample size was identified through experimental design, pre-experimentation, and conventional numerical settings using PASS 15 (a type 1 error [$p = 0.05$], 90% power). The primary hypothesis of this study was comparing the effects of IM administration of alfaxalone alone or in combination with dexmedetomidine on the short ERG protocol in cats. The preliminary data (unpublished) in four cats is as follow. Under the DA 0.01 in ERG, the b-wave values were 58.6 (DEX + ALF), 50.1 (ALF), 52.37 (DEX), and SDs were 13.61 (DEX + ALF), 15.86 (ALF), 16.67 (DEX) respectively. Based on this, PASS 15 calculated the sample size of 8 animals per group would lead to >90% power using a one-way ANOVA with 5% type 1 error. Hence the use of 8 biological replicates in these experiments for accuracy.

3 Result

3.1 Basic information

The age and weight data of cats are presented in Table 1. No significant differences were observed in the age or weight comparisons between cats. The sedation procedures previously mentioned were successfully performed in all cats without any adverse events. Furthermore, the sedation effect was sufficient for completing the ERG examination in all three treatments. Vomiting was observed in two cats from DEX group and one cat from DEX + ALF group following IM injection of dexmedetomidine.

3.2 Sedative and reversal times

The times to head-lift (LH), sternal recumbency (SRr), and standing position (ST) were presented in Table 2. Head-lift times were significantly shorter for cats in ALF group compared to those in DEX or DEX + ALF group ($p < 0.05$).

3.3 Physiological variables

The RT, f_R and HR values were presented in Figure 2. The RT values decreased slightly over time after the drug injection, but remained above 38°C throughout the process in all groups. There were no significant differences in RT values at any time point between the three groups. The HR values increased in ALF group and decreased in DEX and DEX + ALF groups after the injection of drugs. The HR values in ALF group were significantly higher than DEX and DEX + ALF groups at all time points except for baseline, T0, and T5 ($p > 0.05$). ECG monitoring showed no abnormalities during sedation in all three groups. The f_R was significantly lower at T10 ($p = 0.026$) and T25 ($p = 0.018$) in DEX group compared to ALF group. Compared with DEX and ALF groups, the f_R showed no significant differences in DEX + ALF group and was over 20 b/min during the study. The SAP and DAP values were presented in Figure 3. There were no significant differences in SAP and DAP between three groups, except for DAP between DEX and ALF groups at T0 ($p = 0.040$) and T5 ($p = 0.040$).

3.4 IOP and STT-1

All cats could successfully complete the baseline values of IOP and STT-1 examinations. The results of IOP and STT-1 were presented in Table 3. The IOP values of the right and left eye that measured before

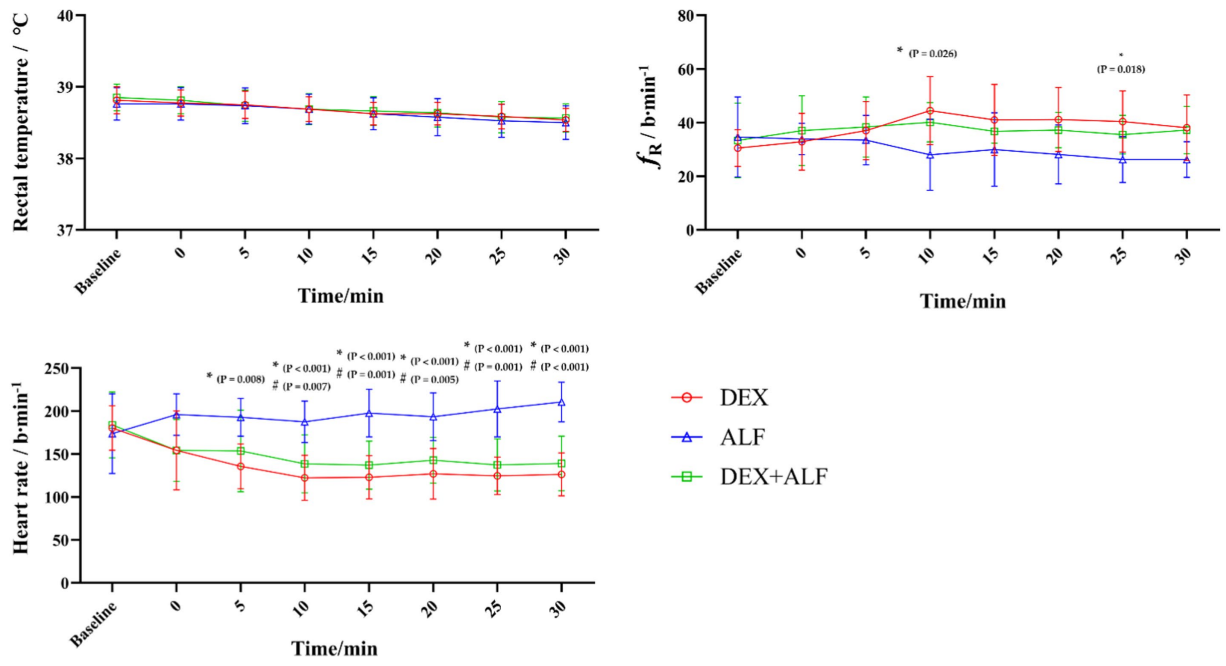

FIGURE 2
The results of rectal temperature (RT) Respiratory rate (f_R), heart rate (HR) after received drugs. DEX + ALF, the group received a combination of dexmedetomidine (5 μg/kg) and alfaxalone (5 mg/kg) intramuscularly; DEX, the group received dexmedetomidine (5 μg/kg) intramuscularly; ALF, the group received alfaxalone (5 mg/kg) intramuscularly, $n = 8$ cats; data are reported as mean ± SD. Baseline values were measured 30 min before the administrated of drugs. Baseline represents baseline values; T0 represents the injection of drugs, the following timepoints are represent as T5, T10, T15, and so on. *Significantly different between the value of DEX and ALF ($p < 0.05$); #Significantly different between the value of DEX + ALF and ALF ($p < 0.05$); †Significantly different between the value of DEX + ALF and DEX ($p < 0.05$).

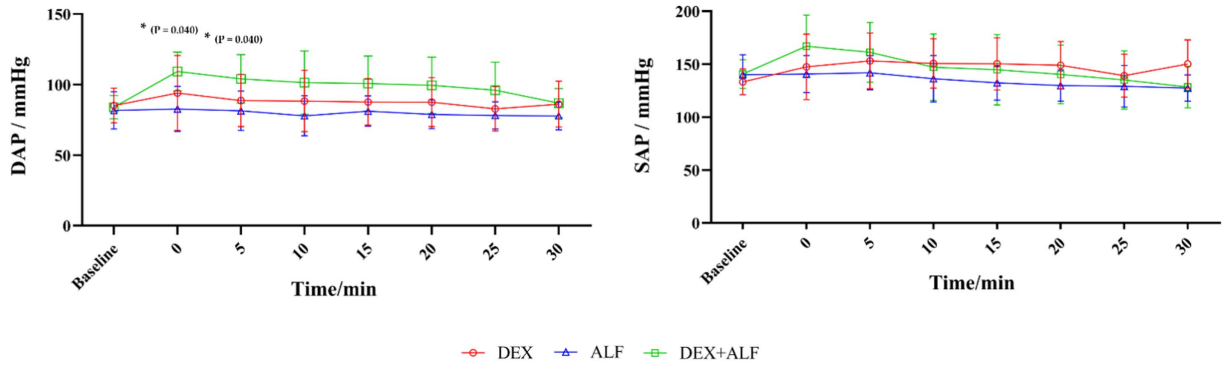

FIGURE 3
The results of systolic arterial pressure (SAP) and diastolic arterial pressure (DAP) after received drugs. DEX + ALF, the group received a combination of dexmedetomidine (5 μg/kg) and alfaxalone (5 mg/kg) intramuscularly; DEX, the group received dexmedetomidine (5 μg/kg) intramuscularly; ALF, the group received alfaxalone (5 mg/kg) intramuscularly, $n = 8$ cats; data are reported as mean ± SD. Baseline values were measured 30 min before the administrated of drugs. Baseline represents baseline values; T0 represents the injection of drugs, the following timepoints are represent as T5, T10, T15, and so on. *Significantly different between the value of DEX and ALF ($p < 0.05$); #Significantly different between the value of DEX + ALF and ALF ($p < 0.05$); †Significantly different between the value of DEX + ALF and DEX ($p < 0.05$).

this study were 21.79 ± 2.78 and 21.38 ± 2.99 mmHg, respectively. Meanwhile, the STT-1 values of the right and left eye were 16.50 ± 3.11 and 17.12 ± 4.10 mm/min. There were no significant differences in the values of IOP or STT-1 between the left and right eye before treatment ($p > 0.05$). In this trial, IOP and STT-1 examinations were only measured on left eye after administration of drugs.

IOP data from the left eyes did not differ significantly among three groups at any time point ($p > 0.05$). There were no significant differences in IOP measurements in all three groups except T15 ($p = 0.044$) in DEX group, T10 ($p = 0.009$) and T30 ($p = 0.031$) in ALF group compared to the baseline values of each group.

STT-1 data from left eyes did not differ significantly among three groups at any time point ($p > 0.05$). STT-1 values reduced significantly in all three groups during the process except T5 ($p = 0.784$) in DEX group compared to the baseline values of each group.

TABLE 3 The results of intraocular pressure (IOP) and Schirmer tear test 1 (STT-1) after received drugs.

Time	IOP (mmHg)			STT-1 (mm/min)		
	DEX	ALF	DEX + ALF	DEX	ALF	DEX + ALF
Baseline	21.00 ± 3.74	20.62 ± 2.88	22.50 ± 2.20	15.00 ± 4.00	19.25 ± 4.59	17.12 ± 2.80
T0	22.75 ± 3.69	22.25 + 3.65	22.12 ± 2.64			
T5	23.88 ± 4.55	25.25 ± 4.40	23.00 ± 3.42	12.62 ± 3.62	13.62 ± 4.75 ☆ ($p = 0.010$)	12.50 ± 2.78 ☆ ($p = 0.043$)
T10	24.62 ± 3.74	25.62 ± 2.77 ☆ ($p = 0.009$)	22.25 ± 3.28			
T15	26.62 ± 7.05 ☆ ($p = 0.044$)	24.00 ± 2.98	22.88 ± 3.93	7.00 ± 3.25 ☆ ($p < 0.001$)	7.00 ± 2.27 ☆ ($p < 0.001$)	7.12 ± 2.03 ☆ ($p < 0.001$)
T20	25.62 ± 4.56	24.88 ± 2.75	22.88 ± 5.33			
T25	26.12 ± 3.18	24.75 ± 2.49	23.12 ± 6.20	3.62 ± 1.68 ☆ ($p < 0.001$)	2.00 ± 1.31 ☆ ($p < 0.001$)	2.88 ± 1.88 ☆ ($p < 0.001$)
T30	24.50 ± 4.57	24.88 ± 2.95 ☆ ($p = 0.031$)	22.75 ± 4.56			

DEX + ALF, the group received a combination of dexmedetomidine (5 μg/kg) and alfaxalone (5 mg/kg) intramuscularly; DEX, the group received dexmedetomidine (5 μg/kg) intramuscularly; ALF, the group received alfaxalone (5 mg/kg) intramuscularly, $n = 8$ cats; data are reported as mean ± SD. Baseline values were measured 30 min before the administrated of drugs. Baseline represents baseline values; T0 represents the injection of drugs, the following timepoints are represent as T5, T10, T15, and so on. *Significantly different from the value of baseline.

3.5 ERG data

The results of ERG were presented in Table 4 and representative electroretinogram response was shown in Figure 4. ERG data from right eyes had no significant differences among three groups at any time point ($p > 0.05$) except for b-wave amplitude in the condition of DA 0.01 between DEX and ALF groups ($p = 0.031$), a-wave amplitude in the condition of LA 3.0 between ALF and DEX + ALF groups ($p = 0.008$).

4 Discussion

Compared with ophthalmoscopic and behavioral examinations, the ERG allows for an objective characterization of specific cell types in the retina and can be used for earlier diagnosis of retinal disease (29). The administration of anesthetic drugs in animals can avoid background noises generated by body or globe movements during ERG recording. It is crucial to regulate IOP and STT-1, especially IOP, to ensure the success of ophthalmic surgery (30), however, there are few reports about the effects of alfaxalone on ocular parameters in cats. Therefore, we evaluated the effect of IM administration of DEX, ALF, or DEX + ALF groups on short ERG protocol, IOP, and STT-1 in cats. All three treatments enabled the cats to tolerate corneal electrodes and subcutaneous needle electrodes. After the reversal with atipamezole in DEX and DEX + ALF groups, head-lift times were significantly shorter than ALF group. The time to recovery from sedation had no significant differences in three treatments.

The short ERG protocol used in this study includes the mixed, rod, and cone responses to light or dark conditions. Three treatments allowed for the successful completion of the ERG examination in cats. ERG changed with different sedation treatments. A higher a-wave amplitude under light-adapted cone response (LA 3.0) conditions was found in DEX + ALF group compared to ALF group, which indicated a difference in the overall assessment of the outer and inner retina in the day vision. Similar to the findings in this study, a previous study observed significant differences in the photopic b-wave amplitude when ketamine was used combined with xylazine or dexmedetomidine in cats (31). And a higher b-wave amplitude under dark-adapted rod response (DA 0.01) conditions was found in DEX group compared to ALF group, which indicated a difference in the rod responses in night vision. Other ERG variables showed no significant changes among three treatments, including: 1. Light-adapted flicker (LA 3.0 flicker) evoked a robust response of the cone pathway; 2. Dark-adapted, mixed, rod and cone response (DA 3.0) that assessed both rod and cones; 3. Dark-adapted mixed, rod and cone response to a higher intensity flash (DA 10.0) that evaluated the retinal function on the media opacity; 4. Dark-adapted oscillatory potentials (DA OPs) extracted from the mixed response by using the 85 Hz bandpass filter, providing more subtle and consistent information about the diffused changes in the inner retina caused by ischemic events or amacrine cell function. Awake cats cannot perform ERG protocol in this trail. But studies have shown that anesthesia and sedation resulted in significant attenuation and delay of ERG responses in dogs (6).

Local anesthesia and mydriasis might potentially influence the measurements of IOP and STT-1, tropicamide and local anesthetic drugs were not used in the left eye in this trial (32–34). There were no significant differences in IOP and STT-1 values between the left and right eyes before the start of sedation, and it had been reported that there were no significant differences between IOP and STT in the left and right eyes after anesthesia (14). Thus we conducted the IOP and STT-1 measurements exclusively on the left eye. Alfaxalone (1–3 mg/kg IM) is reported to significantly increase IOP in dogs that were premedicated with dexmedetomidine or without any premedication (35). Wolfran et al. reported that IM administration of dexmedetomidine (10 μg/kg) reduced IOP and tear production in cats, while a lower dose of 7.5 μg/kg had no significant effect on IOP (36). In dogs receiving intravenous injection of 5 μg/kg dexmedetomidine,

TABLE 4 The results of the short electroretinogram protocol after received drugs.

		Animal group		
		DEX	ALF	DEX + ALF
DA 0.01				
b-wave	Amplitude	55.50 ± 27.34 * (p = 0.031)	45.85 ± 19.41 * (p = 0.031)	60.19 ± 11.26
	Implicit time	48.76 ± 4.80	56.99 ± 7.58	54.42 ± 4.69
DA 3.0				
a-wave	Amplitude	−70.94 ± 31.83	−63.35 ± 33.24	−53.11 ± 29.48
	Implicit time	11.54 ± 0.79	12.71 ± 2.03	11.24 ± 1.36
b-wave	Amplitude	458.25 ± 109.59	366.13 ± 123.34	442.50 ± 160.79
	Implicit time	34.95 ± 3.29	38.16 ± 7.93	38.85 ± 3.77
DA OPs				
	Amplitude	97.30 ± 60.33	90.10 ± 54.56	93.03 ± 33.31
	Implicit time	142.94 ± 24.53	128.61 ± 35.15	143.30 ± 13.85
DA 10.0				
a-wave	Amplitude	−93.03 ± 39.66	−68.29 ± 62.93	−111.63 ± 63.46
	Implicit time	9.98 ± 1.01	10.91 ± 2.10	10.04 ± 1.91
b-wave	Amplitude	483.38 ± 125.32	415.00 ± 134.98	459.13 ± 160.92
	Implicit time	32.85 ± 2.35	35.68 ± 6.12	34.21 ± 3.23
LA 3.0				
a-wave	Amplitude	−7.00 ± 1.53	−5.29 ± 2.23 # (p = 0.008)	−8.90 ± 2.47 # (p = 0.008)
	Implicit time	8.88 ± 0.49	10.41 ± 1.63	9.84 ± 1.90
b-wave	Amplitude	71.64 ± 22.37	70.16 ± 33.69	62.78 ± 21.83
	Implicit time	22.48 ± 5.67	29.99 ± 9.63	23.01 ± 6.29
LA 3.0 flicker				
	Amplitude	78.66 ± 34.51	47.11 ± 17.97	56.38 ± 21.59
	Implicit time	36.93 ± 18.39	24.28 ± 12.16	24.01 ± 12.04

DEX + ALF, the group received a combination of dexmedetomidine (5 μg/kg) and alfaxalone (5 mg/kg) intramuscularly; DEX, the group received dexmedetomidine (5 μg/kg) intramuscularly; ALF, the group received alfaxalone (5 mg/kg) intramuscularly, n = 8 cats; data are reported as mean ± SD. *Significantly different between the value of DEX and ALF (p < 0.05); #Significantly different between the value of DEX + ALF and ALF (p < 0.05).

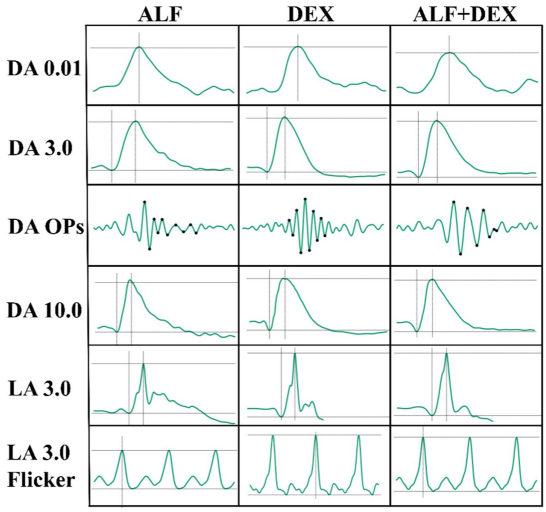

FIGURE 4
Representative electroretinogram response after received drugs. DEX + ALF, the group received a combination of dexmedetomidine (5 μg/kg) and alfaxalone (5 mg/kg) intramuscularly; DEX, the group received dexmedetomidine (5 μg/kg) intramuscularly; ALF, the group received alfaxalone (5 mg/kg) intramuscularly, n = 8 cats. DA 0.01, dark-adapted rod response; DA 3.0, dark-adapted, mixed, rod and cone response; DA Ops, dark-adapted oscillatory potentials; DA 10.0, dark-adapted mixed, rod and cone response to a higher intensity flash; LA 3.0, light-adapted cone response; LA 3.0 flicker, light-adapted 3.0 flicker.

there was no significant difference in IOP measurements within 10 min of drug administration (37, 38). Cats sedation with intramuscular 100 μg/kg medetomidine did not cause a statistically significant change in IOP values (14). In this study, we only observed statistical differences at T15 in DEX group, T10, and T30 in ALF group compared to their baseline, respectively. The lower dose of dexmedetomidine (5 μg/kg) used in our study might explain the discrepancy with the previous study. Additionally, DEX + ALF group could potentially counteract the elevation of IOP compared to ALF group. It was speculated to be related to changes in the production and outflow of aqueous humour (39). But further research is needed to investigate the underlying mechanisms. Corneal injuries are common ocular complications due to the lack of eyelid protection and deficiency of tear production (40). Previous studies demonstrated that medetomidine-ketamine, dexmedetomidine, methadone, dexmedetomidine-methadone and general anaesthesia could reduce tear production (12, 36, 41). Similarly, in the present study, all three treatments reduced tear production in cats.

Notably, even at the lower dose utilized in this study, IM administration of dexmedetomidine (5 μg/kg) resulted in a reduction in HR in cats from the DEX and DEX + ALF groups. These findings are consistent with prior studies indicating that dexmedetomidine administration results in decreased HR in cats, irrespective of dose (26, 42, 43). Alfaxalone treatment demonstrated minimal cardiovascular depression at clinical routine doses (2–10 mg/kg). Previous studies showed that administering supraclinical doses of alfaxalone alone (15 and 50 mg/kg) can lead to dose-dependent decrease in HR and arterial blood pressure in cats (21). The increase in HR is observed after the IM administration of various doses of alfaxalone (1, 2.5, 5, 10 mg/kg) (44). The results of the present trial are similar to these studies, the HR increased following the IM administration of alfaxalone in ALF group. SAP and DAP values displayed a biphasic pattern in DEX + ALF and DEX groups, with blood pressure values initially increased for the

first 10 min after the treatment, subsequently declining gradually to baseline levels. It may be due to the alpha-2 adrenergic agonists such as dexmedetomidine can induce peripheral vasoconstriction by activating post-synaptic alpha-2 receptors in the peripheral vascular smooth muscle, leading to an increase in blood pressure. Blood pressure may subsequently decrease due to a central effect on sympathetic tone (45). The administration of alfaxalone (5 mg/kg, IM) and dexmedetomidine (10, 20, and 40 μg/kg, IM) also showed similar results on arterial blood pressure in cats (26, 46). The administration of alfaxalone in cats caused a dose-dependent suppressive effect on arterial blood pressure (21, 47). In this study, the blood pressure showed a gradual decrease and stabilized after 15 min, no significant suppression was recorded after the administration of alfaxalone.

In the present study, apnea was not observed and f_R was well maintained in all treatments. Apnea after the IV administration of alfaxalone has been reported as an uncommon side effect in cats (47). The IM administration of 10 μg/kg dexmedetomidine and 5 mg/kg alfaxalone with or without 0.2 mg/kg butorphanol in cats has been reported to decrease the respiratory rate which was not observed in this study (46, 48). This might be related to the lower doses of drugs used in the present work.

Some limitations in this study should be noted. Firstly, the relatively small sample size may affect the generalizability of the findings. Furthermore, baseline data of ERG was not obtained as a blank control in cats. Finally, the cats used in this study were young, healthy, spayed female cats, and older, sick, or male cats may respond differently to these treatments.

5 Conclusion

In the present study, we successfully completed the short ERG examination under three protocols in cats. Except for higher photopic a-wave amplitude in DEX + ALF group compared with ALF group, no significant changes in the ERG variables were observed in three treatments. All these treatments resulted in increased IOP values and reduced STT-1 values.

Data availability statement

The original contributions presented in the study are included in the article/Supplementary material, further inquiries can be directed to the corresponding author.

Ethics statement

The animal study was approved by the Institutional Animal Care and Use Committee of Nanjing Agricultural University. The study was conducted in accordance with the local legislation and institutional requirements.

Author contributions

YG: Conceptualization, Data curation, Investigation, Methodology, Visualization, Writing – original draft. SM: Writing – review & editing. ZZ: Writing – review & editing, Project administration, Supervision.

Funding

The author(s) declare that no financial support was received for the research, authorship, and/or publication of this article.

Acknowledgments

The authors wish to thank Xingkai Zhao, Hang Gao and Shuai Li.

Conflict of interest

The authors declare that the research was conducted in the absence of any commercial or financial relationships that could be construed as a potential conflict of interest.

Publisher's note

Supplementary material

The Supplementary material for this article can be found online at: https://www.frontiersin.org/articles/10.3389/fvets.2024.1407928/full#supplementary-material

References

1. Narfstrom K. Electroretinography in veterinary medicine – easy or accurate? *Vet Ophthalmol.* (2002) 5:249–51. doi: 10.1046/j.1463-5224.2002.00252.x

2. Ekesten B, Komáromy AM, Ofri R, Petersen-Jones SM, Narfström K. Guidelines for clinical electroretinography in the dog: 2012 update. *Doc Ophthalmol.* (2013) 127:79–87. doi: 10.1007/s10633-013-9388-8

3. Kerdchuchuen K, Samathayanon K, Phientong P, Chattraphirat S, Jaturakan O, Tuntivanich N. Comparison of intraocular pressure in healthy brachycephalic and nonbrachycephalic cats using the Icare® TONOVET plus rebound tonometer. *Vet Ophthalmol.* (2021) 24:484–90. doi: 10.1111/vop.12929

4. Sebbag L, Uhl LK, Schneider B, Hayes B, Olds J, Mochel JP. Investigation of Schirmer tear test-1 for measurement of tear production in cats in various environmental settings and with different test durations. *J Am Vet Med Assoc.* (2020) 256:681–6. doi: 10.2460/javma.256.6.681

5. Pasmanter N, Petersen-Jones SM. A review of electroretinography waveforms and models and their application in the dog. *Vet Ophthalmol.* (2020) 23:418–35. doi: 10.1111/vop.12759

6. Freeman KS, Good KL, Kass PH, Park SA, Nestorowicz N, Ofri R. Effects of chemical restraint on electroretinograms recorded sequentially in awake, sedated, and anesthetized dogs. *Am J Vet Res.* (2013) 74:1036–42. doi: 10.2460/ajvr.74.7.1036

7. Costa GL, Leonardi F, Interlandi C, Spadola F, Fisichella S, Macrì F, et al. Levobupivacaine combined with cisatracurium in peribulbar anaesthesia in cats undergoing corneal and lens surgery. *Animals*. (2023) 13:170. doi: 10.3390/ani13010170

8. Gelatt KN, MacKay EO. Distribution of intraocular pressure in dogs. *Vet Ophthalmol*. (1998) 1:109–14. doi: 10.1046/j.1463-5224.1998.00024.x

9. Hofmeister EH, Weinstein WL, Burger D, Brainard BM, Accola PJ, Moore PA. Effects of graded doses of propofol for anesthesia induction on cardiovascular parameters and intraocular pressures in normal dogs. *Vet Anaesth Analg*. (2009) 36:442–8. doi: 10.1111/j.1467-2995.2009.00482.x

10. Murphy DF. Anesthesia and intraocular pressure. *Anesth Analg*. (1985) 64:520–30. doi: 10.1213/00000539-198505000-00013

11. Shilo-Benjamini Y, Pe'er O, Abu Ahmad W, Ofri R. Effect of anesthetic induction with propofol, alfaxalone or ketamine on intraocular pressure in cats: a randomized masked clinical investigation. *Vet Anaesth Analg*. (2023) 50:63–71. doi: 10.1016/j.vaa.2022.11.005

12. Di Pietro S, Macrì F, Bonarrigo T, Giudice E, Palumbo Piccionello A, Pugliese A. Effects of a medetomidine-ketamine combination on Schirmer tear test I results of clinically normal cats. *Am J Vet Res*. (2016) 77:310–4. doi: 10.2460/ajvr.77.3.310

13. Mayordomo-Febrer A, Rubio M, Martínez-Gassent M, López-Murcia MM. Effects of morphine-alfaxalone-midazolam premedication, alfaxalone induction and sevoflurane maintenance on intraocular pressure and tear production in dogs. *Vet Rec*. (2017) 180:474. doi: 10.1136/vr.104040

14. Malmasi A, Selk GM. Lack of effects of intramuscular medetomidine on intraocular pressure in clinically normal cats. *J Feline Med Surg*. (2016) 18:315–7. doi: 10.1177/1098612X15583343

15. Grubb T, Sager J, Gaynor JS, Montgomery E, Parker JA, Shafford H, et al. 2020 AAHA anesthesia and monitoring guidelines for dogs and cats. *J Am Anim Hosp Assoc*. (2020) 56:59–82. doi: 10.5326/JAAHA-MS-7055

16. Harrison NL, Simmonds MA. Modulation of the GABA receptor complex by a steroid anaesthetic. *Brain Res*. (1984) 323:287–92. doi: 10.1016/0006-8993(84)90299-3

17. Cottrell GA, Lambert JJ, Peters JA. Modulation of GABA-A receptor activity by alphaxalone. *Br J Pharmacol*. (1987) 90:491–500. doi: 10.1111/j.1476-5381.1987.tb11198.x

18. Interlandi C, Bruno F, Tabbì M, Macrì F, Di Pietro S, Giudice E, et al. Intraoperative isoflurane end-tidal concentration during infusion of fentanyl, tramadol, or fentanyl–tramadol combination in cats. *Vet Sci*. (2024) 11:125. doi: 10.3390/vetsci11030125

19. Child KJ, Davis B, Dodds MG, Twissell DJ. Anaesthetic, cardiovascular and respiratory effects of a new steroidal agent CT 1341: a comparison with other intravenous anaesthetic drugs in the unrestrained cat. *Br J Pharmacol*. (1972) 46:189–200. doi: 10.1111/j.1476-5381.1972.tb06864.x

20. Rodrigo-Mocholí D, Escudero E, Belda E, Laredo FG, Hernandis V, Marín P. Pharmacokinetics and effects of alfaxalone after intravenous and intramuscular administration to cats. *N Z Vet J*. (2018) 66:172–7. doi: 10.1080/00480169.2018.1455541

21. Muir W, Lerche P, Wiese A, Nelson L, Pasloske K, Whittem T. The cardiorespiratory and anesthetic effects of clinical and supraclinical doses of alfaxalone in cats. *Vet Anaesth Analg*. (2009) 36:42–54. doi: 10.1111/j.1467-2995.2008.00428.x

22. Chiu KW, Robson S, Devi JL, Woodward A, Whittem T. The cardiopulmonary effects and quality of anesthesia after induction with alfaxalone in 2-hydroxypropyl-β-cyclodextrin in dogs and cats: a systematic review. *J Vet Pharmacol Ther*. (2016) 39:525–38. doi: 10.1111/jvp.12312

23. Campbell D, Forrester AC, Miller DC, Hutton I, Kennedy JA, Lawrie TD, et al. A preliminary clinical study of CT1341—a steroid ANAESTHETIC agent. *Br J Anaesth*. (1971) 43:14–24. doi: 10.1093/bja/43.1.14

24. Whittem T, Pasloske KS, Heit MC, Ranasinghe MG. The pharmacokinetics and pharmacodynamics of alfaxalone in cats after single and multiple intravenous administration of Alfaxan at clinical and supraclinical doses. *J Vet Pharmacol Ther*. (2008) 31:571–9. doi: 10.1111/j.1365-2885.2008.00998.x

25. Weerink MAS, Struys M, Hannivoort LN, Barends CRM, Absalom AR, Colin P. Clinical pharmacokinetics and pharmacodynamics of dexmedetomidine. *Clin Pharmacokinet*. (2017) 56:893–913. doi: 10.1007/s40262-017-0507-7

26. Rodrigo-Mocholí D, Belda E, Bosmans T, Laredo FG. Clinical efficacy and cardiorespiratory effects of intramuscular administration of alfaxalone alone or in combination with dexmedetomidine in cats. *Vet Anaesth Analg*. (2016) 43:291–300. doi: 10.1111/vaa.12304

27. Carroll GL. *Small animal anesthesia and analgesia*. Hoboken, New Jersey: Wiley (2008).

28. Cremer J, da Cunha A, Aulakh K, Liu CC, Acierno MJ. Validation of the oscillometric blood pressure monitor Vet20 SunTech in anesthetized healthy cats. *Vet Anaesth Analg*. (2020) 47:309–14. doi: 10.1016/j.vaa.2019.12.007

29. Gelatt K, Gilger B, Kern T. *Veterinary ophthalmology*. (2012)

30. Brunson DB. Anesthesia in ophthalmic surgery. *Vet Clin North Am Small Anim Pract*. (1980) 10:481–95. doi: 10.1016/S0195-5616(80)50042-2

31. Del Sole MJ, Nejamkin P, Cavilla V, Schaiquevich P, Moreno L. Comparison of two sedation protocols for short electroretinography in cats. *J Feline Med Surg*. (2018) 20:172–8. doi: 10.1177/1098612X17703011

32. Sarchahi AA, Eskandari M. Effect of four local anesthetics (tetracaine, proparacaine, lidocaine, and bupivacaine) on intraocular pressure in dogs. *Int Ophthalmol*. (2019) 39:1467–74. doi: 10.1007/s10792-018-0969-0

33. Hamor RE, Roberts SM, Severin GA, Chavkin MJ. Evaluation of results for Schirmer tear tests conducted with and without application of a topical anesthetic in clinically normal dogs of 5 breeds. *Am J Vet Res*. (2000) 61:1422–5. doi: 10.2460/ajvr.2000.61.1422

34. Margadant DL, Kirkby K, Andrew SE, Gelatt KN. Effect of topical tropicamide on tear production as measured by Schirmer's tear test in normal dogs and cats. *Vet Ophthalmol*. (2003) 6:315–20. doi: 10.1111/j.1463-5224.2003.00313.x

35. Bauer BS, Ambros B. The effects of intravenous alfaxalone with and without premedication on intraocular pressure in healthy dogs. *Can J Vet Res*. (2016) 80:156–61.

36. Wolfran L, Debiage RR, Lopes DM, Fukushima FB. Ophthalmic effects of dexmedetomidine, methadone and dexmedetomidine-methadone in healthy cats and their reversal with atipamezole. *J Feline Med Surg*. (2022) 24:1253–9. doi: 10.1177/1098612X221077023

37. Artigas C, Redondo JI, López-Murcia MM. Effects of intravenous administration of dexmedetomidine on intraocular pressure and pupil size in clinically normal dogs. *Vet Ophthalmol*. (2012) 15:79–82. doi: 10.1111/j.1463-5224.2011.00966.x

38. Kusolphat P, Soimala T, Sunghan J. Intraocular pressure and cardiovascular effects of dexmedetomidine premedication and tiletamine-zolazepam for anesthetic induction in dogs. *Vet World*. (2022) 15:2929–36. doi: 10.14202/vetworld.2022.2929-2936

39. Rauser P, Pfeifr J, Proks P, Stehlík L. Effect of medetomidine-butorphanol and dexmedetomidine-butorphanol combinations on intraocular pressure in healthy dogs. *Vet Anaesth Analg*. (2012) 39:301–5. doi: 10.1111/j.1467-2995.2011.00703.x

40. Snow JC, Kripke BJ, Norton ML, Chandra P, Woodcome HA. Corneal injuries during general anesthesia. *Anesth Analg*. (1975) 54:465–7. doi: 10.1213/00000539-197507000-00014

41. Peche N, Köstlin R, Reese S, Pieper K. Postanaesthetic tear production and ocular irritation in cats. *Tierarztl Prax Ausg K Kleintiere Heimtiere*. (2015) 43:75–82. doi: 10.15654/TPK-140182

42. McSweeney PM, Martin DD, Ramsey DS, McKusick BC. Clinical efficacy and safety of dexmedetomidine used as a preanesthetic prior to general anesthesia in cats. *J Am Vet Med Assoc*. (2012) 240:404–12. doi: 10.2460/javma.240.4.404

43. Granholm M, McKusick BC, Westerholm FC, Aspegrén JC. Evaluation of the clinical efficacy and safety of dexmedetomidine or medetomidine in cats and their reversal with atipamezole. *Vet Anaesth Analg*. (2006) 33:214–23. doi: 10.1111/j.1467-2995.2005.00259.x

44. Tamura J, Ishizuka T, Fukui S, Oyama N, Kawase K, Itami T, et al. Sedative effects of intramuscular alfaxalone administered to cats. *J Vet Med Sci*. (2015) 77:897–904. doi: 10.1292/jvms.14-0200

45. Dobromylskyj P. Cardiovascular changes associated with anaesthesia induced by medetomidine combined with ketamine in cats. *J Small Anim Pract*. (1996) 37:169–72. doi: 10.1111/j.1748-5827.1996.tb01953.x

46. Grubb TL, Greene SA, Perez TE. Cardiovascular and respiratory effects, and quality of anesthesia produced by alfaxalone administered intramuscularly to cats sedated with dexmedetomidine and hydromorphone. *J Feline Med Surg*. (2013) 15:858–65. doi: 10.1177/1098612X13478265

47. Taboada FM, Murison PJ. Induction of anaesthesia with alfaxalone or propofol before isoflurane maintenance in cats. *Vet Rec*. (2010) 167:85–9. doi: 10.1136/vr.b4872

48. Khenissi L, Nikolayenkova-Topie O, Broussaud S, Touzot-Jourde G. Comparison of intramuscular alfaxalone and ketamine combined with dexmedetomidine and butorphanol for castration in cats. *J Feline Med Surg*. (2017) 19:791–7. doi: 10.1177/1098612X16657951

frontiers | Frontiers in Veterinary Science

TYPE Original Research
PUBLISHED 22 July 2024
DOI 10.3389/fvets.2024.1417244

OPEN ACCESS

EDITED BY
Toshiro Arai,
Nippon Veterinary and Life Science University, Japan

REVIEWED BY
Jingjing Ling,
Elanco, United States
Jaya Bharati,
National Research Centre on Pig (ICAR), India

*CORRESPONDENCE
Shijia Ying
✉ 251510650@qq.com
Min Tang
✉ mt3138@ujs.edu.cn

RECEIVED 14 April 2024
ACCEPTED 08 July 2024
PUBLISHED 22 July 2024

CITATION
Liu Y, Sun D, Xu C, Liu X, Tang M and Ying S (2024) In-depth transcriptome profiling of Cherry Valley duck lungs exposed to chronic heat stress.
Front. Vet. Sci. 11:1417244.
doi: 10.3389/fvets.2024.1417244

In-depth transcriptome profiling of Cherry Valley duck lungs exposed to chronic heat stress

Yi Liu[1,2], Dongyue Sun[3], Congcong Xu[4], Xiaoyong Liu[1], Min Tang[1]*and Shijia Ying[2]*

[1]School of Life Sciences, Jiangsu University, Zhenjiang, Jiangsu, China, [2]Institute of Animal Science, Jiangsu Academy of Agricultural Sciences, Nanjing, China, [3]College of Animal Science and Technology, Nanjing Agricultural University, Nanjing, China, [4]College of Animal Science and Technology, Beijing University of Agriculture, Beijing, China

Amidst rising global temperatures, chronic heat stress (CHS) is increasingly problematic for the poultry industry. While mammalian CHS responses are well-studied, avian-specific research is lacking. This study uses in-depth transcriptome sequencing to evaluate the pulmonary response of Cherry Valley ducks to CHS at ambient temperatures of 20°C and a heat-stressed 29°C. We detailed the CHS-induced gene expression changes, encompassing mRNAs, lncRNAs, and miRNAs. Through protein–protein interaction network analysis, we identified central genes involved in the heat stress response—*TLR7*, *IGF1*, *MAP3K1*, *CIITA*, *LCP2*, *PRKCB*, and *PLCB2*. Subsequent functional enrichment analysis of the differentially expressed genes and RNA targets revealed significant engagement in immune responses and regulatory processes. KEGG pathway analysis underscored crucial immune pathways, specifically those related to intestinal IgA production and Toll-like receptor signaling, as well as Salmonella infection and calcium signaling pathways. Importantly, we determined six miRNAs—miR-146, miR-217, miR-29a-3p, miR-10926, miR-146b-5p, and miR-17-1-3p—as potential key regulators within the ceRNA network. These findings enhance our comprehension of the physiological adaptation of ducks to CHS and may provide a foundation for developing strategies to improve duck production under thermal stress.

KEYWORDS

chronic heat stress, duck rearing, environmental temperature, high-throughput sequencing technology, ceRNA

1 Introduction

The exponential growth of the global population necessitates substantial protein production, placing escalating demands on animal production systems, particularly within tropical and subtropical regions. This factor significantly contributes to ensuring global food security (1, 2). Among these production sectors, the poultry industry emerges as a crucial subsector that substantially fuels economic growth (3, 4). Nevertheless, the implications of global warming have engendered prolonged hyperthermia during the summer months, presenting a formidable challenge to the industry. This challenge has manifested in reduced productivity and substantial economic losses (5). This deleterious phenomenon, recognized as heat stress, has garnered extensive global attention and scrutiny (6).

Heat stress entails an imbalance between heat acquisition and dissipation, resulting in an elevation of poultry body temperature (7–9). It is typically categorized into intense or chronic heat stress (CHS), pertaining to brief or prolonged exposure to elevated ambient temperatures, respectively (10). Unfortunately, both intense and chronic heat stress can exact a toll on avian health (11, 12). This consequence extends to other domestic animals as well. Poultry, in particular, faces heightened vulnerability due to the absence of sweat glands and the majority of their body surface being covered in feathers. Consequently, the role of heat dissipation is largely assumed by the lungs in poultry (13, 14). When the ambient temperature falls within the thermal comfort zone, birds can sustain their body temperature with minimal effort. Typically, the optimal temperature for growing Pekin ducks ranges from 18 to 20°C (15). However, deviations from this range trigger behavioral, physiological, and metabolic adaptations aimed at temperature regulation and mitigating the impact of high temperatures (16–18). These adaptations include panting, reduced food intake, weight loss, and can culminate in undesirable outcomes such as increased feed conversion ratios (FCRs), stunted growth, and compromised meat quality. In cases where efficient heat dissipation is unattainable, multi-organ dysfunction may ensue, potentially leading to fatality (19–21).

Recent strides in high-throughput screening technology have culminated in the routine utilization of transcriptome sequencing for the quantification and identification of RNAs across diverse tissues and cells (22). RNA molecules bear transcribed genetic information that can be translated into proteins or directly/indirectly modulate gene expression levels (23). The variation in the number of different transcripts in response to temperature changes can offer valuable insights into cellular states and stress mechanisms (22, 24). Notably, heat shock proteins (HSPs) and phosphoinositide 3-kinase (PIK3) emerge as key participants in heat stress acclimation, with the genes encoding these proteins showing significant upregulation in heat-treated Fujian shelducks and Shan Ma, Pekin, Muscovy ducks (25–29). Furthermore, non-coding RNAs that play immunoregulatory roles during *Salmonella enteritidis* infection have been revealed through competing endogenous RNA (ceRNA) regulatory networks in Shaoxing ducks (30). Yet, the landscape of ceRNA networks under heat stress conditions remains largely uncharted.

In this pioneering study, we have created a CHS model in CVds—a breed with significant economic value—to explore the comprehensive transcriptomic alterations (31). Our innovative approach employs environmental control chambers for a precise induction of CHS, facilitating the in-depth examination of gene, miRNA, mRNA, and lncRNA expression variations using advanced sequencing techniques. Furthermore, we have delineated lncRNA-miRNA-mRNA networks to elucidate the intricate molecular dialogs during CHS, marking a novel foray into the full-spectrum transcriptomic impact of heat stress on these ducks.

2 Materials and methods

2.1 Animal resources, ethical approval and sample collection

This study was conducted in strict accordance with the regulations outlined by the Administration of Affairs Concerning Experimental Animals (Decree No. 63 of the Jiangsu Academy of Agricultural Science on 8 July 2014). All experimental procedures involving animals received ethical approval from the Research Committee of the Jiangsu Academy of Agricultural Sciences (Nanjing, China).

Following the approach detailed in (15, 32), a batch of 72 newly-hatched CVds with identical genetic backgrounds were procured from a commercial farm. These ducks were subsequently divided into two groups through random allocation, ensuring that there were no significant disparities in phenotypes or weights among any pair of groups. For brevity, these groups were subsequently referred to as W20 and W29. During the initial phase of rearing, all ducks were individually housed in separate pens equipped with an environmental control chamber, providing access to *ad libitum* feed and water (Supplementary Figure S1). Figure 1 illustrates that the ambient temperature was sustained at 35°C for the first 4 days and was subsequently decreased to 34°C for the following 3 days. Over days 8–12, the temperature in the W29 enclosure was gradually lowered by 1°C daily to 29°C, which was then sustained for 30 days. In parallel, the ambient temperature for W20 was similarly reduced by 1°C daily throughout this interval, leading to a steady state at 20°C (33). During the entire rearing phase, humidity was consistently maintained at 74% (34), with all ducks having free access to standard commercial pellet feed and water from a drip-nipple system.

Ultimately, at the market-age of day 43, three samples were collected from each group were humanely stunned with a 36 V electrified pool and then euthanized via jugular vein dissection (35). As the second key organ for heat dissipation, their lungs were carefully excised, promptly frozen in liquid nitrogen and then stored at −80°C prior to dispatch to the sequencing company.

2.2 Microscopic observation of duck lungs

The lungs of each selected duck from both groups were examined under a microscope at a magnification of 20×. Lung tissue samples from CVds were carefully extracted and subsequently fixed in 4% paraformaldehyde for a duration of 24 h to preserve the cellular structure for detailed histological analysis. Subsequently, the samples underwent dehydration using a graded alcohol series. These specimens were then infiltrated and embedded in paraffin, before being sectioned into thin serial slices of approximately 5 μm thickness. These sections

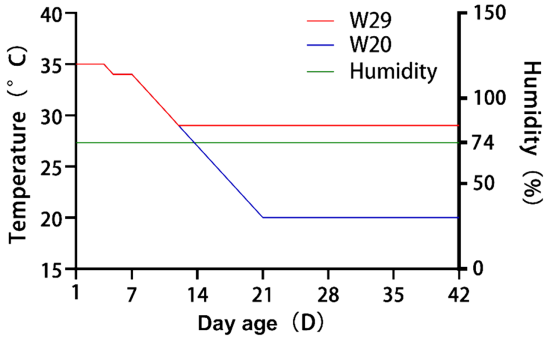

FIGURE 1
Detailed temperature regimens for W20 and W29 cohorts over the course of the investigation.

were mounted onto glass slides, subjected to hematoxylin and eosin staining, and observed using an Olympus microscope (BX53).

2.3 RNA extraction, library preparation and full transcriptome sequencing

For each group, total RNA was isolated from three biological replicates of lung tissue using TRIzol® reagent (Invitrogen, United States), following the manufacturer's protocol, and genomic DNA was removed with DNase I RNase-free (TaKara, Japan). The RNA concentration and integrity were verified using a NanoDrop 2,100 spectrophotometer (Thermo Fisher Scientific, United States) and an Agilent Bioanalyzer 2,100 (Agilent Technologies, United States), respectively. Only high-quality RNA samples (OD260/280 = 1.8 ~ 2.2, OD260/230 ≥ 2.0, RIN ≥ 6.5, 28S:18S ≥ 1.0, >1 μg) were used for sequencing library construction.

Libraries for mRNA and lncRNA were prepared using a ribosomal RNA depletion strategy with the NEBNext® Ultra™ Directional RNA Library Prep Kit for Illumina (New England Biolabs, United States), starting with 3 μg of RNA per sample. miRNA libraries were generated using the QIAseq miRNA Library Kit (Qiagen, Germany), adhering to the supplier's instructions. Based on the length distribution characteristic of miRNA, target fragments (16–35 nt) were isolated by gel excision on a 6% Novex TBE PAGE gel (1.0 mm, 10 well) (Invitrogen, United States). Quantification was performed using the Qubit 4.0 fluorometer (Thermo Fisher Scientific, United States), and sequencing was carried out on an Illumina NovaSeq 6,000 system (Illumina, United States) by Shanghai Majorbio Bio-pharm Biotechnology Co., Ltd. (Shanghai, China).

2.4 Data preprocessing and quality control

After the above deep sequencing, the raw paired-end reads were preprocessed using SeqPrep[1] and Sickle[2] by removing adaptor sequences and filtering low-quality reads (Supplementary Table S1). Clean reads were aligned using HISAT to the high-resolution reference genome of *Anas platyrhynchos* (*A. platyrhynchos* GCF_015476345.1, https://www.ncbi.nlm.nih.gov/genome/2793?genome_assembly_id=1498951) (36, 37). The mapped reads were assembled by StringTie in a reference-based approach (38). Also, the number of reads mapped to each transcript was calculated using RSEM, and the transcripts per million reads (TPM) was estimated to measure the expression level of each gene/transcript (39).

2.5 Bioinformatics analysis at gene expression level and mRNA expression level

Gene expression level is a broader term that encompasses the levels of all products of gene expression, including mRNA, non-coding RNAs, and proteins. mRNA expression level is a subset of this, focusing only on the messenger RNA produced during transcription. The DESeq2 package within R software was employed to identify genes and mRNAs that were differentially expressed between W20 and W29, with an emphasis on those exhibiting a greater than 1.5-fold change and an adjusted padj below 0.05, marking them as statistically significant (40). These findings were further examined for functional relevance using GO and KEGG pathway enrichment via GOATOOLS and KOBAS (41, 42). Additionally, differentially expressed genes (DEGs) were integrated into STRING (version 12.0) and Cytoscape (version 11.0.13) to delineate protein–protein interaction (PPI) networks, highlighting key modules using the cytoHubba plugin (43–45). Enrichment analysis of interactive gene targets was conducted using the BINGO plugin and the clusterProfiler package (46, 47).

2.6 Identification of lncRNA and prediction of target RNAs

Using the StringTie tool (38) with its default settings, we reassembled transcripts from the aligned clean reads. Subsequently, we cross-referenced these merged transcripts against known reference transcripts annotated in GFF/GTF formats and existing lncRNA databases to identify recognized lncRNAs. In addition, we pinpointed putative novel lncRNA transcripts by their length, requiring over 200 base pairs, and by the presence of two or more exons. To assess the coding potential of these transcripts, we employed a suite of tools: CNCI (48) with a score threshold below zero, CPC (49) with a score under 0.5, CPAT (50) with a score below 0.5, and Pfam with an e-value stricter than 1e-3 but not passing the threshold. Transcripts that were consistently predicted to lack protein-coding potential by these metrics were classified as novel lncRNAs. Potential *cis*- and *trans*-acting target mRNAs of lncRNAs were identified through an examination of gene expression patterns and chromosomal positioning, as outlined by (51). For *cis*-acting targets, genes situated within a 100,000 base-pair range flanking the lncRNA were pinpointed utilizing BEDTOOLS software as described by (52). The analysis of lncRNA-mediated trans-regulation was predicated on the correlation coefficient between the expressions of lncRNA and mRNA, with coefficients exceeding 0.9 signifying a potential trans-regulatory interaction.

2.7 Identification of miRNA and prediction of target RNAs

Initially, all clean mapped tags were matched to known miRNAs using the miRBase (version 22.1) database[3]. Subsequently, the remaining tags were cross-referenced with the Rfam and Repbase databases to filter out ribosomal RNA (rRNA), transfer RNA (tRNA), small nuclear RNA (snRNA), small nucleolar RNA (snoRNA), other non-coding RNAs, and repeats. Finally, unannotated tags were evaluated for potential novel miRNAs with miRdeep2 software (53),

1 https://github.com/jstjohn/SeqPrep

2 https://github.com/najoshi/sickle

3 http://www.mirbase.org/

based on their genomic location and the formation of hairpin structures. The miRanda algorithm (54) was applied to animal samples, while psRobot (55) was utilized for insect samples to forecast miRNA targets. Predicted miRNA-target RNAs were then determined by identifying the overlap in the outcomes from both tools.

2.8 Differentially expressed RNAs analysis

The refined datasets for lncRNAs, miRNAs, and mRNAs were obtained by discarding low-quality reads from the initial raw data, ensuring a Phred quality score of at least 20. RNAs that showed no expression in over three samples were excluded from subsequent analyses to maintain data integrity. Consequently, only high-quality filtered datasets were utilized for further analysis. To quantify RNA expression, the polished reads from the lncRNA and mRNA libraries were mapped to the reference genome via the STAR aligner, while the miRNA sequences were aligned to miRBase using the BOWTIE tool. The R software's limma package (56) was utilized for identifying differentially expressed mRNAs, lncRNAs, and miRNAs (DEmRNAs, DElncRNAs, and DEmiRNAs). Significant DEmRNAs and DElncRNAs were detected within the comparison groups, applying a threshold of padj <0.05 and an absolute log2FC greater than 1. For DEmiRNAs, the criteria of an absolute Log2FC greater than 0.585 and a *p*-adjust value below 0.05 were adopted. Functional enrichment analyses for GO terms and KEGG pathways were conducted on the target genes of DEmiRNAs and DElncRNAs, as well as on DEmRNAs, using the GOATOOLS and KOBAS tools (42).

2.9 Construction of the lncRNA-miRNA-mRNA regulatory network

To elucidate the relationships between DEmRNAs, DElncRNAs, and DEmiRNAs, a lncRNA-miRNA-mRNA regulatory network was established rooted in the ceRNA hypothesis. Predictions for miRNA-lncRNA and miRNA-mRNA pairings were conducted utilizing Miranda and Targetscan (57), respectively, while the Spearman correlation coefficient, hinged on expression levels, was employed to assess the interplay among these pairings. Visualization of the intricate network was achieved through Cytoscape software.

2.10 RT-qPCR validation for the expression level of DEmRNAs, DEmiRNAs, and DElncRNAs

The cDNA synthesis for mRNA involved reverse transcription using HiScript III RT SuperMix with gDNA wiper (Vazyme, China) in a thermal cycler, following the protocol provided by the manufacturer. The inverse transcription reaction (ITR) for mRNA was executed in a 20 μL reaction mix, incubated at 37°C for 15 min and 85°C for 5 s, then cooled to 4°C. For lncRNA, cDNA synthesis was performed using the lnRcute lncRNA cDNA First-Strand Synthesis Kit and FastKing One Step First-Strand Synthesis Kit (both from Tiangen, Beijing, China). The cDNA for miRNA was synthesized using the miRNA First Strand cDNA Synthesis (Stem-loop Method) Kit (Sangon Biotech, China), with the ITR for both lncRNA and miRNA conducted as per their respective kits' guidelines.

Primer sets for mRNA were crafted using Primer Premier 6 software, while primer sets for lncRNA and miRNA were designed via Sangon Biotech's online tools[4]. All primers used in this study were synthesized by Genewiz® (China), based on sequences in GenBank and the reference genome. Then, quantitative real-time PCR (RT-qPCR) was carried out using SYBR Green Master Mix (Yeasen, Shanghai, China) on an ABI 7500 Sequence Detector (Applied Biosystem, United States) according to the manufacturer's instructions. The reaction mixture included 10 μL of first-strand cDNA, 0.4 μM each of forward and reverse primers, and 10 μL of 2× SYBR Green Master Mix, totalling 20 μL. For miRNA, the MicroRNAs qPCR Kit (SYBR Green Method) from Sangon Biotech was employed. The RT-qPCR protocol consisted of an initial denaturation at 95°C for 2 min, followed by 34 cycles of 95°C for 10 s and 60°C for 30 s. All assays were performed in triplicate, with GAPDH as the internal control gene for mRNA and lncRNA, and U6 snRNA as the internal control for miRNA expression studies (37, 58). Melting curve analysis confirmed the specificity of the amplification, and relative gene expression was quantified using the $2^{-\Delta\Delta Ct}$ method.

3 Results

3.1 Growth performance and carcass traits

Supplementary Figure S2 reveals that at the 43-day collection point, W20 exhibited superior performance over W29 in the majority of carcass characteristics. For a more comprehensive analysis, please consult our previously published work (1). These findings suggest that the growth rate of CVds decelerates when ambient temperatures rise from 20°C to 29°C, aligning with the findings reported in (4).

3.2 Histopathological examination

In the comparative illustration provided by Figure 2, the lungs of W20 exhibited a robust, reddish color and no exudate, with the alveoli retaining their proper form and exhibiting only minor signs of inflammation. The lung interstitium was also free from any signs of excess fluid. In stark contrast, the W29 samples showed significant exudation and altered alveoli that no longer maintained their usual shape. These samples demonstrated considerable changes including thickened alveolar walls, capillary closure, and the presence of inflammatory cells within the alveolar passages, along with interstitial swelling. Yet, these issues were less pronounced than in previous W29 samples.

4 https://store.sangon.com/newPrimerDesign

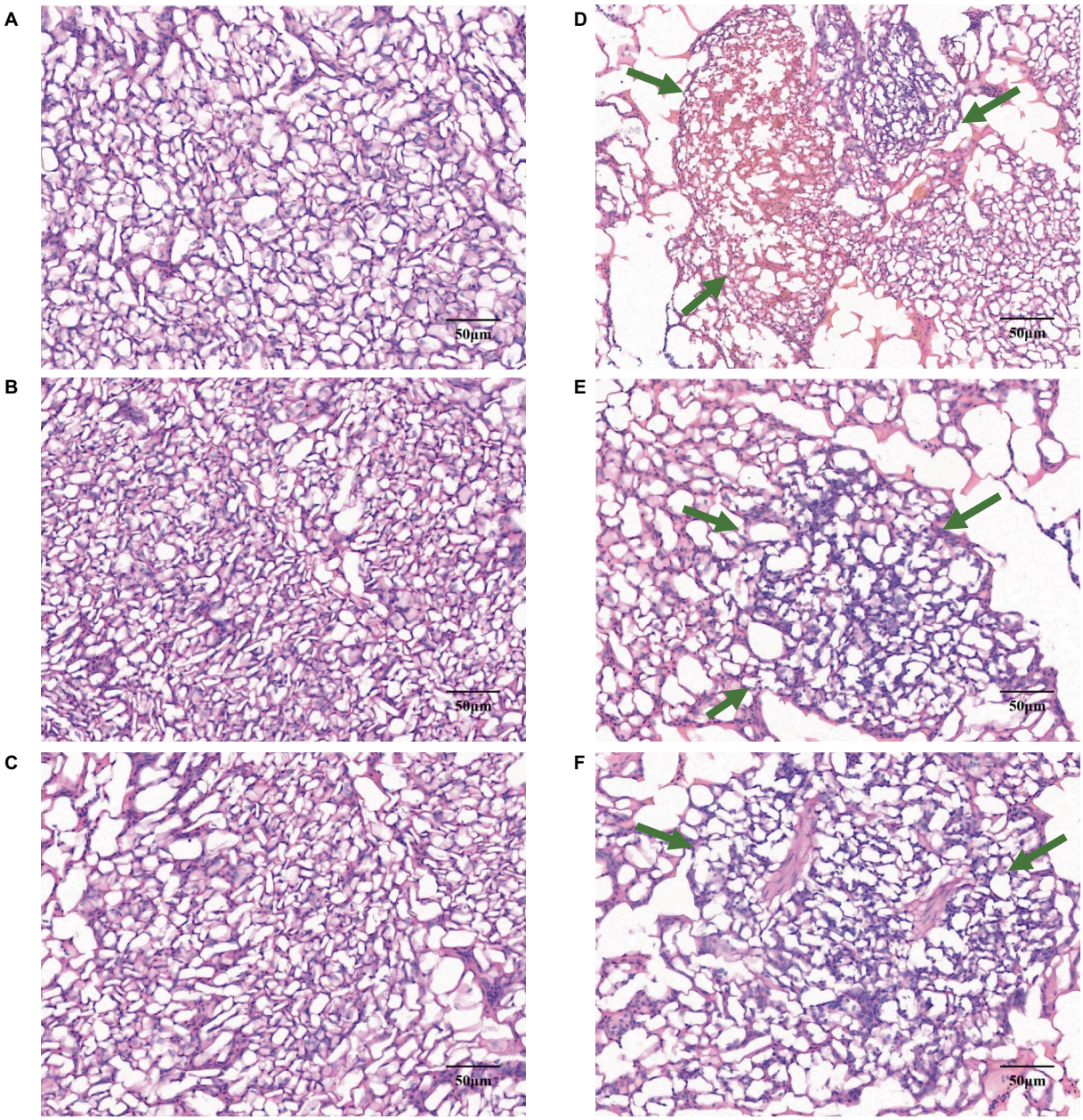

FIGURE 2
Gene expression profiles in CVds at 43 days of age. The cross-sectional areas of CVds lung tissue reared in an environmental control chamber at **(A–C)** 20°C and **(D–F)** 29°C. In panels **(D–F)**, the green arrows point to areas of inflammatory tissue.

3.3 Gene expression divergence and subsequent analysis

To elucidate the genetic underpinnings of heat tolerance in CVds, transcriptomic analyses were conducted on individual lung samples from both W20 and W29 groups using the Illumina NovaSeq 6,000 system. Each of the three cDNA libraries yielded a substantial number of clean reads, amassing billions of nucleotides in total. More than 91% of the clean reads from each library can be mapped to the reference genome of *A. platyrhynchos*. The expression level of each transcript was measured using TPM method. For the evaluation of gene expression variance, the profiles of the longest transcript isoforms were considered. Followed Principal Component Analysis (PCA) demonstrated a marked distinction between the W20 and W29 sample groups (Figure 3A).

Genes exhibiting an absolute fold change of at least 1.5, coupled with a padj under 0.05, were classified as DEGs (Supplementary Table S2). From the W20/W29 comparison, a total of 1,013 DEGs were discovered, among which were 605 up-regulated and 408 down-regulated, as shown in Figures 3B,C. Based on the MCC algorithm and literature research, the top genes were identified as potential hub genes, which were *TLR7*, *IGF1*, *MAP3K1*, *CIITA*, *LCP2*, *PRKCB*, and *PLCB2* (Figure 4).

Subsequently, the GOATOOLS software was employed to pinpoint GO terms significantly enriched within these DEGs. A Fisher's exact test, adjusted for multiple testing with the Benjamin-Hochberg

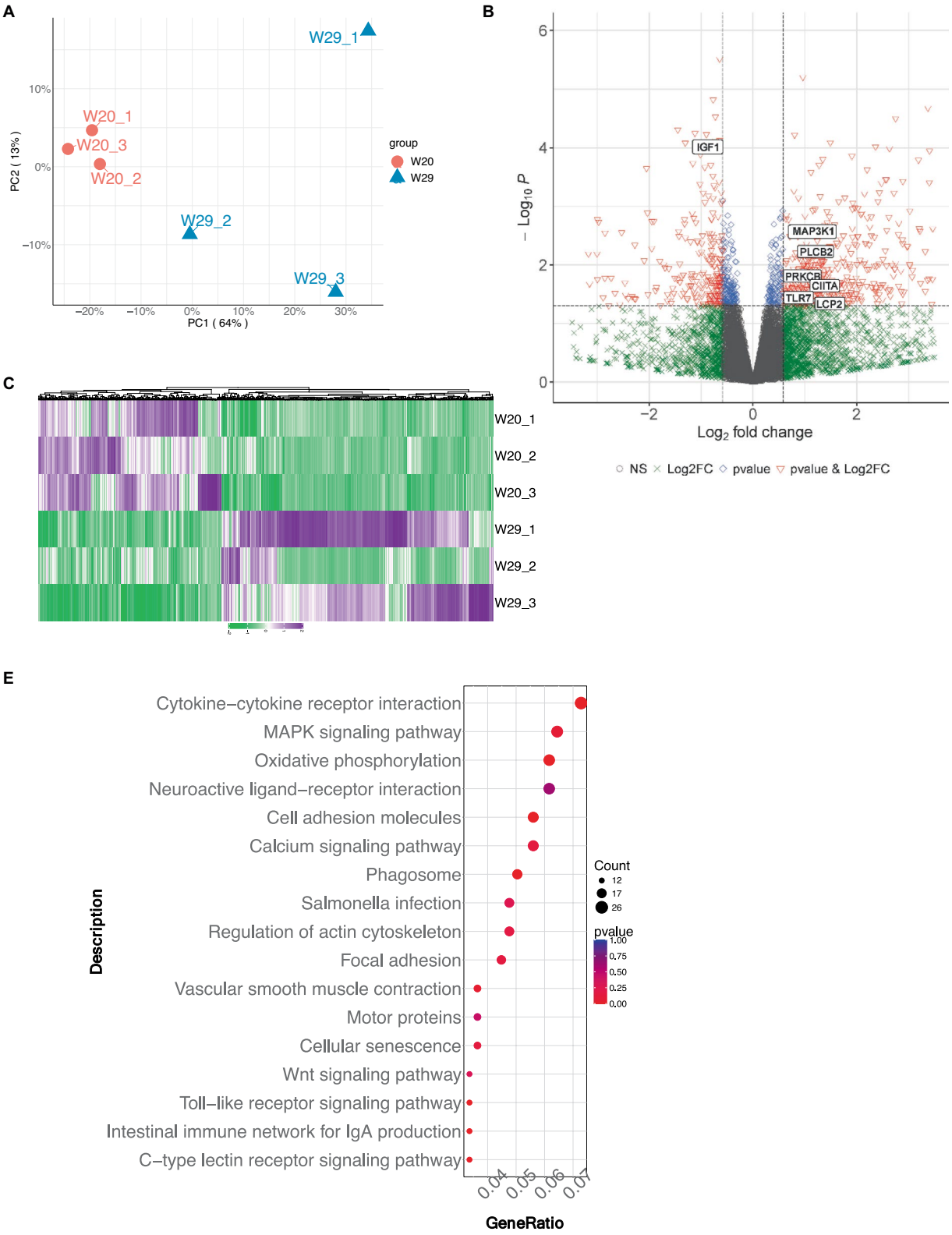

FIGURE 3
Gene expression profile analysis in CVds at 43 days of age. **(A)** Principal Component analysis plot for six samples. **(B)** Volcano plot visualizing the gene expression profile, created using the ComplexHeatmap package in R. **(C)** Heatmap representation of selected differentially expressed genes. **(D)** Gene Ontology enrichment analysis of DEGs. **(E)** Kyoto Encyclopedia of Genes and Genomes pathway enrichment analysis for DEGs.

10.3389/fvets.2024.1417244

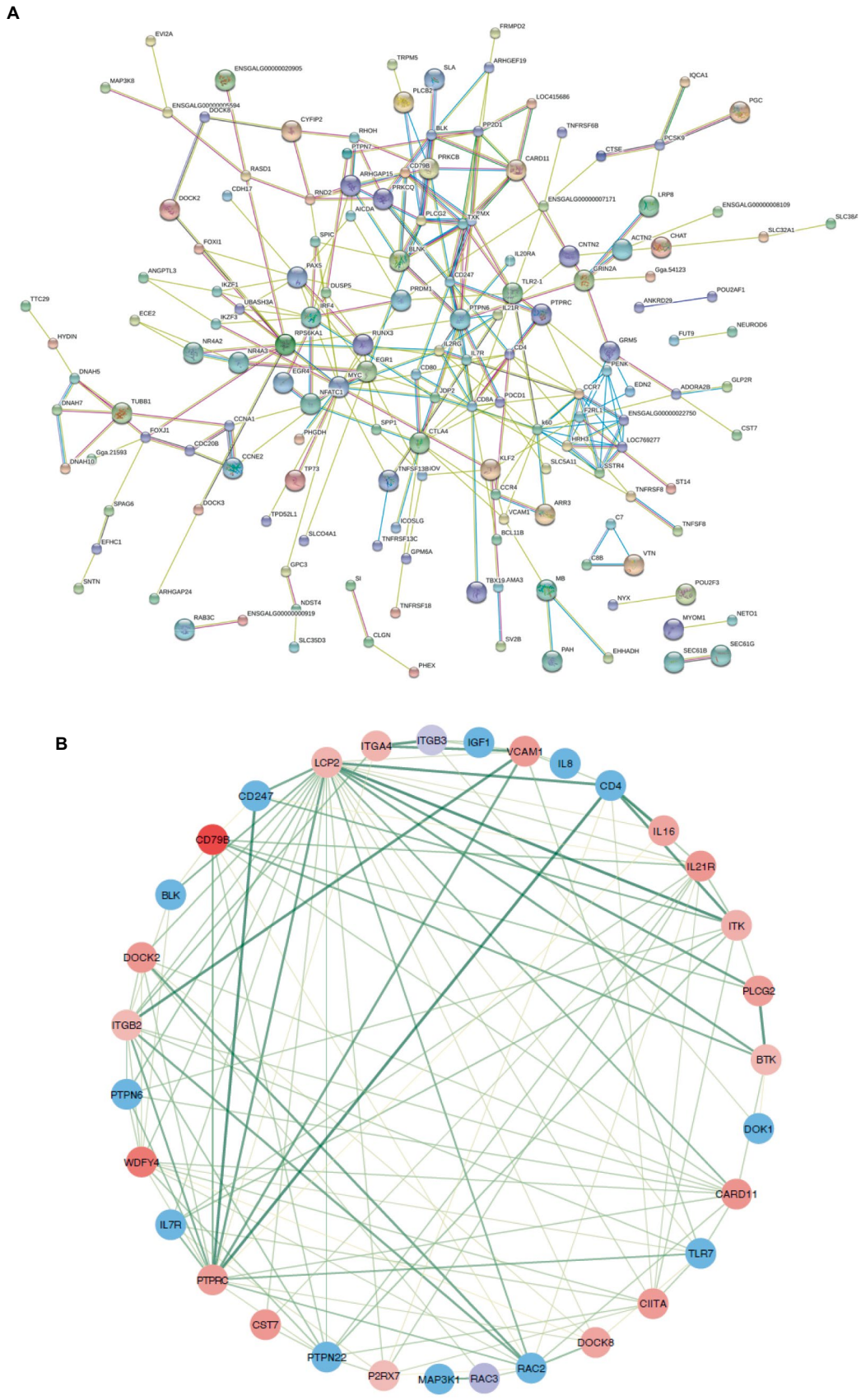

FIGURE 4
Protein–protein interaction networks. **(A)** A comprehensive PPI network for all differentially expressed genes, purged of any isolated nodes; **(B)** a focused subnetwork displayed in a circular layout to emphasize connectivity.

method, flagged GO terms with a false discovery rate less than 0.05 as significantly enriched. Functional annotation of GO terms revealed DEGs predominantly engaged in four biological processes: 'immune response,' 'immune system process,' 'regulation of immune system process,' and 'response to external stimulus,' mirroring findings from multiple other studies. In terms of cellular components, the majority of associated GO terms pertained to membrane-related structures, including 'membrane,' 'mitochondrial inner membrane,' and 'organelle membrane' (Figure 3D). These DEGs were predominantly found to be connected to immune system pathways, including 'intestinal immune network for IgA production,' 'Toll-like receptor signaling pathway,' and 'C-type lectin receptor signaling pathway.' Notably, a significant number of these DEGs were also enriched in pathways related to 'oxidative phosphorylation' and were implicated in 'Salmonella infection' (Figure 3E).

3.4 Characterization and analysis of differentially expressed mRNA

Utilizing quality-assured RNAseq data, we delineated 34,363 protein-encoding mRNAs via custom shell scripts developed in-house. Of which, there were 1,434 mRNA observed to be significantly differentially expressed, with 803 up-regulated and 631 down-regulated (Figures 5A,B).

The GO term functional annotation highlighted that DEmRNAs were actively involved in breakdown processes, including the catabolism of macromolecules and organic substances, as well as protein metabolism. Cellular component analysis showed an abundance of GO terms related to ubiquitin-related enzyme activities, specifically 'ubiquitin-protein transferase activity' and 'ubiquitin-like protein transferase activity' (Figure 5C). Additionally, these DEmRNAs showed a significant presence in immune system pathways, like 'Toll-like receptor signaling' and 'C-type lectin receptor signaling.' Notably, a greater number of terms were associated with infectious diseases, such as those related to 'Herpes simplex virus 1 infection,' 'Influenza A' and 'Salmonella infection' (Figure 5D).

3.5 Characterization and analysis of differentially expressed lncRNA and functional enrichment analysis of predicted targets

In the realm of gene regulation, lncRNAs act as *cis*-regulators, often influencing proximate protein-coding genes. Utilizing refined RNAseq data subjected to quality control, our tailored shell scripts facilitated the identification of 5,352 (4,387 known and 965 novel) lncRNA transcripts. The genomic analysis revealed that while lncRNAs and mRNAs share similar transcript lengths, lncRNAs are more likely to have longer sequences exceeding 3,000 bp. LncRNAs typically feature a greater proportion with 2–5 exons and possess shorter open reading frames (ORFs) and lower expression levels as quantified by FPKM (Figures 6A–D).

Subsequent analysis revealed 217 differentially expressed lncRNAs within the W29 profile, comprising 111 that were up-regulated and the rest displaying down-regulation (Figures 7A,B). Plus, GO and KEGG pathway enrichment analyses were undertaken to decipher the functions and pathways associated with the predicted targets. The enriched GO terms were principally connected to immunoreaction, such as 'immune response,' 'immune system process,' and 'regulation of immune system process' (Figure 7C). The KEGG pathway analysis revealed involvement in immune system (e.g., Intestinal immune network for IgA production) and Infectious disease (e.g., *Salmonella* infection) (Figure 7D).

3.6 Characterization and analysis of differentially expressed miRNA and functional enrichment analysis of predicted targets

In this study, we generated a substantial number of raw reads, totaling 12,706,326, 10,121,409, and 9,982,953 for W20, and 12,311,631, 12,412,586, and 10,192,859 for W29, respectively. Following the removal of adaptor sequences, low-quality sequences, and reads outside the length range of 18 to 32 nucleotides, we obtained high-quality clean reads: 12,553,092, 10,032,226, and 9,858,879 for W20, and 11,971,885, 12,250,135, and 9,864,788 for W29. The majority of these clean reads ranged in length from 20 to 24 nucleotides (Figure 6E). Upon classifying the small RNAs, we discovered that 75.3% of the clean reads were attributed to intronic (61.69%) and exonic (38.24%) regions. Additionally, miRNAs accounted for 19.3% of the reads, small non-coding RNAs (sncRNAs) comprised 0.96, and 4.37% were categorized as other types (Figure 6F).

Additionally, for the miRNA expression profiles, 543 DEmiRNAs were identified in W29, including 413 up-regulated and 130 down-regulated miRNAs (Figures 8A,B). In the target study of W29-specific DEmiRNAs, GO annotation revealed a preponderance linked to molecular functions like receptor activities such as 'neurotransmitter receptor activity,' 'signaling receptor activity,' and 'transmembrane signaling receptor activity.' Cellular component annotations centered around structures such as membranes and organelles, while molecular functions primarily involved binding and catalysis. The enriched GO terms for known DEmiRNAs were associated with catabolic processes (Figure 8C). In KEGG pathway analysis, the targets of DEmiRNAs were involved in MAPK signaling pathway, Calcium signaling pathway, and TGF-beta signaling pathway (Figure 8D).

3.7 CeRNA regulatory network in response to CHS

To elucidate the comprehensive regulatory matrix involving protein-coding RNAs and non-coding RNAs in response to CHS, a complex ceRNA network was established, integrating differentially expressed miRNAs, mRNAs and lncRNAs. This expansive network predicted thousands of mRNAs and dozens of lncRNAs as miRNA targets in the lungs of W29. Filtering interactions by a strong negative correlation revealed several thousand potential miRNA-mRNA and a handful of miRNA-lncRNA linkages. Certain miRNAs (miR-146, miR-217, miR-29a-3p, miR-10926, miR-146b-5p, and miR-17-1-3p) emerged as central hubs, potentially key to regulatory mechanisms, while multiple lncRNAs (LOC101804558, LOC113841824, LOC101798355, LOC119717605, and LOC110353088) were also pinpointed as significant network participants (Figure 9).

10.3389/fvets.2024.1417244

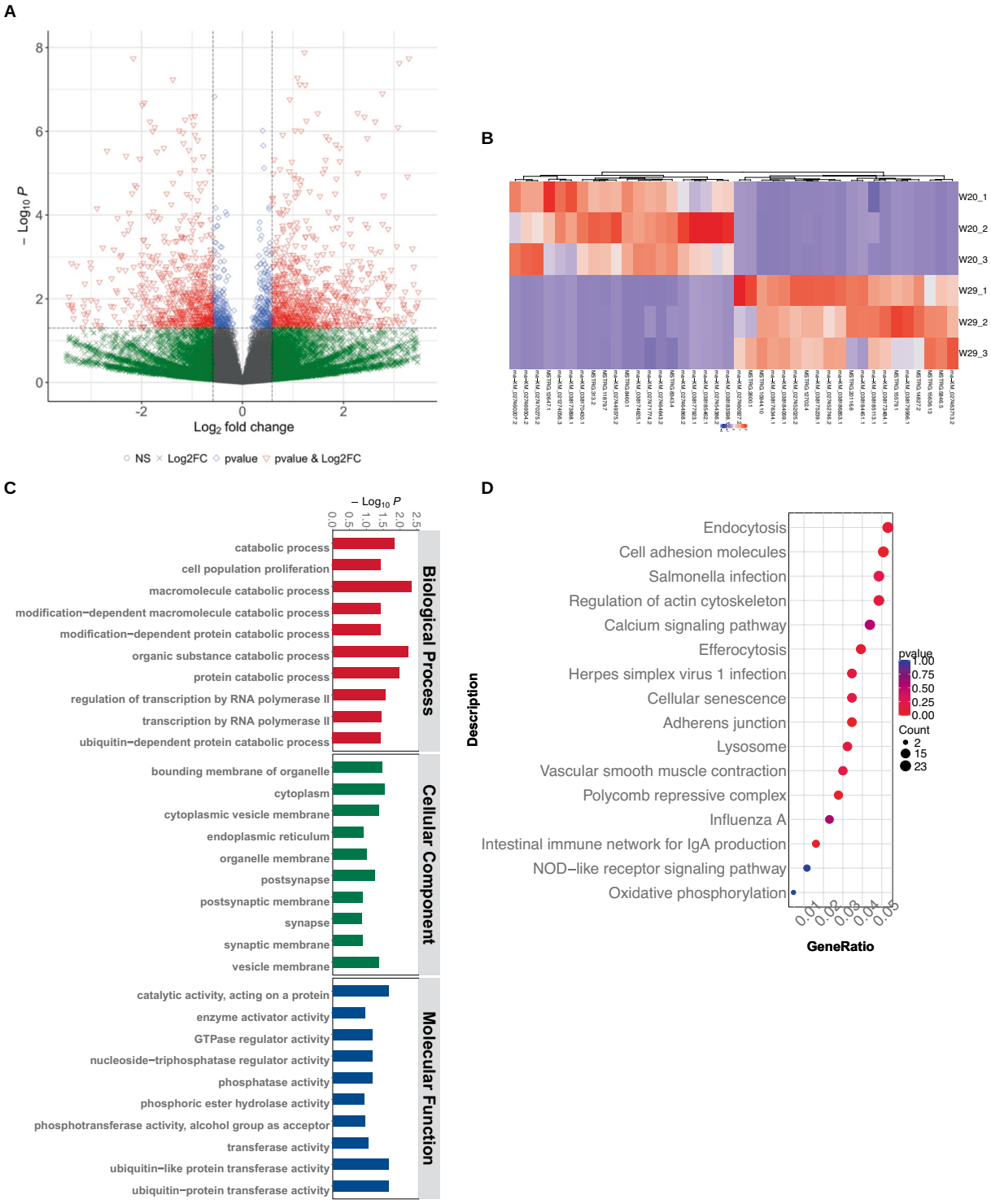

FIGURE 5
Differentially expressed mRNA profiling in CVds at 43 days. **(A)** Volcano plot visualization of mRNA expression profiles generated with the ComplexHeatmap package in RStudio. **(B)** Heatmap depiction of top DEmRNAs. **(C)** GO enrichment analysis of DE-mRNAs. **(D)** KEGG pathway enrichment for DEmRNAs.

3.8 RT-qPCR confirmation of miRNA-ceRNA correlation in CHS responses

To substantiate the RNAseq data and examine the expression correlation between miRNAs and their targets, we selected four key miRNAs—miR-146, miR-217, miR-29a-3p, and miR-10926—and their associated mRNAs and lncRNAs from the ceRNA network for RT-qPCR analysis. The primer sequences for the mRNAs and lncRNAs are itemized in Tables 1, 2, respectively, incorporating GAPDH as the internal reference gene. The primers for the miRNAs are cataloged in Table 3, with U6 employed as the internal

10.3389/fvets.2024.1417244

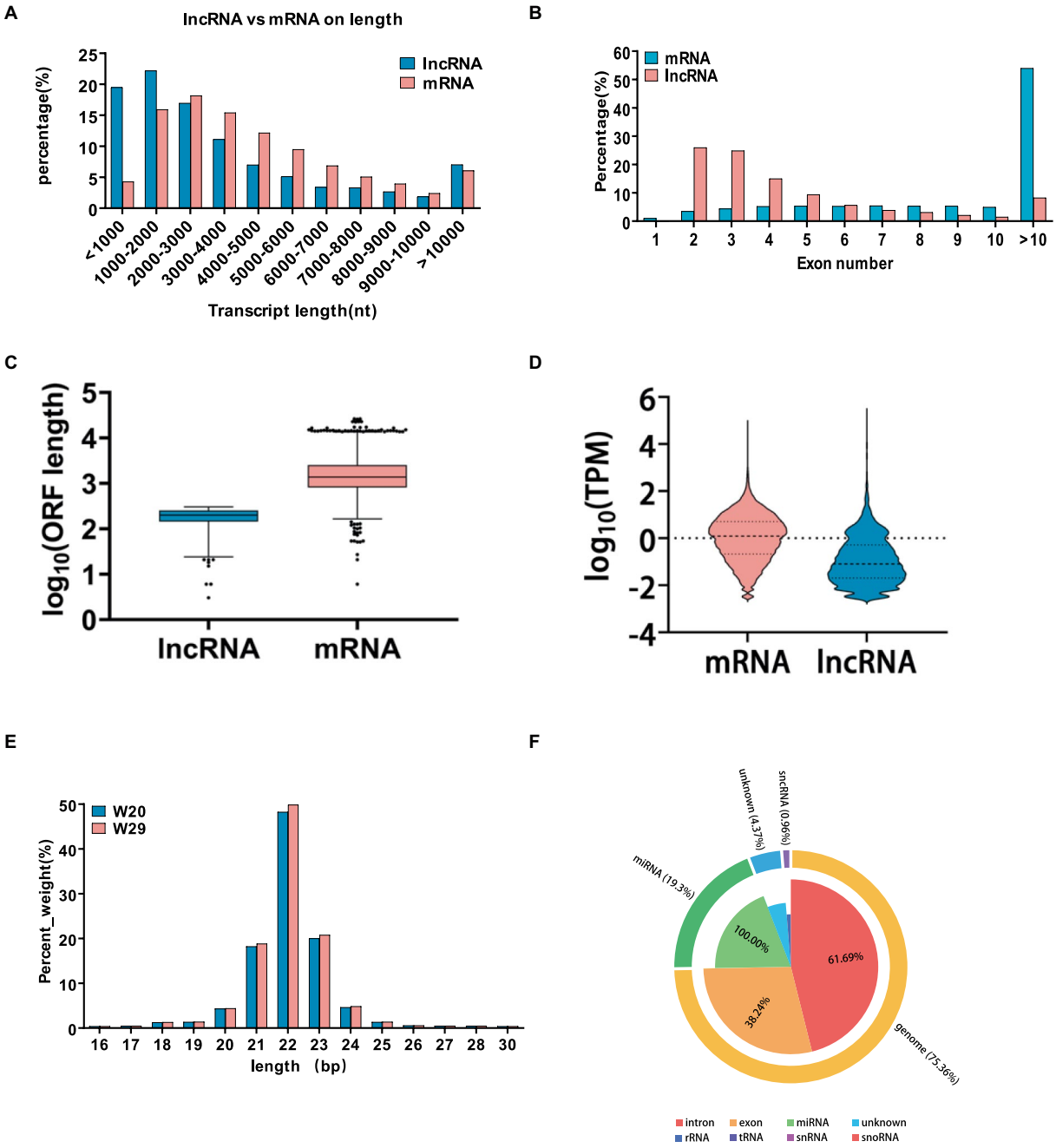

FIGURE 6
Characterization and comparative analysis of differentially expressed lncRNAs under CHS. **(A–D)** Comparative metrics between lncRNAs and mRNAs, including transcript length, exon count, open reading frame size, and expression levels measured as transcripts per million. **(E)** Categorization of the identified small RNAs. **(F)** Distribution of transcript lengths for all identified miRNAs in the two groups.

normalization gene. The analysis affirmed a predominantly accurate reflection of regulatory dynamics, with miRNAs and their respective targets displaying the expected regulatory trends of either up- or down-regulation (Figure 10). Notably, miR-146 was observed to be up-regulated, with its predicted targets being up-regulated, while miR-217 demonstrated down-regulation, accompanied by up-regulation of all its targets. These results not only validate the RNAseq data's accuracy but also the postulated inverse relationship between the expression levels of miRNAs and their corresponding ceRNAs.

4 Discussion

The detrimental physiological effects of CHS on poultry and livestock industries are well-documented. These effects encompass reductions in feed intake, feed efficiency, growth performance, meat and egg production, meat quality, and survival rates (15, 24, 32, 59–67). Moreover, various studies have explored the impact of CHS on inflammatory responses, dysbiosis, reactive oxidative stress (ROS), signal reactions, and energy metabolism (68–76). Some studies have specifically investigated the health status and well-being of ducks

10.3389/fvets.2024.1417244

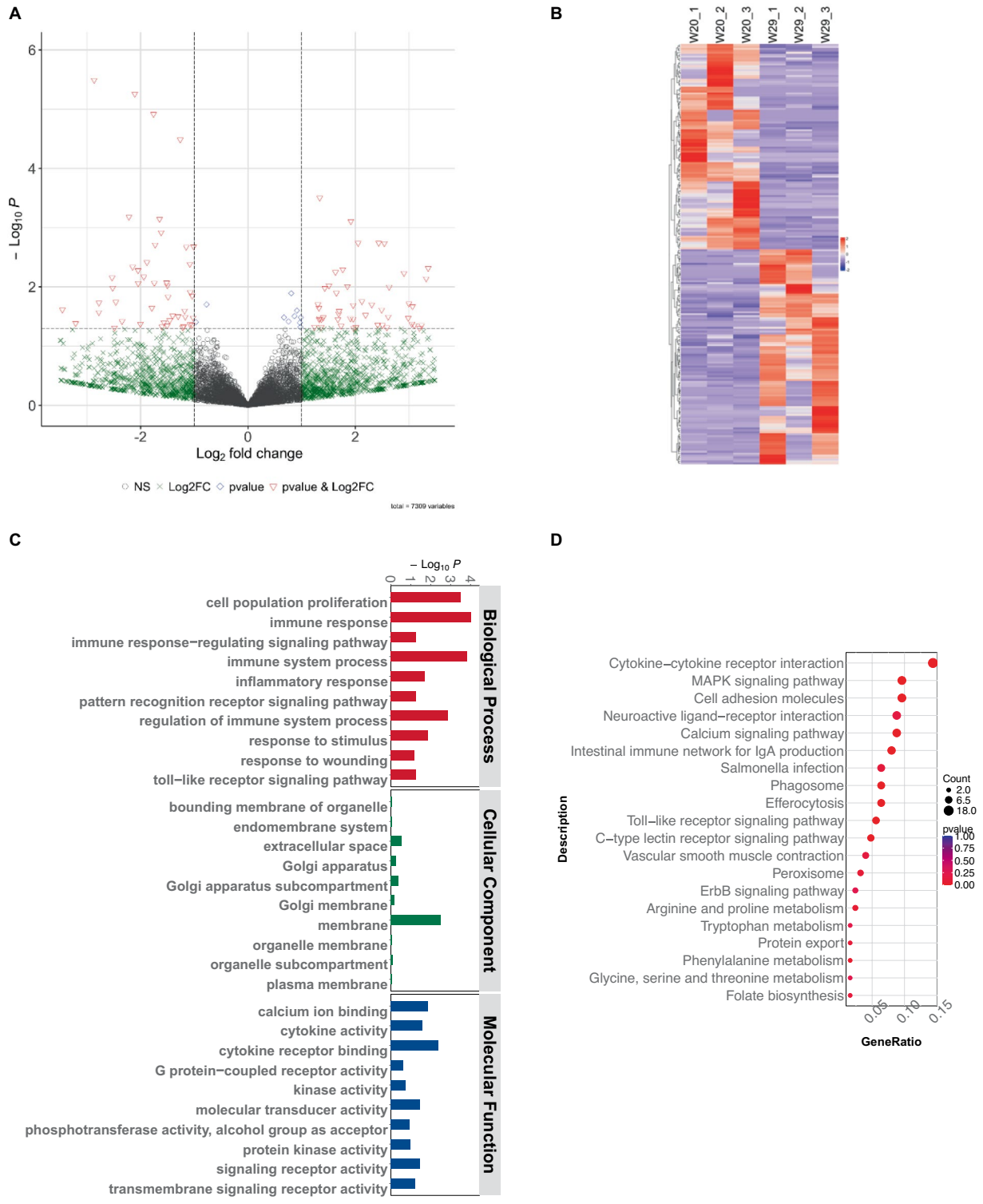

FIGURE 7
Exploring lncRNA variances in CVds at 43 days. **(A)** Visualization of lncRNA expression variations using a volcano plot from the ComplexHeatmap package. **(B)** A heatmap delineating notable DElncRNAs. **(C)** Analysis of GO term enrichment among DElncRNA targets. **(D)** Examination of DElncRNA targets within KEGG pathway frameworks.

under increasing ambient temperatures, focusing on granulosa cells and the jejunum (25, 77). As the one of the main high-throughput sequencing technologies, transcriptomics has been facilitating the poultry rearing in recent years (78). In the current study, we made full transcriptome profiling of lungs detached from two groups of CVds at 43 days of age reared under 20 and 29°C ambient temperatures. In

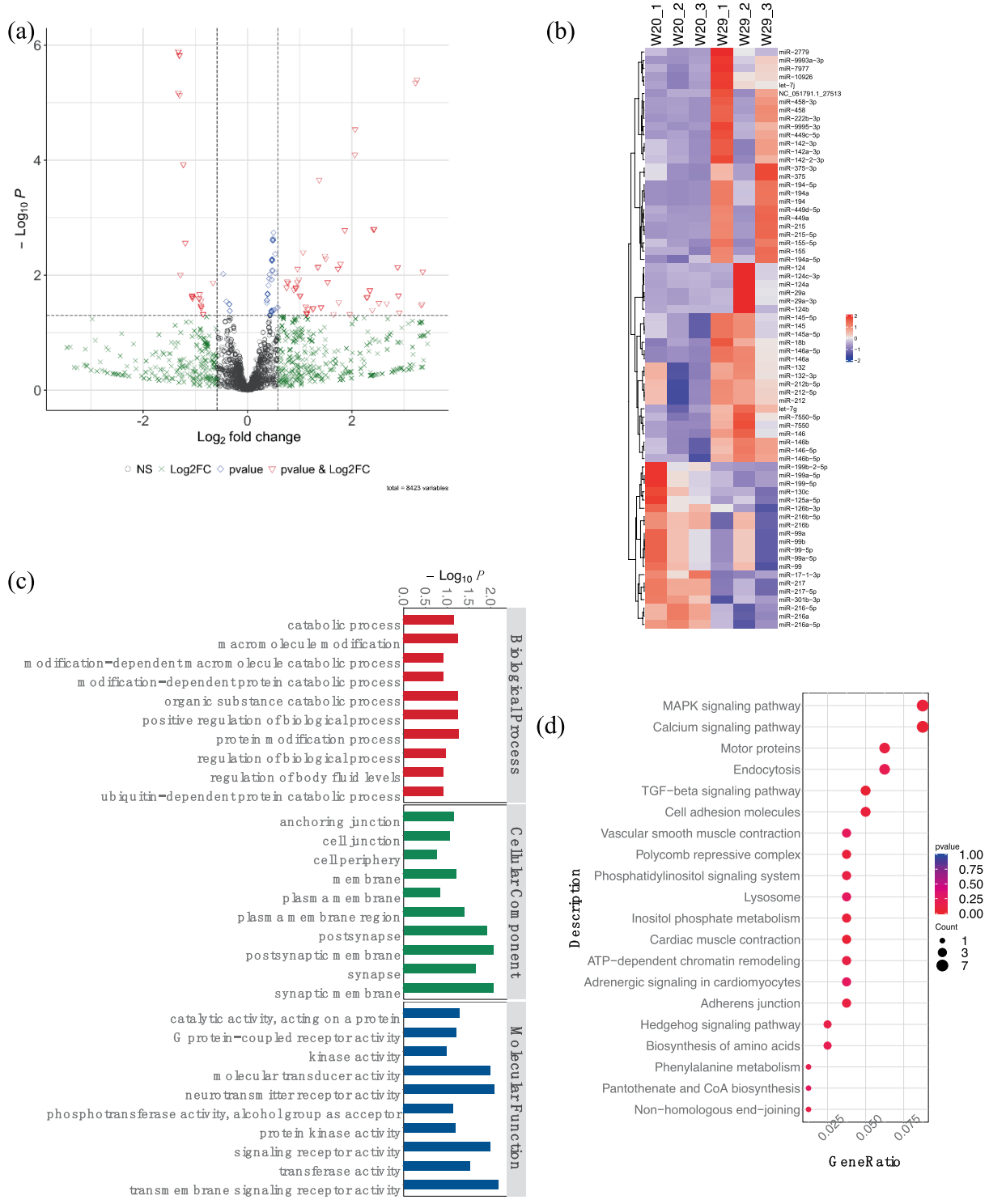

FIGURE 8
Analysis of differentially expressed miRNAs in CVds at 43 days. **(A)** A volcano plot generated with the ComplexHeatmap package in RStudio to visualize miRNA expression profiles. **(B)** Heatmap representation highlighting top DEmiRNAs. **(C)** GO enrichment analysis for predicted targets of DEmiRNAs. **(D)** Assessment of DEmiRNAs within the context of KEGG pathways.

order to understand the molecular mechanism of response to CHS, comprehensive bioinformatics analysis and intensive RT-qPCR experiments was implemented.

Initial findings indicate that CHS significantly modulates a range of physiological aspects in CVds through pivotal genes including *TLR7*, *IGF1*, *MAP3K1*, *CIITA*, *LCP2*, *PRKCB*, and *PLCB2*. Notably, *TLR7*, highly expressed in duck lung tissue, is a key gene in the innate immune defense against viral infections such as influenza (78–80), and also plays a role in egg production (79–83). Immunostimulants are reported to enhance antioxidant and immune efficacy by

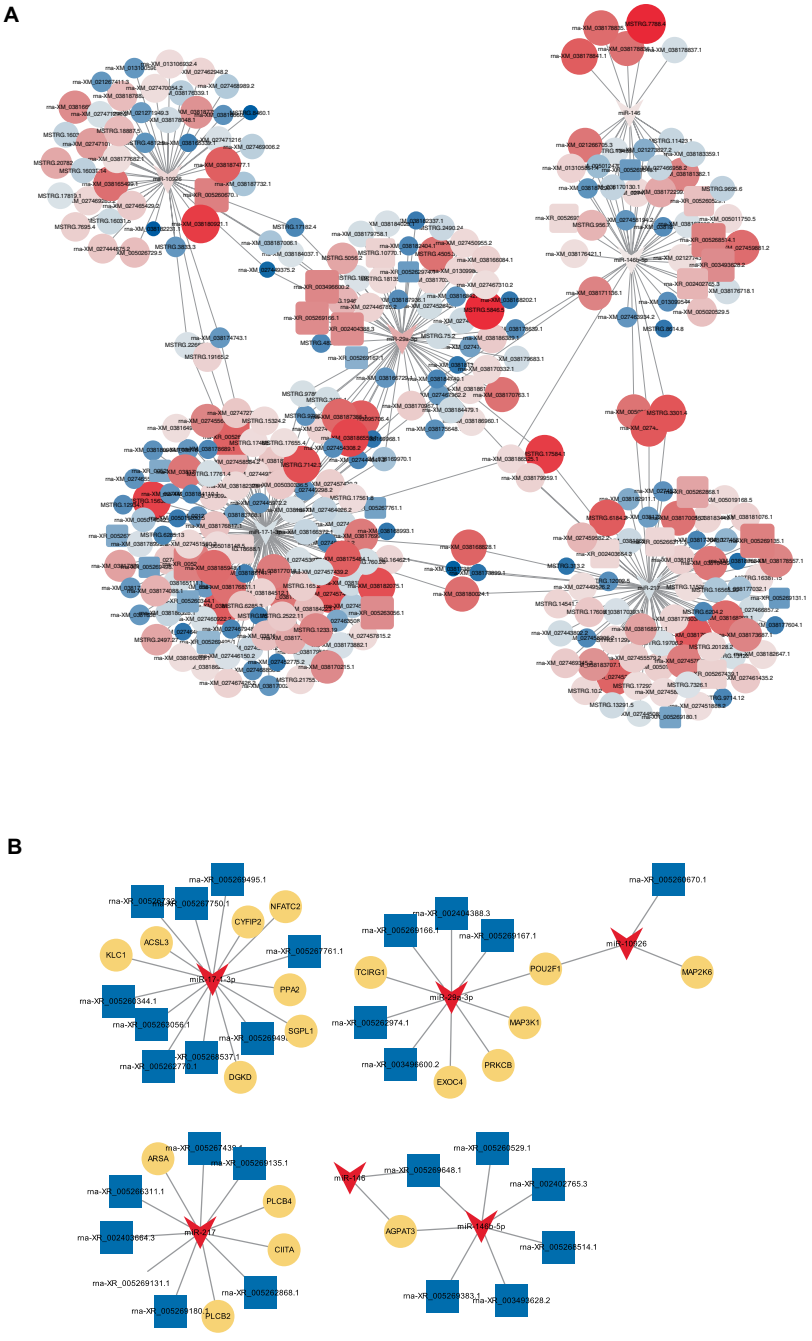

FIGURE 9
CeRNA network. **(A)** A constructed ceRNA network centered around miR-217, miR-146b-5p, miR-29a-3p, miR-10926, miR-17-1-3p, and miR-146. In this network, dark blue arrows represent miRNAs, pink triangles indicate mRNAs, light blue circles denote lncRNAs. **(B)** Depiction of mini-ceRNA network involving six DE-miRNAs and their associated target genes.

stimulating *TLR7* expression (84, 85). *CIITA* (Class II major histocompatibility complex trans-activator) is integral to the innate immune response, functioning as a trans-activator that boosts MHC-II expression in both antigen-presenting and virus-infected cells. This activation sparks antiviral responses in the host, serving as a blockade against viral replication and aiding in the clearance of viral infections (86, 87). *IGF1* is acknowledged as a key gene influencing growth, body composition, and the development of metabolic and skeletal traits, and plays a significant role in the growth of various tissues, including muscle and bone (88–95). Moreover, its correlation with reproductive efficiency underscores its importance in developmental biology and poultry breeding programs (96–100). Publications concerning *MAPK3K1* (mitogen-activated protein kinase kinase kinase 1) (101, 102), *LCP2* (103) are limited, yet these genes are known for their roles in lipid metabolism and the development of fatty liver disease. *PRKCB* (protein kinase C alpha) (104), and *PLCB2* (Phospholipase C Beta 2) are less frequently mentioned. The comprehensive analysis incorporating differential expression and

10.3389/fvets.2024.1417244

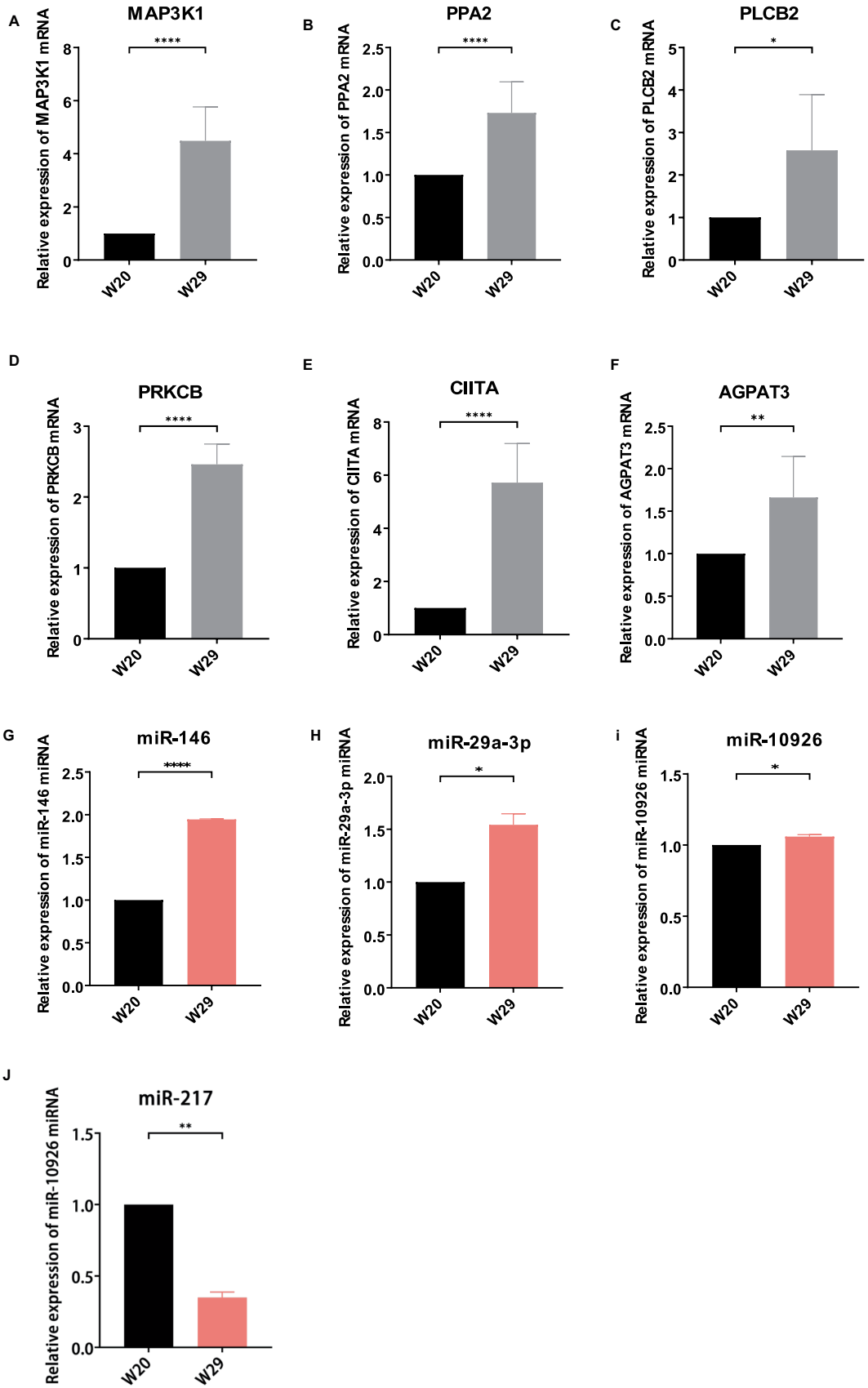

FIGURE 10 (Continued)

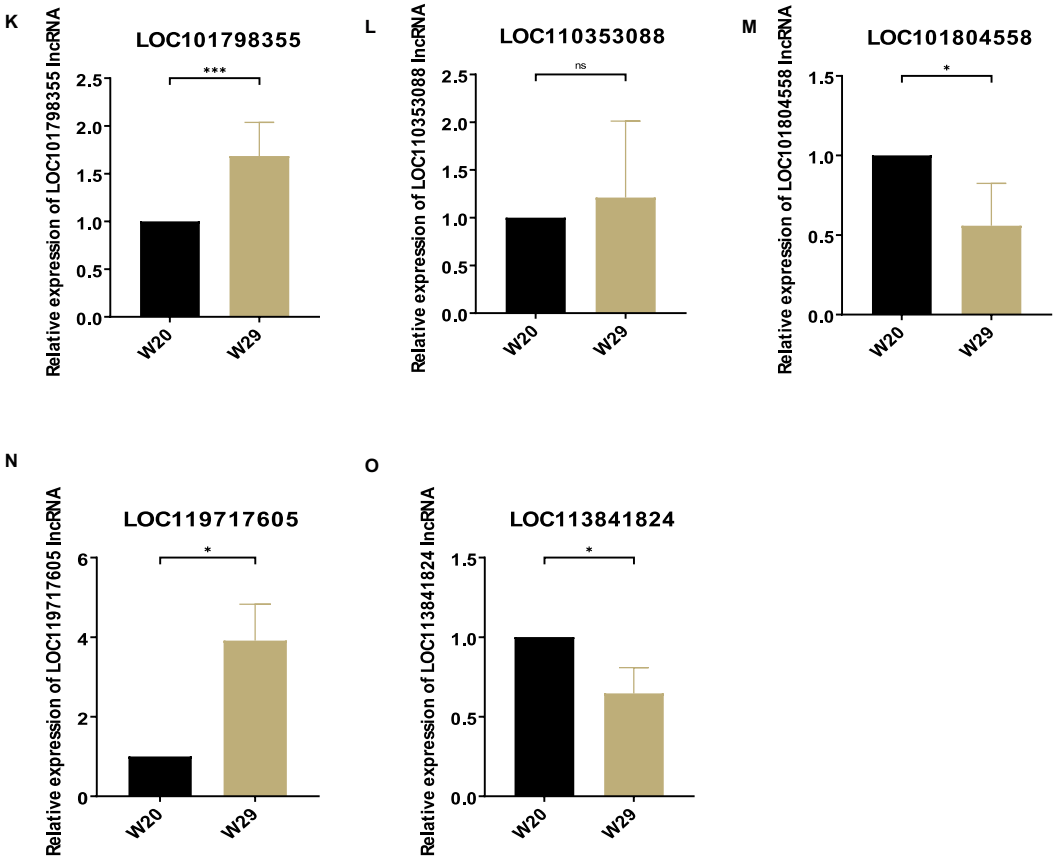

FIGURE 10
Validation of different expressed RNAs via RT-qPCR. **(A–F)** mRNA, **(G–J)** miRNA, **(K–O)** lncRNA. The relative expressions were calculated in triplicate using the method of $2^{-\triangle\triangle}$Ct and presented as mean ± SD. *p-value <0.05, **p-value <0.01, ***p-value <0.001, ****p-value <0.0001.

TABLE 1 Primer sequences for mRNA quantification via RT-qPCR.

mRNA name	GenBank accession No.	Primer sequences (5′–3′)	Product size (bp)
AGPAT3	rna-XM_038172299.1	F: CACAGTTCTCCTCTCGCCTCTC	170
		R: ATTCTTGGTTGCCGTAGCTGGA	
PPA2	MSTRG.7142.3	F: GCCACTGAGGAGCCGTTGAATC	119
		R: GTCTGAGGGAGGGCACCGTAAT	
CIITA	rna-XM_027469345.2	F: AGCAGGAGAAGCAAGTGGAAGA	266
		R: CTGGTGAGTTAGCGAGGTGGAG	
PLCB2	rna-XM_005019168.5	F: GCGATGTGGCTGAAGAGGAACC	295
		R: CGGCTCATCTGTCGCTTGTTGT	
MAP3K1	rna-XM_038170332.1	F: TGCCAACAGTCGAACGAGTCAA	188
		R: CCAGTAGTGCTTGCCAGTTGCT	
PRKCB	rna-XM_038186960.1	F: CCTGACTACATCGCACCTGAGA	202
		R: AGATCGCCACTGCCTCCTTG	
GAPDH	rna-XM_03818058.4	F: GGTTGTCTCCTGCGACTTCA	165
		R: TCCTTGGATGCCATGTGGAC	

F, forward primer sequence; R, reverse primer sequence. GAPDH, internal control gene.

TABLE 2 Primer sequences for miRNA quantification via RT-qPCR.

miRNA name	Target name	GenBank accession No.	Primer sequences (5′–3′)
miR-146	AGPAT3	rna-XM_005012470.5	F: GCGCTGAGAACTGAATTCCA
	AGPAT3	rna-XM_038172299.1	R: GTGCAGGGTCCGAGGT
miR-29a-3p	EXOC4	MSTRG.75.2	F: GCGCTAGCACCATCTGAAAT
	MAP3K1	rna-XM_038170337.1	
	MAP3K1	rna-XM_038170332.1	
	POU2F1	rna-XM_027449375.2	
	POU2F1	rna-XM_038184037.1	R: GTGCAGGGTCCGAGGT
	PRKCB	rna-XM_038186960.1	
	TCIRG1	rna-XM_038179683.1	
miR-10926	MAP2K6	rna-XM_038165339.1	F: GCGCGCATCCCAGCGGTG
	POU2F1	rna-XM_038184037.1	R: GTGCAGGGTCCGAGGT
	POU2F1	rna-XM_027449375.2	
miR-146	LOC101805192	rna-XR_005269648.1	F: GCGCTGAGAACTGAATTCCA
			R: GTGCAGGGTCCGAGGT
miR-29a-3p	LOC119718278	rna-XR_005269166.1	F: GCGCTAGCACCATCTGAAAT
	LOC119715672	rna-XR_005262974.1	
	LOC101791220	rna-XR_003496600.2	R: GTGCAGGGTCCGAGGT
	LOC119718278	rna-XR_005269167.1	
	LOC106018689	rna-XR_002404388.3	
miR-10926	LOC110351219	rna-XR_005260670.1	F: GCGCGCATCCCAGCGGTG
			R: GTGCAGGGTCCGAGGT
U6			F: CTCGCTTCGGCAGCACA
			R: AACGCTTCACGAATTTGCGT

F, forward primer sequence; R, reverse primer sequence. U6, internal control gene.

RT-qPCR suggests the potential of these genes as biomarkers for heat stress in CVds.

Similarly, it was found that biological profiles, inflammation, and stress protein markers were significantly enriched in miRNA target genes in differential genomes, including L1RAPL2, IL7R, TRAF3, TRAF5, HSPA8, etc. IL1RAPL2 is a molecule in the IL1R family that has different biological effects on immune and inflammatory responses. There is evidence to suggest that IL1RAPL2 is a specific biomarker for kidney injury (105). IL7R is often regulated to varying degrees after virus attacks on poultry. Similarly, there is evidence to suggest that IL7R is associated with cellular responses to heat exposure (106). TRAF3 is a key innate immune regulatory factor that plays a crucial role in defending against viral invasion (107, 108). TRAF5 has been found to regulate inflammation and apoptosis of atherosclerosis, steatosis and melanoma cells, and also plays an important role in regulating myocardial I/R injury (109). HSPA8 can significantly affect the proliferation, apoptosis, and immune function of poultry macrophages, while significantly promoting the proliferation of HD11 cells and inhibiting their apoptosis, with pro-inflammatory effects (110).

Subsequent analysis of gene enrichment pointed to CHS significantly bolstering immunological processes, with a particular focus on catabolic pathways in the case of DEmRNAs and targets of DEmiRNAs. Across the differentially expressed RNAs, pathways in the immune system, especially those involved in IgA production and Toll-like receptor signaling, were highlighted. These enrichments align with the literature on CHS's impact on animal health (1, 12, 26, 70, 75, 76). The pathway of *Salmonella* infection consistently appears as one of the most enriched, reflecting the pathogen's notoriety as a leading poultry-associated foodborne illness. This observation aligns with findings that heat stress may compromise the immune defenses, potentially increasing the risk of *Salmonella* infection in poultry, as noted in recent studies (31). The calcium signaling pathway, akin to the *Salmonella* infection pathway, has shown deep involvement in response to heat stress (Figures 3E, 5D, 7D). Elevated temperatures can increase membrane fluidity and permeability, leading to a calcium imbalance and the release of cytochrome c into the cytoplasm, triggering apoptosis through factors like caspases (63). Simultaneously, ROS generated under heat stress can inflict oxidative damage on enzymes responsible for muscle calcium regulation, further disturbing cellular homeostasis. As a result, high temperatures lead to reduced levels of calcium and phosphorus in the plasma of laying hens. These minerals are crucial for egg production and the quality of the eggshell (18, 104, 111).

In addition, this study presents, for the first time, a batch of miRNAs which play a role in CHS response of duck. In the foundational stages of inflammation, miR-146 is upregulated following

TABLE 3 Primer sequences for lncRNA quantification via RT-qPCR.

lncRNA name	GenBank accession No.	Primer sequences (5′–3′)	Product size (bp)
LOC101804558	rna-XR_005269495.1	F: CTGCCTCACCTCTTCGTCTTGG	96
		R: GCTGCTTCTGTCCTTCTCACTCC	
LOC113841824	rna-XR_005267325.1	F: GCAAAGCACAGCCAGCAGTTAC	107
		R: ACAGATACCGCATCCAGAGAAGAAG	
LOC101798355	rna-XR_005260529.1	F: GCAGAGGGTGAGGTGGTTGTC	114
		R: TTCTGGAGGAGCCTTGCATAAGC	
LOC119717605	rna-XR_005267439.1	F: GGAGCAGGACACAGCCACTAAC	127
		R: GCACAGGACAGACGGACAGAC	
LOC110353088	rna-XR_005266311.1	F: CCTGCTGCTGCTGCTCCTG	130
		R: GGGTGGCATCTTCCTCCTTCTTC	
GAPDH	rna- XM_03818058.4	F: GGTTGTCTCCTGCGACTTCA	165
		R: TCCTTGGATGCCATGTGGAC	

F, forward primer sequence; R, reverse primer sequence. GAPDH, internal control gene.

exposure to lipopolysaccharide LPS, a bacterial element detected by *TLR4*. This triggers a series of events where NFκB migrates to the nucleus, initiating the expression of genes responsible for inflammatory mediators (112–114). Research has strengthened miR-146's role in this pathway, underscoring its function in a negative feedback mechanism that tempers the inflammatory response initiated by *TLR4* (115). MiR-146b-5p is typically upregulated in response to *Salmonella enterica* infection, playing a pivotal role in maintaining immune balance by dampening the initiation of the innate immune reaction (116, 117). This miRNA has been shown to facilitate replication of the Duck Tembusu virus through the suppression of the *RPS14* gene, demonstrating its negative regulatory capacity in immune processes (118). miR-217 is noted for its regulatory influence on diverse muscle cell types by modulating critical genes, targeting *ROCK1* in vascular smooth muscle cells and *FGFR2* in skeletal muscle progenitors (119, 120). In the context of chicken liver cancer cells, miR-29a-3p responds to selenium levels and can instigate cell movement and invasion. It does this by focusing on the *COL4A2* gene, leading to the suppression of the *RhoA/ROCK* signaling pathway (121). To date, the roles of miR-10926 and miR-17-1-3p remain unexplored, signaling the need for further investigation into their functions.

However, it's important to acknowledge the limitations of this study. Firstly, we focused solely on morphological changes in lung tissue, and future research should incorporate biochemical tests of lung tissue and morphological tests of skin tissue, as skin is the largest heat dissipation system. Secondly, while the short-read transcriptome sequencing and data analysis provided valuable insights, they do not provide a complete view. The list of DEGs obtained here includes some unreported genes that likely play crucial roles in the CHS-induced response of ducks. These genes should be characterized in future studies. Furthermore, investigating the mechanisms that regulate the expression of these genes is essential, as is the use of other omics approaches (multi-omics studies). Additionally, the present study could benefit from additional examinations, such as assessing amino acid composition, nutritional value, and protein digestibility (122).

As a brief supplement, several strategies have been proposed to mitigate the adverse effects of CHS, such as improving housing, ventilation, and cooling systems (e.g., using little rearing systems and cage rearing systems) (123, 124), dietary supplementation (e.g., with vitamin A, vitamin C, vitamin E, Glutamine, and Herbs) (125–129), feed additives (e.g., probiotics, prebiotics, polyphenols, and palm oils) (130, 131), and other approaches (e.g., feed restrictions and genetic selection for heat tolerance) (132–136).

5 Conclusion

In essence, this study aims to delve into the effects of varying ambient temperatures on the growth performance of CVds and shed light on the underlying mechanisms responding to heat stress using cutting-edge high-throughput sequencing technologies. In conclusion, like other poultry, CVds are also sensitive to high ambient temperatures, and environmental control chambers offer advantages in improving their quality of life (20, 137, 138). Considering the predictions of continued climate change in most models (19, 139), further research is urgently needed to uncover the response mechanisms and regulatory networks of ducks to CHS.

Data availability statement

The original contributions presented in the study are included in the article/Supplementary material, further inquiries can be directed to the corresponding authors.

Ethics statement

The animal study was approved by Administration of Affairs Concerning Experimental Animals (Decree No. 63 of the Jiangsu Academy of Agricultural Science on 8 July 2014). The study was

conducted in accordance with the local legislation and institutional requirements.

Author contributions

YL: Data curation, Formal analysis, Writing – original draft. DS: Resources, Writing – review & editing. CX: Resources, Visualization, Writing – review & editing. XL: Project administration, Resources, Writing – review & editing. MT: Supervision, Writing – review & editing. SY: Funding acquisition, Project administration, Resources, Writing – review & editing.

Funding

The author(s) declare that financial support was received for the research, authorship, and/or publication of this article. This work was supported by the National Natural Science Foundation of China (32002235), Jiangsu Agricultural Science and Technology Innovation Fund (JASTIF) (CX (20) 2010), and China Agriculture Research System (CARS-42-38).

Conflict of interest

The authors declare that the research was conducted in the absence of any commercial or financial relationships that could be construed as a potential conflict of interest.

Publisher's note

Supplementary material

The Supplementary material for this article can be found online at: https://www.frontiersin.org/articles/10.3389/fvets.2024.1417244/full#supplementary-material

References

1. Brugaletta G, Teyssier JR, Rochell SJ, Dridi S, Sirri F. A review of heat stress in chickens. Part I: insights into physiology and gut health. *Front Physiol*. (2022) 13:934381. doi: 10.3389/fphys.2022.934381

2. Qaid MM, Al-Garadi MA. Protein and amino acid metabolism in poultry during and after heat stress: a review. *Animals*. (2021) 11:167. doi: 10.3390/ani11041167

3. Perini F, Cendron F, Rovelli G, Castellini C, Cassandro M, Lasagna E. Emerging genetic tools to investigate molecular pathways related to heat stress in chickens: a review. *Animals*. (2020) 11:46. doi: 10.3390/ani11010046

4. Wasti S, Sah N, Mishra B. Impact of heat stress on poultry health and performances, and potential mitigation strategies. *Animals*. (2020) 10:1266. doi: 10.3390/ani10081266

5. Nawaz AH, Amoah K, Leng QY, Zheng JH, Zhang WL, Zhang L. Poultry response to heat stress: its physiological, metabolic, and genetic implications on meat production and quality including strategies to improve broiler production in a warming world. *Front Vet Sci*. (2021) 8:699081. doi: 10.3389/fvets.2021.699081

6. Naranjo-Gomez JS, Uribe-Garcia HF, Herrera-Sanchez MP, Lozano-Villegas KJ, Rodriguez-Hernandez R, Rondon-Barragan IS. Heat stress on cattle embryo: gene regulation and adaptation. *Heliyon*. (2021) 7:e06570. doi: 10.1016/j.heliyon.2021.e06570

7. Zheng Y, Xie T, Li S, Wang W, Wang Y, Cao Z, et al. Effects of selenium as a dietary source on performance, inflammation, cell damage, and reproduction of livestock induced by heat stress: a review. *Front Immunol*. (2021) 12:820853. doi: 10.3389/fimmu.2021.820853

8. Oladimeji AM, Johnson TG, Metwally K, Farghly M, Mahrose KM. Environmental heat stress in rabbits: implications and ameliorations. *Int J Biometeorol*. (2022) 66:1–11. doi: 10.1007/s00484-021-02191-0

9. Bohler MW, Chowdhury VS, Cline MA, Gilbert ER. Heat stress responses in birds: a review of the neural components. *Biology*. (2021) 10:1095. doi: 10.3390/biology10111095

10. Ahmad R, Yu YH, Hsiao FS, Su CH, Liu HC, Tobin I, et al. Influence of heat stress on poultry growth performance, intestinal inflammation, and immune function and potential mitigation by probiotics. *Animals*. (2022) 12:2297. doi: 10.3390/ani12172297

11. Salem HM, Alqhtani AH, Swelum AA, Babalghith AO, Melebary SJ, Soliman SM, et al. Heat stress in poultry with particular reference to the role of probiotics in its amelioration: An updated review. *J Therm Biol*. (2022) 108:103302. doi: 10.1016/j.jtherbio.2022.103302

12. Liu L, Ren M, Ren K, Jin Y, Yan M. Heat stress impacts on broiler performance: a systematic review and meta-analysis. *Poult Sci*. (2020) 99:6205–11. doi: 10.1016/j.psj.2020.08.019

13. Gonzalez-Rivas PA, Chauhan SS, Ha M, Fegan N, Dunshea FR, Warner RD. Effects of heat stress on animal physiology, metabolism, and meat quality: a review. *Meat Sci*. (2020) 162:108025. doi: 10.1016/j.meatsci.2019.108025

14. Uyanga VA, Oke EO, Amevor FK, Zhao J, Wang X, Jiao H, et al. Functional roles of taurine, L-theanine, L-citrulline, and betaine during heat stress in poultry. *J Anim Sci Biotechnol*. (2022) 13:23. doi: 10.1186/s40104-022-00675-6

15. Sun PX, Shen ZJ, Tang J, Huang W, Hou SS, Xie M. Effects of ambient temperature on growth performance and carcass traits of male growing white Pekin ducks. *Br Poult Sci*. (2019) 60:513–6. doi: 10.1080/00071668.2019.1633011

16. Chen S, Yong Y, Ju X. Effect of heat stress on growth and production performance of livestock and poultry: mechanism to prevention. *J Therm Biol*. (2021) 99:103019. doi: 10.1016/j.jtherbio.2021.103019

17. Rostagno MH. Effects of heat stress on the gut health of poultry. *J Anim Sci*. (2020) 98:98. doi: 10.1093/jas/skaa090

18. Zaboli G, Huang X, Feng X, Ahn DU. How can heat stress affect chicken meat quality?- a review. *Poult Sci*. (2019) 98:1551–6. doi: 10.3382/ps/pey399

19. Kumar M, Ratwan P, Dahiya SP, Nehra AK. Climate change and heat stress: impact on production, reproduction and growth performance of poultry and its mitigation using genetic strategies. *J Therm Biol*. (2021) 97:102867. doi: 10.1016/j.jtherbio.2021.102867

20. Vandana GD, Sejian V, Lees AM, Pragna P, Silpa MV, Maloney SK. Heat stress and poultry production: impact and amelioration. *Int J Biometeorol*. (2021) 65:163–79. doi: 10.1007/s00484-020-02023-7

21. Abdel-Moneim AE, Shehata AM, Khidr RE, Paswan VK, Ibrahim NS, El-Ghoul AA, et al. Nutritional manipulation to combat heat stress in poultry – a comprehensive review. *J Therm Biol*. (2021) 98:102915. doi: 10.1016/j.jtherbio.2021.102915

22. Goel A, Ncho CM, Choi YH. Regulation of gene expression in chickens by heat stress. *J Anim Sci Biotechnol*. (2021) 12:11. doi: 10.1186/s40104-020-00523-5

23. Dai X, Zhang S, Zaleta-Rivera K. RNA: interactions drive functionalities. *Mol Biol Rep*. (2020) 47:1413–34. doi: 10.1007/s11033-019-05230-7

24. Goel A. Heat stress management in poultry. *J Anim Physiol Anim Nutr*. (2021) 105:1136–45. doi: 10.1111/jpn.13496

25. Yang C, Huang XB, Chen SJ, Li XJ, Fu XL, Xu DN, et al. The effect of heat stress on proliferation, synthesis of steroids, and gene expression of duck granulosa cells. *Anim Sci J*. (2021) 92:e13617. doi: 10.1111/asj.13617

26. Zeng T, Li JJ, Wang DQ, Li GQ, Wang GL, Lu LZ. Effects of heat stress on antioxidant defense system, inflammatory injury, and heat shock proteins of Muscovy and Pekin ducks: evidence for differential thermal sensitivities. *Cell Stress Chaperones*. (2014) 19:895–901. doi: 10.1007/s12192-014-0514-7

27. Ma X, Lin Y, Zhang H, Chen W, Wang S, Ruan D, et al. Heat stress impairs the nutritional metabolism and reduces the productivity of egg-laying ducks. *Anim Reprod Sci*. (2014) 145:182–90. doi: 10.1016/j.anireprosci.2014.01.002

28. Kim JM, Lim KS, Byun M, Lee KT, Yang YR, Park M, et al. Identification of the acclimation genes in transcriptomic responses to heat stress of white Pekin duck. *Cell Stress Chaperones*. (2017) 22:787–97. doi: 10.1007/s12192-017-0809-6

29. Yu J, Bao E, Yan J, Lei L. Expression and localization of Hsps in the heart and blood vessel of heat-stressed broilers. *Cell Stress Chaperones*. (2008) 13:327–35. doi: 10.1007/s12192-008-0031-7

30. Zhang Y, Dong X, Hou L, Cao Z, Zhu G, Vongsangnak W, et al. Identification of differentially expressed non-coding RNA networks with potential Immunoregulatory roles during *Salmonella enteritidis* infection in ducks. *Front Vet Sci*. (2021) 8:692501. doi: 10.3389/fvets.2021.692501

31. Ricke SC. Strategies to improve poultry food safety, a landscape review. *Annual Review of Animal Biosciences*. (2021) 9:379–400. doi: 10.1146/annurev-animal-061220-023200

32. Cheng S, He Y, Zeng T, Wang D, He J, Xia Q, et al. Heat stress induces various oxidative damages to myofibrillar proteins in ducks. *Food Chem*. (2022) 390:133209. doi: 10.1016/j.foodchem.2022.133209

33. Shakeri M, Oskoueian E, Le HH, Shakeri M. Strategies to combat heat stress in broiler chickens: unveiling the roles of selenium, vitamin E and vitamin C. *Vet Sci*. (2020) 7:71. doi: 10.3390/vetsci7020071

34. Sun D, Xu C, Liu Y, Dai Z, Pan Z, Chen R, et al. The impact of different relative humidity levels on the production performance, slaughter performance, and meat quality of white Pekin ducks aged 4 to 42 days. *Animals*. (2023) 13:3711. doi: 10.3390/ani13233711

35. Cao Z, Gao W, Zhang Y, Huo W, Weng K, Zhang Y, et al. Effect of marketable age on proximate composition and nutritional profile of breast meat from Cherry Valley broiler ducks. *Poult Sci*. (2021) 100:101425. doi: 10.1016/j.psj.2021.101425

36. Kim D, Langmead B, Salzberg SL. HISAT: a fast spliced aligner with low memory requirements. *Nat Methods*. (2015) 12:357–60. doi: 10.1038/nmeth.3317

37. Li J, Zhang J, Liu J, Zhou Y, Cai C, Xu L, et al. A new duck genome reveals conserved and convergently evolved chromosome architectures of birds and mammals. *Gigascience*. (2021) 10:giaa142. doi: 10.1093/gigascience/giaa142

38. Pertea M, Pertea GM, Antonescu CM, Chang TC, Mendell JT, Salzberg SL. StringTie enables improved reconstruction of a transcriptome from RNA-seq reads. *Nat Biotechnol*. (2015) 33:290–5. doi: 10.1038/nbt.3122

39. Li B, Dewey CN. RSEM: accurate transcript quantification from RNA-Seq data with or without a reference genome. *BMC Bioinformatics*. (2011) 12:323. doi: 10.1186/1471-2105-12-323

40. Love MI, Huber W, Anders S. Moderated estimation of fold change and dispersion for RNA-seq data with DESeq2. *Genome Biol*. (2014) 15:550. doi: 10.1186/s13059-014-0550-8

41. Klopfenstein DV, Zhang L, Pedersen BS, Ramirez F, Warwick Vesztrocy A, Naldi A, et al. GOATOOLS: a python library for gene ontology analyses. *Sci Rep*. (2018) 8:10872. doi: 10.1038/s41598-018-28948-z

42. Xie C, Mao X, Huang J, Ding Y, Wu J, Dong S, et al. KOBAS 2.0: a web server for annotation and identification of enriched pathways and diseases. *Nucleic Acids Res*. (2011) 39:W316–22. doi: 10.1093/nar/gkr483

43. Szklarczyk D, Gable AL, Lyon D, Junge A, Wyder S, Huerta-Cepas J, et al. STRING v11: protein-protein association networks with increased coverage, supporting functional discovery in genome-wide experimental datasets. *Nucleic Acids Res*. (2019) 47:D607–13. doi: 10.1093/nar/gky1131

44. Chin CH, Chen SH, Wu HH, Ho CW, Ko MT, Lin CY. cytoHubba: identifying hub objects and sub-networks from complex interactome. *BMC Syst Biol*. (2014) 8:S11. doi: 10.1186/1752-0509-8-s4-s11

45. Shannon P, Markiel A, Ozier O, Baliga NS, Wang JT, Ramage D, et al. Cytoscape: a software environment for integrated models of biomolecular interaction networks. *Genome Res*. (2003) 13:2498–504. doi: 10.1101/gr.1239303

46. Maere S, Heymans K, Kuiper M. BiNGO: a Cytoscape plugin to assess overrepresentation of gene ontology categories in biological networks. *Bioinformatics*. (2005) 21:3448–9. doi: 10.1093/bioinformatics/bti551

47. Wu T, Hu E, Xu S, Chen M, Guo P, Dai Z, et al. clusterProfiler 4.0: a universal enrichment tool for interpreting omics data. *Innovation*. (2021) 2:100141. doi: 10.1016/j.xinn.2021.100141

48. Sun L, Luo H, Bu D, Zhao G, Yu K, Zhang C, et al. Utilizing sequence intrinsic composition to classify protein-coding and long non-coding transcripts. *Nucleic Acids Res*. (2013) 41:e166. doi: 10.1093/nar/gkt646

49. Kong L, Zhang Y, Ye ZQ, Liu XQ, Zhao SQ, Wei L, et al. CPC: assess the protein-coding potential of transcripts using sequence features and support vector machine. *Nucleic Acids Res*. (2007) 35:W345–9. doi: 10.1093/nar/gkm391

50. Wang L, Park HJ, Dasari S, Wang S, Kocher JP, Li W. CPAT: coding-potential assessment tool using an alignment-free logistic regression model. *Nucleic Acids Res*. (2013) 41:e74. doi: 10.1093/nar/gkt006

51. Fu XZ, Zhang XY, Qiu JY, Zhou X, Yuan M, He YZ, et al. Whole-transcriptome RNA sequencing reveals the global molecular responses and ceRNA regulatory network of mRNAs, lncRNAs, miRNAs and circRNAs in response to copper toxicity in Ziyang Xiangcheng (Citrus junos Sieb. Ex Tanaka). *BMC Plant Biol*. (2019) 19:509. doi: 10.1186/s12870-019-2087-1

52. Quinlan AR, Hall IM. BEDTools: a flexible suite of utilities for comparing genomic features. *Bioinformatics*. (2010) 26:841–2. doi: 10.1093/bioinformatics/btq033

53. Friedlander MR, Mackowiak SD, Li N, Chen W, Rajewsky N. miRDeep2 accurately identifies known and hundreds of novel microRNA genes in seven animal clades. *Nucleic Acids Res*. (2012) 40:37–52. doi: 10.1093/nar/gkr688

54. Enright AJ, John B, Gaul U, Tuschl T, Sander C, Marks DS. MicroRNA targets in Drosophila. *Genome Biol*. (2003) 5:R1. doi: 10.1186/gb-2003-5-1-r1

55. Wu HJ, Ma YK, Chen T, Wang M, Wang XJ. PsRobot: a web-based plant small RNA meta-analysis toolbox. *Nucleic Acids Res*. (2012) 40:W22–8. doi: 10.1093/nar/gks554

56. Ritchie ME, Phipson B, Wu D, Hu Y, Law CW, Shi W, et al. Limma powers differential expression analyses for RNA-sequencing and microarray studies. *Nucleic Acids Res*. (2015) 43:e47. doi: 10.1093/nar/gkv007

57. Agarwal V, Bell GW, Nam JW, Bartel DP. Predicting effective microRNA target sites in mammalian mRNAs. *eLife*. (2015) 4:4. doi: 10.7554/eLife.05005

58. Mueller RC, Ellstrom P, Howe K, Uliano-Silva M, Kuo RI, Miedzinska K, et al. A high-quality genome and comparison of short- versus long-read transcriptome of the palaearctic duck *Aythya fuligula* (tufted duck). *Gigascience*. (2021) 10:giab081. doi: 10.1093/gigascience/giab081

59. Farghly MFA, Abd El-Hack ME, Alagawany M, Saadeldin IM, Swelum AA. Ameliorating deleterious effects of heat stress on growing Muscovy ducklings using feed withdrawal and cold water. *Poult Sci*. (2019) 98:251–9. doi: 10.3382/ps/pey396

60. Oluwagbenga EM, Tetel V, Schober J, Fraley GS. Chronic heat stress part 1: decrease in egg quality, increase in cortisol levels in egg albumen, and reduction in fertility of breeder Pekin ducks. *Front Physiol*. (2022) 13:1019741. doi: 10.3389/fphys.2022.1019741

61. Luo X, Zheng C, Xia W, Ruan D, Wang S, Cui Y, et al. Effects of constant or intermittent high temperature on egg production, feed intake, and hypothalamic expression of antioxidant and pro-oxidant enzymes genes in laying ducks. *J Anim Sci*. (2018) 96:5064–74. doi: 10.1093/jas/sky355

62. Chen XL, Zeng YB, Liu LX, Song QL, Zou ZH, Wei QP, et al. Effects of dietary chromium propionate on laying performance, egg quality, serum biochemical parameters and antioxidant status of laying ducks under heat stress. *Animal*. (2021) 15:100081. doi: 10.1016/j.animal.2020.100081

63. He J, Xia C, He Y, Pan D, Cao J, Sun Y, et al. Proteomic responses to oxidative damage in meat from ducks exposed to heat stress. *Food Chem*. (2019) 295:129–37. doi: 10.1016/j.foodchem.2019.05.073

64. He Y, Zhou M, Xia C, Xia Q, He J, Cao J, et al. Volatile flavor changes responding to heat stress-induced lipid oxidation in duck meat. *Anim Sci J*. (2020) 91:e13461. doi: 10.1111/asj.13461

65. Farghly MFA, Abd El-Hack ME, Alagawany M, Saadeldin IM, Swelum AA. Wet feed and cold water as heat stress modulators in growing Muscovy ducklings. *Poult Sci*. (2018) 97:1588–94. doi: 10.3382/ps/pey006

66. Mashaly MM, Hendricks GL 3rd, Kalama MA, Gehad AE, Abbas AO, Patterson PH. Effect of heat stress on production parameters and immune responses of commercial laying hens. *Poult Sci*. (2004) 83:889–94. doi: 10.1093/ps/83.6.889

67. Hashizawa Y, Kubota M, Kadowaki M, Fujimura S. Effect of dietary vitamin E on broiler meat qualities, color, water-holding capacity and shear force value, under heat stress conditions. *Anim Sci J*. (2013) 84:732–6. doi: 10.1111/asj.12079

68. Akbarian A, Michiels J, Degroote J, Majdeddin M, Golian A, De Smet S. Association between heat stress and oxidative stress in poultry; mitochondrial dysfunction and dietary interventions with phytochemicals. *J Anim Sci Biotechnol*. (2016) 7:37. doi: 10.1186/s40104-016-0097-5

69. Lian P, Braber S, Garssen J, Wichers HJ, Folkerts G, Fink-Gremmels J, et al. Beyond heat stress: intestinal integrity disruption and mechanism-based intervention strategies. *Nutrients*. (2020) 12:734. doi: 10.3390/nu12030734

70. Siddiqui SH, Kang D, Park J, Khan M, Shim K. Chronic heat stress regulates the relation between heat shock protein and immunity in broiler small intestine. *Sci Rep*. (2020) 10:18872. doi: 10.1038/s41598-020-75885-x

71. Huang C, Jiao H, Song Z, Zhao J, Wang X, Lin H. Heat stress impairs mitochondria functions and induces oxidative injury in broiler chickens. *J Anim Sci*. (2021) 93:2144–53. doi: 10.2527/jas.2014-8739

72. Quinteiro-Filho WM, Gomes AV, Pinheiro ML, Ribeiro A, Ferraz-de-Paula V, Astolfi-Ferreira CS, et al. Heat stress impairs performance and induces intestinal inflammation in broiler chickens infected with *Salmonella enteritidis*. *Avian Pathol*. (2012) 41:421–7. doi: 10.1080/03079457.2012.709315

73. Kim WS, Ghassemi Nejad J, Roh SG, Lee HG. Heat-shock proteins gene expression in peripheral blood mononuclear cells as an Indicator of heat stress in beef calves. *Animals*. (2020) 10:895. doi: 10.3390/ani10050895

74. Hosseindoust AR, Lee SH, Kim JS, Choi YH, Kwon IK, Chae BJ. Productive performance of weanling piglets was improved by administration of a mixture of bacteriophages, targeted to control coliforms and Clostridium spp. shedding in a challenging environment. *J Anim Physiol Anim Nutr*. (2017) 101:e98–e107. doi: 10.1111/jpn.12567

75. Cui Y, Gu X. Proteomic changes of the porcine small intestine in response to chronic heat stress. *J Mol Endocrinol*. (2015) 55:277–93. doi: 10.1530/JME-15-0161

76. Lambert GP. Stress-induced gastrointestinal barrier dysfunction and its inflammatory effects. *J Anim Sci*. (2009) 87:E101–8. doi: 10.2527/jas.2008-1339

77. Yang C, Luo P, Chen SJ, Deng ZC, Fu XL, Xu DN, et al. Resveratrol sustains intestinal barrier integrity, improves antioxidant capacity, and alleviates inflammation

in the jejunum of ducks exposed to acute heat stress. *Poult Sci*. (2021) 100:101459. doi: 10.1016/j.psj.2021.101459

78. Li Z, Sun Y, He M, Liu J. Differentially-expressed mRNAs, microRNAs and long noncoding RNAs in intervertebral disc degeneration identified by RNA-sequencing. *Bioengineered*. (2021) 12:1026–39. doi: 10.1080/21655979.2021.1899533

79. Wang B, Zhang J, Chitrakar B, Wang Y, Xu T, Zhou C. Preservation of duck eggs through glycerol monolaurate nanoemulsion coating. *Curr Res Food Sci*. (2021) 4:752–7. doi: 10.1016/j.crfs.2021.10.008

80. Sun J, Wang J, Lin W, Li B, Ma R, Huang Y, et al. Predict the gelling properties of alkali-induced egg white gel based on the freshness of duck eggs. *Food Secur*. (2023) 12:4028. doi: 10.3390/foods12214028

81. Cui H, Yang H, Abdel-Samie MA, Siva S, Lin L. Controlled-release casein/cinnamon essential oil nanospheres for the inactivation of *Campylobacter jejuni* in duck. *Int J Food Microbiol*. (2021) 341:109074. doi: 10.1016/j.ijfoodmicro.2021.109074

82. Sun L, Feng S, Chen C, Liu X, Cai J. Identification of eggshell crack for hen egg and duck egg using correlation analysis based on acoustic resonance method. *J Food Process Eng*. (2020) 43:13430. doi: 10.1111/jfpe.13430

83. Xu F, Huang X, Tian X, Yu S, Zhang X, Zareef M. Application of hyperspectral imaging and colorimetric sensor array coupled with multivariate analysis for quality detection during salted duck eggs processing. *J Food Process Eng*. (2024) 47:14589. doi: 10.1111/jfpe.14589

84. Gu T, Lu L, Xu W, Zeng T, Tian Y, Chen B, et al. Immunopotentiators improve the antioxidant defense, apoptosis, and immune response in Shaoxing ducklings. *Poult Sci*. (2022) 101:101641. doi: 10.1016/j.psj.2021.101641

85. An H, Liu Y, Fang L, Shu M, Zhai Q, Chen J. Placenta-specific 8 facilitates the infection of duck hepatitis a virus type 1 by inhibiting the TLR7 MyD88-dependent signaling pathway. *Poult Sci*. (2023) 102:102724. doi: 10.1016/j.psj.2023.102724

86. Tosi G, Forlani G, Andresen V, Turci M, Bertazzoni U, Franchini G, et al. Major histocompatibility complex class II transactivator CIITA is a viral restriction factor that targets human T-cell lymphotropic virus type 1 Tax-1 function and inhibits viral replication. *J Virol*. (2011) 85:10719–29. doi: 10.1128/JVI.00813-11

87. Li R, Guo M, Lin J, Chai T, Wei L. Molecular cloning, characterization, and anti-avian pathogenic *Escherichia coli* innate immune response of the Cherry Valley duck CIITA gene. *Front Microbiol*. (2017) 8:1629. doi: 10.3389/fmicb.2017.01629

88. Francoeur L, Scoville DM, Johnson PA. Effect of IGF1 and FSH on the function of granulosa cells from pre-hierarchal follicles in chickens dagger. *Biol Reprod*. (2023) 109:498–506. doi: 10.1093/biolre/ioad082

89. Wang WJ, Guo YQ, Xie KJ, Li YD, Li ZW, Wang N, et al. A functional variant in the promoter region of IGF1 gene is associated with chicken abdominal fat deposition. *Domest Anim Endocrinol*. (2021) 75:106584. doi: 10.1016/j.domaniend.2020.106584

90. Gong Y, Yang J, Liu Q, Cai J, Zheng Y, Zhang Y, et al. IGF1 knockdown hinders myocardial development through energy metabolism dysfunction caused by ROS-dependent FOXO activation in the chicken heart. *Oxidative Med Cell Longev*. (2019) 2019:1–31. doi: 10.1155/2019/7838754

91. Zhou H, Mitchell AD, McMurtry JP, Ashwell CM, Lamont SJ. Insulin-like growth factor-I gene polymorphism associations with growth, body composition, skeleton integrity, and metabolic traits in chickens. *Poult Sci*. (2005) 84:212–9. doi: 10.1093/ps/84.2.212

92. Li X, Qiu J, Liu H, Deng Y, Hu S, Hu J, et al. MicroRNA-33a negatively regulates myoblast proliferation by targeting IGF1, follistatin and cyclin D1. *Biosci Rep*. (2020) 40:BSR20191327. doi: 10.1042/BSR20191327

93. Lin J, Guan L, Ge L, Liu G, Bai Y, Liu X. Nanopore-based full-length transcriptome sequencing of Muscovy duck (*Cairina moschata*) ovary. *Poult Sci*. (2021) 100:101246. doi: 10.1016/j.psj.2021.101246

94. Bhattacharya TK, Chatterjee RN, Dushyanth K, Paswan C, Shukla R, Shanmugam M. Polymorphism and expression of insulin-like growth factor 1 (IGF1) gene and its association with growth traits in chicken. *Br Poult Sci*. (2015) 56:398–407. doi: 10.1080/00071668.2015.1041098

95. Hajihoseini Z, Eghbalsaied S. Simultaneous effects of IGF1 and Fadrozole on parthenogenesis and pluripotency markers in chicken embryo. *Theriogenology*. (2018) 114:317–23. doi: 10.1016/j.theriogenology.2018.04.009

96. Ogunpaimo OJ, Ojoawo HT, Wheto MY, Adebambo AO, Adebambo OA. Association of insulin-like growth factor 1 (IGF1) gene polymorphism with the reproductive performance of three dual-purpose chicken breeds. *Transl Anim Sci*. (2021) 5:txab215. doi: 10.1093/tas/txab215

97. Hosnedlova B, Vernerova K, Kizek R, Bozzi R, Kadlec J, Curn V, et al. Associations between IGF1, IGFBP2 and TGFss3 genes polymorphisms and growth performance of broiler chicken lines. *Animals*. (2020) 10:800. doi: 10.3390/ani10050800

98. Ye Q, Xu J, Gao X, Ouyang H, Luo W, Nie Q. Associations of IGF2 and DRD2 polymorphisms with laying traits in Muscovy duck. *PeerJ*. (2017) 5:e4083. doi: 10.7717/peerj.4083

99. Zhao J, Zhao X, Shen X, Zhang Y, Zhang Y, Ye L, et al. CircCCDC91 regulates chicken skeletal muscle development by sponging miR-15 family via activating IGF1-PI3K/AKT signaling pathway. *Poult Sci*. (2022) 101:101803. doi: 10.1016/j.psj.2022.101803

100. Rahaie A, Toghyani M, Eghbalsaied S. Co-treatment of IGF1 and Fadrozole upregulates the expression of RSPO1, SOX9, and AMH in chicken embryos. *Cells Tissues Organs*. (2018) 206:218–28. doi: 10.1159/000499079

101. Zhao Y, Zou M, Sun Y, Zhang K, Peng X. Gga-miR-21 modulates *Mycoplasma gallisepticum* (HS strain)-induced inflammation via targeting MAP3K1 and activating MAPKs and NF-kappaB pathways. *Vet Microbiol*. (2019) 237:108407. doi: 10.1016/j.vetmic.2019.108407

102. Xie HL, Zhang YH, Tan XD, Zheng Y, Ni HY, Dong LP, et al. miR-375 induced the formation and transgenerational inheritance of fatty liver in poultry by targeting MAP3K1. *DNA Cell Biol*. (2022) 41:590–9. doi: 10.1089/dna.2022.0078

103. Pesti D, Hasler-Rapacz J, Rapacz J, McGibbon WH. Immunogenetic studies on low-density lipoprotein allotypes in chickens (Lcp1 and Lcp2). *Poult Sci*. (1981) 60:295–301. doi: 10.3382/ps.0600295

104. Tan GH, Li JZ, Zhang YY, You MF, Liao CM, Zhang YG. Association of PRKCA expression and polymorphisms with layer duck eggshell quality. *Br Poult Sci*. (2021) 62:8–16. doi: 10.1080/00071668.2020.1817329

105. Lin L, Ye K, Chen F, Xie J, Chen Z, Xu Y. Identification of new immune subtypes of renal injury associated with anti-neutrophil cytoplasmic antibody-associated vasculitis based on integrated bioinformatics analysis. *Front Genet*. (2023) 14, 14:1119017. doi: 10.3389/fgene.2023.1119017

106. Habauzit D, Le Quement C, Zhadobov M, Martin C, Aubry M, Sauleau R, et al. Transcriptome analysis reveals the contribution of thermal and the specific effects in cellular response to millimeter wave exposure. *PLoS One*. (2014) 9:e109435. doi: 10.1371/journal.pone.0109435

107. Zhou Y, Zhou Y, Kang X, Meng C, Zhang R, Guo Y, et al. Molecular cloning and functional characterisation of duck (*Anas platyrhynchos*) tumour necrosis factor receptor-associated factor 3. *Br Poult Sci*. (2019) 60:357–65. doi: 10.1080/00071668.2019.1614528

108. Cai W, Pan Y, Luo W, Cheng A, Wang M, Chen S, et al. NS5 hijacks TRAF3 to inhibit type I interferon signaling during duck Tembusu virus infection. *Vet Microbiol*. (2023) 286:109894. doi: 10.1016/j.vetmic.2023.109894

109. Xu W, Zhang L, Ma S, Zhang Y, Cai Z, Zhang K, et al. TRAF5 protects against myocardial ischemia reperfusion injury via AKT signaling. *Eur J Pharmacol*. (2020) 878:173092. doi: 10.1016/j.ejphar.2020.173092

110. Tian H, Ding M, Guo Y, Zhu Z, Yu Y, Tian Y, et al. Effect of HSPA8 gene on the proliferation, apoptosis and immune function of HD11 cells. *Dev Comp Immunol*. (2023) 142:104666. doi: 10.1016/j.dci.2023.104666

111. Scott TA, Balnave D. Comparison between concentrated complete diets and self-selection for feeding sexually-maturing pullets at hot and cold temperatures. *Br Poult Sci*. (1988) 29:613–26. doi: 10.1080/00071668808417088

112. Testa U, Pelosi E, Castelli G, Labbaye C. miR-146 and miR-155: two key modulators of immune response and tumor development. *Noncoding RNA*. (2017) 3:22. doi: 10.3390/ncrna3030022

113. Schulte LN, Westermann AJ, Vogel J. Differential activation and functional specialization of miR-146 and miR-155 in innate immune sensing. *Nucleic Acids Res*. (2013) 41:542–53. doi: 10.1093/nar/gks1030

114. Laanesoo A, Urgard E, Periyasamy K, Laan M, Bochkov YA, Aab A, et al. Dual role of the miR-146 family in rhinovirus-induced airway inflammation and allergic asthma exacerbation. *Clin Transl Med*. (2021) 11:e427. doi: 10.1002/ctm2.427

115. Lee HM, Kim TS, Jo EK. MiR-146 and miR-125 in the regulation of innate immunity and inflammation. *BMB Rep*. (2016) 49:311–8. doi: 10.5483/bmbrep.2016.49.6.056

116. Lee JH, Kim SW, Han JS, Shin SP, Lee SI, Park TS. Functional analyses of miRNA-146b-5p during myogenic proliferation and differentiation in chicken myoblasts. *BMC Mol Cell Biol*. (2020) 21, 21:40. doi: 10.1186/s12860-020-00284-z

117. Hu G, Liu L, Miao X, Zhao Y, Li X. Research note: IsomiRs of chicken miR-146b-5p are activated upon *Salmonella enterica* serovar Enteritidis infection. *Poult Sci*. (2022) 101:101977. doi: 10.1016/j.psj.2022.101977

118. Huang J, Lei L, Cui M, Cheng A, Wang M, Liu M, et al. miR-146b-5p promotes duck Tembusu virus replication by targeting RPS14. *Poult Sci*. (2023) 102:102890. doi: 10.1016/j.psj.2023.102890

119. Zhou W, Ye S, Wang W. miR-217 alleviates high-glucose-induced vascular smooth muscle cell dysfunction via regulating ROCK1. *J Biochem Mol Toxicol*. (2021) 35:e22668. doi: 10.1002/jbt.22668

120. Zhu M, Chen G, Yang Y, Yang J, Qin B, Gu L. miR-217-5p regulates myogenesis in skeletal muscle stem cells by targeting FGFR2. *Mol Med Rep*. (2020) 22:850–8. doi: 10.3892/mmr.2020.11133

121. Hu X, Tan S, Yin H, Khoso PA, Xu Z, Li S. Selenium-mediated gga-miR-29a-3p regulates LMH cell proliferation, invasion, and migration by targeting COL4A2. *Metallomics*. (2020) 12:449–59. doi: 10.1039/c9mt00266a

122. Chowdhury VS, Han G, Eltahan HM, Haraguchi S, Gilbert ER, Cline MA, et al. Potential role of amino acids in the adaptation of chicks and market-age broilers to heat stress. *Front Vet Sci*. (2020) 7:610541. doi: 10.3389/fvets.2020.610541

123. Abo Ghanima MM, Abd El-Hack ME, Othman SI, Taha AE, Allam AA, Eid Abdel-Moneim AM. Impact of different rearing systems on growth, carcass traits, oxidative stress biomarkers, and humoral immunity of broilers exposed to heat stress. *Poult Sci*. (2020) 99:3070–8. doi: 10.1016/j.psj.2020.03.011

124. Farghly MFA, Mahrose KM, Cooper RG, Ullah Z, Rehman Z, Ding C. Sustainable floor type for managing Turkey production in a hot climate. *Poult Sci*. (2018) 97:3884–90. doi: 10.3382/ps/pey280

125. Habibian M, Ghazi S, Moeini MM. Effects of dietary selenium and vitamin E on growth performance, meat yield, and selenium content and lipid oxidation of breast meat of broilers reared under heat stress. *Biol Trace Elem Res*. (2016) 169:142–52. doi: 10.1007/s12011-015-0404-6

126. Wu QJ, Liu N, Wu XH, Wang GY, Lin L. Glutamine alleviates heat stress-induced impairment of intestinal morphology, intestinal inflammatory response, and barrier integrity in broilers. *Poult Sci*. (2018) 97:2675–83. doi: 10.3382/ps/pey123

127. Abd El-Hack ME, Alagawany M, Noreldin AE. Managerial and nutritional trends to mitigate heat stress risks in poultry farms In: Abdel-Wahab RK, Hikal, WM, editors. Sustainability of Agricultural Environment in Egypt: Part II: The Handbook of Environmental Chemistry. Berlin, Germany: Springer (2018). 325–38.

128. Kucuk O, Sahin N, Sahin K. Supplemental zinc and vitamin a can alleviate negative effects of heat stress in broiler chickens. *Biol Trace Elem Res*. (2021) 94:225–36. doi: 10.1385/BTER:94:3:225

129. Sahin K, Smith MO, Onderci M, Sahin N, Gursu MF, Kucuk O. Supplementation of zinc from organic or inorganic source improves performance and antioxidant status of heat-distressed quail. *Poult Sci*. (2005) 84:882–7. doi: 10.1093/ps/84.6.882

130. Yadav S, Jha R. Strategies to modulate the intestinal microbiota and their effects on nutrient utilization, performance, and health of poultry. *J Anim Sci Biotechnol*. (2019) 10:2. doi: 10.1186/s40104-018-0310-9

131. Song J, Xiao K, Ke YL, Jiao LF, Hu CH, Diao QY, et al. Effect of a probiotic mixture on intestinal microflora, morphology, and barrier integrity of broilers subjected to heat stress. *Poult Sci*. (2014) 93:581–8. doi: 10.3382/ps.2013-03455

132. Renaudeau D, Collin A, Yahav S, de Basilio V, Gourdine JL, Collier RJ. Adaptation to hot climate and strategies to alleviate heat stress in livestock production. *Animal*. (2012) 6:707–28. doi: 10.1017/S1751731111002448

133. Duah KK, Essuman EK, Boadu VG, Olympio OS, Akwetey W. Comparative study of indigenous chickens on the basis of their health and performance. *Poult Sci*. (2020) 99:2286–92. doi: 10.1016/j.psj.2019.11.049

134. Ouyang J-h, Xie L, Nie Q-h, Zeng H, Peng Z-j, Zhang D-x, et al. The effects of different sex-linked dwarf variations on Chinese native chickens. *J Integr Agric*. (2012) 11:1500–8. doi: 10.1016/s2095-3119(12)60150-6

135. Yunis R, Cahaner A. The effects of the naked neck (Na) and frizzle (F) genes on growth and meat yield of broilers and their interactions with ambient temperatures and potential growth rate. *Poult Sci*. (1999) 78:1347–52. doi: 10.1093/ps/78.10.1347

136. Dong J, He C, Wang Z, Li Y, Li S, Tao L, et al. A novel deletion in KRT75L4 mediates the frizzle trait in a Chinese indigenous chicken. *Genet Sel Evol*. (2018) 50:68. doi: 10.1186/s12711-018-0441-7

137. Bilal RM, Hassan FU, Farag MR, Nasir TA, Ragni M, Mahgoub HAM, et al. Thermal stress and high stocking densities in poultry farms: potential effects and mitigation strategies. *J Therm Biol*. (2021) 99:102944. doi: 10.1016/j.jtherbio.2021.102944

138. Fathi MM, Galal A, Radwan LM, Abou-Emera OK, Al-Homidan IH. Using major genes to mitigate the deleterious effects of heat stress in poultry: an updated review. *Poult Sci*. (2022) 101:102157. doi: 10.1016/j.psj.2022.102157

139. Kang S, Eltahir EAB. North China plain threatened by deadly heatwaves due to climate change and irrigation. *Nat Commun*. (2018) 9:2894. doi: 10.1038/s41467-018-05252-y

frontiers | Frontiers in Veterinary Science

TYPE Original Research
PUBLISHED 31 July 2024
DOI 10.3389/fvets.2024.1416124

OPEN ACCESS

EDITED BY
Toshiro Arai,
Nippon Veterinary and Life Science University, Japan

REVIEWED BY
Luisa Ragionieri,
University of Parma, Italy
Takahiro Teshima,
Nippon Veterinary and Life Science University, Japan

*CORRESPONDENCE
Elodie Rizzoli
✉ elodie.rizzoli@uliege.be

RECEIVED 11 April 2024
ACCEPTED 22 July 2024
PUBLISHED 31 July 2024

CITATION
Rizzoli E, de Meeûs d'Argenteuil C, Fastrès A, Roels E, Janssen P, Puré E, Garigliany M-M, Marichal T and Clercx C (2024) Fibroblast activation protein is a cellular marker of fibrotic activity in canine idiopathic pulmonary fibrosis. *Front. Vet. Sci.* 11:1416124. doi: 10.3389/fvets.2024.1416124

Fibroblast activation protein is a cellular marker of fibrotic activity in canine idiopathic pulmonary fibrosis

Elodie Rizzoli[1]*, Constance de Meeûs d'Argenteuil[2], Aline Fastrès[1], Elodie Roels[1], Pierre Janssen[3,4], Ellen Puré[5], Mutien-Marie Garigliany[2], Thomas Marichal[3,4,6] and Cécile Clercx[1]

[1]Department of Companion Animal Clinical Sciences, Fundamental and Applied Research for Animals and Health (FARAH), Faculty of Veterinary Medicine, University of Liège, Liège, Belgium, [2]Department of Morphology and Pathology, FARAH, Faculty of Veterinary Medicine, University of Liège, Liège, Belgium, [3]Laboratory of Immunophysiology, GIGA Institute, University of Liège, Liège, Belgium, [4]Department of Functional Sciences, FARAH, Faculty of Veterinary Medicine, University of Liège, Liège, Belgium, [5]Department of Biomedical Sciences, School of Veterinary Medicine, University of Pennsylvania, Philadelphia, PA, United States, [6]Walloon Excellence in Life Sciences and Biotechnology (WELBIO) Department, WEL Research Institute, Wavre, Belgium

Canine idiopathic pulmonary fibrosis (CIPF) is a progressive fibrotic interstitial lung disease of unknown etiology, afflicting aging West Highland white terriers (WHWTs) and leading to progressive respiratory failure. Fibroblast activation protein (FAP), a protease overexpressed in many cancers, is upregulated in idiopathic pulmonary fibrosis in humans. The aim of this study was to investigate FAP as a marker of active fibrosis in lung biopsies from WHWTs affected with CIPF, as well as the potential of plasmatic FAP as a biomarker. After establishing a scoring system to evaluate the severity and activity of fibrosis on histopathological lung sections, anti-FAP immunohistochemistry was performed on healthy and CIPF samples. FAP expression was characterized using both visual and digital quantitative pathology software analyses and then correlated to fibrosis severity and activity. Levels of plasmatic FAP in WHWTs affected with CIPF were measured by enzyme-linked immunosorbent assay and compared with healthy dogs. Lung samples from 22 WHWTs affected with CIPF were collected. According to the fibrosis scoring system, they were classified as cases of mild (5), moderate (9) and severe (8) fibrosis and were attributed scores of fibrosis activity. Fifteen healthy lung samples were classified as non-fibrotic. Healthy lung samples were FAP-negative, whereas fibroblasts were FAP-positive in 20 CIPF samples. FAP immunohistochemical expression correlated mildly with fibrosis severity ($p < 0.05$; $R^2 = 0.22$) but highly with fibrosis activity scores ($p < 0.001$; $R^2 = 0.68$). Digital image analysis detected a higher percentage of FAP-positive cells in areas of active fibrosis ($p < 0.001$) and FAP-positive cells were distributed outside mature fibrosis lesions, clustered in active fibrosis areas or scattered within alveolar septa. On the other hand, plasmatic FAP was significantly lower in dogs affected with CIPF compared with healthy dogs ($p < 0.01$). In conclusion, this study provides a valuable histological scoring system to assess the severity and activity of fibrosis in CIPF. It demonstrates that FAP is a good cellular marker of fibrotic activity in CIPF, and thus constitutes a promising target to be exploited for diagnostic and therapeutic applications. Additionally, it suggests that plasmatic FAP, although non-specific, could be altered in CIPF.

KEYWORDS

dog, lung, fibrosis, idiopathic pulmonary fibrosis, fibroblast activation protein, immunohistochemistry, West Highland white terrier

1 Introduction

Canine idiopathic pulmonary fibrosis (CIPF) is a progressive fibrotic interstitial lung disease of unknown etiology, affecting the West Highland white terrier (WHWT) breed leading to progressive respiratory insufficiency, mimicking idiopathic pulmonary fibrosis (IPF) in humans (1, 2). Currently, there are neither consistent diagnostic or prognostic biomarker nor curative treatment options available for this disease (1, 2).

Fibroblast Activation Protein (FAP), also known as seprase, is a cell surface protease which exhibits both dipeptidyl peptidase activity and endopeptidase activity (3). Among substrates of the endopeptidase activity, FAP cleaves denatured type 1 collagen, thus participating in extracellular matrix (ECM) remodeling (3). The protease also exists as a soluble circulating form called antiplasmin-cleaving enzyme (APCE) (4). FAP is specifically expressed in areas of physiological and pathological active tissue remodeling, including wound healing and scar formation in mammals (5). FAP is usually undetectable in normal tissue (5), although low basal levels have been measured in human adipose tissue, liver and plasma (6, 7).

In human IPF, immunohistochemical studies on lung biopsies showed that FAP is strongly expressed in areas of lung fibrosis, namely in fibroblast foci and interstitium, and is positively correlated with the severity of fibrosis (8, 9). In humans, FAP is also upregulated in other fibrotic diseases (10–12) as well as non-fibrotic diseases (13, 14), and, importantly, in various types of cancers. Indeed, it is expressed in over 90% of carcinomas, including among others non-small-cell lung carcinoma (15–17), colorectal (18, 19), esophageal (20), breast (21–23), and renal (24) cancer. The protease is mainly present in cancer associated fibroblasts, but can also be expressed in other cells in the tumor microenvironment [immune (25) cells or endothelial (19) cells] or in epithelial tumor cells (17, 19). In dogs, overexpression of FAP has already been demonstrated in the stroma of mast cell tumors and mammary carcinomas (26, 27) as well as in the right atrium of beagle dogs with induced atrial fibrillation (28). Moreover, overexpression of the FAP gene has been observed in post-mortem lung biopsies from WHWTs affected with CIPF compared with healthy controls based on microarray analysis and quantitative reverse transcriptase polymerase chain reaction (29).

Recently, FAP-targeted positron emission tomography (PET) imaging using a FAP inhibitor (FAPI) has been described as a non-invasive sensitive tool for advanced tumor staging and monitoring and has a promising potential owing to its ability to accurately depict most malignant tumors (30). Beyond its application in neoplastic disorders, there have been encouraging reports suggesting the utility of FAPI PET in non-neoplastic conditions such as respiratory or cardiac diseases including IPF (9, 31–33). Indeed, the uptake of FAP-targeted tracers (labeled with either ^{68}Ga or ^{18}F) in IPF patients is higher than in healthy volunteers, and also seems to be positively correlated to the pulmonary function decline (9, 33).

Given the potential role of FAP in the pathogenesis of fibrosis and cancer, several therapeutic strategies seek to target this protein, from selective inhibitors (34) to anti-FAP chimeric antigen receptor (CAR)-T cells (35) or even recent theragnostic ligands (36). However, none of these FAP-based therapeutic approaches have been approved in humans yet.

If FAP appears to be a specific marker of active fibrosis in dogs with CIPF, it could represent both an interesting diagnostic and monitoring marker of the disease and importantly, a potential therapeutic target. Therefore, the aim of this study was to gain insight into the implication of FAP in the pathophysiology of CIPF and to confirm its potential as a marker of disease activity. We hypothesized that FAP is expressed in lungs of WHWTs affected with CIPF, as well as in the stroma of canine lung cancers, used as positive controls, but not in healthy lungs. Anti-FAP immunohistochemistry (IHC) staining was thus performed on sections of lung biopsies from WHWTs affected with CIPF, dogs with lung cancer and dogs without pulmonary disease. The pattern of FAP expression was characterized according to the pattern of severity and activity of fibrosis, using both visual and digital quantitative pathology software analyses. Finally, the potential of circulating FAP as a biomarker of CIPF was investigated by measuring the levels of plasmatic FAP in WHWTs affected with CIPF in comparison with healthy dogs.

2 Materials and methods

2.1 Lung sample collection

For this cross-sectional observational study, lung biopsies were obtained from 22 WHWTs affected with CIPF (median age of 12.4 years; range 10.3–15.6; 10 females and 12 males), 15 dogs of various breeds [WHWT (4), Beagle (3), Yorkshire Terrier (3), mixed breed (2), American Staffordshire Terrier, Bull Terrier, Leonberger, and Shih Tzu] exempt from lung disease (median age of 13.2 years; range 7.3–16.8; 4 females and 11 males) and 7 dogs of different breeds [WHWT (4), mixed breed (2), Weimaraner] with lung neoplasia (median age of 12.0 years; range 8.2–14.2; 5 females and 2 males). In WHWTs, CIPF diagnosis was based on clinical signs, physical examination, 6-min walk test, hematology, serum biochemistry, arterial blood gas analysis, cardiac ultrasonography, thoracic high-resolution computed tomography, bronchoscopy and analysis of bronchoalveolar lavage fluid (1, 37). CIPF and healthy WHWTs were recruited as part of a longitudinal study conducted at the University of Liège and approved by the Animal Ethics Committee of the University of Liège (approval #20–2245). Healthy controls were euthanized for reasons unrelated to the study and had no

Abbreviations: BSA, bovine serum albumin; CAR, chimeric antigen receptor; CIPF, canine idiopathic pulmonary fibrosis; DPBS, Dulbecco's Phosphate-Buffered Saline; ELISA, enzyme-linked immunosorbent assay; EPT, endpoint titer; FAP, fibroblast activation protein; FAPI, fibroblast activation protein inhibitor; HE, hematoxylin and eosin; IHC, immunohistochemistry; IPF, idiopathic pulmonary fibrosis; PET, positron emission tomography; UIP, usual interstitial pneumonia; WHWT, West Highland white terrier.

respiratory clinical signs and normal lung histopathology. Five post-mortem lung biopsies were collected: one in the periphery of the right cranial and accessory lobes, two in the periphery of the right diaphragmatic lobe – one ventrally and one dorsally – and one centrally in the right middle lobe. Biopsies of pulmonary neoplasia, collected after either lobectomy or necropsy, were also retrieved. All biopsies were fixed in formalin 10% and embedded in paraffin until further use. All samples were obtained with informed owner consent.

2.2 Histopathology and fibrosis scoring

Formalin-fixed, paraffin-embedded specimens were sliced into 5 µm sections with a motorized microtome (Microm HM355S, Thermo Fisher Scientific). Hematoxylin and eosin (HE) staining was initially performed. All slides were evaluated by the first author and by a diplomate of the European College of Veterinary Pathology (MMG), who were blinded to the clinical records. For each healthy and CIPF case, one representative section was selected and additional serial slides were stained with Masson's trichrome and Picro Sirius red for further use. All sections were digitalized with NDP NanoZoomer (Hamamatsu) and Picro Sirius red slides were additionally digitalized under polarized light with ZEISS Axioscan 7.

For each selected section, a scoring system of fibrosis was applied, based on both HE and Masson's trichrome. For this purpose, a list of criteria was established, as detailed in Table 1, based on previously reported histopathological examinations of CIPF lung sections (37, 38) and the latest consensus for histopathological diagnosis of human IPF (39). Categories of criteria included the pattern of interstitial fibrosis (evaluating the severity of fibrosis in the subpleural area, in peribronchiolar area as well as within alveolar septa) based on Masson's trichome stained sections, the maturity of fibrosis and its extent over the section (based on HE and Masson's trichrome), and alveolar epithelial and luminal changes (based on HE). Regarding the maturity of fibrosis, each case was assigned a score of active fibrosis from 0 to 3 reflecting the proportion of the section affected by active fibrosis, which was defined as immature, highly cellular, fibroblast-dominant fibrosis (38). Another score from 0 to 3 was attributed according to the contribution of mature fibrosis, which was defined as inactive fibrosis and characterized by dense collagen deposition and low cellularity consisting of a few fibrocytes (38). An overall grade of fibrosis severity was attributed according to the total score as follows: 0–3 (non-fibrotic), 4–7 (mild), 8–11 (moderate) and 12–16 (severe). For lung tumor cases, the histopathological diagnosis was established as precisely as possible based on medical records and HE stained slides.

2.3 Tissular FAP immunohistochemistry

2.3.1 Staining

Anti-FAP IHC was performed on additional serial sections of formalin-fixed, paraffin-embedded biopsies of CIPF, healthy lungs and

TABLE 1 Scoring system used to evaluate fibrosis in canine idiopathic pulmonary fibrosis lung biopsies.

Histopathological features	Criteria	Scores			
		0	1	2	3
Interstitial fibrosis pattern					
Subpleural	Increase in pleural width	0	2x	≥3x	NA
Peribronchiolar fibrous metaplasia	Smooth muscle over lamina propria and adventitia thickness ratio	>0.34	≤0.34	NA	NA
Diffuse	Increase in septa width by fibrosis	0	2x	3–4x	≥5x
	Atelectasis, alveolar distortion, consolidation, and/or honeycombing	Absent	NA	NA	Present
Maturity of fibrosis					
Immature, active, cellular, fibroblast-dominant*	Proportion of the section affected by active fibrosis	0%	1–33%	34–66%	≥67%
Mature, inactive, fibrous, few fibrocytes*	Proportion of the section affected by mature fibrosis	0%	1–33%	34–66%	≥67%
Alveolar epithelial and luminal changes					
Type II pneumocyte hyperplasia/ bronchiolar metaplasia	Alveolar epithelium	Normal	Type II pneumocyte hyperplasia and/or atypia	Pseudo-stratification	NA
Numerous alveolar macrophages	Alveolar macrophages count per alveolar space	1–2	≥3	NA	NA

The grade of severity of fibrosis was attributed by calculating the sum of the score attributed for each criteria: 0–3 (non-fibrotic), 4–7 (mild), 8–11 (moderate) and 12–16 (severe). *As the sum of both percentages cannot exceed 100% (whole section), the sum of the scores from these 2 categories is maximum 4.

lung cancers, which were used as positive controls. The slides were deparaffinized in xylene and rehydrated in graded alcohol series. Antigen retrieval was performed using 10 mM sodium citrate buffer for 5 min at 100°C. Slides were washed at room temperature and hydrated in Phosphate-Buffered Saline. Endogenous peroxidase activity was blocked with 3% hydrogen peroxide incubation for 30 min. Sections were then washed with distilled water. Nonspecific antibody binding was blocked by incubation for 30 min in a blocking buffer containing 0.5% blocking reagent provided in the TSA Plus DNP kit (Akoya Biosciences #NEL747A001KT). Sections were incubated overnight at 4°C temperature with rabbit anti-human fibroblast activation protein alpha monoclonal primary antibody (1:100, Abcam #ab207178, RRID:AB_2864720) or with rabbit isotype IgG control antibody (1:1600, Jackson ImmunoResearch Labs #011–000-003, RRID:AB_2337118) to later screen for non-specific staining. Biotinylated goat anti-rabbit secondary antibody (1,1000, Thermo Fisher Scientific #65–6,140, RRID:AB_2533969) was then incubated for 1 h at room temperature. The slides were incubated for 30 min with streptavidin-horseradish peroxidase (Invitrogen #S911), and signal was amplified using a TSA Plus DNP kit (Akoya Biosciences #NEL747A001KT). Signal development was achieved with a metal enhanced diaminobenzidine substrate kit (Thermo Fisher Scientific #34065). Slides were counterstained with hematoxylin for 30 s, then dehydrated and mounted. Each slide was digitalized using NDP NanoZoomer (Hamamatsu).

2.3.2 Visual assessment of FAP expression

Two independent observers, including the first author and a diplomate of the European College of Veterinary Pathology (MMG), blinded to the histopathological diagnosis, assessed all healthy and CIPF digitalized sections to determine a staining index for the whole section, that represents the expression of FAP. There was 91% agreement between the two observers and the final index was obtained after a consensus was reached. An area of parenchymal lung was identified as FAP-positive if at least 25% of the cells exhibited FAP staining. The FAP expression index (from 0 to 3) was then attributed according to the percentage of the whole section occupied by FAP-positive areas. An index of 0 (no expression) was attributed if less than 1% of the section was occupied by FAP-positive areas, 1 (low expression) if FAP-positive areas occupied from 1 to 10% of the whole section, 2 (intermediate expression) from 11 to 50% and 3 (high expression) for more than 50%. In all CIPF cases, correlation analyses were conducted between the FAP expression index and the fibrosis severity score, as well as with the fibrosis activity score attributed during the scoring of fibrosis.

2.3.3 Digital analysis of FAP expression

Whole slide images were analyzed with an open-source automated software analysis program for digital pathology (QuPath version 0.4.3) (40). Briefly, lesional areas were determined manually on the HE slides and classified into 'active fibrosis' or 'mature fibrosis.' Ten areas of 200,000 μm^2 each representative of active fibrosis or mature fibrosis were selected. Automated tissue detection was performed in the lesional area to correct for alveolar blank spaces. Thereafter, for fibrosis quantification, built-in algorithms for pixel classification of QuPath and machine learning were used on sequential Picro Sirius red slides for measuring collagen content in lesional areas. The accuracy of collagen detection was then verified by assessing the same area digitalized under polarized light. On FAP-stained sections, the percentage of FAP-positive cells within the lung interstitium for the 20 areas was calculated by applying the deep learning algorithm StarDist method for cell nuclei segmentation and applying a single threshold to the cell detection to obtain positive cell detection. To visualize the spatial distribution of FAP positive cells in fibrotic areas, image superposition of Picro Sirius red slides and FAP-stained slides was done by using the Warpy extension in QuPath.

2.4 Plasmatic FAP measurement

2.4.1 Test samples

For the plasmatic FAP measurement, we used plasma samples from the day of death of 6 WHWTs affected with CIPF for which positive FAP expression in the lungs was confirmed by the methods described above. They had a median age of 12.6 years (range 10.3–15.6; 3 females and 3 males). For the control group, we used the plasma leftover from the analysis of blood donations from 9 healthy canine blood donors of various breeds [Border Collie (4), Golden Retriever (3), Akita Inu, Bull Terrier] with a median age of 6.6 years (range 3.9–7.3), including 4 females and 5 males. Dogs were considered healthy based on the absence of clinical signs or physical exam abnormalities, a complete blood analysis and a screening for infectious diseases. In all dogs, blood was collected in a citrated tube before being centrifuged and plasma was isolated and stored at −80°C until the day of the experiment. The assay was performed in citrate plasma in all cases because it was the type of plasma that was available for the higher number of cases in our biobank. Plasma samples underwent maximum 2 freeze–thaw cycles before analysis. Plasma samples were diluted in 1% bovine serum albumin (BSA, Sigma #A7906) in Dulbecco's Phosphate-Buffered Saline (DPBS) in four dilutions (1:50, 1:100, 1:200, 1:400) for titration. The reactivity of the assay with canine FAP was verified by using a homogenate of a FAP-rich metastasis of mammary carcinoma as positive control. A snap frozen biopsy of a lung metastasis of a mammary carcinoma that highly overexpressed FAP in IHC was homogenized using a previously described protocol (41). This canine FAP-containing solution was then diluted 1:5, 1:10, 1:25, 1:50 in 1% BSA DPBS in the assay for titration. Recombinant human FAP (Abcam #ab79623) with known concentration was used as positive control and standard. Negative control was 1% BSA DPBS.

2.4.2 Assay

Plasma levels of FAP were measured using a double-antibody sandwich enzyme-linked immunosorbent assay (ELISA). First, 96-well microplates were coated with a mouse IgG monoclonal anti-canine FAP antibody (5.125 µg/mL, Puré lab, University of Pennsylvania, 4G5) that cross-reacts with human FAP (35) and incubated overnight at 4°C. The following day, plates were blocked with 1% BSA in DPBS for 1 h before test samples were added in duplicates and incubated overnight at 4°C with agitation. For detection, a biotinylated polyclonal sheep anti-human FAP antibody (0.4 µg/µl, R&D Systems #BAF3715, RRID:AB_2057508) was added and incubated for 90 min. Plates were then incubated with avidin horseradish peroxidase (1:1000 dilution, Thermo Fisher Scientific #18–4100-94) for 30 min, after which 3,3′,5,5′-tetramethylbenzidine (TMB, Life Technologies #SB02) was added. After a 10 min-incubation

in the dark, reaction was stopped using 50 µL/well of H2SO4 1 M. Plates were read by an optical density reader (Multiskan FC, Thermo Fisher Scientific #51119000) set at 450 nm. Between each step until the chromogenic reaction, 3 to 5 rinses were performed with a wash solution of Tween-20 5% (Thermo Fisher Scientific #233360010) in DPBS.

Because of the lack of commercially available purified canine FAP protein to act as standard, the exact amount of soluble FAP in biological samples could not be calculated. Instead, we expressed results in endpoint titers (EPT). Using a plot of the optical density on the log base 2 of the dilutions, we defined the cutoff line at half the optical density of recombinant human FAP at 78.13 ng/mL concentration. The log2 of the endpoint titer was obtained from the point where the linear line crosses the cutoff line.

2.5 Statistical analysis

Statistical analyses were conducted using the R Commander interface (42) to the R statistical software. Normal distribution was assessed using Shapiro–Wilk normality test. For normally distributed data, parametric tests were used and results were expressed in mean and standard deviation. A Fisher test was used to verify homoscedasticity between groups. When variances were significantly different between groups, comparisons of means were performed using a Welsh two sample *t*-test. For non-normally distributed data, non-parametric tests were employed and results were expressed in median and interquartile range (P25-P75). For correlation analyses of non-normally distributed data, Spearman's rank correlation rho test was used. For the comparison of medians between two groups, a Mann–Whitney test was used. Significance was established at a *p*-value lower than 0.05.

3 Results

3.1 Histopathological analysis

After scoring fibrosis in CIPF sections, five were characterized as mild (scores ranging from to 4 to 7), nine as moderate (scores ranging from 8 to 11) and eight as severe fibrosis (scores ranging from 12 to 16). Control lung sections were attributed scores from 0 to 3 and were considered as non-fibrotic. Seven cases of lung neoplasia, including six primary pulmonary adenocarcinomas and one metastasis of mammary carcinoma, served as positive controls for IHC.

3.2 Tissular FAP expression

FAP was expressed in cells interpreted as fibroblasts in the lungs of 20 out of 22 WHWTs affected with CIPF. Using a visual semi-quantitative scoring system, an index of high, intermediate, low and zero FAP expression were attributed in, respectively, 4, 4, 12, and 2 WHWTs. Healthy lung biopsies from WHWTs and other breeds all had an index of zero FAP expression. In primary pulmonary adenocarcinomas and in the metastasis of mammary carcinoma, cancer-associated fibroblasts were strongly FAP-positive. Cancer cells were also FAP-positive in four out of six cases of primary adenocarcinoma. Figure 1 illustrates examples of FAP staining in lung sections. Within CIPF cases, there was a statistically significant but poorly relevant positive correlation ($p < 0.05$; $R^2 = 0.22$) between the FAP expression index and the score of fibrosis severity. However, the index of FAP expression was highly positively correlated to the score of active fibrosis ($p < 0.001$; $R^2 = 0.68$), as illustrated in Figure 2.

Using quantitative digital analysis, we analyzed 20 areas originating from 11 different cases which were previously attributed with various indices of FAP expression and of fibrosis activity. QuPath automated detection of collagen content in lesional areas accurately reflected the mature collagen fibers visualized by polarized light microscopy (Supplementary Figure 1). The mean collagen content was significantly higher in representative areas of mature fibrosis (32.95 ± 15.28%) than in representative areas of active fibrosis (11.20 ± 7.34%; $p < 0.001$; Figure 3A). This validated our visual, semiquantitative assessment of the maturity of fibrosis. The mean percentage of FAP-positive cells was significantly higher ($p < 0.001$) in representative areas of active (27.73 ± 8.57%) compared with mature fibrosis (9.64 ± 4.02%; Figure 3B). Visual superimposition of serial Picro Sirius red and FAP-stained sections (Figure 4) revealed that FAP-positive cells were rare within highly collagenic mature fibrosis areas (Figures 4A–D). However, FAP-positive cells were clustered in areas of active fibrosis within alveolar septa (Figures 4E–H) or dispersed at the periphery of mature fibrotic lesions, where collagen content is lower (Figures 4I–L).

3.3 Plasmatic FAP quantification

The plasmatic levels of soluble FAP, as illustrated in Figure 5, were significantly lower ($p < 0.01$) in WHWTs with CIPF (EPT 0.74 [0.24–2.38]) than in healthy dogs (EPT 16.50 [4.78–63.84]).

4 Discussion

In this study, we established a semiquantitative scoring system destined to evaluate the severity and activity of fibrosis on histopathological sections of CIPF, which in this study exhibited mild to severe fibrosis. As expected, the FAP IHC study revealed that healthy lung sections were FAP-negative, and that cancer-associated fibroblasts from lung tumors were strongly positive. In the majority of CIPF samples, FAP was expressed by cells consistent with fibroblasts at various indices and only 2 samples were negative. FAP expression correlated weakly with fibrosis severity but highly with fibrosis activity. Indeed, automated image analysis detected a higher percentage of FAP-positive cells in areas of active fibrosis. It is also noticeable on superimposition of images that FAP-positive cells are located at the periphery of mature fibrosis lesions and clustered in areas of active fibrosis. Another finding of this study is that plasmatic FAP was significantly lower in WHWTs affected with CIPF compared with healthy dogs.

We established a system of scoring of the histological severity and activity of fibrosis in CIPF. This scoring system aimed to objectively distinguish lung biopsies of old healthy dogs from mild CIPF as well as mild from moderate and severe cases of CIPF. While attributing scores, a particular consideration was given to the distinction between active (immature) and inactive (mature) fibrosis

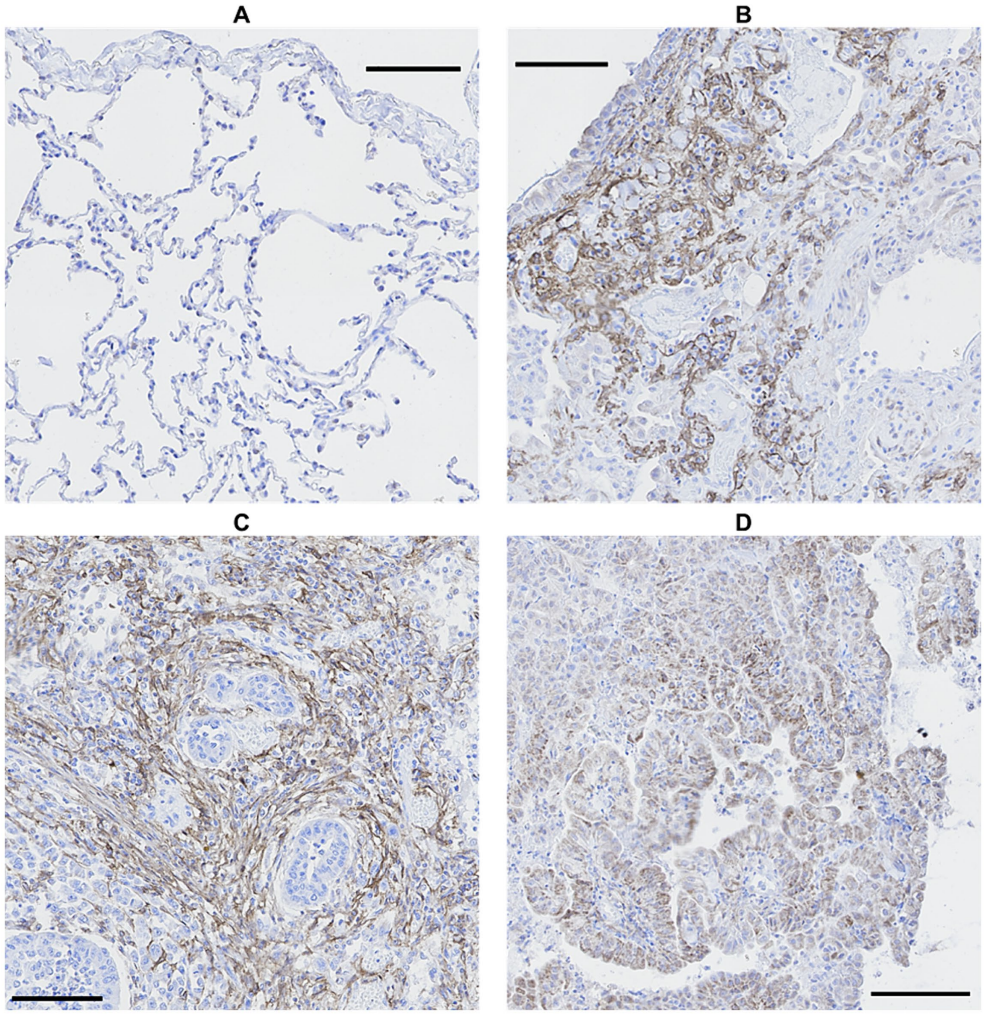

FIGURE 1
Comparison of FAP immunostaining in canine lung biopsies. No FAP expression in healthy lung **(A)** and high FAP expression in CIPF **(B)** and primary pulmonary adenocarcinoma, either in cancer-associated fibroblasts **(C)** or in cancer cells **(D)**. Immunoperoxidase-diaminobenzidine, hematoxylin counterstain (bar: 100 μm). FAP, fibroblast activation protein; CIPF, canine idiopathic pulmonary fibrosis.

for the purpose of subsequently establishing correlation with FAP IHC analyses. The Ashcroft scoring system (43) used for IPF cannot be applied to CIPF as human and canine IPF do not have the same histological pattern. Indeed, in humans, IPF is characterized by usual interstitial pneumonia (UIP) (39, 44). UIP diagnosis is based on patchy dense fibrosis accompanied by architectural distortion (with destructive scarring and/or honeycombing) with a predilection for subpleural and paraseptal parenchyma, and the presence of fibroblast foci (39, 44). CIPF shares features with UIP but also with non-specific interstitial pneumonia, which is characterized by diffuse interstitial fibrosis (37, 38). Indeed, in WHWTs affected with CIPF, histology reveals a mild to moderate diffuse mature interstitial fibrosis with multifocal subpleural or peribronchial areas of accentuation. Besides, no fibroblast foci are described (37, 38). The absence of fibroblast foci, as well as the high heterogeneity of fibrosis within a lung biopsy from a CIPF case, also prevented the application of scoring systems used for IHC studies of human IPF sections. This underlines the need for a specific scoring system adapted to dogs, as presented here.

This study confirmed the presence of FAP in lung biopsies from WHWTs affected with CIPF, and its absence in normal lungs, as anticipated from studies of human IPF (8, 9). Based on the assessment of their morphology and localization, FAP-positive cells appeared as fibroblasts. Nonetheless, the simultaneous expression of other fibroblast markers would be needed to confirm with certainty the precise identity of FAP-positive cells, although previous studies in human IPF reported a FAP expression restricted to activated fibroblasts (8, 9). The majority of cases were assigned a low FAP expression index according to the semiquantitative scoring system. This outcome, which might initially appear disappointing, is actually due to the fact that the scoring system assesses the overall expression across the entire section since CIPF exhibits a more diffuse interstitial fibrosis pattern than UIP (38). As a whole section of CIPF biopsy can be highly heterogeneous, with varying ratios of mature and active fibrosis, this heterogeneity significantly influences the proportion of the section occupied by FAP-positive areas.

In cases of CIPF, the FAP expression index exhibited a mild correlation with the severity score of fibrosis, aligning with findings

from previous studies that have explored the association between FAP expression and fibrosis severity at both histological and clinical level in humans (8, 9). Nevertheless, a good correlation emerged when focused on the activity of fibrosis in lung biopsies. In UIP, the histologic pattern of human IPF, FAP expression is restricted to areas of ongoing tissue injury (8). FAP is indeed strongly expressed in fibroblast foci, which are interstitial clusters of proliferating fibroblasts and myofibroblasts near the injured alveolar epithelium (8). Despite the absence of fibroblast foci in CIPF, it is consistent that FAP is mostly expressed in highly fibroblastic active areas, and not in poorly cellular regions that are consolidated by dense amounts of collagen fibers. The identified positive correlation between FAP expression and fibrosis activity underscores FAP's potential as a promising marker for fibroplasia, providing substantial support for the hypothesis that FAP plays a crucial role in the pathophysiology of the disease.

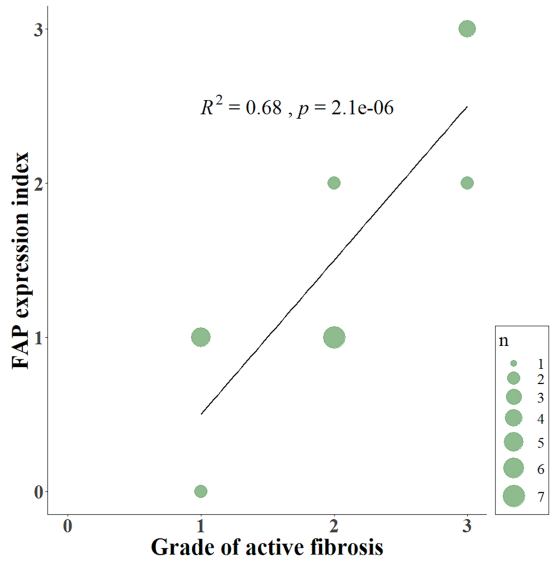

FIGURE 2
Scatterplot displaying the relationship between the FAP expression index and the grade of active fibrosis. The index of FAP expression (from 0 to 3) is positively correlated ($p < 0.001$; $R^2 = 0.68$) to the score of active fibrosis (from 0 to 3) in lung sections of CIPF. FAP, fibroblast activation protein; CIPF, canine idiopathic pulmonary fibrosis; n, number of cases.

Automated quantitative image analysis technologies were used to confirm these results with a more sensitive and objective method. Digital image analysis using artificial intelligence solutions is emerging in the field of histopathology and IHC, providing promising techniques for scoring quantification of tissue fibrosis in human IPF or to quantify FAP positivity in IHC images (9, 43). Such quantifying tools allowed us to validate our semiquantitative scoring system of fibrosis used to select areas by their representativity of a type of maturity of fibrosis (active or mature) with a precise quantification of the collagen content of the area, which is an established marker of mature fibrosis (43). Then, it was confirmed that the proportion of FAP-positive cells was significantly higher in areas occupied by active fibrosis than in those occupied by mature fibrosis. Digital superimposition of FAP-positive cell detections onto Picro Sirius red stained sections allowed us to witness the spatial distribution of FAP-positive cells in relation to the lesions of fibrosis within the sections. FAP-positive cells, consistent with activated fibroblasts, are sparse within mature lesions and are mainly scattered in alveolar septa that are not yet burdened by large layers of collagen fibers. FAP-positive active fibrosis areas seem to be located in the periphery of mature lesions. In this view, FAP-positive cells appear to play a driving role in fibrosis.

The small cohort of primary pulmonary adenocarcinomas used in this study showed a strong expression of FAP by cancer-associated fibroblasts, and occasionally by cancer cells themselves, aligning with expectations based on both veterinary and human literature (17, 26,

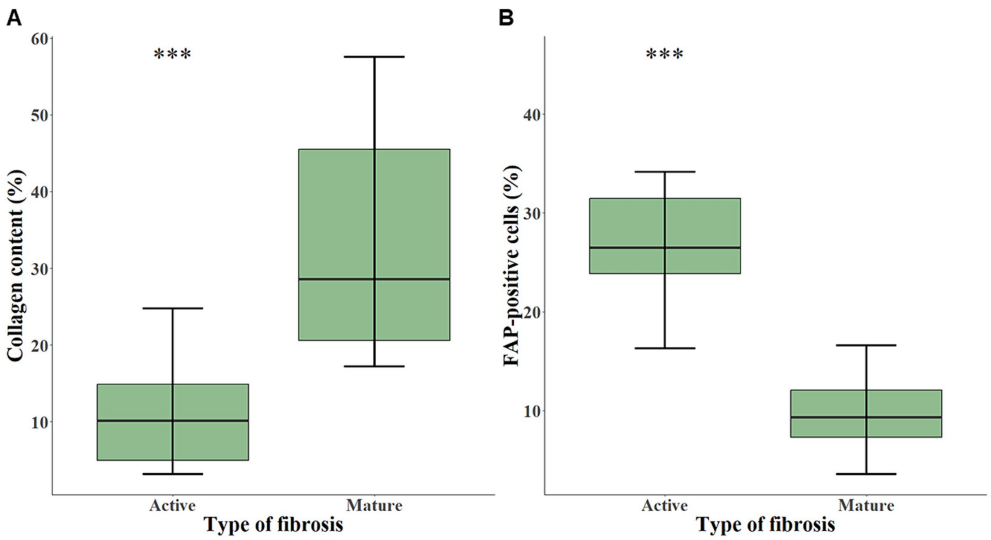

FIGURE 3
Box-and-whisker plots of collagen content **(A)** and of FAP-positive cells **(B)** in areas representing either active ($n = 10$) or mature fibrosis ($n = 10$), calculated with quantitative digital analysis in CIPF lung sections. The box represents the median and interquartile range. The whiskers represent the values within 1.5 times the interquartile range. Significance level: *** indicates a p-value below 0.001. FAP, fibroblast activation protein.

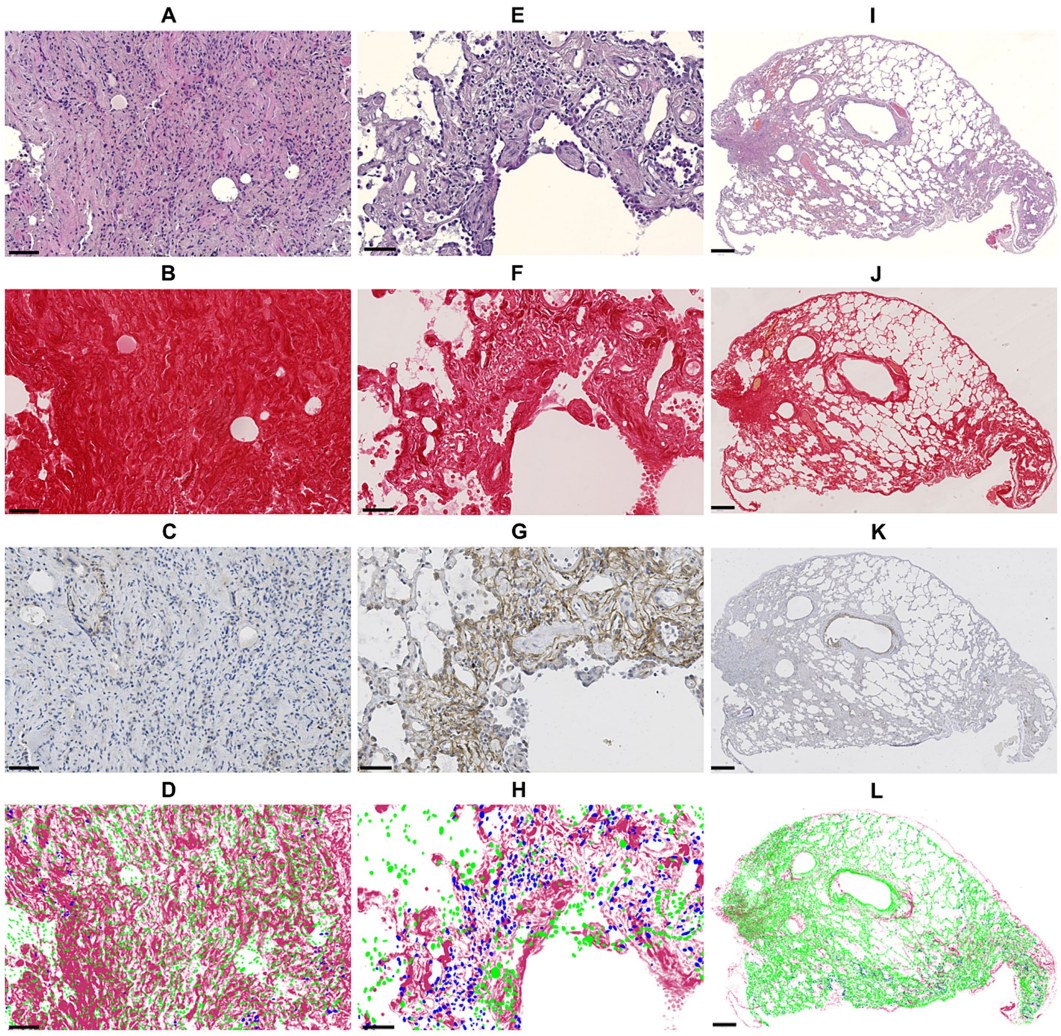

FIGURE 4
Panel showing sequential sections in HE staining (1st row), Picro Sirus red staining (2nd row), anti-FAP immunohistochemistry staining (3rd row) and the superimposition of cell detections (blue: FAP-positive, green: FAP-negative) based on anti-FAP immunohistochemistry onto Picro Sirus red-stained collagen (4th row). Images **(A–D)** show an area of strongly collagenic mature fibrosis with rare FAP-positive cells (bar: 50 µm). Images **(E–H)** illustrate an area of active fibrosis with low collagen content and numerous FAP-positive cells (bar: 50 µm). Images **(I–L)** show an entire section with mixed fibrosis pattern: few FAP-positive cells within highly collagenic mature fibrosis areas, from which less collagenic, FAP-rich areas extend (bar: 500 µm). FAP, fibroblast activation protein.

27). This provides a foundation for potential extended investigations about the prognostic significance of FAP in lung cancer. Indeed canine lung cancers of advanced stage still carry a poor prognosis and could benefit from novel therapeutic strategies (45, 46).

This analysis revealed lower plasmatic FAP levels in WHWTs affected with CIPF compared with healthy dogs. To date, the variation of plasmatic FAP in humans affected with IPF is not known. However, it has been studied in various other conditions, notably in patients with cancer (18, 20, 24), inflammatory bowel disease (47) or acute heart failure (48), who also exhibited a lower plasmatic FAP concentration compared with healthy volunteers, despite an overexpression of FAP in diseased tissues. The reason for such decrease, as well as the source of the soluble form of FAP, are still unknown, including whether it results from shedding from the cellular membrane or from alternative splicing (7, 49, 50). Current hypotheses suggest that multiple organs may contribute to a low basal level of circulating FAP, which would decrease due to a systemic reaction to the disease (20, 48, 51). Interestingly, other studies showed an increase of circulating FAP in patients with liver fibrosis and support the hypothesis that the liver constitutes a major source of elevated circulating FAP (7, 52, 53). Further studies on a greater number of cases are thus required to explain why circulating FAP is decreased in CIPF.

This study of plasmatic FAP concentrations is based on a small number of dogs which could expose us to sampling biases. Furthermore, due to the nature of the selection criteria for blood donation (dogs of less than 10 years old and more than 20 kg), the control group is not matched for age and breed with the study population. Nonetheless, a strong association between age and circulating FAP levels has never been established in existing literature (32). However, it appears that various conditions can influence the level of plasmatic FAP, such as malignant, inflammatory, metabolic, cardiac, or other organs fibrotic conditions (24, 47, 48, 52, 53). Although plasmatic FAP appears significantly decreased in dogs with CIPF, we do not believe that it would constitute a useful biomarker of CIPF since it does not seem specific to the disease.

As perspectives, the sensitivity of FAP to identify active fibrosis specifically localized within the lungs in cases of CIPF can be harnessed

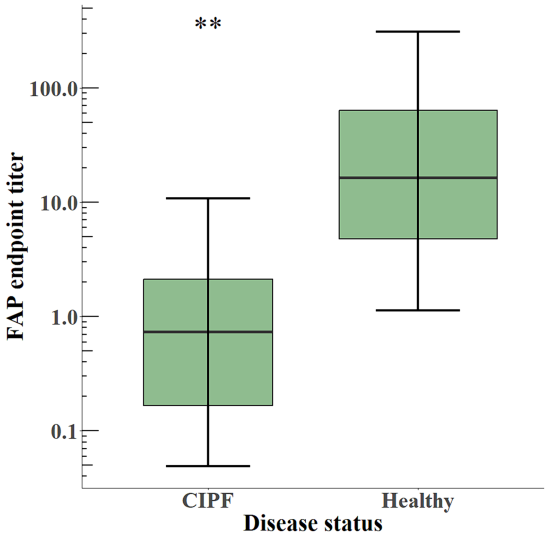

FIGURE 5
Box-and-whisker plot of plasma levels of soluble FAP in dogs with CIPF ($n = 6$) and in healthy dogs ($n = 9$). The box represents the median and interquartile range, and the whiskers represent the values within 1.5 times the interquartile range. Significance level: ** indicates a p-value below 0.01. FAP, fibroblast activation protein; CIPF, canine idiopathic pulmonary fibrosis.

by FAP-targeted PET examinations. FAPI-based PET/CT are emerging in preclinical and clinical studies on interstitial lung disease (such as IPF) or cancer and are presented as non-invasive tools to monitor disease progression or response to treatment (31, 54). This promising technique would allow to assess FAP expression in dogs *in vivo* and thus enable an early detection of CIPF and evaluation of progression or response to treatment. In this field, FAP-targeted therapies (such as anti-FAP CAR-T cells or FAPI-based theragnostic) emerge as promising prospects, given the current lack of available treatments for CIPF. Considering that CIPF is regarded as a spontaneous preclinical model of IPF, human patients could also gain advantages from these findings.

In conclusion, this study shows new insights into the pathology of CIPF by describing the cellular expression of FAP in progressing active immature lesions of fibrosis. These findings position tissular FAP – but not plasmatic FAP – as a promising marker of activity of the disease, which could be exploited by multiple diagnostic and therapeutic applications.

Data availability statement

The raw data supporting the conclusions of this article will be made available by the authors, without undue reservation.

Ethics statement

The animal studies were approved by the Animal Ethics Committee of the University of Liège. The studies were conducted in accordance with the local legislation and institutional requirements. Written informed consent was obtained from the owners for the participation of their animals in this study.

Author contributions

ERi: Conceptualization, Data curation, Formal analysis, Investigation, Methodology, Validation, Visualization, Writing – original draft, Writing – review & editing, Resources. CM: Resources, Writing – review & editing, Formal analysis, Methodology, Software, Visualization. AF: Resources, Writing – review & editing. ERo: Resources, Writing – review & editing. PJ: Formal analysis, Investigation, Methodology, Writing – review & editing. EP: Conceptualization, Investigation, Methodology, Resources, Supervision, Writing – review & editing. M-MG: Conceptualization, Formal analysis, Investigation, Methodology, Resources, Supervision, Validation, Writing – review & editing. TM: Conceptualization, Methodology, Resources, Supervision, Writing – review & editing. CC: Conceptualization, Funding acquisition, Project administration, Resources, Supervision, Writing – review & editing, Validation.

Funding

The author(s) declare that financial support was received for the research, authorship, and/or publication of this article. ERi is a Research Fellow of the Fonds de la Recherche Scientifique - FNRS and this work was supported by the Special Research Funds of the University of Liège.

Acknowledgments

Preliminary results were partly presented as an abstract at the 32nd congress of the European College of Veterinary Internal Medicine – Companion Animals (ECVIM-CA), Göteborg, Sweden, 1-3 September 2022. We gratefully thank Yue Li, Pranidhi Baddam, and Leslie Hopper for their help with the IHC staining and the management of the slides.

Conflict of interest

The authors declare that the research was conducted in the absence of any commercial or financial relationships that could be construed as a potential conflict of interest.

The author(s) declared that they were an editorial board member of Frontiers, at the time of submission. This had no impact on the peer review process and the final decision.

Publisher's note

Supplementary material

The Supplementary material for this article can be found online at: https://www.frontiersin.org/articles/10.3389/fvets.2024.1416124/full#supplementary-material

References

1. Clercx C, Fastrès A, Roels E. Idiopathic pulmonary fibrosis in West Highland white terriers: an update. *Vet J*. (2018) 242:53–8. doi: 10.1016/j.tvjl.2018.10.007

2. Laurila HP, Rajamäki MM. Update on canine idiopathic pulmonary fibrosis in West Highland white terriers. *Vet Clin North Am Small Anim Pract*. (2020) 50:431–46. doi: 10.1016/j.cvsm.2019.11.004

3. Christiansen VJ, Jackson KW, Lee KN, McKee PA. Effect of fibroblast activation protein and α2-antiplasmin cleaving enzyme on collagen types I, III, and IV. *Arch Biochem Biophys*. (2007) 457:177–86. doi: 10.1016/j.abb.2006.11.006

4. Lee KN, Jackson KW, Christiansen VJ, Chung KH, McKee PA. A novel plasma proteinase potentiates α2-antiplasmin inhibition of fibrin digestion. *Blood*. (2004) 103:3783–8. doi: 10.1182/blood-2003-12-4240

5. Fitzgerald AA, Weiner LM. The role of fibroblast activation protein in health and malignancy. *Cancer Metastasis Rev*. (2020) 39:783–803. doi: 10.1007/s10555-020-09909-3

6. Roberts EW, Deonarine A, Jones JO, Denton AE, Feig C, Lyons SK, et al. Depletion of stromal cells expressing fibroblast activation protein-α from skeletal muscle and bone marrow results in cachexia and anemia. *J Exp Med*. (2013) 210:1137–51. doi: 10.1084/jem.20122344

7. Keane FM, Yao TW, Seelk S, Gall MG, Chowdhury S, Poplawski SE, et al. Quantitation of fibroblast activation protein (FAP)-specific protease activity in mouse, baboon and human fluids and organs. *FEBS Open Biol*. (2014) 4:43–54. doi: 10.1016/j.fob.2013.12.001

8. Acharya PS, Zukas A, Chandan V, Katzenstein ALA, Puré E. Fibroblast activation protein: a serine protease expressed at the remodeling interface in idiopathic pulmonary fibrosis. *Hum Pathol*. (2006) 37:352–60. doi: 10.1016/j.humpath.2005.11.020

9. Yang P, Luo Q, Wang X, Fang Q, Fu Z, Li J, et al. Comprehensive analysis of fibroblast activation protein expression in interstitial lung diseases. *Am J Respir Crit Care Med*. (2023) 207:160–72. doi: 10.1164/rccm.202110-2414OC

10. Levy M, McCaughan G, Marinos G, Gorrell M. Intrahepatic expression of the hepatic stellate cell marker fibroblast activation protein correlates with the degree of fibrosis in hepatitis C virus infection. *Liver*. (2002) 22:93–101. doi: 10.1034/j.1600-0676.2002.01503.x

11. Dienus K, Bayat A, Gilmore BF, Seifert O. Increased expression of fibroblast activation protein-alpha in keloid fibroblasts: implications for development of a novel treatment option. *Arch Dermatol Res*. (2010) 302:725–31. doi: 10.1007/s00403-010-1084-x

12. Rovedatti L, Di Sabatino A, Knowles CH, Sengupta N, Biancheri P, Corazza GR, et al. Fibroblast activation protein expression in Crohn's disease strictures. *Inflamm Bowel Dis*. (2011) 17:1251–3. doi: 10.1002/ibd.21446

13. Milner JM, Kevorkian L, Young DA, Jones D, Wait R, Donell ST, et al. Fibroblast activation protein alpha is expressed by chondrocytes following a pro-inflammatory stimulus and is elevated in osteoarthritis. *Arthritis Res Ther*. (2006) 8:R23. doi: 10.1186/ar1877

14. Tillmanns J, Hoffmann D, Habbaba Y, Schmitto JD, Sedding D, Fraccarollo D, et al. Fibroblast activation protein alpha expression identifies activated fibroblasts after myocardial infarction. *J Mol Cell Cardiol*. (2015) 87:194–203. doi: 10.1016/j.yjmcc.2015.08.016

15. Liao Y, Ni Y, He R, Liu W, Du J. Clinical implications of fibroblast activation protein-α in non-small cell lung cancer after curative resection: a new predictor for prognosis. *J Cancer Res Clin Oncol*. (2013) 139:1523–8. doi: 10.1007/s00432-013-1471-8

16. Kilvaer TK, Khanehkenari MR, Hellevik T, Al-Saad S, Paulsen EE, Bremnes RM, et al. Cancer associated fibroblasts in stage I-IIIA NSCLC: prognostic impact and their correlations with tumor molecular markers. *PLoS One*. (2015) 10:e0134965. doi: 10.1371/journal.pone.0134965

17. Shi J, Hou Z, Yan J, Qiu W, Liang L, Meng M, et al. The prognostic significance of fibroblast activation protein-α in human lung adenocarcinoma. *Ann Transl Med*. (2020) 8:224. doi: 10.21037/atm.2020.01.82

18. Solano-Iturri JD, Beitia M, Errarte P, Calvete-Candenas J, Etxezarraga MC, Loizate A, et al. Altered expression of fibroblast activation protein-α (FAP) in colorectal adenoma-carcinoma sequence and in lymph node and liver metastases. *Aging*. (2020) 12:10337–58. doi: 10.18632/aging.103261

19. Iwasa S, Jin X, Okada K, Mitsumata M, Ooi A. Increased expression of seprase, a membrane-type serine protease, is associated with lymph node metastasis in human colorectal cancer. *Cancer Lett*. (2003) 199:91–8. doi: 10.1016/S0304-3835(03)00315-X

20. Liao Y, Xing S, Xu B, Liu W, Zhang G. Evaluation of the circulating level of fibroblast activation protein α for diagnosis of esophageal squamous cell carcinoma. *Oncotarget*. (2017) 8:30050–62. doi: 10.18632/oncotarget.16274

21. Ariga N, Sato E, Ohuchi N, Nagura H, Ohtani H. Stromal expression of fibroblast activation protein/seprase, a cell membrane serine proteinase and gelatinase, is associated with longer survival in patients with invasive ductal carcinoma of breast. *Int J Cancer*. (2001) 95:67–72. doi: 10.1002/1097-0215(20010120)95:1<67::AID-IJC1012>3.0.CO;2-U

22. Hua X, Yu L, Huang X, Liao Z, Xian Q. Expression and role of fibroblast activation protein-alpha in microinvasive breast carcinoma. *Diagn Pathol*. (2011) 6:111. doi: 10.1186/1746-1596-6-111

23. Jia J, Martin TA, Ye L, Jiang WG. FAP-α (fibroblast activation protein-α) is involved in the control of human breast cancer cell line growth and motility via the FAK pathway. *BMC Cell Biol*. (2014) 15:16. doi: 10.1186/1471-2121-15-16

24. Solano-Iturri JD, Errarte P, Etxezarraga MC, Echevarria E, Angulo J, López JI, et al. Altered tissue and plasma levels of fibroblast activation protein-α (FAP) in renal tumours. *Cancers*. (2020) 12:3393. doi: 10.3390/cancers12113393

25. Arnold JN, Magiera L, Kraman M, Fearon DT. Tumoral immune suppression by macrophages expressing fibroblast activation protein-alpha and heme oxygenase-1. *Cancer Immunol Res*. (2014) 2:121–6. doi: 10.1158/2326-6066.CIR-13-0150

26. Giuliano A, dos Santos HR, Constantino-Casas F, Hoather T, Dobson J. Expression of fibroblast activating protein and correlation with histological grade, mitotic index and Ki67 expression in canine mast cell tumours. *J Comp Pathol*. (2017) 156:14–20. doi: 10.1016/j.jcpa.2016.10.004

27. Ettlin J, Clementi E, Amini P, Malbon A, Markkanen E. Analysis of gene expression signatures in cancer-associated stroma from canine mammary tumours reveals molecular homology to human breast carcinomas. *Int J Mol Sci*. (2017) 18:1101. doi: 10.3390/ijms18051101

28. Li L, Gao J, Chen BX, Liu X, Shi L, Wang Y, et al. Fibroblast activation protein imaging in atrial fibrillation: a proof-of-concept study. *J Nucl Cardiol*. (2023) 30:2712–20. doi: 10.1007/s12350-023-03352-x

29. Krafft E, Laurila HP, Peters IR, Bureau F, Peeters D, Day MJ, et al. Analysis of gene expression in canine idiopathic pulmonary fibrosis. *Vet J*. (2013) 198:479–86. doi: 10.1016/j.tvjl.2013.08.018

30. Nakamoto Y, Baba S, Kaida H, Manabe O, Uehara T. Recent topics in fibroblast activation protein inhibitor-PET/CT: clinical and pharmacological aspects. *Ann Nucl Med*. (2024) 38:10–9. doi: 10.1007/s12149-023-01873-6

31. Röhrich M, Leitz D, Glatting FM, Wefers AK, Weinheimer O, Flechsig P, et al. Fibroblast activation protein-specific PET/CT imaging in fibrotic interstitial lung diseases and lung cancer: a translational exploratory study. *J Nucl Med Off Publ Soc Nucl Med*. (2022) 63:127–33. doi: 10.2967/jnumed.121.261925

32. Lavis P, Pingitore J, Doumont G, Garabet A, Van Simaeys G, Lacroix S, et al. Usefulness of FAPα assessment in bronchoalveolar lavage as a marker of fibrogenesis: results of a preclinical study and first report in patients with idiopathic pulmonary fibrosis. *Respir Res*. (2023) 24:254. doi: 10.1186/s12931-023-02556-6

33. Mori Y, Kramer V, Novruzov E, Mamlins E, Röhrich M, Fernández R, et al. Initial results with [18F]FAPI-74 PET/CT in idiopathic pulmonary fibrosis. *Eur J Nucl Med Mol Imaging*. (2023) 51:1605–11. doi: 10.1007/s00259-023-06564-y

34. Jung HJ, Nam EH, Park JY, Ghosh P, Kim IS. Identification of BR102910 as a selective fibroblast activation protein (FAP) inhibitor. *Bioorg Med Chem Lett*. (2021) 37:127846. doi: 10.1016/j.bmcl.2021.127846

35. Lee IK, Noguera-Ortega E, Xiao Z, Todd L, Scholler J, Song D, et al. Monitoring therapeutic response to anti-FAP CAR T cells using [18F]AlF-FAPI-74. *Clin Cancer Res Off J Am Assoc Cancer Res*. (2022) 28:5330–42. doi: 10.1158/1078-0432.CCR-22-1379

36. Fu K, Pang Y, Zhao L, Lin L, Wu H, Sun L, et al. FAP-targeted radionuclide therapy with [177Lu]Lu-FAPI-46 in metastatic nasopharyngeal carcinoma. *Eur J Nucl Med Mol Imaging*. (2022) 49:1767–9. doi: 10.1007/s00259-021-05634-3

37. Heikkilä HP, Lappalainen AK, Day MJ, Clercx C, Rajamäki MM. Clinical, bronchoscopic, histopathologic, diagnostic imaging, and arterial oxygenation findings in West Highland white terriers with idiopathic pulmonary fibrosis. *J Vet Intern Med*. (2011) 25:433–9. doi: 10.1111/j.1939-1676.2011.0694.x

38. Syrjä P, Heikkilä HP, Lilja-Maula L, Krafft E, Clercx C, Day MJ, et al. The histopathology of idiopathic pulmonary fibrosis in West Highland white terriers shares features of both non-specific interstitial pneumonia and usual interstitial pneumonia in man. *J Comp Pathol*. (2013) 149:303–13. doi: 10.1016/j.jcpa.2013.03.006

39. Raghu G, Remy-Jardin M, Richeldi L, Thomson CC, Inoue Y, Johkoh T, et al. Idiopathic pulmonary fibrosis (an update) and progressive pulmonary fibrosis in adults: an official ATS/ERS/JRS/ALAT clinical practice guideline. *Am J Respir Crit Care Med*. (2022) 205:e18–47. doi: 10.1164/rccm.202202-0399ST

40. Bankhead P, Loughrey MB, Fernández JA, Dombrowski Y, McArt DG, Dunne PD, et al. QuPath: open source software for digital pathology image analysis. *Sci Rep*. (2017) 7:16878. doi: 10.1038/s41598-017-17204-5

41. Vanneste D, Bai Q, Hasan S, Peng W, Pirottin D, Schyns J, et al. Maf B-restricted local monocyte proliferation precedes lung interstitial macrophage differentiation. *Nat Immunol*. (2023) 24:827–40. doi: 10.1038/s41590-023-01468-3

42. Fox J, Munoz Marquez M, Bouchet-Valat M. Rcmdr: R commander. (2023). Available at: https://socialsciences.mcmaster.ca/jfox/Misc/Rcmdr/

43. Testa LC, Jule Y, Lundh L, Bertotti K, Merideth MA, O'Brien KJ, et al. Automated digital quantification of pulmonary fibrosis in human histopathology specimens. *Front Med*. (2021) 8:607720. doi: 10.3389/fmed.2021.607720

44. Hochhegger B, Marchiori E, Zanon M, Rubin AS, Fragomeni R, Altmayer S, et al. Imaging in idiopathic pulmonary fibrosis: diagnosis and mimics. *Clinics*. (2019) 74:e225. doi: 10.6061/clinics/2019/e225

45. Lee BM, Clarke D, Watson M, Laver T. Retrospective evaluation of a modified human lung cancer stage classification in dogs with surgically excised primary pulmonary carcinomas. *Vet Comp Oncol*. (2020) 18:590–8. doi: 10.1111/vco.12582

46. McPhetridge JB, Scharf VF, Regier PJ, Toth D, Lorange M, Tremolada G, et al. Distribution of histopathologic types of primary pulmonary neoplasia in dogs and outcome of affected dogs: 340 cases (2010-2019). *J Am Vet Med Assoc*. (2021) 260:234–43. doi: 10.2460/javma.20.12.0698

47. Corsi F, Sorrentino L, Albasini S, Colombo F, Cigognini M, Massari A, et al. Circulating fibroblast activation protein as potential biomarker in patients with inflammatory bowel disease. *Front Med*. (2021) 8:725726. doi: 10.3389/fmed.2021.725726

48. Delgado-Arija M, Genovés P, Pérez-Carrillo L, González-Torrent I, Giménez-Escamilla I, Martínez-Dolz L, et al. Plasma fibroblast activation protein is decreased in acute heart failure despite cardiac tissue upregulation. *J Transl Med*. (2024) 22:124. doi: 10.1186/s12967-024-04900-w

49. Lee KN, Jackson KW, Christiansen VJ, Lee CS, Chun JG, McKee PA. Antiplasmin-cleaving enzyme is a soluble form of fibroblast activation protein. *Blood*. (2006) 107:1397–404. doi: 10.1182/blood-2005-08-3452

50. Tillmanns J, Widera C, Habbaba Y, Galuppo P, Kempf T, Wollert KC, et al. Circulating concentrations of fibroblast activation protein α in apparently healthy individuals and patients with acute coronary syndrome as assessed by sandwich ELISA. *Int J Cardiol*. (2013) 168:3926–31. doi: 10.1016/j.ijcard.2013.06.061

51. Javidroozi M, Zucker S, Chen WT. Plasma seprase and DPP4 levels as markers of disease and prognosis in cancer. *Dis Markers*. (2012) 32:309–20. doi: 10.1155/2012/706745

52. Uitte De Willige S, Keane FM, Bowen DG, Malfliet JJMC, Zhang HE, Maneck B, et al. Circulating fibroblast activation protein activity and antigen levels correlate strongly when measured in liver disease and coronary heart disease. *PLoS One*. (2017) 12:e0178987. doi: 10.1371/journal.pone.0178987

53. Williams KH, Viera de Ribeiro AJ, Prakoso E, Veillard AS, Shackel NA, Bu Y, et al. Lower serum fibroblast activation protein shows promise in the exclusion of clinically significant liver fibrosis due to non-alcoholic fatty liver disease in diabetes and obesity. *Diabetes Res Clin Pract*. (2015) 108:466–72. doi: 10.1016/j.diabres.2015.02.024

54. Rosenkrans ZT, Massey CF, Bernau K, Ferreira CA, Jeffery JJ, Schulte JJ, et al. Ga]Ga-FAPI-46 PET for non-invasive detection of pulmonary fibrosis disease activity. *Eur J Nucl Med Mol Imaging*. (2022) 49:3705–16. doi: 10.1007/s00259-022-05814-9

frontiers | Frontiers in Veterinary Science

TYPE Original Research
PUBLISHED 08 August 2024
DOI 10.3389/fvets.2024.1437648

OPEN ACCESS

EDITED BY
Scott J. Roberts,
Royal Veterinary College (RVC),
United Kingdom

REVIEWED BY
Valerie Johnson,
Michigan State University, United States
Luca Melotti,
University of Padua, Italy

*CORRESPONDENCE
Takahiro Teshima
✉ teshima63@nvlu.ac.jp

RECEIVED 24 May 2024
ACCEPTED 22 July 2024
PUBLISHED 08 August 2024

CITATION
Yasumura Y, Teshima T, Nagashima T, Michishita M, Taira Y, Suzuki R and Matsumoto H (2024) Effective enhancement of the immunomodulatory capacity of canine adipose-derived mesenchymal stromal cells on colitis by priming with colon tissue from mice with colitis. *Front. Vet. Sci.* 11:1437648. doi: 10.3389/fvets.2024.1437648

Effective enhancement of the immunomodulatory capacity of canine adipose-derived mesenchymal stromal cells on colitis by priming with colon tissue from mice with colitis

Yuyo Yasumura[1], Takahiro Teshima[1,2]*, Tomokazu Nagashima[3], Masaki Michishita[3], Yoshiaki Taira[1], Ryohei Suzuki[1] and Hirotaka Matsumoto[1]

[1]Laboratory of Veterinary Internal Medicine, School of Veterinary Medicine, Faculty of Veterinary Science, Nippon Veterinary and Life Science University, Musashino, Japan, [2]Research Center for Animal Life Science, Nippon Veterinary and Life Science University, Musashino, Japan, [3]Laboratory of Veterinary Pathology, School of Veterinary Medicine, Faculty of Veterinary Science, Nippon Veterinary and Life Science University, Musashino, Japan

Introduction: The therapeutic efficacy of mesenchymal stromal cells (MSCs) in inflammatory bowel disease is not completely known and is not consistent. Priming with inflammatory cytokines has been proposed to adapt MSCs to an inflammatory environment to have them ready to counteract it, but may have undesirable effects on MSCs, such as increased immunogenicity. In this study, we hypothesized that priming MSCs with inflamed intestinal tissue would more effectively enhance their therapeutic effect on intestinal inflammation.

Methods: The capacity of canine adipose-derived MSCs (cADSCs) primed with colon tissue homogenates from mice with experimentally induced colitis or a combination of tumor necrosis factor-α and interferon-γ to inhibit T-cell proliferation was analyzed, along with their own apoptosis, proliferation, cell surface marker expression, and transcriptome. In addition, colitis mice were treated with the primed cADSCs to assess colitis severity and immune cell profile.

Results: Priming with cytokines induced apoptosis, decreased cell proliferation, and major histocompatibility complex-II gene expression in cADSCs, but these adverse effects were mild or absent with colitis-tissue priming. cADSCs primed with colitis tissue reduced the severity of colitis via the induction of M2 macrophages and T-regulatory cells and suppression of T-helper (Th)1/Th17-cell responses, and their effects were comparable to those of cytokine-primed cells.

Discussion: Our results emphasize the importance of the activation of MSCs by the appropriate microenvironment to maximize their therapeutic effect.

KEYWORDS

mesenchymal stromal cell, priming, immunomodulatory, inflammatory bowel disease, chronic inflammatory enteropathy, dextran sulfate sodium-induced colitis, microenvironment, stem cell therapy

1 Introduction

Inflammatory bowel disease (IBD), including Crohn's disease and ulcerative colitis, is a naturally occurring gastrointestinal disorder in humans caused by multiple etiologies, such as genetic factors, environmental factors, and abnormalities in gut microbiota and immune response (1). Patients' quality of life is severely compromised by chronic gastrointestinal symptoms that repeatedly go into remission and recur, and by complications such as fistulas, abscesses, and colorectal cancer (2). Current treatments for human IBD include aminosalicylic acid, glucocorticoids, immunosuppressants, and tumor necrosis factor (TNF)-α inhibitors, but nearly 30% of patients do not respond to these treatments and 50% of patients become refractory over time (1, 2). Chronic inflammatory enteropathy (CIE) is a multifactorial gastrointestinal disorder that occurs spontaneously in dogs, and its symptoms, pathogenesis, and treatment are similar in many ways to those of human IBD (3). CIE is clinically classified by treatment responsiveness into food-responsive enteropathy, antimicrobial-responsive enteropathy, and immunosuppressant-responsive enteropathy (3). Dogs that do not respond to these treatments are classified as having non-responsive enteropathy and reportedly account for 5% to 27% of dogs with CIE (4). Against this background, the development of new therapeutic strategies for human IBD and canine CIE is desirable.

Since their discovery by Friedenstein in 1966, mesenchymal stromal cells (MSCs) have been intensively studied as a cell source for tissue regeneration because of their stemness, including self-renewal and multilineage differentiation potential (5). Recently, MSCs have attracted attention for their stromal properties, including immunomodulatory and angiogenic capacities mediated by secreted factors, and many studies on them have been conducted not only in human medicine but also in veterinary medicine as a cell source for treating inflammatory and immune-mediated diseases (5, 6). MSCs can be isolated from almost all tissues of the body, including bone marrow, adipose tissue, umbilical cord, dental pulp, muscle, and synovium. Adipose-derived mesenchymal stromal cells (ADSCs) are one of the most common cell sources in humans and dogs due to their relatively low invasiveness, high-yield isolation, and high proliferative potential (5, 6). In fact, therapeutic effects of ADSCs have been observed in dogs as well as in humans for cutaneous, musculoskeletal, ocular, hepatic, respiratory, and neurological diseases (6, 7).

MSCs are expected to be a novel treatment for IBD and CIE and, indeed, have been shown to effectively ameliorate gastrointestinal inflammation in a number of preclinical studies using experimental animal models (8). However, the success of these preclinical studies has not been replicated in clinical trials (9). This may be attributable to the heterogeneity of MSCs caused by differences in sources such as donors and tissues, autologous or allogeneic origin, manufacturing steps such as isolation, culture, and cryopreservation methods, and application steps such as administration methods and patient conditions (10, 11). In veterinary medicine, two studies have reported fairly promising therapeutic effects of canine ADSCs (cADSCs) on CIE, but both were open-label studies without control groups in a small number of dogs by the same research group (12, 13). Therefore, there is a need to conduct larger-scale clinical trials to verify the efficacy and safety of MSCs, as well as for efforts to stabilize the quality of MSC products.

Priming approaches have been proposed as a way to enhance the inconsistent therapeutic effects of MSCs (11, 14). Priming, also known as preconditioning or licensing, has been demonstrated in several studies to affect MSC function by modulating biological, biochemical, and biophysical factors to enhance therapeutic efficacy (14). Among these, priming MSCs with inflammatory cytokines or hypoxic conditions is the most studied approach to enhance their immunomodulatory capacity by mimicking the inflamed microenvironment in the body (15). However, priming with inflammatory cytokines such as TNF-α and interferon (IFN)-γ may have adverse effects on MSCs for therapeutic application, such as by increasing their immunogenicity (15). MSCs exist as pericytes or fibroblast-like cells in the stromal tissue of almost all organs and work to maintain tissue homeostasis (16). Once tissue inflammation or damage occurs, MSCs are activated in response to the microenvironment and contribute to tissue repair through immunomodulation and matrix remodeling (17, 18). Although the cues in the disease microenvironment that activate MSCs are still unclear, it is suggested that a variety of factors act in combination to enhance their repair capacity. However, to the best of our knowledge, no studies have examined whether canine MSCs enhance their therapeutic potential in response to the disease microenvironment.

Based on the above, the purpose of our study was to investigate whether priming canine MSCs with disease tissue including components of the disease microenvironment would enhance their therapeutic efficacy on the original disease. In the context of studies to improve the therapeutic efficacy of MSCs for CIE, canine MSCs primed with inflammatory intestinal tissue from dogs with enteritis should be administered to canine models of enteritis to determine if the therapeutic efficacy is enhanced, but such a canine model has not been established. Therefore, we decided to test our hypothesis using a mouse model of dextran sulfate sodium (DSS)-induced colitis, a preclinical model of IBD and CIE commonly used in MSC xenotransplantation studies (8). If this study demonstrates that priming with colitis tissue from colitis mice enhances the immunomodulatory and therapeutic efficacy of cADSCs on mice with DSS-induced colitis, it will provide the basis for further studies to evaluate the functional changes of canine MSCs primed with inflamed intestinal mucosal samples from dogs with CIE and their efficacy on CIE patients.

2 Results

2.1 Priming with colon tissue homogenate from mice with colitis enhances the capacity of cADSCs to inhibit lymphocyte proliferation in a concentration-dependent manner

We first determined the concentration of colon tissue homogenate derived from colitis mice suitable for priming

cADSCs. For this purpose, cADSCs were incubated with colon homogenates at graded concentrations for 24 h, followed by evaluation of primed cell morphology and cell viability. Colon priming at concentrations up to 0.1 mg/mL had no apparent effect on the morphology of the cADSCs, but at higher concentrations the cells were observed to "aggregate" (Figure 1A). The viability of primed cells, assessed by trypan blue exclusion, maintained above 98% at concentrations up to 0.5 mg/mL, but reduced mildly to about 94% at concentrations of 1.0 mg/mL (Supplementary Figure 1). After this experiment, primed cADSCs were co-cultured for 3 days with $CD4^+$ T-helper (Th) cells derived from the spleen of colitis mice stimulated with anti-CD3/CD28-coated beads, followed by flow cytometry measurement of Th cell proliferation (Figure 1B). Priming with colon homogenate at concentrations up to 0.5 mg/mL enhanced the capacity of cADSCs to inhibit Th-cell proliferation in a concentration-dependent manner (Figure 1C). However, priming with colon homogenate at 1.0 mg/mL as the total protein concentration did not further enhance the capacity of cADSCs to inhibit Th-cell proliferation (Figure 1D). Therefore, the concentration of 0.1 mg/mL in colon priming that best enhanced the capacity of cADSCs to inhibit lymphocyte proliferation without affecting their cell morphology and survival was used in subsequent *in vivo* experiments.

2.2 cADSCs primed with colon homogenate strongly inhibit proliferation of $CD4^+$ Th cells from mice with colitis, as do those primed with TNF-α+IFN-γ

To compare the effects of priming on the capacity of cADSCs to inhibit Th-cell proliferation, cADSCs were primed with colon homogenate as well as purified inflammatory cytokines (TNF-α+IFN-γ), serum or liver homogenate from colitis mice for 24 h, after which co-culture assays were performed with primed cells and Th cells derived from mice with colitis. Based on the finding that colon priming enhances the capacity of cADSCs to inhibit Th-cell proliferation in a concentration-dependent manner up to 0.5 mg/mL, in this experiment, cADSCs were primed with mouse-derived substances at two different concentrations. However, priming with 0.5 mg/mL serum resulted in most cells aggregating after 24 h, so they were excluded from the experiment. Th-cell proliferation was significantly inhibited after 72 h in co-cultures with naïve or any primed cADSCs compared with that in mono-culture (Figure 2A). Priming with liver homogenate as well as colon homogenate significantly enhanced the capacity of cADSCs to inhibit Th-cell proliferation in a concentration-dependent manner (Figure 2B). The capacity to inhibit Th-cell proliferation was strongest for cADSCs primed colon homogenate at high concentrations, followed by cADSCs primed with colon homogenate at low concentrations, liver homogenate at high concentrations, and TNF-α+IFN-γ.

2.3 Colon priming could avoid adverse effects on cADSCs

Priming may affect the survival, proliferation, and immunogenicity of MSCs, as well as their immunomodulatory capacity (14). Therefore, we next investigated the effect of priming with diseased tissue on the properties of cADSCs. To examine the effect of priming on survival, cADSCs were primed with TNF-α+IFN-γ, liver homogenate, and a low or high concentration of colon homogenate for 24 h, after which the frequency of Annexin-V and propidium iodide (PI)-positive apoptotic cell was measured by flow cytometry (Figure 3A). Priming with these conditions was chosen because TNF-α+IFN-γ application is a well-studied priming method, liver represents a non-primary lesion organ in colitis, and low and high concentrations of colon homogenate allow the study of concentration-dependent effects. Apoptosis of cADSCs was induced drastically by TNF-α+IFN-γ priming and mildly by liver priming, while colon priming did not induce apoptosis at levels exceeding that of naive cADSCs, even at a high concentration (Figure 3B).

As with apoptosis, cADSCs were primed for 24 h under each condition, followed by passaging of primed cADSCs and analysis of cell proliferation after 1–4 days. Differences in the proliferation of cADSCs primed with different conditions were observed day by day, and after 4 days, cADSCs primed with colon homogenate at a concentration of 0.1 mg/mL showed better cell proliferation than those under the other conditions (Figure 3C). In contrast, the proliferation of cADSCs primed with TNF-α+IFN-γ or liver homogenate was rather suppressed compared with that of naive cADSCs.

2.4 cADSCs primed with colon homogenate were showed enriched expression of genes associated with cell proliferation in addition to inflammation-related genes

To further characterize the biological response of cADSCs to priming with colon homogenate representing diseased tissue, gene expression profiling was performed using RNA sequencing (RNA-seq) and the results were compared to the transcriptomes of naive and TNF-α+IFN-γ-primed cADSCs. Primary analysis of sequencing reads obtained by RNA-seq detected the expression of 17,863 genes among naive cADSCs, and cADSCs primed with TNF-α+IFN-γ or colon homogenate (Supplementary Table 1). Principal component analysis (PCA) showed that priming markedly altered the gene expression of cADSCs, with variation among the different strains of cADSCs (Figure 4A). In particular, to identify the genes of cADSCs affected by priming in common between the two different conditions and the genes specifically affected by each type of priming, differentially expressed genes (DEGs) were detected from each dataset using DESeq2 and Venn diagram analysis was performed. TNF-α+IFN-γ priming and colon priming upregulated 957 and 628 genes, respectively, of which 264 genes were in common (Figures 4B, C, Supplementary Figures 2A, B,

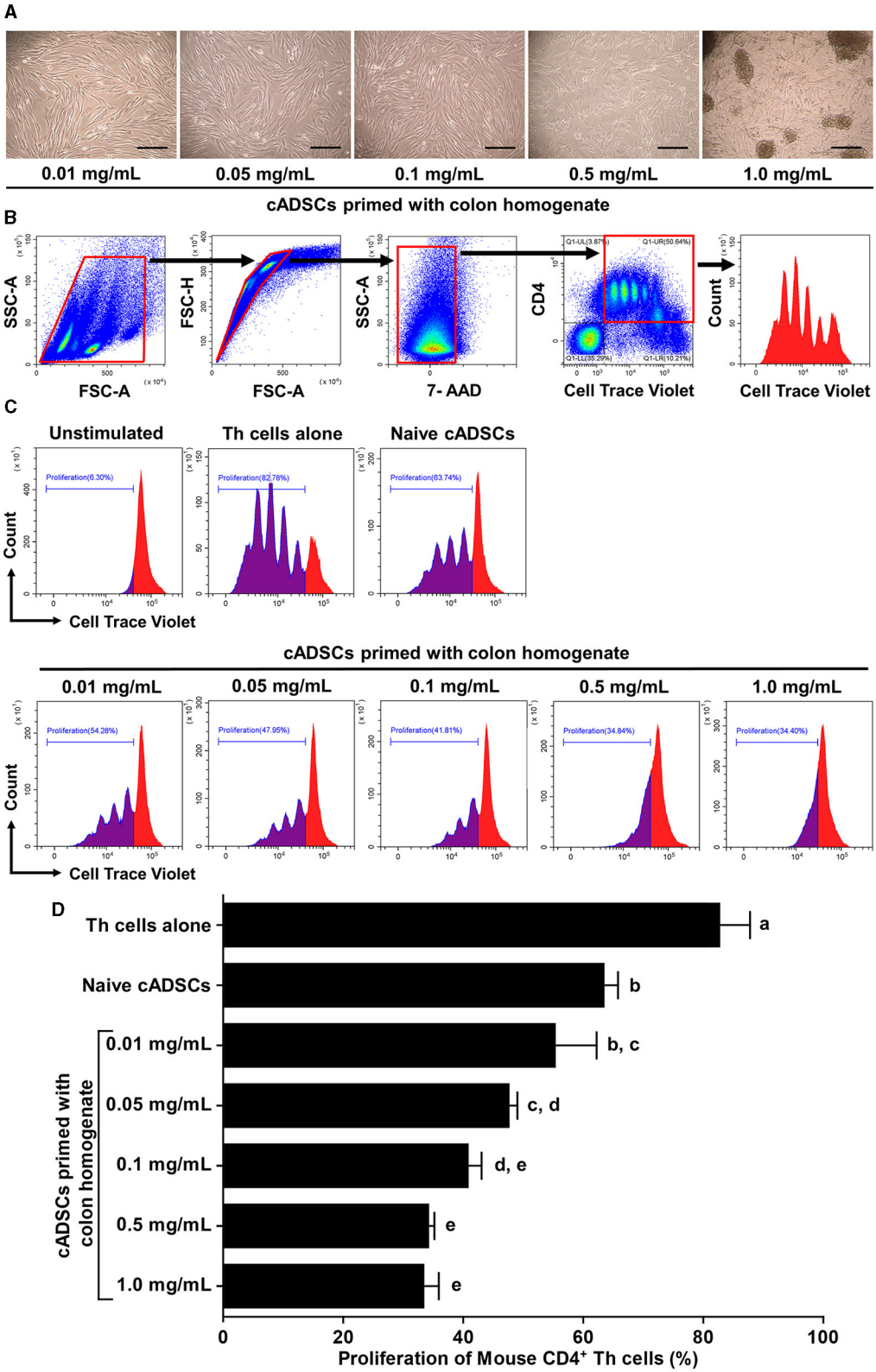

FIGURE 1
Effect of priming concentration of colon tissue homogenate from mice with colitis on the morphology of canine adipose-derived mesenchymal stromal cells (cADSCs) and their capacity to inhibit $CD4^+$ T-helper (Th)-cell proliferation. **(A)** Microscopic morphology of cADSCs primed with colitis colon at graded concentrations. Scale bar = 200 μm. **(B)** Gating method in flow cytometry for analyzing Th-cell proliferation. Panels from left to right show gating of lymphocyte fractions, removal of doublets, removal of dead cells, gating of $CD4^+$ cells, and histogram of cell trace violet-positive cells, with red boxes indicating gating regions. **(C)** Histogram of cell trace violet-positive cells showing $CD4^+$ Th-cell division in each condition. **(D)** Comparison of $CD4^+$ Th-cell proliferation in each condition. The proliferation of Th cells was quantified using the percentage of cell trace $violet^{low}$ cells. The same lower-case letter beside the bars indicates that there is no significant difference between the groups ($p > 0.05$). Data are expressed as the mean ± standard deviation from experiments performed in triplicate; $n = 5$.

10.3389/fvets.2024.1437648

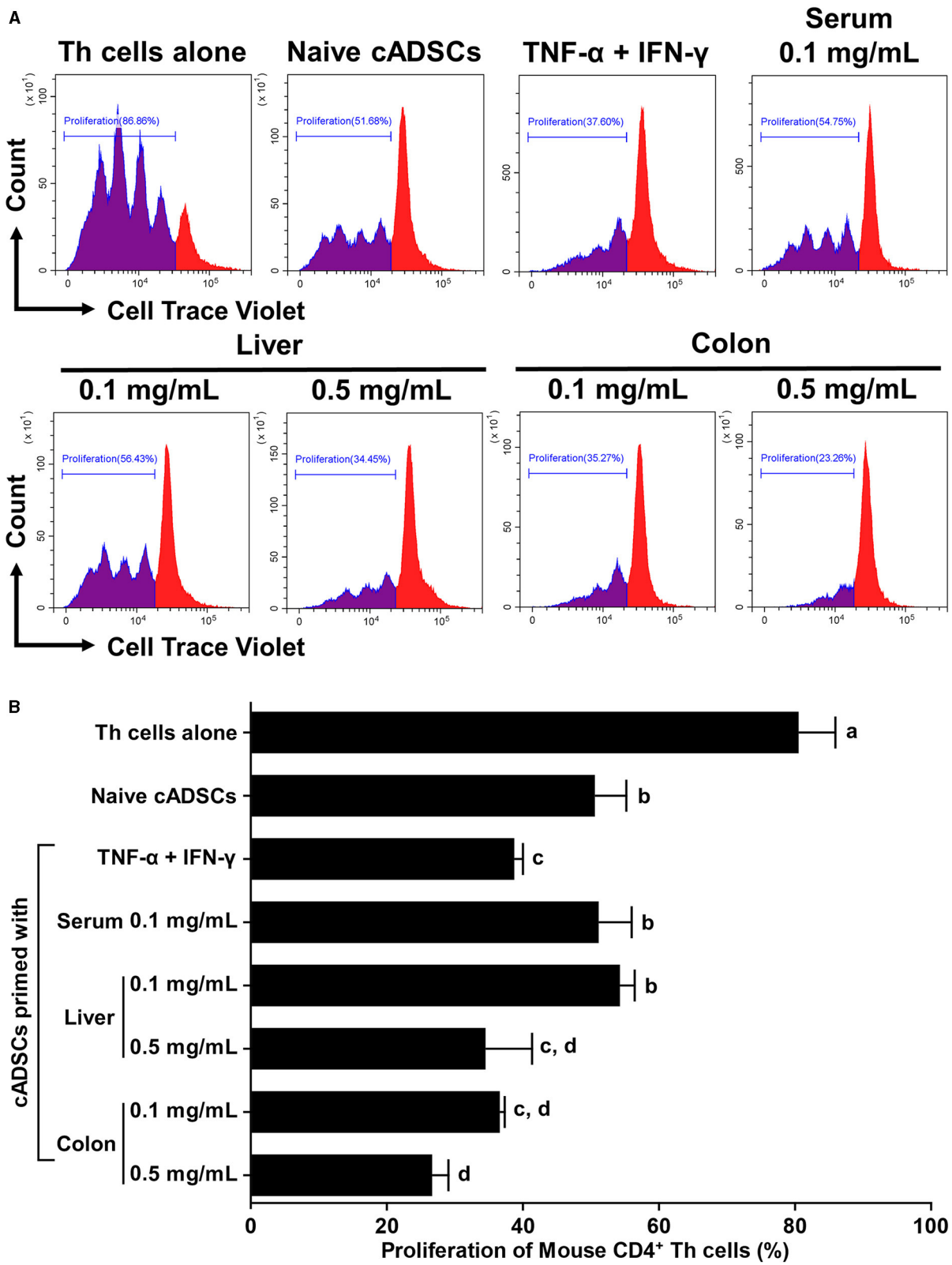

FIGURE 2
Effect of priming with different conditions on the capacity of cADSCs to inhibit Th-cell proliferation. **(A)** Histogram of cell trace violet-positive cells showing division of $CD4^+$ Th cells co-cultured with primed cADSCs with each condition. **(B)** Comparison of Th-cell proliferation in each condition. cADSCs primed with colon homogenate at a low concentration inhibited Th-cell proliferation to the same extent as cADSCs primed with liver homogenate at a high concentration or tumor necrosis factor (TNF)-α+interferon (IFN)-γ. The same lower-case letter beside bars indicates that there is no significant difference between the groups ($p > 0.05$). Data are expressed as the mean ± standard deviation from experiments performed in triplicate; $n = 5$.

10.3389/fvets.2024.1437648

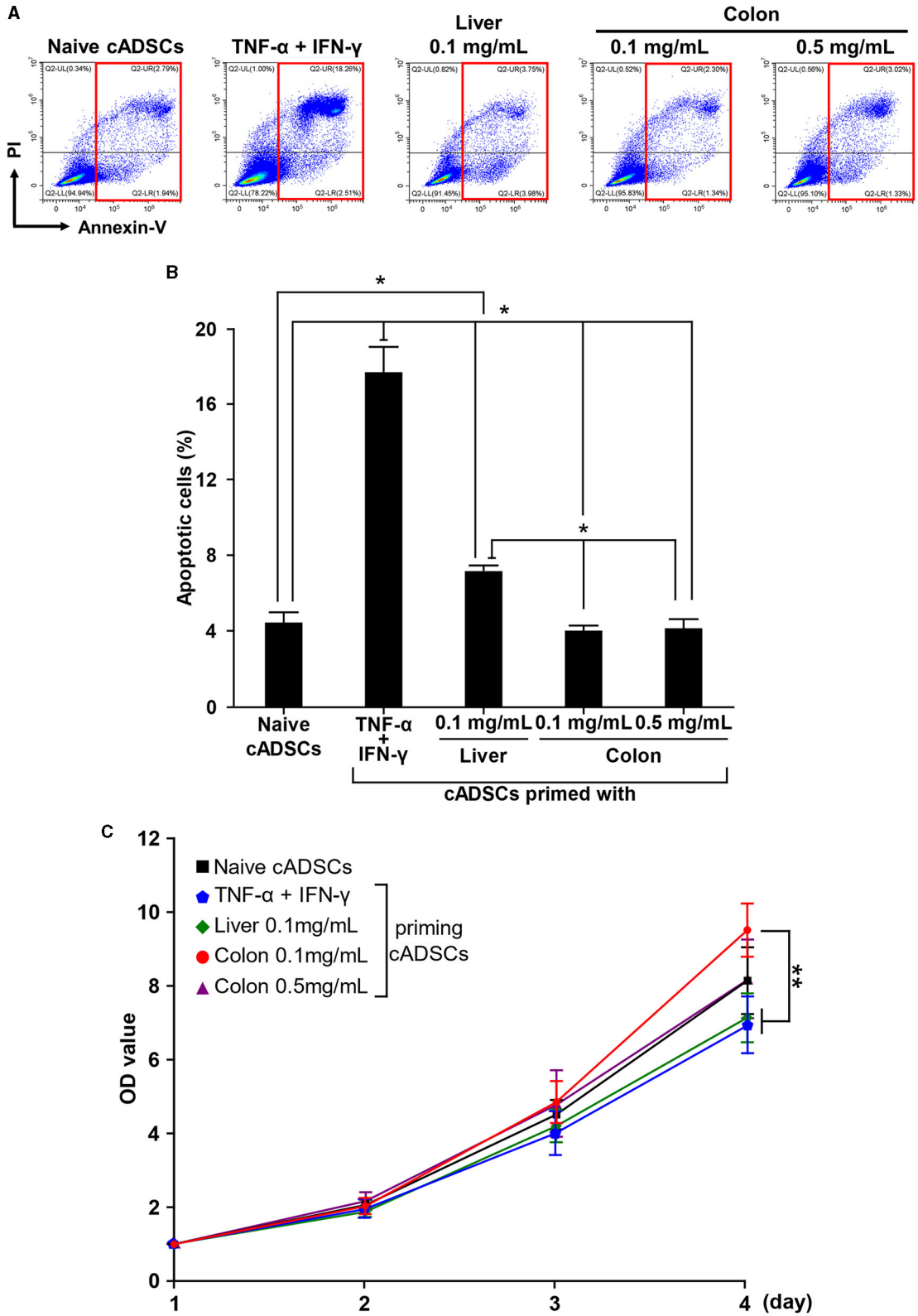

FIGURE 3
Different effects of various priming conditions on the properties of cADSCs. **(A)** Flow cytometric detection of apoptosis in primed cADSCs. The sum of the percentages of cells positive for Annexin V alone or in combination with propidium iodide (PI), indicated by red boxes, was measured as representative of apoptotic cells. **(B)** Comparison of the percentage of apoptotic cells in cADSCs primed with each condition. TNF-α+IFN-γ priming significantly induced apoptosis in cADSCs, but colon priming did not. **(C)** Proliferation of cADSCs after 1–4 days of priming measured spectrophotometrically. Optical density (OD) values after 2–4 days of priming were normalized by OD values after 1 day. Cell proliferation after 4 days of priming was best induced by priming with colitis colon at a low concentration. Data are expressed as the mean ± standard deviation from experiments performed in triplicate; $n = 5$; $^{*}p < 0.05$, $^{**}p < 0.01$.

Supplementary Table 2). At the same time, the downregulated genes numbered 371 and 489 for TNF-α+IFN-γ priming and colon priming, respectively, of which 186 genes were in common (Supplementary Figures 2A–D, Supplementary Table 3). Enrichment analysis based on the Molecular Signatures Database (MSigDB) hallmark gene set was performed to reveal the biological relevance of the gene sets that were specifically or commonly up- or downregulated by each priming condition. The top-ranked pathways associated with the 264 commonly upregulated genes were inflammation-related pathways such as TNF-α signaling via nuclear factor-kappa B (NFκB), inflammatory response, IFN-γ response, and complement, as well as apoptosis (Figures 4D, E, Supplementary Table 4). Similarly, the pathways associated with the 693 genes that were specifically upregulated by TNF-α+IFN-γ priming were inflammation-related pathways, including TNF-α signaling via NFκB, inflammatory response, IFN-γ response, and IFN-α response, but also allograft rejection pathways (Figure 4F). In contrast, pathways associated with the 364 genes specifically upregulated in colon priming were cell proliferation-related pathways such as the G2M checkpoint, mitotic spindle, and E2F targets, as well as hypoxia (Figure 4G). Enrichment analysis of the gene sets downregulated by the different priming conditions revealed that late estrogen response was associated with both types of priming; epithelial–mesenchymal transition was specifically associated with TNF-α+IFN-γ priming; and E2F targets, cholesterol homeostasis, and Notch signaling pathways were specifically associated with colon priming (Supplementary Figures 2E–H, Supplementary Tables 4, 5).

2.5 Colon priming improves the therapeutic effect of cADSCs on colitis to the same extent as TNF-α+IFN-γ priming

To assess whether exposure to diseased tissues specifically enhances the therapeutic effect of cADSCs on the original disease, cADSCs primed with each condition were administered intraperitoneally to mice on day 2 of colitis induction by DSS (Figure 5A). The mice used in a series of experiments investigating the therapeutic effects of primed cADSCs *in vivo* were different from those used for homogenate preparation and co-culture assays. On day 10 of the experiment, compared with that in the colitis mice receiving phosphate-buffered saline (PBS), body weight loss was mildly but significantly suppressed in colitis mice receiving naive cADSCs and cADSCs primed with TNF-α+IFN-γ or colon homogenate (Figure 5B), and disease activity index (DAI) was significantly reduced in mice receiving cADSCs primed with TNF-α+IFN-γ or colon homogenate (Figure 5C). Meanwhile, in the assessment of the length of the mouse colon after sacrifice, only cADSCs primed with colon homogenate showed improvement in shortening (Figures 5D, E). Histological evaluation of the colon showed no significant ameliorative effect of primed cADSCs, although some mice treated with cADSCs primed with TNF-α+IFN-γ or colon homogenate had relatively mild histological severity (Figures 5F, G).

2.6 cADSCs primed with colon homogenate markedly shift macrophage polarity to M2 phenotype

We next performed phenotypic analysis of macrophages to determine the modulatory effects of primed cADSCs on these cells, which are important mediators in the pathogenesis of DSS-induced colitis in mice (19). Peritoneal macrophages from colitis mice treated with cADSCs primed with each condition were isolated and the frequencies of $F4/80^+$ $CD80^+$ proinflammatory M1 macrophages and $F4/80^+$ $CD206^+$ anti-inflammatory M2 macrophages were determined using flow cytometry. Both naive cADSCs and cADSCs primed with any condition reduced $F4/80^+$ $CD80^+$ M1 macrophages, which were drastically increased by colitis induction, but cADSCs primed with TNF-α+IFN-γ or colon homogenate in particular significantly and markedly reduced them (Supplementary Figures 3A, B). Concurrently, $F4/80^+$ $CD206^+$ M2 macrophages increased to higher levels than in healthy control mice with the administration of any cADSCs, and were most increased with administration of cADSCs primed with colon homogenate (Supplementary Figures 3C, D). The ratio of M1 to M2 phenotypes of macrophages was greatly polarized toward M1 dominance by induction of colitis, but was significantly skewed toward M2 dominance by administration of cADSCs primed with any conditions, especially by administration of cADSCs primed with colon homogenate (Figure 6A).

2.7 cADSCs primed with colon homogenate effectively suppress Th1/Th17-cell responses

Among the various Th-cell subsets, activation of the Th1/Th17-cell response, characterized by a cytokine profile featuring components such as TNF-α, IFN-γ, interleukin (IL)-6, and IL-17, also contributes to the development of the acute phase of DSS-induced colitis (20). Therefore, we investigated the effect of priming with diseased tissue on the capacity of cADSCs to modulate an imbalanced Th-cell paradigm by the phenotypic analysis of $CD4^+$ Th cells from mice with colitis. To this end, $CD4^+$ Th cells were isolated from the spleens of colitis mice treated with cADSCs primed with each condition, and the frequencies of Th1 cells expressing IFN-γ as an intracellular cytokine, Th2 cells expressing IL-4, Th17 cells expressing IL-17A, and T-regulatory (Treg) cells expressing both CD25 on the cell surface and the transcription factor Foxp3 in the nucleus were determined using flow cytometry.

The frequency of $CD4^+$ IFN-γ^+ Th1 cells did not show statistically significant changes in any of the treated mice compared to the control group (Supplementary Figures 4A, B). Even though the frequency of Th1 cells tended to increase in colitis mice without cADSC treatment and not in mice with primed cADSC treatment, the reason statistical significance was not detected is suggested by the high variability in the colitis mice without cADSC. For $CD4^+$ IL-4^+ Th2 cells, the induction of colitis by DSS and treatment with any cADSCs did not cause consistent and obvious changes (Supplementary Figures 4C, D). The ratio of Th1 to Th2 cell frequencies, representing the Th1/Th2 balance,

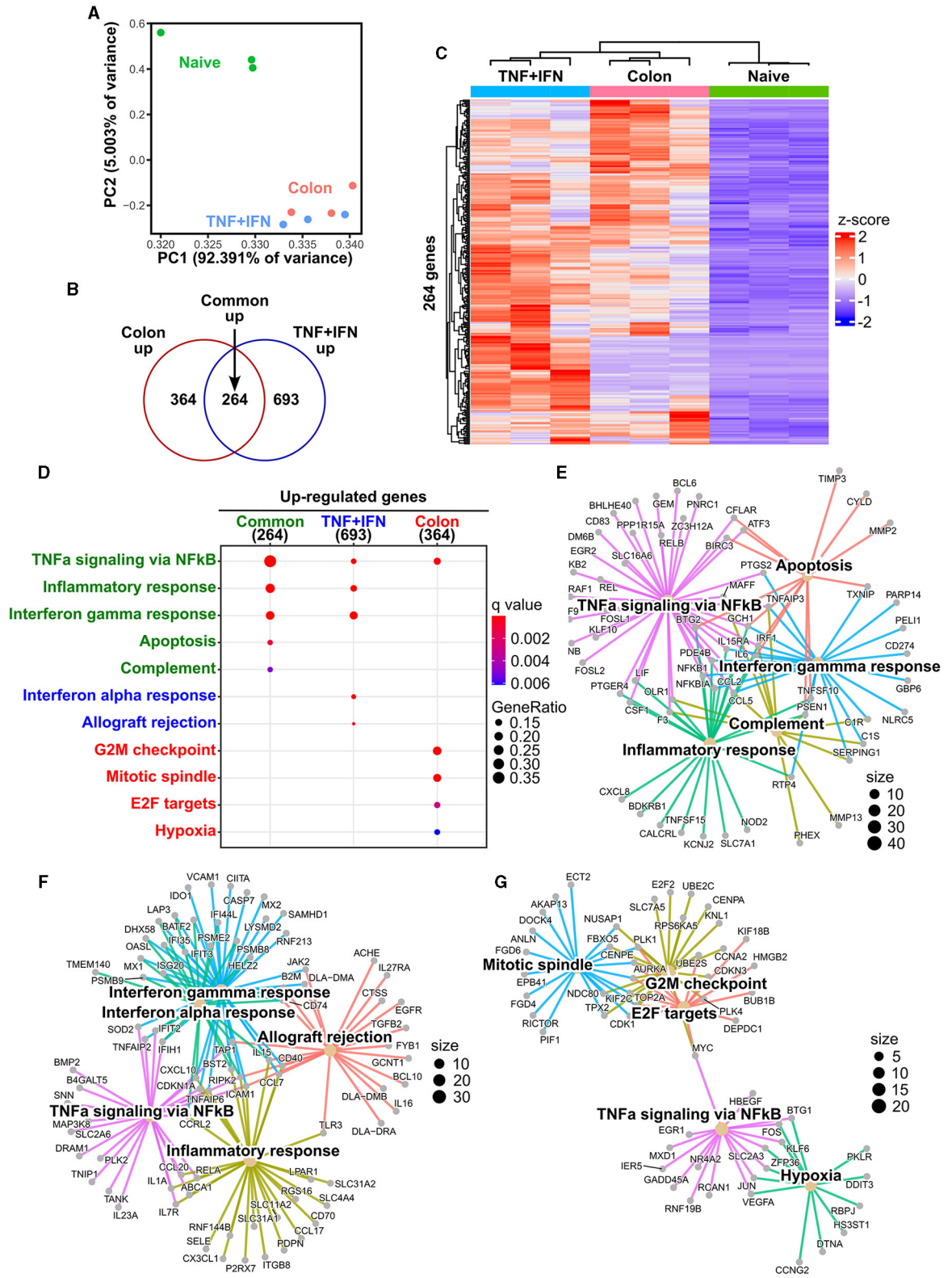

FIGURE 4
Effects of TNF-α+IFN-γ priming and colon priming on the transcriptome of cADSCs. **(A)** Biplot obtained from principal component analysis (PCA) for transcriptomes of naive cADSCs and those primed with TNF-α+IFN-γ or colon homogenate. **(B)** Venn diagram of genes significantly upregulated by priming with TNF-α+IFN-γ or colon homogenate. Differentially expressed gene (DEG) analysis was performed using DESeq2; $n = 3$; fold change >2, false discovery rate (FDR) < 0.05. **(C)** Integrated heatmap of genes commonly upregulated in both types of priming. **(D)** Top-ranked functional pathways enriched in gene sets upregulated by priming, including 264 common genes (green), 693 genes specific to TNF-α+IFN-γ priming (blue), and 364 genes specific to colon priming (red); FDR < 0.05. **(E)** Gene-concept network (cnet) plot of pathways enriched for upregulated gene sets common to each type of priming. **(F)** cnet plot of pathways enriched for gene sets specifically upregulated by TNF-α+IFN-γ priming. **(G)** cnet plot of pathways enriched for gene sets specifically upregulated by colon priming.

10.3389/fvets.2024.1437648

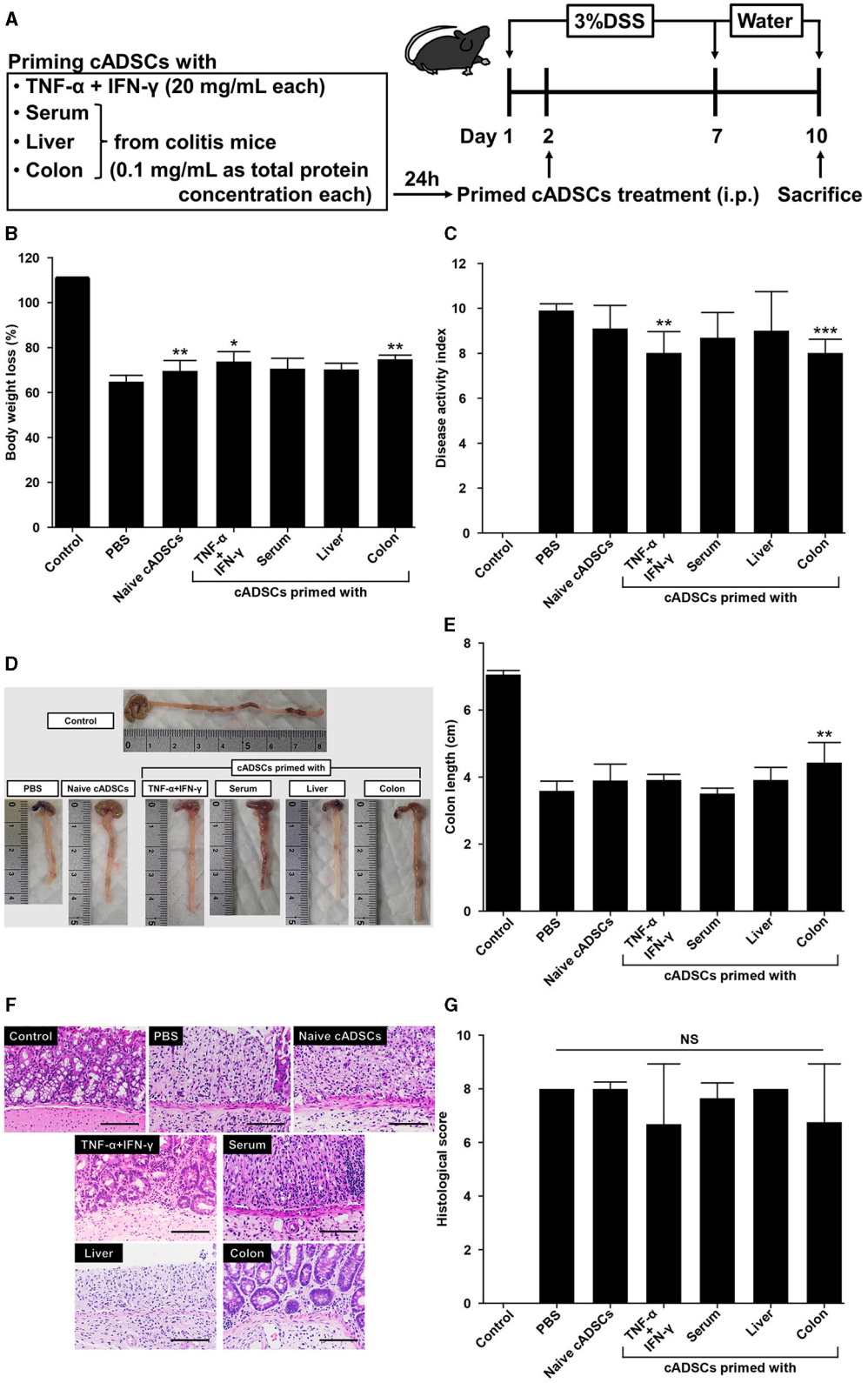

FIGURE 5
Effect of priming conditions on the therapeutic efficacy of cADSCs in dextran sulfate sodium (DSS)-induced colitis. **(A)** Scheme for priming and administering cADSCs and induction of colitis by DSS. **(B)** Comparison of body weight loss on day 10 in mice receiving cADSCs primed with each condition. Control represents healthy mice that received neither DSS nor cADSCs. **(C)** Comparison of disease activity index (DAI) at day 10 of the experiment. Colon-primed cADSCs most significantly reduced DAI. **(D)** Gross images of the colon of mice treated with cADSCs primed with each condition. The length of the colon, excluding the cecum, was measured. **(E)** Colon-primed cADSCs significantly improved colon shortening. **(F)** Histological images of the colon of mice treated with primed cADSCs. Some mice treated with cADSCs primed with TNF-α+IFN-γ or colon homogenate had relatively mild mucosal epithelial injury. Bar = 100 μm. **(G)** Comparison of histological scores in each group. Data are expressed as the mean ± standard deviation; $n = 5$; *$p < 0.05$, **$p < 0.01$, ***$p < 0.001$, NS, not significant.

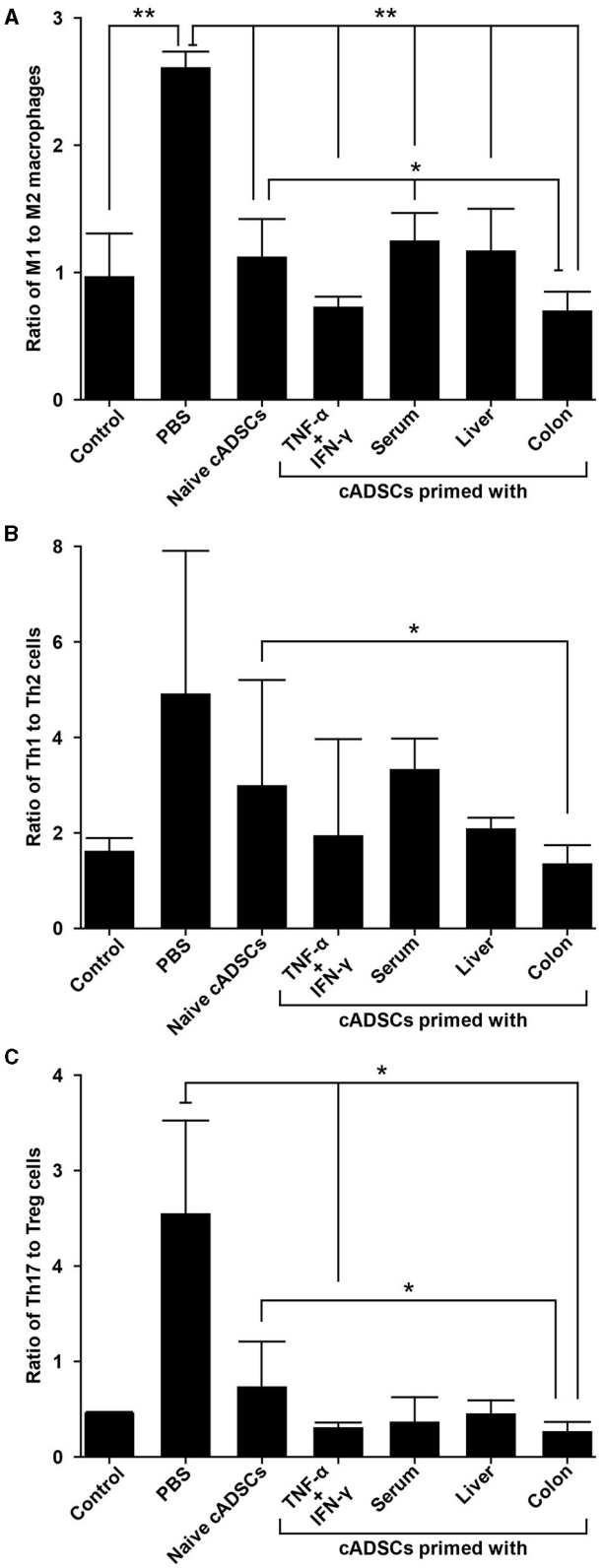

FIGURE 6
Differential capacity of cADSCs primed with variable conditions to modulate macrophage polarity and Th cell paradigm. **(A)** The ratio of M1 to M2 macrophage frequencies. cADSCs primed with TNF-α+IFN-γ or colon homogenate markedly shifted macrophage polarity toward M2 dominance. **(B)** Balance of the Th1/Th2-cell paradigm as indicated by the ratio of Th1 to Th2-cell frequencies. *(Continued)*

FIGURE 6 (Continued)
The cADSCs primed with colon homogenate modulated the Th1/Th2 balance by inhibiting Th1-cell activation. **(C)** Balance of the Th17/T regulatory (Treg)-cell paradigm as indicated by the ratio of Th17 to Treg cells. Priming with any condition effectively enhanced the capacity of cADSCs to suppress Th17-cell responses and induce Treg-cells, but the effect was particularly pronounced with TNF-α+IFN-γ or colon-priming. Data are expressed as the mean ± standard deviation; $n = 5$; $^{*}p < 0.05$, $^{**}p < 0.01$.

was significantly reduced in mice treated with cADSCs primed with colon homogenate to the same level as in healthy controls, in contrast to the level in mice treated with naive cADSCs (Figure 6B). Again, because of the high variability in the PBS group, no statistically significant difference between the PBS group and the colon primed group was detected.

The naive and all primed cADSCs consistently reduced the frequency of $CD4^{+}$ IL-$17A^{+}$ Th17 cells increased by colitis induction, similar to the suppression pattern in Th1 cells, and especially cADSCs primed with colon homogenate significantly reduced Th17 cells (Supplementary Figures 5A, B). In contrast, the frequency of $CD4^{+}$ $CD25^{+}$ $Foxp3^{+}$ Treg cells was clearly increased in mice treated with all primed cADSCs, and those treated with cADSCs primed with TNF-α+IFN-γ or colon homogenate in particular showed significant and marked increases in this frequency compared with PBS-treated mice (Supplementary Figures 5C, D). The ratio of Th17- to Treg-cell frequencies as a measure of the balance of the Th17/Treg-cell paradigm was significantly reduced in mice treated with cADSCs primed with TNF-α+IFN-γ or colon homogenate compared with that in mice without cADSC treatment (Figure 6C). In summary, all priming methods enhanced the capacity of cADSCs to suppress Th1/Th17-cell responses and induce Treg cells in colitis mice, with colon priming having the strongest enhancing effect.

3 Discussion

Various priming approaches have been proposed to improve the therapeutic efficacy of MSCs, including cytokines, growth factors, hypoxia, drugs, and biomaterials (14). Among them, the priming of MSCs with inflammatory cytokines aimed at increasing the secretion of anti-inflammatory and immunomodulatory factors has been the subject of numerous studies. Yang et al. reported that priming cADSCs with a combination of TNF-α and IFN-γ markedly enhanced the capacity of these cells to suppress the expression of proinflammatory cytokines in lipopolysaccharides (LPS)-activated macrophage cell lines and canine peripheral blood mononuclear cells via upregulation of the cyclooxygenase (COX)-2/prostaglandin E2 (PGE2) pathway (21). The same group also showed that TNF-α-primed cADSCs ameliorated colitis by promoting the polarization of M2 macrophages in mice with DSS-induced colitis via the hypersecretion of PGE2 and TNF-α-stimulated gene/protein 6 (TSG-6) (22), and that extracellular vesicles (EVs) derived from cADSCs primed with TNF-α and IFN-γ effectively suppressed colitis by inducing Treg cells

and M2 macrophages (23). Consistent with the above studies, priming of cADSCs with a combination of TNF-α and IFN-γ in this study drastically enhanced the capacity of cADSCs to induce M2 macrophages and Treg cells, suppress Th1/Th17-cell responses, and inhibit Th-cell proliferation, thereby reducing the severity of colitis, with the upregulation of COX-2 and TSG-6 (Supplementary Table 1). Enrichment analysis showed that pathways such as TNF-α signaling via NFκB, IFN-γ responses, and inflammatory responses were enriched as expected, but surprisingly these pathways were also commonly enriched upon priming with colitis tissue. Furthermore, the enhancing effect of cADSCs on immunomodulatory capacity was equally observed upon priming with colitis tissue. The colon of mice with DSS-induced colitis expresses high levels of TNF-α and IFN-γ compared with that of healthy mice, but at picogram levels (24, 25). Therefore, cytokine concentrations much lower than those used in this study (20 ng/mL) may be sufficient to enhance the immunomodulatory capacity of cADSCs, and the inclusion of cytokines at concentrations and types more closely resembling the inflammatory environment may appropriately enhance the therapeutic effect of cADSCs. This is supported by studies reporting that exposure of human ADSCs to synovial fluid from patients with rheumatoid arthritis or plasma from patients with graft-vs.-host disease, which contain picogram levels of multiple inflammatory cytokines such as TNF-α, exerts better immunomodulatory effects (26, 27).

Priming is a good way to enhance MSC function, but one must consider that it may affect MSC survival, proliferation, and immunogenicity (15). In this regard, Li et al. showed that treatment of mouse bone marrow-derived MSCs (BMSCs) for 48 h with 10 ng/mL each of TNF-α and IFN-γ synergistically induced cell apoptosis, which was mediated by nitric oxide (28). In addition, Domenis et al. reported that priming of human ADSCs with graded concentrations of TNF-α and IFN-γ from 10 to 40 ng/mL for 48 h caused concentration-dependent changes in cell morphology and decreased proliferation (29). Regarding the effect on immunogenicity, Montesinos et al. demonstrated that stimulation of human BMSCs with a low concentration of TNF-α (0.5 ng/mL) or IFN-γ (5 ng/mL) for 24 h increased the expression of major histocompatibility complex (MHC)-I (30). Meanwhile, MHC-II expression of human BMSCs was not induced by TNF-α, but was markedly induced by IFN-γ, after 24 h (31, 32). Similar to these reports, in the present study, cADSC priming with the combination of TNF-α and IFN-γ induced apoptosis, decreased cell proliferation, and MHC-II gene (*DLA-DRA* and *DLA-DQA1*) expression, while enrichment analysis revealed enrichment of the apoptotic and allograft rejection pathways. A marked upregulation of MHC-II gene expression in cytokine-primed cells was revealed by RNA-seq (Supplementary Table 1). In contrast, priming of cADSCs with colitis tissue did not induce cell apoptosis, even at high concentrations, but rather promoted cell proliferation, and MHC-II gene expression was marginal. Priming with colitis tissue also showed upregulation of the apoptotic pathway in common, while the upregulation of cell proliferation and hypoxic pathways was specifically observed. Several studies have shown that priming MSCs under hypoxic conditions improves the survival and proliferative potential of the cells (33, 34). The detailed mechanisms by which the hypoxia and cell proliferation pathways were upregulated are unknown, but activation of these pathways may have protected cADSCs primed with colitis tissue from apoptosis. With regard to immunogenicity, priming human BMSCs with IL-17 alone or a cocktail of IL-1β, IL-6, and IL-23, cytokines secreted by Th17 cells, has been reported to enhance immunomodulatory capacity without increasing the expression of MHC-II or co-stimulatory molecules (35, 36). Considering the activation of Th17 cells that occurs in the colon of mice with DSS-induced colitis, it is suggested that not only low concentrations of TNF-α and IFN-γ in colitis tissue, but also Th17 cytokines, may be responsible for the enhanced function of cADSCs without increasing their immunogenicity. Similar priming effects that enhance function without adversely affecting MSCs are also provided by exposure of human ADSCs to the inflammatory environment produced by activated T cells, synovial fluid from rheumatoid arthritis patients, or plasma from graft-vs.-host disease patients (26, 27, 37).

MSCs are well known to change their properties and functions in response to the surrounding microenvironment (18). Therefore, the aim of this study was to investigate whether *ex vivo* exposure of cADSCs to inflamed colon tissue from mice would more effectively enhance the therapeutic effect of cADSCs on colitis in mice. DSS-induced colitis is a representative disease model used in preclinical studies of human IBD and canine CIE (38). Actually, some studies have reported that xenotransplantation of canine MSC ameliorate DSS-induced colitis in mice via immunomodulatory effects (21, 22, 39). In this study, to determine whether the original disease microenvironment enhances the immunomodulatory and therapeutic effects of canine MSCs on DSS-induced colitis in mice, cADSCs were primed with colon homogenates from colitis mice rather than dogs and the enhancing effects were compared to other priming conditions. DSS is toxic to mucosal epithelial cells of the colon, and when 40–50 kDa DSS is added at a concentration of 1–5% to drinking water and fed to mice for 5–10 days, it disrupts the integrity of the epithelial barrier and causes acute colitis (40). In addition to epithelial cell damage, macrophages play an important role in the pathogenesis of colitis, and stimulated and subsequently activated proinflammatory M1 macrophages not only cause direct colonic mucosal injury via the secretion of proinflammatory cytokines such as TNF-α, IL-1β, and IL-6, but also cause the infiltration of neutrophils and $CD4^+$ Th cells into the mucosal epithelium via the secretion of IL-23 (41). Meanwhile, the adaptive immune system is not essential for the development of colitis, but the Th1/Th17-cell response, characterized by cytokines such as IFN-γ, IL-6, and IL-17, contributes to the progression of colitis (20, 42). Although the mechanism by which MSCs improve the pathogenesis of this model is not fully understood, they have been reported to improve the severity of colitis by reprogramming macrophages, modifying the Th-cell paradigm, and inducing regulatory immune cells via the secretion of indoleamine 2,3-dioxygenase (IDO), PGE2, transforming growth factor-β1, TSG-6, and EVs, among others (8). It has also been reported that intravenously administered rat BMSCs engraft onto damaged colon epithelium and restore the integrity of the epithelial barrier by rebuilding the tight junction protein claudin (43). Consistent with many previous reports, our intraperitoneally administered cADSCs, even naive

ones, shifted the macrophage phenotype from M1 to M2 polarity, suppressed activation of Th1/Th17-cell responses, and directly inhibited Th-cell proliferation. However, their immunomodulatory capacity and were particularly enhanced in cADSCs primed with a combination of the inflammatory cytokines TNF-α and IFN-γ and in cADSCs primed with colon homogenate from colitis mice. These results emphasize the importance of activating MSCs by exposure to an inflammatory environment in order to maximize their therapeutic efficacy.

Although MSCs are not constitutively immunosuppressive, several studies have shown that their immunomodulatory function is activated by the host inflammatory environment (44). Therefore, in DSS-induced colitis, delivery of MSCs to inflamed colonic tissues may effectively activate their immunomodulatory function. Differences in the migration of MSCs to the inflamed colon that depend on the route of administration have been reported. For example, Castelo-Branco et al. showed that the intraperitoneal administration of allogeneic ADSCs to rats with trinitrobenzene sulfonic acid (TNBS)-induced colitis improved inflammation via the migration of ADSCs into the inflamed colon, but intravenous administration did not improve inflammation as the cells did not migrate into the colon (45). Li et al. also reported that the intravenous administration of human BMSCs to mice with TNBS-induced colitis resulted in most of them being trapped in the lungs and spleen, but the overexpression of CXCL2 on the cells markedly increased migration to the colon (46). In contrast, Gonçalves et al. reported that allogeneic ADSCs administered intravenously to mice with DSS-induced colitis induced high levels of IFN-γ in mouse serum, thereby activating the immunomodulatory function of ADSCs and showing increased T-cell apoptosis in the inflamed colon and improvement of inflammation, although this did not occur upon intraperitoneal administration (47). Furthermore, Pan et al. showed that allogeneic umbilical cord-derived MSCs administered intraperitoneally or intravenously to mice with DSS-induced colitis migrate into the colon by either route and improve colitis by improving local microcirculation, repairing epithelial barriers, and exerting immunomodulatory effects, with the effect of intraperitoneal administration being shown to be superior (48). Although the biodistribution of administered cADSCs was not analyzed in this study, it is possible that some of the intraperitoneally administered cADSCs migrated to the inflamed colon and were activated by its microenvironment, as suggested by the fact that even naive cADSCs exhibited immunomodulatory effects. Thus, intraperitoneal administration may be a more appropriate route of administration to enhance the therapeutic effect of MSCs in colitis in mice. However, the intraperitoneal administration of MSCs is not practical in large animals such as dogs or in humans due to the large volume of their abdominal cavity. With the exception of fistula-type Crohn's disease, local administration of MSCs is difficult in canine CIE and human IBD because of the diffuse or multiple lesions in the intestine, which is much larger and longer than in mice, and MSCs are almost always administered intravenously (8, 10). Although no studies have yet examined the biodistribution of intravenously administered MSCs in dogs with CIE or patients with IBD, intravenously administered MSCs in these species are often trapped early in the lungs and then redistributed to the spleen, liver, and kidney, but rarely in the intestinal tract (49). Furthermore, proteins, including cytokines, in the blood do not accurately reflect the state of inflammation in the gastrointestinal tract, as evidenced by the absence of established blood biomarkers (50). In summary, because intravenously administered MSCs in dogs and humans are less exposed to the inflammatory microenvironment, priming MSCs with inflammatory tissue may be a promising approach for successful MSC therapy not only in rodent experimental animal models but also in canine CIE and human IBD patients.

Hepatobiliary disorders are common extraintestinal manifestations of IBD (51). Similarly, in DSS-induced colitis, disruption of the colonic mucosal epithelial barrier increases intestinal permeability, allowing inflammatory cytokines and toxins such as LPS to reach the liver via the portal vein and cause inflammatory damage (52). In addition, during the acute phase of colitis caused by DSS, serum from C57BL/6J mice exhibits a cytokine expression pattern characterized by TNF-α, IFN-γ, and IL-6 from M1 macrophages/Th1 cells and IL-17 from Th17 cells similar to the expression pattern found in colon (24, 25). Therefore, we also primed cADSCs with serum and liver as non-colon tissues derived from colitis mice to test the specificity of priming with colitis tissue in enhancing the therapeutic effect of MSCs on colitis. Our results showed that priming with colitis tissue enhanced the immunomodulatory and therapeutic effects of cADSCs more than priming with other tissues, suggesting that the enhancing effects were specific. Given that the factors contained in each tissue sample are diverse, including not only cytokines but also EVs, miRNAs, and extracellular matrix, this study cannot clarify the mechanisms involved in the enhancement of cADSC function by priming, but it is possible that not only factors induced by inflammation but also components of colon tissue played an important role. To further validate this site-specific potentiation effect, it is necessary to compare the therapeutic effect of cADSCs primed with liver homogenates or colon homogenates on hepatitis models, for example.

Taken together, priming with colitis tissue homogenate enhanced the immunomodulatory capacity of cADSCs as much as priming with a combination of TNF-α and IFN-γ, a priming method that is well known to enhance the immunosuppressive capacity of MSCs. Furthermore, priming with colitis tissue enhanced the function of cADSCs without inducing apoptosis, decreased cell proliferation, or immunogenicity. Therefore, priming MSCs with diseased tissues may be an alternative method of priming MSCs to that of cytokines. We believe that if future studies demonstrate the safety of primed cells in dogs, they can be considered for use in individual cases in the clinic. The lack of direct quantification of cytokines and other proteins contained in the mouse-derived tissue samples used for priming or secreted by the primed cADSCs is a major limitation of this study, but given the diversity of factors contained in the samples and the lack of clarity on the mechanism of action of cADSCs, an exhaustive proteomic analysis is needed to investigate them. Detailed analysis of the mechanisms by which inflammatory tissue enhances MSC function was not within the scope of this study, but should be conducted in the future. If the factors involved in MSC activation are identified for this priming method, they may be purified and combined, making this a disease-specific and scalable method. In

addition, it will be necessary to investigate the effects of primed cADSCs on the function as well as phenotype of macrophages and Th cell subsets. However, to the best of our knowledge, this is the first study to report that exposure of cADSCs to colitis tissue appropriately enhances their immunomodulatory and therapeutic effects on the original disease, colitis. Based on this finding, better therapeutic efficacy may be achieved by priming MSCs with mucosal samples obtained in a relatively non-invasive manner by endoscopic gastrointestinal mucosal biopsy, an essential step in the definitive diagnosis of canine CIE and human IBD. To achieve this, further studies are needed to elucidate the mechanisms mediating the functional enhancement of MSCs by priming, as well as to analyze characteristics and functions of primed MSCs in more detail.

4 Materials and methods

4.1 cADSC isolation and characterization

cADSCs were isolated from the falciform ligament fat of five healthy beagles (males; mean age: 1.8 years; mean weight: 11.0 kg), as previously described (53). This study was approved by the Bioethics Committee of Nippon Veterinary and Life Science University (approval number 2023S-5; 31 March, 2023). The animals were handled in accordance with the animal care guidelines of the Institute of Laboratory Animal Resources, Nippon Veterinary and Life Science University, Japan. Briefly, collected adipose tissue was digested in Dulbecco's Modified Eagle's Medium (DMEM) containing 0.15% collagenase type I (Sigma-Aldrich, St. Louis, MO, USA) with gentle agitation at 37°C for 1 h. After centrifugation, the pellet containing the stromal vascular fraction was resuspended in DMEM, filtered through a 100 μm nylon mesh, plated into a T-75 culture flask containing DMEM complete medium [DMEM supplemented with 10% fetal bovine serum (FBS; Capricorn, Hessen, Germany) and 1% penicillin–streptomycin (Thermo Fisher Scientific, Waltham, MA, USA)], and incubated overnight in a humidified atmosphere with 5% CO_2 at 37°C. The cells were detached using trypsin-EDTA solution (Sigma-Aldrich) upon reaching 80–90% confluence and passaged. As shown in our previous studies, cADSCs were characterized by flow cytometry for expression pattern of CD29, CD44, and CD90 positive, CD34, CD45, and HLA-DR negative cell surface markers (53). In addition, the trilineage differentiation potential of these cells for adipogenesis, osteogenesis, and chondrogenesis was confirmed. All experiments were performed using cADSCs at passages 2–3.

4.2 Mouse colon, liver homogenate, and serum preparation

To obtain mouse-derived samples and prepare homogenates for priming cADSCs, fifteen 6-week-old male C57BL/6J mice were purchased from Jackson Laboratory Japan (Kanagawa, Japan) and fed *ad libitum* on sterile water and standard experimental chow in a temperature- and light-controlled room. Mice in which colitis had been induced by 7 days of 3% DSS (36–50 kDa; MP Biomedical, Solon, OH, USA) solution administration were euthanized by CO_2 asphyxiation, and colon, liver, and whole-blood samples were collected. The colon and liver samples were washed well in PBS and immediately frozen in liquid nitrogen, followed by manual homogenization on ice using a tapered tissue grinder. After adding 1 mL of PBS per 100 mg of homogenate, the samples were centrifuged at 10,000 × g for 20 min at 4°C, and the supernatant was collected and filtered through a 20 μm mesh filter for sterilization. The collected whole blood was centrifuged at 1,200 × g for 15 min at 4°C, and the supernatant was collected to obtain serum. Total protein concentrations of colon and liver homogenates and serum were determined using a Qubit protein assay kit (Thermo Fisher Scientific), in accordance with the manufacturer's instructions. Homogenates and sera were stored frozen in liquid nitrogen until use.

4.3 cADSC priming protocols

cADSCs were thawed and suspended in DMEM complete medium and plated on 100 mm cell culture dishes. After 3–5 days, when cADSCs reached 70–80% confluence, the medium was removed and washed twice with PBS, after which DMEM complete medium containing 0.1 mg of homogenate or serum as total protein per mL, or containing 20 ng of recombinant mouse TNF-α (Miltenyi Biotec, Bergisch Gladbach, Germany) and recombinant mouse IFN-γ (Miltenyi Biotec) per mL was added and incubated with 5% CO_2 at 37°C. After 24 h, cells were detached with trypsin-EDTA solution and used for subsequent experiments.

4.4 Lymphocyte proliferation inhibition assay

cADSCs primed with colon homogenate at graded concentrations of 0.01 to 1.0 mg/mL, primed with liver homogenate or serum at concentrations of 0.1 mg/mL and 0.5 mg/mL, or primed with 20 ng/mL mouse TNF-α and mouse IFN-γ were plated in six-well plates. After 24 h, cADSC adhesion was confirmed and the medium of the wells was removed, followed by the addition of 1×10^6 splenic Th cells from colitis mice without cADSC treatment pre-labeled with 5 μM Cell Trace Violet (Thermo Fisher Scientific) in RPMI-1640 complete medium (RPMI-1640 supplemented with 10% FBS, 1% penicillin–streptomycin, and 50 μM 2-mercaptoethanol) to the wells with or without 2×10^5 naive or primed cADSCs. The cells were then co-cultured with or without cADSCs in the presence of anti-mouse CD3/CD28 antibody-loaded Anti-Biotin MACSiBead particles (Miltenyi Biotec) at 37°C with 5% CO_2 for 72 h. Th cells and cADSCs were cultured with direct contact in the wells. Finally, Th cells were collected and stained with an anti-CD4-APC antibody (Clone: RM4-5; BioLegend) or the isotype control, and proliferation was measured by flow cytometry.

4.5 cADSC apoptosis assay

Naive cADSCs or cADSCs primed for 24 h with 20 ng/mL of each of TNF-α and IFN-γ, 0.1 mg/mL liver homogenate, or 0.1 mg/mL or 0.5 mg/mL colon homogenate were stained with the FITC Annexin-V Apoptosis Detection Kit with PI (BioLegend, San Diego, CA, USA), in accordance with the manufacturer's instructions, and then apoptotic cells were measured by flow cytometry as the sum of the percentages of cells positive for Annexin V alone or in combination with PI.

4.6 cADSC proliferation assay

Naive cADSCs or cADSCs primed for 24 h with 20 ng/mL of each of TNF-α and IFN-γ, 0.1 mg/mL liver homogenate, or 0.1 mg/mL or 0.5 mg/mL colon homogenate were plated in 96-well plates at 2×10^3 cells each. After incubation at 37°C and 5% CO_2 for 1–4 days, Cell Counting Kit-8 (CCK-8; Dojindo, Kumamoto, Japan) was added to the wells, in accordance with the manufacturer's instructions and cell proliferation was measured as OD values at a wavelength of 450 nm with a Synergy HT Microplate Reader (BioTek, Winooski, VT, USA). OD values after day 2 were normalized by OD values on day 1.

4.7 RNA sequencing

Total RNA was extracted from naive cADSCs or cADSCs primed for 24 h with 20 ng/mL of each of TNF-α and IFN-γ, or 0.1 mg/mL colon homogenate using a NucleoSpin RNA kit (TaKaRa, Shiga, Japan), in accordance with the manufacturer's instructions. Construction of the cDNA library was performed with 1 μg of total RNA using Illumina NEBNext Ultra II RNA Library Prep Kit, in accordance with the manufacturer's instructions, followed by paired-end sequencing (2×150 bp) using a NovaSeq 6000 instrument. An average of 16–20 million read pairs were generated for each library. Primary analysis of RNA-seq raw data was carried out on the web using RaNa-seq (https://ranaseq.eu/; accessed on 22 February, 2024) (54). In this way, FASTQ files were pre-processed with the FASTp tool (55), expression was quantified with Salmon (56) against the genome assembly CanFam3.1, and raw count data and count data normalized by transcripts per million (TPM) were output. Secondary analysis of RNA-seq data was performed on the web by inputting these count data into RNAseqChef (https://imeg-ku.shinyapps.io/RNAseqChef/; accessed on 10 March, 2024) (57). For the pairwise comparison analysis, DEG detection was performed using DESeq2 with fold change and false discovery rate (FDR) cut-off values of >2 and <0.05, respectively. To compare DEGs from different data sets, Venn diagram analysis was performed. Functional enrichment analysis was performed using clusterProfiler (58) with an FDR cut-off of >0.05 based on the MSigDB hallmark gene set.

4.8 Mouse colitis induction and cADSC treatment

To evaluate the therapeutic effect of cADSCs primed with each condition on colitis *in vivo*, 35 6-week-old c57BL/6J mice were purchased separately from the mice used for homogenate preparation and lymphocyte proliferation inhibition assays. To induce colitis, mice received 3% DSS solution in drinking water for 7 days, followed by sterile water for 3 days. On day 2 of colitis induction, mice received 200 μL of PBS or 2×10^6 cells of naive or primed cADSCs intraperitoneally. In contrast, healthy control mice received only sterile water to drink and the intraperitoneal administration of PBS. Each group included 5 mice. The mice were sacrificed by CO_2 asphyxiation on day 10, and colon tissues and immune cells were harvested for subsequent histological evaluation and phenotypic analysis.

4.9 Evaluation of colitis severity

The severity of colitis was assessed based on the DAI, colon length, and the histological score of the colon. The DAI was calculated as the sum of three scores, namely, percent weight loss from initial weight (grades 0–4: 0, none; 1, 1–5% loss; 2, 6–10% loss; 3, 11–20% loss; 4, >20% loss), stool consistency (grades 0–3: 0, normal; 1, soft; 2, loose; 3, watery), and rectal bleeding (grades 0–3: 0, none; 1, occult blood; 2, visible bleeding; 3, gross bleeding), and was compared among the groups. Colon length was measured with a ruler from colon samples harvested on day 10. Two pathologists evaluated hematoxylin and eosin-stained colon tissue sections in a blinded fashion, and histological scores were calculated in accordance with previously reported methods (23) as follows: inflammatory cell infiltration (score 0–4: 0, no filtration; 1, infiltrate around crypt bases; 2, infiltrate reaching the lamina muscularis mucosa with abundant edema; 3, extensive infiltration reaching the muscularis mucosa with abundant edema; 4, infiltration of the submucosal layer) and epithelial damage (score 0–4: 0, normal morphology; 1, loss of goblet cells; 2, loss of goblet cells in large areas; 3, loss of crypts; 4, loss of crypts in large areas).

4.10 Phenotypic analysis of mouse peritoneal macrophages and splenic $CD4^+$ Th cells

To investigate the effect of primed cADSCs on the immune system of mice with DSS-induced colitis, immune cells were harvested from these mice with and without cADSC treatment. Isolation and phenotypic analysis of mouse peritoneal macrophages and splenic $CD4^+$ Th cells were performed as previously described (24). In brief, peritoneal macrophages were isolated by collecting and centrifuging PBS injected into the abdominal cavity of mice, and splenic $CD4^+$ Th cells were isolated from cell suspensions obtained by mechanical mashing of the spleen by negative magnetic selection using a mouse $CD4^+$ T-cell isolation kit (Miltenyi Biotec), in accordance with the manufacturer's instructions.

For flow cytometric phenotyping of macrophages, the cells were stained with the following antibodies or their respective isotype controls: anti-F4/80-FITC (clone: BM8; BioLegend), anti-CD80-APC (clone: 16-10A1; BioLegend), and anti-CD206-PE (clone: C068C2; BioLegend).

For intracellular cytokine detection, Th cells were stimulated with phorbol 12-myristate 13-acetate (50 ng/mL; Sigma-Aldrich) and ionomycin (1 μg/mL; Sigma-Aldrich) for 6 h and brefeldin A (10 μg/mL; Sigma-Aldrich) for 4 h, and then stained with an anti-CD4-APC antibody (Clone: RM4-5; BioLegend) or isotype control. The cells were fixed and permeabilized with Cyto-Fast Fix/Perm Buffer Set (BioLegend) and then stained with anti-IFN-γ-PE (clone: XMG1.2; BioLegend), anti-IL-4-PE (clone: 11B11; BioLegend), and anti-IL-17A-PE (clone: TC11-18H10.1; BioLegend) antibodies, or their respective isotype controls.

For flow cytometric detection of Treg cells, Th cells were stained with anti-CD4-APC and anti-CD25-PE (clone: PC61; BioLegend) antibodies or their respective isotype controls, followed by fixing and permeabilizing with True-Nuclear Transcription Factor Buffer Set (BioLegend) and staining with an anti-Foxp3-Alexa Fluor488 antibody (clone: MF-14; BioLegend) or isotype control. All samples were measured using a CytoFLEX instrument (Beckman Coulter, Brea, CA, USA) and data were analyzed using CytExpert ver. 2.0 analysis software.

4.11 Statistical analysis

All results are presented as the mean ± standard deviation. Data were tested for distribution normality using the Shapiro-Wilks normality test. Differences among multiple groups were assessed by one-way analysis of variance for normally distributed data and compared using the Dunnett's or Tukey–Kramer multiple comparison *post hoc* test, and assessed by Kruskal-Wallis test for non-normally distributed data and compared using Steel-Dwass post hock test. $p < 0.05$ was considered statistically significant. Statistical analyses were performed using R Commander 4.1.2.

Data availability statement

The original contributions presented in the study are included in the article/Supplementary material, further inquiries can be directed to the corresponding author.

Ethics statement

The animal study was approved by the Bioethics Committee of Nippon Veterinary and Life Science University. The study was conducted in accordance with the local legislation and institutional requirements.

Author contributions

YY: Conceptualization, Data curation, Formal analysis, Investigation, Methodology, Project administration, Validation, Visualization, Writing – original draft. TT: Conceptualization, Data curation, Formal analysis, Funding acquisition, Investigation, Methodology, Project administration, Resources, Supervision, Visualization, Writing – review & editing. TN: Investigation, Writing – review & editing. MM: Investigation, Writing – review & editing. YT: Investigation, Writing – review & editing. RS: Investigation, Writing – review & editing. HM: Investigation, Writing – review & editing.

Funding

The author(s) declare that financial support was received for the research, authorship, and/or publication of this article. This research was funded by JSPS KAKENHI grant number JP21H02373.

Acknowledgments

We thank Edanz (https://jp.edanz.com/ac) for editing a draft of this manuscript, and FUJIFILM Wako Bio Solutions Corporation and VERITAS Inc. for help with the RNA-seq.

Conflict of interest

The authors declare that the research was conducted in the absence of any commercial or financial relationships that could be construed as a potential conflict of interest.

Publisher's note

Supplementary material

The Supplementary Material for this article can be found online at: https://www.frontiersin.org/articles/10.3389/fvets.2024.1437648/full#supplementary-material

References

1. Chang JT. Pathophysiology of inflammatory bowel diseases. *N Engl J Med.* (2020) 383:2652–64. doi: 10.1056/NEJMra2002697

2. Catalan-Serra I, Brenna Ø. Immunotherapy in inflammatory bowel disease: novel and emerging treatments. *Hum Vaccin Immunother.* (2018) 14:2597–611. doi: 10.1080/21645515.2018.1461297

3. Jergens AE, Heilmann RM. Canine chronic enteropathy-current state-of-the-art and emerging concepts. *Front Vet Sci.* (2022) 9:923013. doi: 10.3389/fvets.2022.923013

4. Dandrieux JRS, Mansfield CS. Chronic enteropathy in canines: prevalence, impact and management strategies. *Vet Med (Auckl).* (2019) 10:203–14. doi: 10.2147/VMRR.S162774

5. Mastrolia I, Foppiani EM, Murgia A, Candini O, Samarelli AV, Grisendi G, et al. Challenges in clinical development of mesenchymal stromal/stem cells: concise review. *Stem Cells Transl Med.* (2019) 8:1135–48. doi: 10.1002/sctm.19-0044

6. Voga M, Adamic N, Vengust M, Majdic G. Stem cells in veterinary medicine-current state and treatment options. *Front Vet Sci.* (2020) 7:278. doi: 10.3389/fvets.2020.00278

7. Bunnell BA. Adipose tissue-derived mesenchymal stem cells. *Cells.* (2021) 10:3433. doi: 10.3390/cells10123433

8. Lopez-Santalla M, Garin MI. Improving the efficacy of mesenchymal stem/stromal-based therapy for treatment of inflammatory bowel diseases. *Biomedicines.* (2021) 9:1507. doi: 10.3390/biomedicines9111507

9. Ciccocioppo R, Baumgart DC, Dos Santos CC, Galipeau J, Klersy C, Orlando G. Perspectives of the international society for cell & gene therapy gastrointestinal scientific committee on the intravenous use of mesenchymal stromal cells in inflammatory bowel disease (PeMeGi). *Cytotherapy.* (2019) 21:824–39. doi: 10.1016/j.jcyt.2019.05.003

10. Teshima T. Heterogeneity of mesenchymal stem cells as a limiting factor in their clinical application to inflammatory bowel disease in dogs and cats. *Vet J.* (2024) 304:106090. doi: 10.1016/j.tvjl.2024.106090

11. Zhou T, Yuan Z, Weng J, Pei D, Du X, He C, et al. Challenges and advances in clinical applications of mesenchymal stromal cells. *J Hematol Oncol.* (2021) 14:24. doi: 10.1186/s13045-021-01037-x

12. Pérez-Merino EM, Usón-Casaús JM, Zaragoza-Bayle C, Duque-Carrasco J, Mariñas-Pardo L, Hermida-Prieto M, et al. Safety and efficacy of allogeneic adipose tissue-derived mesenchymal stem cells for treatment of dogs with inflammatory bowel disease: Clinical and laboratory outcomes. *Vet J.* (2015) 206:385–90. doi: 10.1016/j.tvjl.2015.08.003

13. Cristóbal JI, Duque FJ, Usón-Casaús JM, Ruiz P, Nieto EL, Pérez-Merino EM. Effects of allogeneic mesenchymal stem cell transplantation in dogs with inflammatory bowel disease treated with and without corticosteroids. *Animals (Basel).* (2021) 11:2061. doi: 10.3390/ani11072061

14. Noronha NC, Mizukami A, Caliári-Oliveira C, Cominal JG, Rocha JLM, Covas DT, et al. Priming approaches to improve the efficacy of mesenchymal stromal cell-based therapies. *Stem Cell Res Ther.* (2019) 10:131. doi: 10.1186/s13287-019-1224-y

15. López-García L, Castro-Manrreza ME. TNF-α and IFN-γ participate in improving the immunoregulatory capacity of mesenchymal stem/stromal cells: importance of cell-cell contact and extracellular vesicles. *Int J Mol Sci.* (2021) 22:9531. doi: 10.3390/ijms22179531

16. Klimczak A, Kozlowska U. Mesenchymal stromal cells and tissue-specific progenitor cells: their role in tissue homeostasis. *Stem Cells Int.* (2016) 2016:4285215. doi: 10.1155/2016/4285215

17. Shi Y, Su J, Roberts AI, Shou P, Rabson AB, Ren G. How mesenchymal stem cells interact with tissue immune responses. *Trends Immunol.* (2012) 33:136–43. doi: 10.1016/j.it.2011.11.004

18. Bernardo ME, Fibbe WE. Mesenchymal stromal cells: sensors and switchers of inflammation. *Cell Stem Cell.* (2013) 13:392–402. doi: 10.1016/j.stem.2013.09.006

19. Lin Y, Yang X, Yue W, Xu X, Li B, Zou L, et al. Chemerin aggravates DSS-induced colitis by suppressing M2 macrophage polarization. *Cell Mol Immunol.* (2014) 11:355–66. doi: 10.1038/cmi.2014.15

20. Yang F, Wang D, Li Y, Sang L, Zhu J, Wang J, et al. Th1/Th2 balance and Th17/Treg-mediated immunity in relation to murine resistance to dextran sulfate-induced colitis. *J Immunol Res.* (2017) 2017:7047201. doi: 10.1155/2017/7047201

21. Yang HM, Song WJ, Li Q, Kim SY, Kim HJ Ryu MO, et al. Canine mesenchymal stem cells treated with TNF-α and IFN-γ enhance anti-inflammatory effects through the COX-2/PGE2 pathway. *Res Vet Sci.* (2018) 119:19–26. doi: 10.1016/j.rvsc.2018.05.011

22. Song WJ, Li Q, Ryu MO, Nam A, An JH, Jung YC, et al. Canine adipose tissue-derived mesenchymal stem cells pre-treated with TNF-alpha enhance immunomodulatory effects in inflammatory bowel disease in mice. *Res Vet Sci.* (2019) 125:176–84. doi: 10.1016/j.rvsc.2019.06.012

23. An JH, Li Q, Bhang DH, Song WJ, Youn HY. TNF-α and INF-γ primed canine stem cell-derived extracellular vesicles alleviate experimental murine colitis. *Sci Rep.* (2020) 10:2115. doi: 10.1038/s41598-020-58909-4

24. Alex P, Zachos NC, Nguyen T, Gonzales L, Chen TE, Conklin LS, et al. Distinct cytokine patterns identified from multiplex profiles of murine DSS and TNBS-induced colitis. *Inflamm Bowel Dis.* (2009) 15:341–52. doi: 10.1002/ibd.20753

25. Kim JJ, Shajib MS, Manocha MM, Khan WI. Investigating intestinal inflammation in DSS-induced model of IBD. *J Vis Exp.* (2012) 3678. doi: 10.3791/3678-v

26. Sayegh S, El Atat O, Diallo K, Rauwel B, Degboé Y, Cavaignac E, et al. Rheumatoid synovial fluids regulate the immunomodulatory potential of adipose-derived mesenchymal stem cells through a TNF/NF-κB-dependent mechanism. *Front Immunol.* (2019) 10:1482. doi: 10.3389/fimmu.2019.01961

27. Silva-Carvalho AÉ, Rodrigues LP, Schiavinato JL, Alborghetti MR, Bettarello G, Simões BP, et al. GVHD-derived plasma as a priming strategy of mesenchymal stem cells. *Stem Cell Res Ther.* (2020) 11:156. doi: 10.1186/s13287-020-01659-x

28. Li X, Shang B, Li YN, Shi Y, Shao C. IFNγ and TNFα synergistically induce apoptosis of mesenchymal stem/stromal cells via the induction of nitric oxide. *Stem Cell Res Ther.* (2019) 10:18. doi: 10.1186/s13287-018-1102-z

29. Domenis R, Cifù A, Quaglia S, Pistis C, Moretti M, Vicario A, et al. Pro inflammatory stimuli enhance the immunosuppressive functions of adipose mesenchymal stem cells-derived exosomes. *Sci Rep.* (2018) 8:13325. doi: 10.1038/s41598-018-31707-9

30. Montesinos JJ, López-García L, Cortés-Morales VA, Arriaga-Pizano L, Valle-Ríos R, Fajardo-Orduña GR, et al. Human bone marrow mesenchymal stem/stromal cells exposed to an inflammatory environment increase the expression of ICAM-1 and release microvesicles enriched in this adhesive molecule: analysis of the participation of TNF-α and IFN-γ. *J Immunol Res.* (2020) 2020:8839625. doi: 10.1155/2020/8839625

31. Prasanna SJ, Gopalakrishnan D, Shankar SR, Vasandan AB. Pro-inflammatory cytokines, IFNgamma and TNFalpha, influence immune properties of human bone marrow and Wharton jelly mesenchymal stem cells differentially. *PLoS ONE.* (2010) 5:e9016. doi: 10.1371/journal.pone.0009016

32. Takeshita K, Motoike S, Kajiya M, Komatsu N, Takewaki M, Ouhara K, et al. Xenotransplantation of interferon-gamma-pretreated clumps of a human mesenchymal stem cell/extracellular matrix complex induces mouse calvarial bone regeneration. *Stem Cell Res Ther.* (2017) 8:101. doi: 10.1186/s13287-017-0550-1

33. Lavrentieva A, Majore I, Kasper C, Hass R. Effects of hypoxic culture conditions on umbilical cord-derived human mesenchymal stem cells. *Cell Commun Signal.* (2010) 8:18. doi: 10.1186/1478-811X-8-18

34. Li B, Li C, Zhu M, Zhang Y, Du J, Xu Y, et al. Hypoxia-induced mesenchymal stromal cells exhibit an enhanced therapeutic effect on radiation-induced lung injury in mice due to an increased proliferation potential and enhanced antioxidant ability. *Cell Physiol Biochem.* (2017) 44:1295–310. doi: 10.1159/000485490

35. Sivanathan KN, Rojas-Canales D, Grey ST, Gronthos S, Coates PT. Transcriptome profiling of IL-17A preactivated mesenchymal stem cells: a comparative study to unmodified and ifn-γ modified mesenchymal stem cells. *Stem Cells Int.* (2017) 2017:1025820. doi: 10.1155/2017/1025820

36. Pourgholaminejad A, Aghdami N, Baharvand H, Moazzeni SM. The effect of pro-inflammatory cytokines on immunophenotype, differentiation capacity and immunomodulatory functions of human mesenchymal stem cells. *Cytokine.* (2016) 85:51–60. doi: 10.1016/j.cyto.2016.06.003

37. Crop MJ, Baan CC, Korevaar SS, Ijzermans JN, Pescatori M, Stubbs AP, et al. Inflammatory conditions affect gene expression and function of human adipose tissue-derived mesenchymal stem cells. *Clin Exp Immunol.* (2010) 162:474–86. doi: 10.1111/j.1365-2249.2010.04256.x

38. Okayasu I, Hatakeyama S, Yamada M, Ohkusa T, Inagaki Y, Nakaya R, et al. novel method in the induction of reliable experimental acute and chronic ulcerative colitis in mice. *Gastroenterology.* (1990) 98:694–702. doi: 10.1016/0016-5085(90)90290-H

39. Yasumura Y, Teshima T, Nagashima T, Michishita M, Takano T, Taira Y, et al. Immortalized canine adipose-derived mesenchymal stem cells maintain the immunomodulatory capacity of the original primary cells. *Int J Mol Sci.* (2023) 24:17484. doi: 10.3390/ijms242417484

40. Randhawa PK, Singh K, Singh N, Jaggi AS. A review on chemical-induced inflammatory bowel disease models in rodents. *Korean J Physiol Pharmacol.* (2014) 18:279–88. doi: 10.4196/kjpp.2014.18.4.279

41. Katsandegwaza B, Horsnell W, Smith K. Inflammatory bowel disease: a review of pre-clinical murine models of human disease. *Int J Mol Sci.* (2022) 23:9344. doi: 10.3390/ijms23169344

42. Dieleman LA, Ridwan BU, Tennyson GS, Beagley KW, Bucy RP, Elson CO. Dextran sulfate sodium-induced colitis occurs in severe combined immunodeficient mice. *Gastroenterology.* (1994) 107:1643–52. doi: 10.1016/0016-5085(94)90803-6

43. Yabana T, Arimura Y, Tanaka H, Goto A, Hosokawa M, Nagaishi K, et al. Enhancing epithelial engraftment of rat mesenchymal stem cells restores epithelial barrier integrity. *J Pathol.* (2009) 218:350–9. doi: 10.1002/path.2535

44. Krampera M. Mesenchymal stromal cell 'licensing': a multistep process. *Leukemia.* (2011) 25:1408–14. doi: 10.1038/leu.2011.108

45. Castelo-Branco MT, Soares ID, Lopes DV, Buongusto F, Martinusso CA, do Rosario A Jr, et al. Intraperitoneal but not intravenous cryopreserved mesenchymal stromal cells home to the inflamed colon and ameliorate experimental colitis. *PLoS ONE.* (2012) 7:e33360. doi: 10.1371/journal.pone.0033360

46. Li Q, Lian Y, Deng Y, Chen J, Wu T, Lai X, et al. mRNA-engineered mesenchymal stromal cells expressing CXCR2 enhances cell migration and improves recovery in IBD. *Mol Ther Nucleic Acids.* (2021) 26:222–36. doi: 10.1016/j.omtn.2021.07.009

47. Gonçalves Fda C, Schneider N, Pinto FO, Meyer FS, Visioli F, Pfaffenseller B, et al. Intravenous vs intraperitoneal mesenchymal stem cells administration: what is the best route for treating experimental colitis? *World J Gastroenterol.* (2014) 20:18228–39. doi: 10.3748/wjg.v20.i48.18228

48. Pan XH, Li QQ, Zhu XQ Li ZA, Cai XM, Pang RQ, et al. Mechanism and therapeutic effect of umbilical cord mesenchymal stem cells in inflammatory bowel disease. *Sci Rep.* (2019) 9:17646. doi: 10.1038/s41598-019-54194-y

49. Sanchez-Diaz M, Quiñones-Vico MI, Sanabria de la Torre R, Montero-Vílchez T, Sierra-Sánchez A, Molina-Leyva A, et al. Biodistribution of mesenchymal stromal cells after administration in animal models and humans: a systematic review. *J Clin Med.* (2021) 10:2925. doi: 10.3390/jcm10132925

50. Siel D, Beltrán CJ, Martínez E, Pino M, Vargas N, Salinas A, et al. Elucidating the role of innate and adaptive immune responses in the pathogenesis of canine chronic inflammatory enteropathy-a search for potential biomarkers. *Animals (Basel).* (2022) 12:1645. doi: 10.3390/ani12131645

51. Uko V, Thangada S, Radhakrishnan K. Liver disorders in inflammatory bowel disease. *Gastroenterol Res Pract.* (2012) 2012:642923. doi: 10.1155/2012/642923

52. Gäbele E, Dostert K, Hofmann C, Wiest R, Schölmerich J, Hellerbrand C, et al. DSS induced colitis increases portal LPS levels and enhances hepatic inflammation and fibrogenesis in experimental NASH. *J Hepatol.* (2011) 55:1391–9. doi: 10.1016/j.jhep.2011.02.035

53. Yasumura Y, Teshima T, Taira Y, Saito T, Yuchi Y, Suzuki R, et al. Optimal intravenous administration procedure for efficient delivery of canine adipose-derived mesenchymal stem cells. *Int J Mol Sci.* (2022) 23:14681. doi: 10.3390/ijms232314681

54. Prieto C, Barrios D. RaNA-Seq: interactive RNA-Seq analysis from FASTQ files to functional analysis. *Bioinformatics.* (2019) 36:1955–1956. doi: 10.1093/bioinformatics/btz854

55. Chen S, Zhou Y, Chen Y, Gu J. fastp: an ultra-fast all-in-one FASTQ preprocessor. *Bioinformatics.* (2018) 34:i884–90. doi: 10.1093/bioinformatics/bty560

56. Patro R, Duggal G, Love MI, Irizarry RA, Kingsford C. Salmon provides fast and bias-aware quantification of transcript expression. *Nat Methods.* (2017) 14:417–9. doi: 10.1038/nmeth.4197

57. Etoh K, Nakao M, A. web-based integrative transcriptome analysis, RNAseqChef, uncovers the cell/tissue type-dependent action of sulforaphane. *J Biol Chem.* (2023) 299:104810. doi: 10.1016/j.jbc.2023.104810

58. Wu T, Hu E, Xu S, Chen M, Guo P, Dai Z, et al. clusterProfiler 40: A universal enrichment tool for interpreting omics data. *Innovation (Camb).* (2021) 2:100141. doi: 10.1016/j.xinn.2021.100141

frontiers | Frontiers in Veterinary Science

TYPE Original Research
PUBLISHED 24 October 2024
DOI 10.3389/fvets.2024.1437805

OPEN ACCESS

EDITED BY
Francisco Javier Salguero,
UK Health Security Agency, United Kingdom

REVIEWED BY
Maria Elena Gelain,
University of Padua, Italy
Shingo Ishikawa,
Osaka Metropolitan University, Japan

*CORRESPONDENCE
Koh Kawasumi
✉ kawasumi224@nvlu.ac.jp

RECEIVED 31 May 2024
ACCEPTED 25 September 2024
PUBLISHED 24 October 2024

CITATION
Kusaba A, Tago E, Kusaba H and Kawasumi K (2024) Study of age-related changes in plasma metabolites and enzyme activity of healthy small dogs that underwent medical checkups.
Front. Vet. Sci. 11:1437805.
doi: 10.3389/fvets.2024.1437805

Study of age-related changes in plasma metabolites and enzyme activity of healthy small dogs that underwent medical checkups

Akio Kusaba[1,2], Erika Tago[1], Haruna Kusaba[2] and Koh Kawasumi[1]*

[1]Laboratory of Veterinary Biochemistry, Nippon Veterinary and Life Science University, Musashino, Japan, [2]Muromi Animal Hospital, Fukuoka, Japan

Introduction: In Japan, the importance of medical checkups for pet dogs is increasing. In this study, we retrospectively explored the effects of age on plasma biomarkers in healthy small dogs that underwent medical checkups.

Methods: Based on the modified American Animal Hospital Association Canine Life Stage Guidelines, 52 healthy small dogs were divided into 3 groups according to their life stage: young adult (1–4 years old), mature adult (5–11 years old), senior (12–15 years old). None of the dogs were obese. Plasma was collected from animals that underwent medical checkups at Muromi Animal Hospital (Fukuoka, Japan). Plasma glucose, triglyceride (TG), total protein, blood urea nitrogen (BUN), creatinine, total cholesterol, and albumin concentrations; alanine aminotransferase, aspartate aminotransferase, and alkaline phosphatase (ALP) activities; c-reactive protein (CRP), non-esterified fatty acid, malondialdehyde (MDA), serum amyloid A (SAA), insulin, and adiponectin (ADN) concentrations; glutathione peroxidase (GPx), superoxide dismutase (SOD), malate dehydrogenase (MDH), and lactate dehydrogenase (LDH) activities; and M/L ratio (MDH/LDH) were examined. Changes in the abovementioned plasma biomarker levels were compared between canines in different life stages.

Results: Plasma ADN concentrations and GPx, SOD, and MDH activities significantly decreased with age, whereas plasma ALP, BUN, TG, and MDA concentrations gradually increased. Plasma SAA levels measured by the latex agglutination method in 51 of the 52 small dogs that underwent medical checkups were below the detection limit.

Conclusion: Plasma ADN concentrations, GPx, SOD activity, and BUN levels may be important biomarkers for clarifying the effect of age in healthy dogs that undergo medical checkups. However, plasma SAA values obtained by the latex agglutination method were not considered an age-related inflammation marker for healthy dogs.

KEYWORDS

adiponectin, age-related inflammation, healthy dog, medical checkup, SAA

1 Introduction

In the field of veterinary medicine, as in human medicine, there is a growing movement to promote "prevention" and "prevention of disease." There is a particularly growing awareness of the importance of aging-related care in pets (1–6), as aged dogs are likely to become obese and develop other metabolic diseases that induce chronic inflammation. Senescent cells secrete various factors such as inflammatory cytokines, chemokines, and extracellular matrix-degrading enzymes that have inflammatory and carcinogenic effects, causing a phenomenon called the senescence-associated secretory phenotype (7–10), which is associated with a variety of diseases (11).

The emphasize on prevention of disease increased the need for medical checkups for pets, as regular medical checkup programs for laboratory dogs are essential for their well-being (12). In Japan, veterinary medical checkups for pets include general inspection tests such as 15–20 blood tests, urinalysis, stool tests, and definitive diagnostic tests, such as chest/abdominal x-ray examinations, abdominal ultrasound tests, electrocardiograms, blood pressure measurements, and thyroid hormone tests. A medical checkup is a detailed examination to detect diseases that may be overlooked during an annual health checkup performed at the time of rabies vaccination. However, even in animals that undergo annual medical checkups and are diagnosed as healthy, illnesses can be discovered before 1 year. Moreover, almost all tests that can be performed without anesthesia are performed at primary care facilities. Therefore, it is necessary to consider whether there are any items that can detect metabolic changes earlier by measuring additional aging and metabolic biomarkers that may not be routinely assessed in the hospital.

Franceschi et al. (13) proposed the term "inflammaging," which refers to a proinflammatory state associated with the low-grade inflammation associated with aging. Several researchers in veterinary medicine have also reported inflammaging (14–21). Levels of acute phase protein, an acute-phase inflammatory marker, has also been used to investigate chronic inflammatory conditions. Particularly, serum amyloid A protein (SAA) levels increase with age in various diseases. Currently, SAA values are considered disease onset markers (22, 23). SAA is thought to be a major contributor to the obesity-associated inflammatory response (24). SAA promotes the lipolysis of adipose tissue through the NF-κB system, increases blood free fatty acid concentration, and induces insulin resistance and vascular damage (25). However, it remains unclear whether increased plasma SAA levels are caused by obesity-induced or age-related inflammation (inflammaging) in aged obese dogs.

Therefore, in this study, we examined the changes in plasma biomarker values such as plasma metabolites, hormone concentrations, and enzyme activities in healthy dogs without obesity that underwent medical checkups, and life stage differences were investigated. In addition, we investigated whether plasma SAA levels measured by the latex agglutination method could be used as an indicator of age-related inflammation in healthy aging dogs. Notably, because the lifespan of dogs varies depending on size—small dogs tend to live longer than larger animals (26)—and the age of small dogs corresponding to humans is less than that of larger dogs (27, 28), the effect of age on metabolism should be evaluated using a uniform size. Therefore, because small dogs account for the largest population in our country (29), we focused on small healthy dogs that underwent medical checkups to detect age-related inflammation.

2 Materials and methods

2.1 Animals

Fifty-two clinically healthy small dogs that underwent medical checkups at the Muromi Animal Hospital (Fukuoka City) were recruited. Based on the modified AAHA Canine Life Stage Guidelines (30), the animals were divided into three groups: young adult (1–4 years old), mature adult (5–11 years old), senior (12–15 years old).

Ethical approval was obtained from Muromi Animal Hospital (R23-1). Written informed consent was obtained from each owner. The frozen plasma samples collected during the medical checkups were taken to Nippon Veterinary and Life Science University, and plasma biomarkers were examined.

2.2 Body type classification

Considering the species of dogs in this study, those weighing less than 9 kg were regarded as small dogs (28).

2.3 Body weight (BW) and body conditioning score (BCS) measurement

BW was measured during the medical checkups. To evaluate the BCS of the dogs, we employed a 9-point system: 1/9, emaciated; 2/9, very thin; 3/9, thin; 4/9, underweight; 5/9, ideal; 6/9, overweight; 7/9, heavy; 8/9, obese; and 9/9, severely obese (31).

2.4 Blood sampling and analysis

Fasting blood was collected from the lateral saphenous vein into heparinized tubes after at least 8 h of fasting. Plasma was collected by centrifugation at 3500G for 5 min at room temperature and stored at −80°C until use. Glucose, triglyceride (TG), total protein (TP), blood urea nitrogen (BUN), creatinine (CRE), total bilirubin, total cholesterol (TC), albumin (ALB) concentrations and alanine aminotransferase, aspartate aminotransferase (AST), alkaline phosphatase (ALP) activities, C-reactive protein (CRP) were measured at Muromi Animal Hospital (Fukuoka, Japan) using an automatic biochemical analyzer, FUJI dry chem 7,000 V (Fujifilm Medical Co., Ltd., Tokyo, Japan).

Abbreviations: ADN, Adiponectin; ALB, Albumin; ALP, Alkaline phosphatase; ANOVA, Analysis of variance; AST, Aspartate aminotransferase; BCS, Body condition score; BUN, Blood urea nitrogen; BW, Body weight; CRE, Creatinine; CRP, C-reactive protein; GPx, Glutathione peroxidase; LALP, Liver alkaline phosphatase; LDH, Lactate dehydrogenase; MDA, Malondialdehyde; MDH, Malate dehydrogenase; M/L, Malate dehydrogenase/lactate dehydrogenase ratio; NEFA, Non-esterified fatty acid; SAA, Serum amyloid A; SE, Standard error; SOD, Superoxide dismutase; TC, Total cholesterol;; TG, Triglyceride; TP, Total protein.

Using the remaining plasma samples collected for medical checkups, non-esterified fatty acids (NEFA), malondialdehyde (MDA), serum amyloid A protein (SAA), insulin, adiponectin (ADN) concentrations, glutathione peroxidase (GPx), superoxide dismutase (SOD), malate dehydrogenase (MDH), lactate dehydrogenase (LDH) activity, and M/L ratio (MDH/LDH) were measured retrospectively at the Veterinary Biochemistry Laboratory, Nippon Veterinary and Life Science University (Tokyo, Japan). NEFA levels were measured using a commercial kit (NEFA C-Test Wako; Fujifilm Wako Pure Chemical Industries, Ltd. Tokyo, Japan). MDA was measured using a commercial kit (NWLSSTM Malondialdehyde Assay Kit, NWLSS [#NWK-MDA01], Northwest Life Science Specialties, LLC, Vancouver, Canada). Insulin was measured using a commercial kit (REVIS® Insulin-Rat T, Fujifilm Wako Shibayagi Co., Ltd., Gunma, Japan). ADN levels were measured using a commercial kit (mouse/rat adiponectin ELISA kit; Otsuka Pharmaceutical Co., Ltd., Tokyo, Japan). Fifty-thousand-fold diluted plasma samples were used for ADN measurement. The acceptable detection limit was estimated to be from 0.25 ng/mL to 8.0 ng/mL by calibration curve (32). GPx levels were measured using a commercial kit (NWLSS Glutathione Peroxidase Assay Kit; Northwest Life Science Specialties, LLC, Vancouver, Canada). SOD activity was measured using a commercial kit (Superoxide Dismutase ELISA Kit, Northwest Life Science Specialties, LLC, Vancouver, Canada). LDH and MDH activities were measured using the methods reported by Kaloustian et al. (1969) (33) and Bergmeyer and Bernt (1974) (34), respectively. LDH activity was calculated by measuring the change in absorbance at 340 nm for 180 s using an absorbance meter while MDH activity was calculated by measuring the change in absorbance at 340 nm for 300 s using an absorbance meter. The M/L ratio was calculated by dividing the MDH level by the LDH level.

Plasma SAA values were measured at the Research and Development Department of Eiken Chemical Co., Ltd. (Tochigi, Japan) using a Hitachi 7,180 automatic analyzer with the measurement reagent VET-SAA (Eiken Chemical, Tokyo, Japan). Age-related changes in the abovementioned plasma biomarkers were compared according to canine life stages.

2.5 Statistical analysis

Results are presented as mean ± standard error (SE). Statistical significance was determined using one-way analysis of variance (ANOVA). The significance level was set at $p < 0.05$ or $p < 0.01$. Correlation coefficients and p-values between age and the examined parameters were calculated using multivariate regression analysis. Significance levels were set at $p < 0.05$ or $p < 0.01$. Correlation coefficients were evaluated as follows: |0.7–1.0|: excellent, |0.4–0.7|: moderate, |0.2–0.4|: weak, |0–0.2|: no correlation.

3 Results

As shown in Table 1, the 52 healthy small dogs that underwent medical checkups were divided into 3 groups according to their life stage: 6 young adults, 35 mature adults, and 11 seniors. The mean ± SE of body weight for the 52 small dogs was 5.68 ± 0.30 kg. Among the 52 dogs, there were 3 Miniature Schnauzers, 2 Miniature Dachshunds, 19 Toy Poodles, 1 West Highland White Terrier, 2 Cavaliers, 5 Shizu dogs, 2 Shiba dogs, 3 Chihuahuas, 2 Pugs, 3 Pekingese dogs, 3 Pomeranians, 1 Maltese, 3 Yorkshire Terriers, and 3 mixed breeds. Fifty-one of the 52 small dogs had a BCS of 5 on a 9-point scale and were not obese.

Although statistical significance was not observed, plasma BUN, TG, and MDA levels tended to gradually increase with age, whereas plasma ADN concentrations in the senior group were significantly decreased compared with those of young adult group and mature adult group (one-way ANOVA, $p = 0.0048$, $p = 0.0241$, respectively: Table 2). Although the difference was not significant, plasma TP levels tended to increase with age, whereas plasma ALB levels tended to decrease with age.

The GPx and MDH activities in the senior group were significantly lower than those in the mature group (one-way ANOVA, $p = 0.0049$ and $p = 0.0182$, respectively; Table 3). Plasma SOD activity in the mature adult group was significantly lower than that in the young adult group ($p = 0.044$).

As shown in Table 4, the plasma SAA levels in 51 of the 52 healthy small dogs that underwent medical checkups were below the lower detection limit, which was calculated as 3.54 mg/L (35). One dog without severe inflammation (age: 9.5 years, BCS: 6/9; with cataracts, pupillary atrophy, and mild periodontal disease) had a plasma SAA value of 12.3 mg/L.

The correlation coefficients and p-values between age and biomarker levels were calculated using multivariable regression analysis (Table 5). The following markers were positively correlated with age: BUN levels, moderately positive (coefficient 0.499, $p = 0.000$); CRE levels, moderately positive (coefficient 0.467, $p = 0.001$); TG levels, weakly positive (coefficient 0.237, $p = 0.138$); ALP levels, weakly positive (coefficient 0.297, $p = 0.024$); and TP levels, weakly positive (coefficient 0.204, $p = 0.246$). Negative correlations were as follows: ADN levels, moderately negative (coefficient − 0.478, $p = 0.007$); GPx activity, moderately negative

TABLE 1 Changes in BW and BCS in healthy small dogs examined in medical checkups.

		Young adult (6)			Mature adult (35)			Senior (11)		
Age	(Years)	3.9	±	0.6	9.0	±	0.3	14.0	±	0.4
Weight	(kg)	6.6	±	1.1	5.8	±	0.4	4.7	±	0.5
BCS	(/9)	5.5	±	0.3	5.5	±	0.2	5.0	±	0.1

Data are presented as mean ± SE.
The numbers in parentheses indicate the number of animal examined.
BW, body weight; BCS, body condition score; SE, standard error.

TABLE 2 Changes in plasma metabolites and hormone concentrations in healthy small dogs examined in medical checkups.

		Young adult (6)			Mature adult (35)			Senior (11)		
GLU	(mg 100 mL^{-1})	106.7	±	7.5	102.7	±	1.4	104.0	±	2.4
TG	(mg 100 mL^{-1})	61.7	±	6.7	94.6	±	15.3	157.6	±	50.0
TC	(mg 100 mL^{-1})	223.7	±	39.6	217.8	±	14.0	227.6	±	18.8
NEFA	(mEq L^{-1})	1.25	±	0.3	1.18	±	0.10	1.05	±	0.17
TP	(g 100 mL^{-1})	6.3	±	0.2	6.4	±	0.1	6.6	±	0.3
ALB	(g 100 mL^{-1})	3.5	±	0.2	3.4	±	0.1	3.3	±	0.1
CRE	(mg 100 mL^{-1})	0.7	±	0.1	0.7	±	0.0	0.9	±	0.1
BUN	(mg 100 mL^{-1})	16.1	±	1.5	16.3	±	1.3	34.3	±	6.3
MDA	(μmol L^{-1})	0.7	±	0.4	0.9	±	0.3	1.1	±	0.4
CRP	(mg 100 mL^{-1})		NT		0.8	±	0.2	0.9	±	0.2
INS	(ng mL^{-1})	0.2	±	0.1	0.4	±	0.2	0.2	±	0.1
ADN	(μmol mL^{-1})	40.4	±	10.3*	26.8	±	3.3*	12.5	±	2.3

Data are presented as mean ± SE.
The numbers in parentheses indicate the number of animals examined.
* Significant ($p < 0.05$) compared to the senior group (one-way ANOVA).
ADN, adiponectin; ALB, albumin; ANOVA, analysis of variance; BUN, blood urea nitrogen; CRP, c-reactive protein; CRE, creatinine; GLU, glucose; INS, insulin; MDA, malondialdehyde; NEFA, non-esterified fatty acid; SE, standard error; TC, total cholesterol; TG, triglyceride; TP, total protein.

TABLE 3 Changes in plasma enzymes activities in healthy small dogs examined in medical checkups.

		Young adult (6)			Mature adult (35)			Senior (11)		
AST	(U/L)	31.2	±	3.9	33.2	±	2.5	28.1	±	2.2
ALT	(U/L)	44.3	±	4.4	77.2	±	8.6	86.5	±	23.1
ALP	(U/L)	95.4	±	28.8	170.3	±	39.4	325.9	±	79.4
GPx	(mU/mL)	26.0	±	4.3	24.3	±	1.3	18.7	±	2.8**
SOD	(unit/mL)	44.7	±	23.4**	19.3	±	3.3	11.0	±	1.7
MDH	(IU/L)	59.8	±	19.5	73.1	±	6.2	44.6	±	6.0**
LDH	(IU/L)	88.0	±	24.3	109.0	±	9.6	91.6	±	12.6
M/L		0.6	±	0.1	0.8	±	0.2	0.5	±	0.1

The data are expressed as mean ± SE.
The numbers in parentheses indicate the number of animals examined.
** Significant ($p < 0.05$) when compared against mature adult group (One-way ANOVA).
ALP, alkaline phosphatase; ALT, alanine aminotransferase; ANOVA, analysis of variance; AST, aspartate aminotransferase; GPx, glutathione peroxidase; LDH, lactate dehydrogenase; MDH, malate dehydrogenase; M/L, malate dehydrogenase/lactate dehydrogenase ratio; SE, standard error; SOD, superoxide dismutase.

(coefficient − 0.414, p = 0.007); SOD activity, weakly negative (coefficient − 0.267, $p = 0.127$); and AST levels, weakly negative (coefficient − 0.242, $p = 0.132$). Plasma MDH activity (an energy metabolism marker) and plasma SAA level (an inflammatory marker) did not correlate with age (coefficient − 0.144, p = 0.007; coefficient 0.065, $p = 0.683$, respectively).

4 Discussion

The characteristics of medical checkups in Japan are different from those of health checkups conducted once a year. During medical checkups, more detailed examinations are performed based on the wishes of pet owners concerned about the onset of potential diseases. Therefore, even in pets that are diagnosed as healthy during health checkups, we check for the presence or absence of various internal abnormalities in the body, such as latent inflammatory diseases and tumors, as early as possible.

Since small dogs are more commonly kept compared to medium and large dogs in Japan, we focused on small dogs in this study. The equivalent age at each life stage differs between small, medium, and large dogs, and it is impossible to evaluate the effects of age on metabolic changes in the same way.

4.1 Changes in plasma enzyme activities

GPx is an enzyme belonging to the selenoprotein family that catalyzes the reduction of hydrogen peroxide and lipid peroxides (36). Four types of GPx (GPx-1–4) have been identified in mammals (37). GPx4 is an antioxidant enzyme known to directly reduce phospholipid hydroperoxides in membranes and lipoproteins and

10.3389/fvets.2024.1437805

TABLE 4 Plasma SAA levels in 52 small dogs.

	Young adult (6)				Mature adult (35)						Senior (11)			
Age (dog)	1	3	4	5	6	7	8	9	10	11	12	13	14	15
(Human)	15	28	32	36	40	44	48	52	56	60	64	68	72	76
SAA ($mg\,L^{-1}$)	0.6	0.6	0.4	0.8	0.7	0.6	0.5	0.7	0.4	1.0	0.9	1.2	0.5	0.7
			0.5	0.8	0.6	0.7	0.6	0.8	0.3	0.6	1.0	0.9	1.7	2.0
			0.9		0.3	0.1	0.8	0.3	0.6	0.8	1.3	0.2		0.8
			0.6		0.6	0.5	0.8	0.5	0.9	0.5				
						2.0		0.5		0.0				
								12.3		0.8				
								1.1						
								0.3						
								0.7						
								0.3						
AV	0.6	0.6	0.6	0.8	0.6	0.8	0.7	1.8	0.6	0.6	1.1	0.8	1.1	1.2

SAA, serum amyloid A.

TABLE 5 Correlation coefficients and *P* values between the age and examined parameters in 52 healthy dogs.

	Correlation coefficient	*P* value
BW	−0.198	0.105
BCS	−0.168	0.150
GLU	−0.015	0.713
TC	0.044	0.262
TG	0.237	0.138
NEFA	−0.025	0.837
MDA	0.129	0.482
AST	−0.242	0.132
ALT	0.133	0.379
ALP	0.297	0.024
MDH	−0.144	0.007
LDH	0.015	0.727
M/L ratio	−0.087	0.439
SOD	−0.267	0.127
GPx	−0.414	0.007
ADN	−0.478	0.007
INS	0.004	0.983
TP	0.204	0.246
ALB	−0.033	0.419
BUN	0.499	0.000
CRE	0.467	0.001
SAA	0.065	0.683

Correlation coefficients were evaluated as follows: |0.7–1.0|: excellent, |0.4–0.7|: moderate, |0.2–0.4|: weak, |0–0.2|: no correlation using Pearson analysis. *P*-values were evaluated using multivariable regression analysis.

ADN, adiponectin; ALB, albumin; ALP, alkaline phosphatase; ALT, alanine aminotransferase; AST, aspartate aminotransferase; BCS, body condition score; BUN, blood urea nitrogen; BW, body weight; CRE, creatinine; GLU, glucose; GPx, glutathione peroxidase; INS, insulin; LDH, lactate dehydrogenase; MDA, malondialdehyde; M/L, malate dehydrogenase/lactate dehydrogenase ratio; NEFA, non-esterified fatty acid; SAA, serum amyloid A; SOD, superoxide dismutase; TC, total cholesterol; TG, triglyceride.

cooperates with α-tocopherol to suppress lipid peroxidation (38). In this study, plasma GPx and SOD activities tended to decrease in aged dogs that underwent medical checkups. This suggests that the protective function against cytotoxicity owing to the strong oxidizing action of superoxide may weaken with age.

4.2 MDH, M/L ratio

MDH (L-malate: NAD oxidoreductase [EC 1.1.1.37]) catalyzes the NAD/NADH-dependent interconversion of the substrates, malate and oxaloacetate. This reaction plays an important role in the malate/

aspartate shuttle across the mitochondrial membrane and the tricarboxylic acid cycle within the mitochondrial matrix (39).

In this study, MDH activity significantly decreased at the senior stage compared to that at the mature adult stage. This suggests a decrease in energy metabolism in the senior stage, as has been observed in humans. The M/L ratio, calculated by dividing the activity value by the LDH activity value, is thought to be an index for evaluating the metabolic state of animal tissues (40). It is used as a sensitive marker of increased energy metabolism, including increased ATP production, in tissues (41). Previous research on the relationship between aging and the M/L ratio in riding horses also found no significant difference in the M/L ratio between young and old groups (42). To investigate age-related energy metabolism, MDH activity may be more appropriate than the M/L ratio.

4.3 ALP

ALP [orthophosphoric-monoester phosphorylase (EC 3.1.3.1)] is an enzyme with low substrate specificity that hydrolyzes phosphate monoester bonds under alkaline conditions (pH 9–11). In clinical practice in dogs, it is primarily used as an indicator of liver and biliary tract diseases (43). In dog serum, three ALP isoenzymes are known: bone ALP, liver ALP (LALP), and corticosteroid-induced ALP (44). LALP accounted for less than 10% of young dogs, but more than 50% of total ALP in middle-aged and elderly dogs (45). In this study, the age-related increase in plasma ALP levels was suggested to be due to an increase in LALP levels.

4.4 Changes in plasma metabolites

Plasma TG levels tended to increase with age. This indicates that lipid metabolism tends to decline with age, even if it does not manifest as an abnormality.

Due to decreased lipid metabolism, fat accumulates in areas other than the visceral fat and adipose tissue, leading to obesity, and the ectopic accumulation of fat in the muscle and liver induces inflammation (46). In addition, obesity activates aging signals in adipose tissue and promotes immunosenescence (47). However, in this study, not all dogs that underwent pet medical checkups displayed obesity-related inflammation, considering their BCS and plasma SAA levels.

An increase in plasma TP levels and decrease in plasma ALB levels indicate an increase in plasma globulin levels. In such cases, chronic inflammation such as periodontal disease is often observed.

Plasma BUN values are influenced by three factors: ingested proteins and protein catabolism, urea synthesis by the liver and excretion by the kidneys, and changes depending on the amount of urea filtered glomerular filtration. Therefore, it is considered less reliable than CRE levels (48). However, an increase in plasma BUN levels accompanied by an increase in plasma CRE levels in the senior stage may be an important indicator of kidney disease. Consequently, urine specific gravity, urine protein, and blood pressure measurements should be considered. In obese cats, serum BUN levels significantly increased during the geriatric stage (49).

MDA is a relatively stable end product of the peroxidation of polyunsaturated fatty acids and is considered an indicator of oxidative stress (50, 51). The measurement results showed a tendency for plasma MDA levels to increase in dogs with age, although the difference was not significant. We hypothesized that oxidative stress may increase in aged dogs undergoing medical checkups. In addition, the levels of GPx and SOD, which have antioxidant effects, significantly decrease with age. These antioxidant effects were consistent with an increase in plasma MDA levels. Notably, many aging phenomena are suggested to be related to oxidative stress. In dogs and cats, it is said to be related to degenerative changes in the renal tubules (52). It was speculated that the increase in BUN and CRE is due to oxidative stress, which leads to early kidney disease. Previously, we attributed elevated BUN levels to increased protein intake in aging patients. By measuring GPx, SOD, and MDA, we may be able to differentiate between oxidative stress and excessive protein intake as potential causes.

Plasma ADN concentrations showed the highest levels (40.4 ± 10.3 μg/mL) at the young adult stage. Subsequently, the concentrations decreased with age. This suggests that the anti-inflammatory effect might decrease, and insulin resistance might increase in healthy aged dogs who undergo medical checkups, even if they are not obese. In a previous study, we examined plasma ADN concentrations in experimentally induced healthy obese dogs fed a high-fat diet. ADN concentrations at the young adult life stages were at the same level as in this study (38.8 ± 7.8 μg/mL) (53). In addition, the positive correlation of TG and ALP with age suggests that decreased ADN activity may lead to reduced fat burning and bile stagnation in the liver and elevated TG levels due to decreased AMP kinase activation, which increases ALP levels. Moreover, serum ALP activity increases in dogs and cats are reportedly due to intrahepatic or extrahepatic cholestasis (43). Since the owners of animals undergoing medical checkups are very health-conscious, they may not be obese according to BCS, but they may have accumulated visceral fat. In Japan, many owners feed their dogs jerky as a treat, and many of these snacks contain artificial additives. If a small dog continues to ingest additives every day, it puts more strain on the liver and liver enzymes rise. In cases of high TG and TC levels or cases of elevated liver enzymes without abnormalities in the liver parenchyma on ultrasonography, we have prescribed dietary foods (high fiber foods) or low fat foods. However, if we can confirm a decrease in ADN in our hospital, supplementing with 5-aminolevulinic acid might be beneficial, as it has been shown to reduce TG levels and liver enzymes (54, 55).

4.5 SAA

At the beginning of this study, we hypothesized that plasma SAA levels, measured using Vet SAA (Eiken Chemical), could serve as an indicator of age-related inflammation. A paper comparing apolipoprotein-A1 in septic shock and multiple organ dysfunction syndrome using Eiken Chemical's Vet SAA (the same one we used) reported that both CRP and SAA showed high values (56). This paper reported that the average values of SAA in 21 cases of septic shock were 400 μg/mL and CRP values were 23.6 mg/dL. We expected that Vet SAA (Eiken Chemical) would have a higher value and wider detection range during the same inflammation compared to CRP, an apolipoprotein-A1 commonly used in dogs.

As mentioned above, it is assumed that slight inflammation occurs in the animals' bodies due to oxidative stress caused by aging, and it was hypothesized that the onset of this very small inflammation could be detected using Vet SAA, which would result in differences between groups. In addition, the young adult group is excluded from the test items in our hospital's medical checkups because they are young and

often do not have inflammation, but the CRP levels measured in the mature adult and senior groups were low at 0.8 ± 0.2 and 0.9 ± 0.2 mg/dL, respectively, but were above the reference range. Therefore, some kind of inflammation may have begun to occur in the body. However, almost all the plasma SAA levels were below the detection limit. Therefore, although it has been confirmed that plasma SAA levels measured by the latex agglutination method are elevated in cases of severe inflammatory diseases, it may be difficult to detect the onset of inflammation that we are looking for using SAA. Furthermore, to apply other detection methods such as ELISA and chemiluminescence, it is necessary to verify plasma SAA levels as a marker of age-related inflammation.

Dogs are important for the investigation of age-related diseases in humans (57). Like humans, elderly dogs tend to become obese (58). In aged obese dogs, it is difficult to determine whether inflammation is induced by aging or obesity. To verify the onset of inflammation due to aging, we measured the degree of inflammation in clinically healthy dogs without obesity, by measuring plasma SAA levels using the latex agglutination method. As a result, the plasma SAA level was below the detection limit, and no pathological inflammation related to aging was observed. Future studies should investigate whether the latex agglutination test for SAA remains below the detection limit in obese senior dogs. Notably, only one of the 52 dogs in this study had a measurable SAA level, and this dog had a BCS of 6/9. Healthy dogs that have undergone pet checkups do not show the pathological inflammation associated with aging. Pet owners are afraid of latent inflammatory illnesses that cannot be identified through health checkups. In this study, the plasma SAA levels in healthy dogs provided sufficient information to pet owners.

4.6 Limitations

None of the small dogs recruited in this study were obese, and they had no clinical symptoms, although Miniature Schnauzers have breed-specific altered TG metabolism (59, 60) and are likely to become hyperlipidemic with age (61). Therefore, we do not believe that these results are representative of all small dogs bred in Japan. However, our results regarding the characteristics on age-related changes in plasma enzyme activities, hormones, and metabolites may be a characteristic of healthy small dogs that have undergone medical checkups.

Although we targeted small dogs that underwent medical checkups in this study, small dogs that undergo regular health examinations may have different physiological characteristics, such as obesity. Therefore, it is necessary to conduct further studies on dogs from other populations to clarify the effects of age. Since medium-sized and large dogs have different lifespans than small dogs, they are thought to have different age-related metabolic characteristics. Therefore, we need to verify the characteristics of age-related inflammation separately. Plasma SAA measurements using latex agglutination tests can also be performed in dogs with inflammatory diseases. Therefore, it may be difficult to detect early-stage age-related inflammation in non-obese small dogs.

5 Conclusion

In this study, age-related changes in plasma BUN levels, ADN concentrations, and GPx, SOD and MDH activities were found in healthy small dogs that underwent medical checkups. These may complement in-hospital testing and contribute to earlier detection of disease. Further studies on more biomarkers are required to better understand age-related inflammation. We measured SAA using the latex agglutination method to determine whether it could be used as an indicator of age-related inflammation. However, this test was unable to detect age-related inflammation in dogs without inflammatory diseases because most of the clinically healthy canine samples were below the lower detection limits. We confirmed that the healthy dogs that underwent medical checkups had no inflammation in their inner bodies.

Data availability statement

The original contributions presented in the study are included in the article/supplementary material, further inquiries can be directed to the corresponding author/s.

Ethics statement

The animal studies were approved by the Ethical approval was obtained from Muromi Animal Hospital (R23-1). The studies were conducted in accordance with the local legislation and institutional requirements. Written informed consent was obtained from the owners for the participation of their animals in this study.

Author contributions

AK: Formal analysis, Investigation, Writing – original draft, Writing – review & editing. ET: Data curation, Formal analysis, Writing – original draft, Conceptualization, Investigation, Methodology. HK: Investigation, Writing – original draft. KK: Data curation, Formal analysis, Supervision, Writing – review & editing, Writing – original draft.

Funding

The author(s) declare that no financial support was received for the research, authorship, and/or publication of this article.

Acknowledgments

We would like to thank the staff of Muromi Animal Hospital for sampling plasma. We would like to thank Editage (www.editage.jp) for English language editing.

Conflict of interest

The authors declare that the research was conducted in the absence of any commercial or financial relationships that could be construed as a potential conflict of interest.

Publisher's note

References

1. Wallis LJ, Radford AD, Belshaw Z, Jackson J, Kubinyi E, German AJ, et al. "just old age"-a qualitative investigation of owner and veterinary professional experiences of and attitudes to ageing in dogs in the UK. *J Small Anim Pract*. (2023) 64:425–33. doi: 10.1111/jsap.13610

2. Belshaw Z, Dean R, Asher L. Could it be osteoarthritis? How dog owners and veterinary surgeons describe identifying canine osteoarthritis in a general practice setting. *Prev Vet Med*. (2020) 185:105198. doi: 10.1016/j.prevetmed.2020.105198

3. Belshaw Z, Robinson NJ, Dean RS, Brennan ML. Motivators and barriers for dog and cat owners and veterinary surgeons in the United Kingdom to using preventative medicines. *Prev Vet Med*. (2018) 154:95–101. doi: 10.1016/j.prevetmed.2018.03.020

4. Enlund KB, Brunius C, Hanson J, Hagman R, Höglund OV, Gustås P, et al. Dental home care in dogs - a questionnaire study among Swedish dog owners, veterinarians and veterinary nurses. *BMC Vet Res*. (2020) 16:90. doi: 10.1186/s12917-020-02281-y

5. Larsen JA, Villaverde C. Scope of the problem and perception by owners and veterinarians. *Vet Clin North Am Small Anim Pract*. (2016) 46:761–72. doi: 10.1016/j.cvsm.2016.04.001

6. Chapagain D, Range F, Huber L, Virányi Z. Cognitive aging in dogs. *Gerontology*. (2018) 64:165–71. doi: 10.1159/000481621

7. Rodier F, Campisi J. Four faces of cellular senescence. *J Cell Biol*. (2011) 192:547–56. doi: 10.1083/jcb.201009094

8. van Vliet T, Varela-Eirin M, Wang B, Borghesan M, Brandenburg SM, Franzin R, et al. Physiological hypoxia restrains the senescence-associated secretory phenotype via AMPK-mediated mTOR suppression. *Mol Cell*. (2021) 81:2041–52.e6. doi: 10.1016/j.molcel.2021.03.018

9. Birch J, Gil J. Senescence and the SASP: many therapeutic avenues. *Genes Dev*. (2020) 34:1565–76. doi: 10.1101/gad.343129.120

10. Kumari R, Jat P. Mechanisms of cellular senescence: cell cycle arrest and senescence associated secretory phenotype. *Front Cell Dev Biol*. (2021) 9:645593. doi: 10.3389/fcell.2021.645593

11. Ohtani N. The roles and mechanisms of senescence-associated secretory phenotype (SASP): can it be controlled by senolysis? *Inflamm Regen*. (2022) 42:11. doi: 10.1186/s41232-022-00197-8

12. Lee GH, Jo W, Park JS, Kang TK, Sung SE, Oh T, et al. Regular medical checkup program (in K-MEDI hub) to enhance the welfare of laboratory dogs and pigs. *Lab Anim Res*. (2023) 39:24. doi: 10.1186/s42826-023-00170-7

13. Franceschi C, Garagnani P, Parini P, Giuliani C, Santoro A. Inflammaging: a new immune-metabolic viewpoint for age-related diseases. *Nat Rev Endocrinol*. (2018) 14:576–90. doi: 10.1038/s41574-018-0059-4

14. Jiménez AG. Inflammaging in domestic dogs: basal level concentrations of IL-6, IL-1β, and TNF-α in serum of healthy dogs of different body sizes and ages. *Biogerontology*. (2023) 24:593–602. doi: 10.1007/s10522-023-10037-y

15. Day MJ. Ageing, immunosenescence and inflammageing in the dog and cat. *J Comp Pathol*. (2010) 142:S60–9. doi: 10.1016/j.jcpa.2009.10.011

16. Piotti P, Pierantoni L, Albertini M, Pirrone F. Inflammation and behavior changes in dogs and cats. *Vet Clin North Am Small Anim Pract*. (2024) 54:1–16. doi: 10.1016/j.cvsm.2023.08.006

17. Jimenez AG, Downs CJ, Lalwani S, Cipolli W. Cellular metabolism and IL-6 concentrations during stimulated inflammation in primary fibroblasts from small and large dog breeds as they age. *J Exp Biol*. (2021) 224:jeb 233734. doi: 10.1242/jeb.233734

18. Jiménez AG. A revisiting of "the hallmarks of aging" in domestic dogs: current status of the literature. *GeroScience*. (2024) 46:241–55. doi: 10.1007/s11357-023-00911-5

19. Panickar KS, Jewell DE. The beneficial role of anti-inflammatory dietary ingredients in attenuating markers of chronic low-grade inflammation in aging. *Horm Mol Biol Clin Investig*. (2015) 23:59–70. doi: 10.1515/hmbci-2015-0017

20. Withers SS, Moore PF, Chang H, Choi JW, McSorley SJ, Kent MS, et al. Multi-color flow cytometry for evaluating age-related changes in memory lymphocyte subsets in dogs. *Dev Comp Immunol*. (2018) 87:64–74. doi: 10.1016/j.dci.2018.05.022

21. Alexander JE, Colyer A, Haydock RM, Hayek MG, Park J. Understanding how dogs age: longitudinal analysis of markers of inflammation, immune function, and oxidative stress. *J Gerontol A Biol Sci Med Sci*. (2018) 73:720–8. doi: 10.1093/Gerona/glx182

22. Yoon JS, Yu DH, Park J. Changes in the serum protein electrophoresis profile in dogs with pyometra. *Front Vet Sci*. (2021) 8:626540. doi: 10.3389/fvets.2021.626540

23. Tecles F, Spiranelli E, Bonfanti U, Cerón JJ, Paltrinieri S. Preliminary studies of serum acute-phase protein concentrations in hematologic and neoplastic diseases of the dog. *J Vet Intern Med*. (2005) 19:865–70. doi: 10.1111/j.1939-1676.2005.tb02779.x

24. Zhao Y, He X, Shi X, Huang C, Liu J, Zhou S, et al. Association between serum amyloid a and obesity: a meta-analysis and systematic review. *Inflamm Res*. (2010) 59:323–34. doi: 10.1007/s00011-010-0163-y

25. Kumon Y. Inflammatory adipokines. *Clin Chem*. (2008) 37:261–71. doi: 10.14921/jscc1971b.37.3_264

26. Fan R, Olbricht G, Baker X, Hou C. Birth mass is the key to understanding the negative correlation between lifespan and body size in dogs. *Aging (Albany NY)*. (2016) 8:3209–22. doi: 10.18632/aging.101081

27. Loos S. How to convert dog years to human years. Pet MD. (2020). Available at: https://www.petmd.com/dog/general-health/pet-myths-dog-years-human-years (Accessed April 1, 2024).

28. Willems A, Paepe D, Marynissen S, Smets P, Van de Maele I, Picavet P, et al. Results of screening of apparently healthy senior and geriatric dogs. *J Vet Intern Med*. (2017) 31:81–92. doi: 10.1111/jvim.14587

29. Pet medical support (in Japanese) (2024). Available at: https://prtimes.jp/main/html/rd/p/000000005.000057917.html (Accessed April 1, 2024).

30. Creevy KE, Grady J, Little SE, Moore GE, Strickler BG, Thompson S, et al. 2019 AAHA canine life stage guidelines. *J Am Anim Hosp Assoc*. (2019) 55:267–90. doi: 10.5326/JAAHA-MS-6999

31. Association for Pet obesity prevention body condition score (BCS) for dogs. (2024). Available at: https://www.petobesityprevention.org/pet-weight-check (Accessed February 1, 2024).

32. Pharmaceutical Ostuka. Mouse/rat adiponectin ELISA kit. TI25462309 (instruction manual in Japanese). (2006). Available at: https://www.otsuka.co.jp/pharmaceutical-business/products/pdf/direction-sheet02.pdf (Accessed April 1, 2024).

33. Kaloustian HD, Stolzenbach FE, Everse J, Kaplan NO. Lactic dehydrogenase of lobster (*Homanus americanus*) tail muscle. I. Physical and chemical properties. *J Biol Chem*. (1969) 244:2891–901. doi: 10.1016/S0021-9258(18)91709-6

34. Bergmeyer HU, Bernt E. Malate dehydrogenase UV-Assay In: HU Bergmeyer, editor. Methods of enzymatic analysis, vol. *1*. *2nd* ed. New York: Academic Press (1974). 613–7.

35. Eiken Chemical Co., Ltd., Eiken VS. Analytical performance: Horse, cat, dog, and cow. Available at: https://www.eiken.co.jp/en/products/vet_saa/ (Accessed February 1, 2024).

36. Arthur JR. The glutathione peroxidases. *Cell Mol Life Sci*. (2000) 57:1825–35. doi: 10.1007/pl00000664

37. Sneddon AA, Wu HC, Farquharson A, Grant I, Arthur JR, Rotondo D, et al. Regulation of selenoprotein GPx4 expression and activity in human endothelial cells by fatty acids, cytokines and antioxidants. *Atherosclerosis*. (2003) 171:57–65. doi: 10.1016/j.atherosclerosis.2003.08.008

38. Yant LJ, Ran Q, Rao L, Van Remmen H, Shibatani T, Belter JG, et al. The selenoprotein GPX4 is essential for mouse development and protects from radiation and oxidative damage insults. *Free Radic Biol Med*. (2003) 34:496–502. doi: 10.1016/s0891-5849(02)01360-6

39. Minárik P, Tomásková N, Kollárová M, Antalík M. Malate dehydrogenases--structure and function. *Gen Physiol Biophys*. (2002) 21:257–65.

40. Washizu T, Nakamura M, Izawa N, Suzuki E, Tsuruno S, Washizu M, et al. The activity ratio of the cytosolic MDH/LDH and the isoenzyme pattern of LDH in the peripheral leukocytes of dogs, cats and rabbits. *Vet Res Commun*. (2002) 26:341–6. doi: 10.1023/a:1016278409138

41. Li G, Lee P, Mori N, Yamamoto I, Arai T. Long term intensive exercise training leads to a higher plasma malate/lactate dehydrogenase (M/L) ratio and increased level of lipid mobilization in horses. *Vet Res Commun*. (2012) 36:149–55. doi: 10.1007/s11259-012-9515-0

42. Kawasumi K, Yamamoto M, Koide M, Okada Y, Mori N, Yamamoto I, et al. Aging effect on plasma metabolites and hormones concentrations in riding horses. *Open Vet J*. (2015) 5:154–7. doi: 10.5455/OVJ.2015.v5.i2.p154

43. Oikonomidis IL, Milne E. Clinical enzymology of the dog and cat. *Aust Vet J*. (2023) 101:465–78. doi: 10.1111/avj.13291

44. Itoh H, Kakuta T, Genda G, Sakonju I, Takase K. Canine serum alkaline phosphatase isoenzymes detected by polyacrylamide gel disk electrophoresis. *J Vet Med Sci*. (2002) 64:35–9. doi: 10.1292/jvms.64.35

45. Syakalima M, Takiguchi M, Yasuda J, Hashimoto A. The age dependent levels of serum ALP isoenzymes and the diagnostic significance of corticosteroid-induced ALP during long-term glucocorticoid treatment. *J Vet Med Sci*. (1997) 59:905–9. doi: 10.1292/jvms.59.905

46. Lumeng CN, Saltiel AR. Inflammatory links between obesity and metabolic disease. *J Clin Invest*. (2011) 121:2111–7. doi: 10.1172/JCI57132

47. Yang H, Youm YH, Vandanmagsar B, Rood J, Kumar KG, Butler AA, et al. Obesity accelerates thymic aging. *Blood*. (2009) 114:3803–12. doi: 10.1182/blood-2009-03-213595

48. Son D, Nangaku M. 3. Metabolism of BUN and creatinine -policy of differential diagnosis with increased creatinine level. *J Jpn Soc Intern Med*. (2008) 97:929–33. doi: 10.2169/naika.97.929, (in Japanese)

49. Mizorogi T, Kobayashi M, Ohara K, Okada Y, Yamamoto I, Arai T, et al. Effects of age on inflammatory profiles and nutrition/energy metabolism in domestic cats. *Vet Med*. (2020) 11:131–7. doi: 10.2147/VMRR.S277208

50. Kunitomo M. Oxidative stress and atherosclerosis. *Yakugaku Zasshi*. (2007) 127:1997–2014. doi: 10.1248/yakushi.127.1997

51. Del Rio D, Stewart AJ, Pellegrini N. A review of recent studies on malondialdehyde as toxic molecule and biological marker of oxidative stress. *Nutr Metab Cardiovasc Dis*. (2005) 15:316–28. doi: 10.1016/j.numecd.2005.05.003

52. Yu S, Paetau-Robinson I. Dietary supplements of vitamins E and C and beta-carotene reduce oxidative stress in cats with renal insufficiency. *Vet Res Commun*. (2006) 30:403–13. doi: 10.1007/s11259-006-3269-5

53. Kawasumi K, Murai T, Mizorogi T, Okada Y, Yamamoto I, Suruga K, et al. Changes in plasma metabolites concentrations in obese dogs supplemented with anti-oxidant compound. *Front Nutr*. (2018) 5:74. doi: 10.3389/fnut.2018.00074

54. Megumi K, Saitou Y, Tsuchiya K, Abe F, Tanaka T, Horinouchi I, et al. Effects of 5-aminolevulinic acid on a murine model of diet-induced obesity. *J Clin Biochem Nutr*. (2015) 57:145–50. doi: 10.3164/jcbn.13-58

55. Sakai A, Iwatani N, Harada K. Improvement effect of 5-aminolevulinic acid on hyperlipidemia in miniature schnauzer dogs: an open study in 5 cases of one pedigree. *Yonago Acta Med*. (2020) 63:234–8. doi: 10.33160/yam.2020.08.006

56. Bulgarelli C, Ciuffoli E, Troia R, Goggs R, Dondi F, Giunti M. Apolipoprotein A1 and serum amyloid a in dogs with sepsis and septic shock. *Front Vet Sci*. (2023) 10:1098322. doi: 10.3389/fvets.2023.1098322

57. Jin K, Hoffman JM, Creevy KE, O'Neill DG, Promislow D. Multiple morbidities in companion dogs: a novel model for investigating age-related disease. *Pathobiol Aging Age Relat Dis*. (2016) 6:33276. doi: 10.3402/pba.v6.33276

58. Hoffman JM, Creevy KE, Franks A, O'Neill DG, Promislow DEL. The companion dog as a model for human aging and mortality. *Aging Cell*. (2018) 17:e12737. doi: 10.1111/acel.12737

59. Xenoulis PG, Steiner JM. Canine hyperlipidaemia. *J Small Anim Pract*. (2015) 56:595–605. doi: 10.1111/jsap.12396

60. Xenoulis PG, Steiner JM. Lipid metabolism and hyperlipidemia in dogs. *Vet J*. (2018) 183:12–21. doi: 10.1016/j.tvjl.2008.10.011

61. Mori N, Lee P, Muranaka S, Sagara F, Takemitsu H, Nishiyama Y, et al. Predisposition for primary hyperlipidemia in miniature schnauzers and Shetland sheepdogs as compared to other canine breeds. *Res Vet Sci*. (2010) 88:394–9. doi: 10.1016/j.rvsc.2009.12.003

Frontiers in Veterinary Science

Transforms how we investigate and improve animal health

The third most-cited veterinary science journal, bridging animal and human health with a comparative approach to medical challenges. It explores innovative biotechnology and therapy for improved health outcomes.

Discover the latest Research Topics

See more →

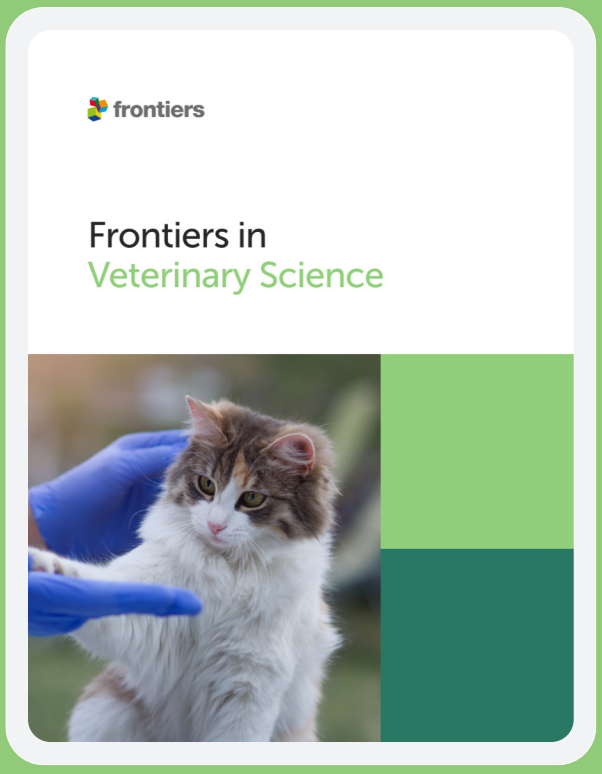

Frontiers

Avenue du Tribunal-Fédéral 34
1005 Lausanne, Switzerland
frontiersin.org

Contact us

+41 (0)21 510 17 00
frontiersin.org/about/contact